

https://dspace.org/

A risk based methodology to improve the definition of geotechnical design sectors in slope design

Bester, Marnus

2019
https://hdl.handle.net/10539/32939

Downloaded from a DSpace repository. https://dspace.org/

A RISK BASED METHODOLOGY TO IMPROVE THE DEFINITION OF GEOTECHNICAL DESIGN SECTORS IN SLOPE DESIGN

Marnus Bester

A thesis submitted to the Faculty of Engineering and the Built Environment, University of the Witwatersrand, Johannesburg, in fulfilment of the requirements for the degree of Doctor of Philosophy.

Johannesburg, 2019

DECLARATION

The work described in this thesis was carried out while in full time employment of Kumba Iron Ore, a division of Anglo American. The research was supervised by Professor T.R. Stacey of the School of Mining Engineering at the University of the Witwatersrand. These studies represent original work by the author and where use has been made of work of others, it is duly acknowledged. The thesis is being submitted to the Degree of Doctor of Philosophy to the University of the Witwatersrand, Johannesburg. It has not been submitted before for any degree or examination to any other University.

Signature of candidate



……

Marnus Bester

Date

28 day of November, 2019

ABSTRACT

In open pit mines, the slope design process is widely utilised in a relatively standard format. Data from geological, structural, rock mass and hydrogeological models are used to formulate and populate geotechnical models. The volume of interest is divided into geotechnical domains, wherein structural and rock strength data are key inputs to define conceptual failure modes or models. Subdivision of domains, which contain structurally-controlled and/or anisotropic materials, into design sectors should result in practical slope designs.

However, in the planning of open pit mines, it is often difficult to determine the shapes and sizes of slope design sectors prior to their analysis, particularly in structurally-complex geological environments. The most challenging aspects of design, in moderately- to heavily-jointed rock masses, relate to the impacts of in-situ geological features on rock mass behaviour. In addition, joint density and persistence must be considered relative to the volume of interest, as rock mass properties can exhibit significant scale-dependence. This problem is exacerbated in sectors encompassing significant strike changes of lithological units or contacts. This variability in strike is often poorly-addressed/represented via the application of median values, or averages for key parameters, thereby increasing uncertainty and risk.

In order to address the fact that slope instability is one of the major sources of risk in open pit mining, largely due to data uncertainties, the discrete fracture network (DFN) and synthetic rock mass (SRM) approaches are applied herein to elucidate the effect that anisotropy has on slope design.

The thesis presents the analysis of the interaction of complex geological features with slope geometry, utilising the input from synthetic rock mass modelling and thereby exploiting the integration of structural geology with slope design.

The interaction of a geological plane (e.g. foliation, bedding or contact) with a vertical surface within a pit design, results in a calculable apparent dip (AD). Continuous AD maps augment the use of 2D design sections, by providing a rational and dynamic methodology to improve the definition of design sectors, as inputs to the mine planning process, from a very early project stage.

The technique shows the spatial variability in the apparent dip of anisotropic units or geological features, using fully-constrained, implicit 3D geological models. Apparent dip is plotted spatially and binned into categories that show its inward or outward dipping attitude with respect to the pit. This binning may be arbitrary or guided by input from SRM analysis or may rely on critical friction angles. This is particularly important where the main plane of anisotropy shows significant changes in dip direction, which may warrant further domain subdivision. This technique is also particularly useful where the pit surface shows a dramatic change in orientation with respect to strike or dip direction in a given part of a domain. Improved design sector classification highlights possible areas of favourable or

unfavourable interactions of anisotropic lithologies, with slope geometries in current mining faces, future pushbacks or on final/design faces. This allows for focused data acquisition and practical sector- (or sub-sector)-specific design parameters as input for mine design, in turn leading to optimised designs and early risk mitigation.

Utilising the input from the SRM analysis, the new 3D geometrical analysis methodology was successfully applied at the Heuningkranz project in the Northern Cape of South Africa, resulting in the definition of early stage design sectors. A geotechnical block model was developed, constrained with design sectors and populated with geotechnical design parameters as input in the mine planning process. Early stage, focussed geotechnical data acquisition was also planned and implemented based on results obtained from the 3D geometrical analysis. New data were included in the geological and geotechnical databases to inform model updates. The application of the new methodology at the Heuningkranz exploration project showed how early front-end loading of a project, utilising the suggested iterative process, greatly improves the design process to achieve the objectives of the project stage (concept), i.e. to look for fatal flaws and to refine the investigation with new data. From a geotechnical engineering point of view, this was achieved, as focussed data acquisition targets potential risk areas early on, to allow for optimised ramp and waste dump placement, leading to improved slope designs. It therefore increases the confidence in one of the major drivers of this project, viz. the strip ratio, that is vital in the economic viability of the project.

A case study at Sishen Mine, in the Northern Cape of South Africa, demonstrates that an ongoing, risk-based approach, described in this thesis, leads to a higher-confidence, dynamically-updatable geotechnical model, thereby allowing for an integrated mine design process that achieves early risk mitigation and at the same time, delivers optimised designs that unlock significant value without compromising the geotechnical risk profile of the mine.

Another case study at Kolomela Mine, also in the Northern Cape of South Africa, further validates the approach described in this thesis, that leads to early risk identification and successful mitigation of potential slope instability. Increased confidence in slope design by addressing geological uncertainty led to pit layout optimisation opportunities, unlocking significant value. This was achieved without any fall of ground (FoG) related accidents, due to the early identification and effective management of geotechnical risk through effective collaboration by the Geotechnical Engineering, Mine Planning and Mining Operations Departments.

At Jwaneng Mine in Botswana, the application of this new methodology has greatly assisted in the early identification of potential risk areas and allows for forward prediction of stability implications based on still-to-be-mined benches with respect to the mine design. This information leads to a better definition of the design, and early risk mitigation through execution of the solution design (in this case, dip slope mining). Business risks associated with personnel and equipment safety, as well as economic risks, could have had devastating impacts on the mine's sustainability

and, as Jwaneng provides a large part of Botswana's GDP, a deleterious impact on the country's economy.

ACKNOWLEDGEMENTS

I would like to express my appreciation to my supervisor, Professor T.R. Stacey, for his advice and guidance throughout the duration of this study.

The contribution of the following towards this work is also acknowledged:

- Dr Ian Basson from TECT Geological Consulting and the TECT Team (Dr Corné Koegelenberg, Pieter Creus, Chris Anthonissen and Ben Stoch) for their dedicated assistance throughout this study.
- Dr Loren Lorig and Alex Cabrera from Itasca Consulting Group for their excellent support and assistance. SRM analyses were carried out under contract by Itasca Consulting Group according to instructions provided to them, using project input data provided to them. Subsequent to workshops and discussions, the results of the analyses were presented by Itasca in contract reports to Kumba Iron Ore, and, as internal documents, these have not been referenced in the reference list.
- Dr Ian Basson, Peter Terbrugge from SRK Consulting, and Roger Johnson, former Head of Geotechnical Engineering for Anglo American, for their initial motivation and support to embark on this journey.
- The whole Kumba Iron Ore Geotechnical Engineering team with Chief Engineers, Richard Carey at Sishen Mine, Ivan Smit at Kolomela Mine and Thandile Dlokweni at Head Office.

My thanks also to Kumba Iron Ore, a division of Anglo American, for the opportunity to complete this study.

Last but not least, I would like to dedicate this work to my loving parents, Hendrik and Rina Bester, to whom I'm eternally grateful for my education and providing me with every opportunity I needed to embark on my chosen career. Then, also to my wife, Annelize, and children, Annerine and Ruan, for without their love and support, none of this is worthwhile.

LIST OF FIGURES **10**

LIST OF TABLES **15**

NOMENCLATURE **16**

1. INTRODUCTION **18**

1.1. PROBLEM STATEMENT 19
1.2. OBJECTIVES OF THE RESEARCH 19
1.3. FORMAT OF THE THESIS 21

2. SYNTHETIC ROCK MASS MODELLING **23**

2.1. INTRODUCTION 23
2.2. METHODOLOGY 24
2.3. SYNTHETIC ROCK MASS MODELLING FOR SISHEN MINE 27
2.3.1. Background *27*
2.3.2. Geological setting of Sishen Mine *28*
2.3.3. Banded Iron Formation (BIF) *34*
2.3.4. Shale (SH) *41*
2.4. SYNTHETIC ROCK MASS MODELLING FOR KOLOMELA MINE 45
2.4.1. Background *45*
2.4.2. Geological setting of Kolomela Mine *46*
2.4.3. Banded Iron Formation (BIF) *46*
2.4.4. Shale (SH) *50*
2.5. SYNTHETIC ROCK MASS MODELLING (CONCEPTUAL) FOR THE HEUNINGKRANZ PROJECT 59
2.5.1. Background *59*
2.5.2. Geological Setting of Heuningkranz *61*
2.5.3. Banded Iron Formation (BIF) *61*
2.5.4. Shale (SH) *67*
2.6. SUMMARY AND CONCLUSIONS 73

3. A NEW 3D GEOMETRICAL ANALYSIS METHODOLOGY **77**

3.1. INTRODUCTION 77
3.2. DEVELOPMENT OF THE METHODOLOGY 80
3.3. CALCULATION OF APPARENT DIP 81
3.4. CONTOURING AND BINNING OF AD RESULTS 84
3.5. APPLYING THE NEW METHODOLOGY AT DIFFERENT STAGES OF A PROJECT'S LIFE CYCLE 88
3.5.1. Early-Stage Projects (Limited Data) *88*
3.5.2. Operational Stage Project (Denser Data Sets) *89*
3.6. THE DEFINITION OF GEOTECHNICAL DESIGN SECTORS 90
3.7. SUMMARY AND CONCLUSIONS 92

4. THE SLOPE DESIGN PROCESS **93**

4.1. INTRODUCTION 93
4.2. APPLYING THE NEW METHODOLOGY TO IMPROVE THE SLOPE DESIGN PROCESS 94
4.2.1. Concept stage *96*
4.2.2. Pre-Feasibility Stage *104*
4.2.3. Feasibility Stage *104*
4.2.4. Design and Construction Stage *104*
4.2.5. Operations *104*
4.2.6. Mine Closure *113*
4.3. THE GEOTECHNICAL BLOCK MODEL AS THE MAIN OUTPUT FROM THE GEOTECHNICAL ENGINEERING FUNCTION 114

4.3.1. The Geological Wireframe Model and Geological Block Model 115
4.3.2. Creating a Geotechnical Block Model 115
4.3.3. Assign Geotechnical Attributes and Design Parameters to the Geotechnical Block Model 117
4.3.4. Interpolation and Population of the Geotechnical Block Model 123
4.4. SUMMARY AND CONCLUSION 123

5. APPLICATION OF THE DESIGN PROCESS, SYNTHETIC ROCK MASS MODELS AND 3D GEOMETRICAL ANALYSIS METHODOLOGY TO CASE STUDIES IN PROJECT PHASE 124

5.1. CONCEPTUAL STAGE PROJECT – HEUNINGKRANZ PROJECT 124
5.1.1. Introduction 124
5.1.2. Discussion of results: Application of 3D Geometrical Analysis Methodology 124
5.2. SUMMARY AND CONCLUSIONS 130

6. APPLICATION OF THE DESIGN PROCESS, SYNTHETIC ROCK MASS MODELS AND 3D GEOMETRICAL ANALYSIS METHODOLOGY TO CASE STUDIES IN THE OPERATIONAL PHASE 131

6.1. SISHEN MINE 131
6.1.1. Introduction 131
6.1.2. Discussion of results: Application of synthetic rock mass models and 3D geometrical analysis methodology 131
6.1.3. Summary and Conclusions 152
6.2. KOLOMELA MINE 153
6.2.1. Introduction 153
6.2.2. Discussion of results: Application of 3D geometrical analysis methodology 153
6.2.3. Summary and conclusions 159
6.3. JWANENG MINE 160
6.3.1. Introduction 160
6.3.2. Geological Setting of Jwaneng Mine 161
6.3.3. Discussion of Results: Application of 3D Geometrical Analysis Methodology 164
6.3.4. Summary and Conclusions 172

7. VALUA ADDED BY FOLLOWING THE METHODOLOGY DESCRIBED 174

7.1. INTRODUCTION 174
7.2. VALUE ADD AT SISHEN MINE 174
7.3. VALUE ADD AT KOLOMELA MINE 175
7.4. CONCLUSIONS 176

8. CONCLUSIONS 177

8.1. SYNTHETIC ROCK MASS MODELLING 178
8.2. A NEW 3D GEOMETRICAL ANALYSIS METHODOLOGY 178
8.3. THE SLOPE DESIGN PROCESS 179
8.4. APPLICATION OF THE DESIGN PROCESS, SYNTHETIC ROCK MASS MODELS AND 3D GEOMETRICAL ANALYSIS METHODOLOGY TO CASE STUDIES IN PROJECT PHASE 180
8.5. APPLICATION OF THE DESIGN PROCESS, SYNTHETIC ROCK MASS MODELS AND 3D GEOMETRICAL ANALYSIS METHODOLOGY TO CASE STUDIES IN THE OPERATIONAL PHASE 180
8.6. VALUE ADDED BY FOLLOWING THE METHODOLOGY DESCRIBED 181
8.7. SUGGESTIONS FOR FURTHER RESEARCH 181
8.7.1. The Impact of Technology 182

REFERENCES 183

APPENDICES 193

APPENDIX 1: EXAMPLES OF A MINE PLANNING CYCLE (ANNUAL OR BI-ANNUAL) AND A MORE DETAILED PROCESS JOINTLY PERFORMED BY THE MINE PLANNING AND GEOTECHNICAL ENGINEERING FUNCTIONS. 194
APPENDIX 2: FAULT CONFIDENCE RATING TABLE. 196
APPENDIX 3: GEOLOGICAL SETTING OF THE HEUNINGKRANZ PROJECT. 198
APPENDIX 4: SISHEN MINE GEOTECHNICAL DATA. 206
APPENDIX 5: GEOLOGICAL SETTING OF KOLOMELA MINE. 208
APPENDIX 6: KOLOMELA MINE GEOTECHNICAL DATA. 212
APPENDIX 7: KOLOMELA MINE LEEUWFONTEIN PIT STABILITY ANALYSIS RESULTS. 214

LIST OF FIGURES

FIGURE 1 AVERAGE STRENGTH RESULTS FOR SISHEN BIF FOR 3 AND 6 ITERATIONS.....26
FIGURE 2 LOCALITY MAP OF KUMBA IRON ORE OPERATIONS 28
FIGURE 3 DETAILED SISHEN STRATIGRAPHIC SUCCESSION (VENTER & DEACON, 2017).....29
FIGURE 4 STEREONETS FOR BEDDING PLANES AND ORTHOGONAL JOINTS IN BIF AT SISHEN MINE. 35
FIGURE 5 SPACING HISTOGRAM (WITH MEDIAN AND EQUIVALENT FRACTURE FREQUENCY FF) FOR BEDDING PLANES AND ORTHOGONAL JOINTS IN BIF. 36
FIGURE 6 PERSISTENCY HISTOGRAM FOR ORTHOGONAL JOINTS IN BIF. 37
FIGURE 7 3DEC SAMPLE FOR BIF UNIT TEST WITH 10° INCLINATION FOR BEDDING PLANES. 37
FIGURE 8 STRENGTH RESULTS IN PA (MAGENTA CURVE) FOR BIF UNIT TEST WITH EXPLICIT HORIZONTAL BEDDING PLANES. COMPARATIVE LOAD RESULTS (YELLOW AND ORANGE CURVES) AT BOTH ENDS OF THE SAMPLE (IN NEWTON).....39
FIGURE 9 STRENGTH RESULTS FOR THE BIF UNIT FOR EXPLICIT TESTS AT ALL ANALYSED INCLINATIONS.....40
FIGURE 10 COMPARISON OF RESULTS FOR BIF UNIT TESTS ON ANISOTROPIC ROCK. 41
FIGURE 11 SPACING HISTOGRAM (WITH MEDIAN AND EQUIVALENT FRACTURE FREQUENCY FF) FOR BEDDING PLANES AND ORTHOGONAL JOINTS IN THE SH UNIT.....42
FIGURE 12 PERSISTENCY HISTOGRAM FOR ORTHOGONAL JOINTS IN SH. 43
FIGURE 13 3DEC SAMPLE FOR THE SH UNIT TEST WITH 10° INCLINATION FOR BEDDING.....43
FIGURE 14 STRENGTH RESULTS FOR SH FOR EXPLICIT TESTS, AT ALL ANALYSED INCLINATIONS....44
FIGURE 15 COMPARISON OF NUMERICAL ANISOTROPIC STRENGTH RESULTS FOR IMPLICIT AND EXPLICIT REPRESENTATIONS OF JOINTS IN SH. 45
FIGURE 16 STEREONETS FOR BEDDING PLANES AND ORTHOGONAL JOINTS IN BIF AT KOLOMELA MINE. 46
FIGURE 17 3DEC SAMPLE FOR KOLOMELA BIF TEST WITH 29° INCLINATION FOR BEDDING PLANES. 47
FIGURE 18 STRENGTH RESULTS IN PA (MAGENTA CURVE) FOR A BIF TEST AT KOLOMELA MINE WITH EXPLICIT INCLINED BEDDING PLANES (20°). COMPARATIVE LOAD RESULTS (SUPERIMPOSED YELLOW AND ORANGE CURVE) IN BOTH ENDS OF THE SAMPLE (IN NEWTONS). 48
FIGURE 19 STRENGTH RESULTS FOR BIF AT KOLOMELA MINE FOR EXPLICIT TESTS AT ALL ANALYSED INCLINATIONS.....49
FIGURE 20 COMPARISON OF RESULTS FOR BIF TESTS AT KOLOMELA MINE ON ANISOTROPIC ROCK MASS. 50
FIGURE 21 STEREONETS FOR BEDDING PLANES AND ORTHOGONAL JOINTS IN LEEUWFONTEIN PIT SHALE. 51
FIGURE 22 STEREONETS FOR BEDDING PLANES AND ORTHOGONAL JOINTS IN KLIPBANKFONTEIN PIT SHALE. 52
FIGURE 23 STEREONETS FOR BEDDING PLANES AND ORTHOGONAL JOINTS IN KAPSTEVEL NORTH PIT SHALE. 52
FIGURE 24 SPACING HISTOGRAM FOR BEDDING PLANES AND ORTHOGONAL JOINTS IN SHALE AT KOLOMELA MINE (LEEUWFONTEIN, KLIPBANKFONTEIN AND KAPSTEVEL NORTH PITS). 53
FIGURE 25 3DEC SAMPLE FOR SHALE IN THE LEEUWFONTEIN PIT WITH 13° INCLINATION FOR BEDDING PLANES (ORIGINAL ORIENTATION).....54
FIGURE 26 STRENGTH RESULTS FOR SHALE AT LEEUWFONTEIN PIT FOR EXPLICIT TESTS AT ALL ANALYSED INCLINATIONS.....55
FIGURE 27 STRENGTH RESULTS FOR SHALE AT KLIPBANKFONTEIN PIT FOR EXPLICIT DISCONTINUITY REPRESENTATION AT VARIOUS INCLINATIONS. 56
FIGURE 28 STRENGTH RESULTS FOR SHALE AT KAPSTEVEL NORTH PIT FOR EXPLICIT TESTS AT ALL THE ANALYSED INCLINATIONS.....57
FIGURE 29 COMPARISON OF RESULTS FOR SHALE TESTS AT LEEUWFONTEIN PIT ON ANISOTROPIC ROCK MASS.....58

FIGURE 30 COMPARISON OF RESULTS FOR SHALE TESTS AT KLIPBANKFONTEIN PIT ON ANISOTROPIC ROCK MASS. 58
FIGURE 31 COMPARISON OF RESULTS FOR SHALE TESTS AT KAPSTEVEL NORTH PIT ON ANISOTROPIC ROCK MASS. 59
FIGURE 32 LOCATION OF HEUNINGKRANZ PROJECT ON THE MAREMANE DOME REGIONAL INTERPRETATION 60
FIGURE 33 STEREO NETS FOR BEDDING PLANES AND ORTHOGONAL JOINTS IN BIF AT THE HEUNINGKRANZ PROJECT. NOTE THAT THE DATA IS IN MINE GRID (180° ROTATED). 62
FIGURE 34 SPACING HISTOGRAMS FOR BEDDING PLANES AND ORTHOGONAL JOINTS IN BIF AT HEUNINGKRANZ. 63
FIGURE 35 3DEC SAMPLE FOR A BIF TEST WITH 14° INCLINATION FOR BEDDING PLANES (ORIGINAL ORIENTATION). 64
FIGURE 36 STRENGTH RESULTS IN PA (MAGENTA CURVE) FOR A BIF TEST FOR THE HEUNINGKRANZ PROJECT WITH EXPLICIT INCLINED BEDDING PLANES (20°). COMPARATIVE LOAD RESULTS (SUPERIMPOSED YELLOW AND ORANGE CURVE) AT BOTH ENDS OF THE SAMPLE (IN NEWTONS). 65
FIGURE 37 STRENGTH RESULTS FOR BIF AT THE HEUNINGKRANZ PROJECT FOR EXPLICIT TESTS AT ALL THE ANALYSED INCLINATIONS. 66
FIGURE 38 COMPARISON OF RESULTS FOR BIF TESTS AT THE HEUNINGKRANZ PROJECT ON ANISOTROPIC ROCK MASS. 67
FIGURE 39 STEREONETS FOR BEDDING PLANES AND ORTHOGONAL JOINTS IN SHALE AT THE HEUNINGKRANZ PROJECT. NOTE THAT THE DATA IS IN MINE GRID (180° ROTATED). 68
FIGURE 40 SPACING HISTOGRAMS FOR BEDDING PLANES AND ORTHOGONAL JOINTS IN SHALE AT THE HEUNINGKRANZ PROJECT. 69
FIGURE 41 3DEC SAMPLE FOR A SHALE TEST WITH 16° INCLINATION FOR BEDDING PLANES (ORIGINAL ORIENTATION). 70
FIGURE 42 STRENGTH RESULTS IN PA (MAGENTA CURVE) FOR A SHALE TEST AT THE HEUNINGKRANZ PROJECT, WITH EXPLICIT VERTICAL BEDDING PLANES (90°). COMPARATIVE LOAD RESULTS (YELLOW AND ORANGE CURVE) AT BOTH ENDS (IN NEWTONS). 71
FIGURE 43 STRENGTH RESULTS FOR THE SHALE UNIT AT HEUNINGKRANZ PROJECT FOR EXPLICIT TESTS AT ALL ANALYSED INCLINATIONS. 72
FIGURE 44 COMPARISON OF RESULTS FOR SHALE TESTS AT THE HEUNINGKRANZ PROJECT ON ANISOTROPIC ROCK MASS. 73
FIGURE 45 COMPARISON OF RESULTS FOR BIF TESTS AT KUMBA OPERATIONS IN THE NORTHERN CAPE. 74
FIGURE 46 COMPARISON OF RESULTS FOR SHALE TESTS AT KUMBA OPERATIONS IN THE NORTHERN CAPE. 74
FIGURE 47 ILLUSTRATION OF GEOTECHNICAL DESIGN SECTORS. 79
FIGURE 48 AN EXAMPLE OF A CONCEPTUAL FAILURE MODEL. 81
FIGURE 49 STEREONET ILLUSTRATING THE PRINCIPAL OF APPARENT DIP CALCULATION (BESTER, BASSON, & KOEGELENBERG, 2015). 82
FIGURE 50 CALCULATING APPARENT DIP (CREUS, ET AL., 2019) 83
FIGURE 51 RANGES OF BINS ARE BASED ON RESULTS OBTAINED FROM THE STRENGTH CURVE OF THE ANISOTROPIC STRENGTH RESPONSE FROM SRM MODELLING. 85
FIGURE 52 EXAMPLE OF RESULTS OF OBTAINED FOR SISHEN MINE UTILISING SRM INPUT FOR BIF AND SHALE. 87
FIGURE 53 FLOWCHART ILLUSTRATING THE PROCESS OF APPLYING THE 3D GEOMETRICAL ANALYSIS METHODOLOGY WITH A LIMITED DATASET 89
FIGURE 54 FLOWCHART ILLUSTRATING THE PROCESS OF APPLYING THE 3D GEOMETRICAL ANALYSIS METHODOLOGY WITH A DENSE DATASET. 90
FIGURE 55 EXAMPLE OF GEOTECHNICAL DESIGN SECTORS (BESTER, BASSON, & KOEGELENBERG, 2015) 91
FIGURE 56 THE SLOPE DESIGN PROCESS (READ AND STACEY, 2009) 93
FIGURE 57 THE ENGINEERING CIRCLE OR WHEEL OF DESIGN (STACEY, 2009) 95

FIGURE 58 THE METHODOLOGY IMPROVES THE SLOPE DESIGN PROCESS DURING EARLY PROJECT STAGES. 96
FIGURE 59 EXAMPLE OF WHITTLE SHELL DRAPED WITH GEOLOGY (LEFT) AND APPARENT DIP (RIGHT). APPARENT DIP WAS BINNED AND CONTOURED TO SHOW FAVOURABLE (DIPPING AWAY, 0 TO -90 DEGREES, BLUE) VS. UNFAVOURABLE (DIPPING INTO, 0 TO 90 DEGREES, RED) INTERACTION OF BEDDING PLANES WITH FUTURE SLOPE ORIENTATIONS. 99
FIGURE 60 EXAMPLE OF APPARENT DIP ANALYSIS ON EARLY STAGE PIT LAYOUT {NOTE THAT LAYOUT HAS NO RAMPS YET AND APPARENT DIPS ONLY CONTOURED TO SHOW DIPPING INTO THE PIT (RED) AND DIPPING OUT OF THE PIT (BLUE)}. 101
FIGURE 61 EXAMPLE OF DOWNHOLE SURVEY LOG (OTV) SHOWING 23 – 29 M INTERVAL ON THE LEFT AND 83 – 88M INTERVAL ON THE RIGHT. JOINTS AND BEDDING ARE INTERPRETED FROM THE LOG WITH, IN THIS EXAMPLE, GREEN AND RED PINS EACH WITH DIP AND DIP DIRECTION. 102
FIGURE 62 THE METHODOLOGY IMPROVES THE SLOPE DESIGN PROCESS DURING IMPLEMENTATION. 105
FIGURE 63 A SUMMARY OF THE DESIGN PROCESS FOR MINE DEWATERING ACCORDING TO ENGINEERING DESIGN PRINCIPLES (BESTER, NEL, & MC GAVIGAN, 2013) 107
FIGURE 64 RAW HIGH-DENSITY SCANNER POINT CLOUD (LEFT) VERSUS POINT CLOUD WITH CONCURRENT PHOTOGRAPHIC OVERLAY (RIGHT) (BESTER, RUSSELL, & CAREY, 2018). 109
FIGURE 65 ORIENTATION, SPACING AND PERSISTENCY MEASUREMENTS TAKEN USING THE GEOTECHNICAL AND CAD FUNCTIONALITIES OF I-SITE STUDIO (BESTER, RUSSELL, & CAREY, 2018). 109
FIGURE 66 EXAMPLE OF AN OVERLAY OF ACTUAL MAPPED (GREEN ARROWS) AND INFERRED BEDDING ORIENTATION MEASUREMENTS FROM THE GEOLOGICAL MODEL (RED AND BLUE ARROWS) (BESTER, RUSSELL, & CAREY, 2018). 110
FIGURE 67 EXAMPLE OF CONFORMANCE BETWEEN ACTUAL MEASURED DIP DIRECTION AND INFERRED DIP DIRECTION BASED ON LITHOLOGICAL CONTACTS (INFERRED DATA POINTS WITHIN 100M OF MAPPING FACE CENTROIDS). EXAMPLE FACE CENTROIDS – LEFT, DISTRIBUTION IN DEVIATION FOR MODEL WIDE FACE MAPPING DATA – RIGHT (BESTER, RUSSELL, & CAREY, 2018). 112
FIGURE 68 EXAMPLE OF INFERRED FAULTS VERSUS A MEASURED FAULT LOCATION IN AN EXPOSED PORTION OF A HIGH WALL (BESTER, RUSSELL, & CAREY, 2018). 113
FIGURE 69 *SUGGESTED* APPROACH FOR GEOTECHNICAL AND HYDROGEOLOGICAL INPUT TO MINE CLOSURE ACCORDING TO THE MINE PLANNING CYCLE. 114
FIGURE 70 AN ILLUSTRATION OF THE SISHEN GEOTECHNICAL BLOCK MODEL (BELOW) UP-BLOCKED FROM THE GEOLOGICAL BLOCK MODEL (ABOVE) WITH A CROSS SECTION THROUGH BOTH MODELS. 116
FIGURE 71 THE SISHEN GEOTECHNICAL BLOCK MODEL INTERSECTED WITH THE PIT LAYOUT INDICATING A BIF BLOCK WITH ITS SLOPE DESIGN PARAMETERS. 118
FIGURE 72 GEOTECHNICAL LOGGING SEQUENCE 125
FIGURE 73 RESULTS OF EARLY STAGE 3D GEOMETRICAL ANALYSIS BASED ON SRM STRENGTH ENVELOPE RESULTS. 126
FIGURE 74 CONCEPT LEVEL DESIGN SECTORS WERE DELINEATED BASED ON 3D GEOMETRICAL ANALYSIS. 128
FIGURE 75 PLAN OF DEDICATED GEOTECHNICAL DRILL HOLES TARGETING POTENTIAL UNFAVOURABLE AREAS. 129
FIGURE 76 LOCATION OF GR35 AND GR80 AREAS OF SISHEN MINE. 132
FIGURE 77 CONCEPTUAL DEFINITION OF THE AREA INFLUENCED BY BLAST DAMAGE (D) – HA AND HB REFERS TO SLOPE HEIGHT. 135
FIGURE 78 3DEC SECTION WITH DAMAGE FACTOR APPLIED IN DEPTH, FROM 1 ON SURFACE TO 0 IN DEPTH. 136
FIGURE 79 AREA OF CONCERN IN THE CENTRAL PART OF SISHEN MINE (GR35) 137
FIGURE 80 FAULT NW1 WAS MODELLED EXPLICITLY AND THE SLOPE FAULT MODELLED AS A ZONE OF WEAK MATERIAL. 137

FIGURE 81 LITHOLOGIES IN THE GR35 NUMERICAL MODEL. 138
FIGURE 82 BIF-CH AND BIF-DYKE LITHOLOGICAL CONTACTS EXPLICITLY REPRESENTED IN THE NUMERICAL MODEL. 139
FIGURE 83 A SECTION SHOWING ANISOTROPY ORIENTATIONS IN BIF AND SHALE. 140
FIGURE 84 DEFINITION OF STABLE VS. UNSTABLE BEHAVIOUR IN TERMS OF NUMERICAL VELOCITIES. 140
FIGURE 85 FACTOR OF SAFETY RESULTS FOR THE GR 35 ANALYSIS. 141
FIGURE 86 SECTION IN GR 35 SHOWING THE FACTOR OF SAFETY RESULTS. 142
FIGURE 87 SECTION IN GR 35 SHOWING DISPLACEMENT MAGNITUDES. 142
FIGURE 88 AREA OF CONCERN (GR80) IN FUTURE PUSHBACK IN NORTHERN PART OF SISHEN MINE. 143
FIGURE 89 GEOTECHNICAL DRILLING TO CONFIRM BEDDING ORIENTATION AND TECTONIC UNCONFORMITY 144
FIGURE 90 GR 80 FAULTS AND TECTONIC UNCONFORMITY MODELLED IN 3DEC. 144
FIGURE 91 PLAN VIEW AND SECTION OF 3DEC NUMERICAL MODEL 145
FIGURE 92 FACTOR OF SAFETY RESULTS FOR THE GR80 STABILITY ANALYSIS. 145
FIGURE 93 SECTION IN GR 80 SHOWING THE INFLUENCE OF THE TECTONIC UNCONFORMITY 146
FIGURE 94 SECTION IN GR 80 SHOWING MECHANICS OF POTENTIAL MOVEMENT. 146
FIGURE 95 SECTION IN GR 80 SHOWING THE AREA WITH FACTOR OF SAFETY OF 1.3 – 1.4. 147
FIGURE 96 FACTOR OF SAFETY RESULTS FOR GR80 SENSITIVITY ANALYSES (INCREASED FRICTION ANGLE LEFT AND INCREASED RESIDUAL COHESION RIGHT). 147
FIGURE 97 FACTOR OF SAFETY RESULTS FOR GR 80 SENSITIVITY ANALYSIS WITH DECREASED COHESION ON FAULTS. 148
FIGURE 98 FACTOR OF SAFETY RESULTS FOR GR 80 SENSITIVITY ANALYSIS WITH PORE PRESSURE APPLIED IN THE SURFACE AQUIFER. 149
FIGURE 99 FACTOR OF SAFETY RESULTS FOR GR 80 SENSITIVITY ANALYSIS WITH PORE PRESSURE APPLIED IN THE SURFACE AQUIFER AS WELL AS STRUCTURES. 149
FIGURE 100 THE GEOTECHNICAL MANAGEMENT PROCESS EMPLOYS CRITICAL CONTROLS AT ALL LEVELS – FROM DESIGN TO IMPLEMENTATION. 150
FIGURE 101 LOCATION OF SOLAR POWERED DEPRESSURISATION HOLES WITH DISCHARGE INTO LINED STORM WATER CANAL. 151
FIGURE 102 DEPRESSURISATION RESULTS ACHIEVED (NOTE THE QUICK RESPONSE TO RAINFALL). 151
FIGURE 103 RESULTS OF THE 3D GEOMETRICAL ANALYSIS OF LEEUWFONTEIN PIT AT KOLOMELA MINE. 154
FIGURE 104 CARBONIFEROUS SHALE EXPOSED ON THE NORTH-EASTERN SIDE OF THE LEEUWFONTEIN PIT. 155
FIGURE 105 MODEL WITH SECTION ILLUSTRATING DOLOMITE / CHERT CONTACT EXPOSED IN THE FACE IN NORTHERN FAULT BLOCK. 156
FIGURE 106 IMAGE (ABOVE) AND RADAR IMAGE (BELOW) OF INSTABILITY EVENT IN THE LEEUWFONTEIN PIT. 157
FIGURE 107 REMEDIATION OF FAILURE IN THE LEEUWFONTEIN PIT AT KOLOMELA MINE (NOTE THE INSTALLATION OF DRAPE MESH). 158
FIGURE 108 PLAN OF GEOTECHNICAL DRILL HOLES AND AN ILLUSTRATION OF INCLINATIONS DRILLED. 159
FIGURE 109 LOCALITY MAP OF JWANENG MINE (DEBSWANA DIAMOND COMPANY (PTY) LTD, 2015). 161
FIGURE 110 CROSS-SECTION OF THE CENTRE OF THE PIT. JWANENG KIMBERLITES ARE INFERRED TO OCCUR WITHIN, OR CLOSE TO THE EDGE OF A HORST-LIKE STRUCTURE (CREUS, ET AL., 2018). 162
FIGURE 111 SCHEMATIC OF THE DEFORMATION EVENTS AT JWANENG MINE: D_1 COMPRESSION FORMING BREACHED FOLDS AND LOW-ANGLE THRUSTS (LEFT); D_2 EXTENSION EXPLOITING FANNING AXIAL PLANAR CLEAVAGE (RIGHT) (BASSON, GABANAKGOSI, MOGOROSI, BESTER, & CREUS, 2016). 163

FIGURE 112 3D GEOLOGICAL MODEL CLIPPED TO DESIGN PIT SURFACE SHOWING DAYLIGHTING OR INTERSECTING COUNTRY ROCK LITHOLOGIES (BASSON, GABANAKGOSI, MOGOROSI, BESTER, & CREUS, 2016). 166
FIGURE 113 SUB-DOMAINING OF BEDDING READINGS FROM PIT MAPPING INTO FAULT-BOUNDED BLOCKS. ANOMALOUSLY STEEPER DIPS FROM DOMAIN 7A ARE HIGHLIGHTED (BASSON, GABANAKGOSI, MOGOROSI, BESTER, & CREUS, 2016). 167
FIGURE 114 CONTOURED PLOT OF APPARENT DIP FOR QS, CS, LS (DOLOMITE AND SILL IS EXCLUDED), BINNED ACCORDING TO AVERAGE FRICTION ANGLE (37 DEG) AND SENSE OF DIP (INTO VS. OUT OF FACE). THE PLOT HIGHLIGHTS A ZONE OF RELATIVELY STEEPER BEDDING, COMPARED TO THE UNDERLYING DESIGN SURFACE, WITHIN DOMAIN 7A AND TRENDING NE-SW THROUGH DOMAINS 8 AND 9 (BASSON, GABANAKGOSI, MOGOROSI, BESTER, & CREUS, 2016). 167
FIGURE 115 NW-SE TRENDING CROSS-SECTION SHOWING THE 3D MODEL CLIPPED TO THE DESIGN SURFACE AND THE RELATIVELY STEEPER BEDDING FOR DOMAIN 7A (INDICATED) (BASSON, GABANAKGOSI, MOGOROSI, BESTER, & CREUS, 2016). 168
FIGURE 116 PLANAR TYPE BENCH FAILURES AT JWANENG MINE CUT 8. 169
FIGURE 117 GEOTECHNICAL MAPPING COVERAGE FOR JWANENG MINE (GABANAKGOSI, ET AL., 2018) 170
FIGURE 118 BLAST BLOCK DESIGNS FOR DIP SLOPE BENCHES. (GABANAKGOSI, ET AL., 2018) 171
FIGURE 119 AN EXCAVATOR SCALING AND LOADING A FINAL PIT BOUNDARY (GABANAKGOSI, ET AL., 2018). 172
FIGURE 120 SECTION ILLUSTRATING ORE TARGETED FOR OPTIMISATION. 176

LIST OF TABLES

TABLE 1 STRUCTURE SET DEFINITION IN BIF AT SISHEN MINE 34
TABLE 2 INTACT ROCK PROPERTIES FOR BIF UNIT FOR EXPLICIT SRM TEST 38
TABLE 3 EXPLICIT STRUCTURE PROPERTIES FOR BIF UNIT SRM TEST 38
TABLE 4 ROCK MASS PROPERTIES, FOR BIF FOR IMPLICIT SRM TEST 40
TABLE 5 INTACT ROCK PROPERTIES FOR SH FOR EXPLICIT SRM TEST 44
TABLE 6 EXPLICIT STRUCTURE PROPERTIES FOR THE SH UNIT SRM TEST 44
TABLE 7 ROCK MASS PROPERTIES FOR SH FOR THE IMPLICIT SRM TEST 45
TABLE 8 STRUCTURE SETS DEFINITION IN BIF FOR KOLOMELA MINE 46
TABLE 9 ROCK MASS PROPERTIES FOR BIF AT KOLOMELA MINE FOR IMPLICIT SRM TEST 49
TABLE 10 STRUCTURE SETS DEFINITION IN SHALE FOR DIFFERENT PITS AT KOLOMELA MINE 51
TABLE 11 INTACT ROCK PROPERTIES FOR SHALE FOR THE EXPLICIT SRM TEST 54
TABLE 12 ROCK MASS PROPERTIES FOR SHALE MATERIAL AT THE DIFFERENT KOLOMELA PITS FOR IMPLICIT SRM TESTS. 57
TABLE 13 STRUCTURE SETS DEFINITION IN BIF 61
TABLE 14 ROCK MASS PROPERTIES FOR BIF AT THE HEUNINGKRANZ PROJECT FOR IMPLICIT SRM TEST 66
TABLE 15 STRUCTURE SETS DEFINITION IN SHALE 67
TABLE 16 ROCK MASS PROPERTIES FOR SHALE AT THE HEUNINGKRANZ PROJECT FOR IMPLICIT SRM TEST 72
TABLE 17 SUGGESTED TARGET LEVELS OF DATA CONFIDENCE (READ & STACEY, 2009) 97
TABLE 18: JOINT PLANE SPACING (JPS) 120
TABLE 19: ROCK MASS DESCRIPTION (RMD) 121
TABLE 20: JOINT PLANE ORIENTATION (JPO) 121
TABLE 21 GEOTECHNICAL UNITS AT SISHEN MINE 133
TABLE 22 GEO-MECHANICAL PROPERTIES FOR ISOTROPIC GEOTECHNICAL UNITS AT SISHEN MINE. 133
TABLE 23 GEO-MECHANICAL PROPERTIES FOR CLAY MATERIALS AT SISHEN MINE. 134
TABLE 24 GEO-MECHANICAL PROPERTIES FOR FAULTS AND CONTACTS AT SISHEN MINE. 134
TABLE 25 GEO-MECHANICAL PROPERTIES FOR THE TECTONIC UNCONFORMITY IN GR 80. 135
TABLE 26 EXPLANATION OF LITHOLOGICAL CODES AT JWANENG MINE. 165
TABLE 27 SUMMARY OF VALUE ADDED THROUGH PROCESS DRIVEN SLOPE OPTIMISATION AT SISHEN UTILISING THE NEW METHODOLOGY. 175
TABLE 28 SUMMARY OF VALUE ADDED THROUGH PROCESS DRIVEN SLOPE OPTIMISATION AT KOLOMELA UTILISING THE NEW METHODOLOGY 176

NOMENCLATURE

Anisotropy	Anisotropy is the property of being directionally dependent, which implies different properties in different directions, as opposed to isotropy.
Apparent Dip (AD):	Apparent dip is the inclination of a geological feature as seen from any vertical cross Section not perpendicular to the strike.
Bedding	Geological formation or stratigraphic rock series marked by well-defined divisional planes (bedding planes) separating it from layers above and below.
Bench:	Standard height of a mining block
Burden:	Distance between blast hole rows parallel to the free face.
Deformation:	A change in shape or size of a solid body.
Dilation	An indicator of volumetric increase during rock deformation. The most common concept used to describe dilation is the dilation angle.
Dip:	Angle at which a stratum or other planar feature is inclined from the horizontal.
Discrete Fracture Network (DFN)	A Discrete Fracture Network (DFN) model is a mathematical representation of fracture characteristics
Factor of Safety (FoS)	The ratio of shear resistance to driving force along a potential failure plane.
Foliation	Repetitive layering in metamorphic rocks.
Geotechnical Design Sector:	Defined area based on geotechnical domains considering failure modes (structure and strength)
Geotechnical Domain:	Lithological unit or grouped units with similar geotechnical characteristics
Isosurface	An isosurface is a three-dimensional analogue of an isoline. It is a surface that represents points of a constant value within a volume of space; in other words, it is a level set of a continuous function whose domain is 3D-space.
Limit blasting:	All forms of blasting designed to preserve the integrity of the remaining

	rock mass (e.g. smooth blasting, presplitting, post-splitting, buffer blasting).
OTV / ATV	Optical Televiewer and Acoustic Televiewer
Poisson's ratio:	The ratio of transverse contraction strain to longitudinal extension strain in the direction of stretching force. Tensile deformation is considered positive and compressive deformation is considered negative.
Ramp:	Inclined haul road designed into the pit highwalls so that material can be transported out of the pit.
Rock mass:	Rock as it occurs in- situ, including its discontinuities.
Rockfall (fall of ground):	Fall of a rock fragment without the simultaneous occurrence of a seismic event.
Strike:	Direction of the azimuth of a horizontal line in the plane of an inclined stratum (or another planar feature) within a rock-mass.
Synthetic Rock Mass Model (SRM)	(SRM) modelling is a new approach for simulating the mechanical behaviour of jointed rock mass utilising a numerical model.
Ubiquitous Joint Rock Mass (UJRM)	The term "ubiquitous" means that the joints may occur at any point in the rock mass and they do not have a fixed location.
Unconformity	A buried erosional or non-depositional surface separating two rock masses or strata of different ages, indicating that sediment deposition was not continuous.
Uniaxial compressive strength (UCS)	The maximum axial compressive stress that a right-cylindrical sample of material can withstand before failing.
Young's Modulus:	A measure of elasticity, usually the linear relationship between the stress acting on a substance to the strain produced.

1. INTRODUCTION

The research described in this thesis deals with open pit mining and the inherent risk of dealing with variable geology. Certain degrees of safety, economic and financial risk have always been implicit in all mining operations (Read & Stacey, 2009). Therefore, it is increasingly required by Management to be involved in the decision-making process for slope designs. Subsequently, the requirement for the quantification and effective management of geotechnical risks has developed (Read & Stacey, 2009).

To address this, the planning and design of large open pit mines in most mining companies are typically performed by mine planning engineers and geotechnical engineers. Due to the volatility of several critical financial parameters (commodity price, exchange rate, inflation/cost etc.) influencing the mine plan, most companies also follow a mine planning cycle to periodically review or adjust their mine plans to maintain profitability as far as possible. This mine planning cycle generally includes the following high-level aspects:

Pit Optimisation – This process involves the economic evaluation of the mine to produce an optimum pit shell using tools like Whittle (Dassault Systèmes, 2019) and mine financial evaluation models. Geotechnical input during this step involves slope angle input to produce an optimum pit shell (lowest strip ratio) that will adhere to industry standards pertaining to geotechnical risk (safety and economics).

Practical Pit Layout Construction - During this phase, a practical pit layout is constructed using detailed input from geotechnical engineers. The practical layout will take into account infrastructure such as treatment plants and waste dumps to produce an optimum layout with efficient ramp systems.

Scheduling – The aim of this step is to provide a Life of Mine production schedule that delivers the desired production volume. Iterations and scenarios are evaluated during this phase to deliver an optimised cash flow and Net Present Value (NPV), taking into account certain constraints that may exist (e.g. rail constraints).

Geomechanical analysis and geotechnical risk assessment – Once the practical pit is available, geotechnical engineers can geomechanically analyse the pit layout to determine if it adheres to company and industry standards. This should be an iterative process to ensure adherence to acceptability criteria. Once a mine schedule is available, detailed geotechnical risk assessments can be conducted (e.g., fault and event tree analyses). Effective controls need to be put in place to ensure residual geotechnical risk levels are acceptable. The pit layout and production schedules are also used during this phase to evaluate groundwater risk and to design and plan dewatering / depressurisation systems if required.

Resource and Reserve Reporting Process – The Life of Mine Plan forms the basis of annual Resource and Reserves reporting as required by various governance codes, e.g. Australasian Joint Ore Reserves Committee (JORC), the South African

Code for the Reporting of Exploration Results, Mineral Resources and Mineral Reserves (SAMREC) etc.

Notwithstanding aforementioned robust processes being in place, slope instability remains one of the major sources of risk, largely due to data uncertainties.

1.1. Problem Statement

In planning open pit mines, it is often difficult to determine the sizes and extents of slope design sectors, *prior* to analysis, particularly in large, structurally- complex environments. This problem is exacerbated when a defined sector encompasses a dramatic change in the strike of its contained lithological units and fabrics, which change is poorly addressed via the application of median values or averages for key parameters, thereby increasing uncertainty and risk. This typically results in a time-consuming, iterative process of constructing pits using software tools such as Surpac, Datamine and Vulcan, followed by stability analyses, then reconstruction or modification of pit layouts based on stability assessment results, until the results of these analysis cycles accord with industry standards. Furthermore, complex environments necessitate the use of numerous design sections around pits or sub-pits.

Routinely-applied geotechnical data are typically sparse or focused only on a narrow volume around vertical, 2D design cross-sections, which are typically radially-oriented with respect to the centre of a pit or sub-pit. Furthermore, the simulation of the effects of anisotropic rock mass strength, scale effects and deformation behaviour on pit slope stability is challenging. As for data availability for early planning of pushbacks, early mining phases or early-stage projects, only drill hole information, (usually) limited surface mapping and a preliminary geological model are available.

1.2. Objectives of the Research

The aim of the research is the pioneering application of Synthetic Rock Mass (SRM) modelling for anisotropic Banded Iron Formation (BIF) and Shale (SH) units, in the Northern Cape Province of South Africa, utilizing the ubiquitous joint rock mass (UJRM) modelling technique to effectively account for rock mass anisotropy and scale effects utilising the numerical software code, *3DEC*. Subsequently, the study aims to demonstrate that the use of vertical 2D design sections in slope designs may be augmented by a new and better methodology that established the sizes and geometries of design sectors from conceptual-phase projects (exploration phase) to operational mines, based on fully-constrained, implicit 3D models and inputs from synthetic rock mass (SRM) modelling. This results in a more robust and practical suite of sector-specific design parameters, in block model format, as inputs for mine design across several commodities. Application of this new methodology results in a dynamic geotechnical model that may be continuously updated and calibrated with new information (e.g. mapping from benches or mined slopes as well as downhole data for future mining areas).

Such an ongoing process will lead to optimised designs and early risk mitigation, ultimately unlocking maximum value while maintaining zero harm.

The results of this methodology are dependent on the quality and quantity of input data. However, the methodology also allows one to focus ongoing and future data acquisition in areas of concern, by considering available data and, moreover, based on maps that show the continuous variation of certain parameters throughout the volume of interest. The methodology follows a risk-based approach, as the resulting focused data acquisition mitigates risk cost effectively from early project stages. It therefore addresses the fact that slope instability is one of the major sources of risk in open pit mining, largely due to data uncertainties. This was achieved as follows:

- Collect and statistically analyse data on the banded iron formation and shale units of the Northern Cape.
- Perform Synthetic Rock Mass Modelling - Develop Discrete Fracture Networks (DFN) for the Banded Iron Formation and Shale units found in the Northern Cape utilising the ubiquitous joint rock mass (UJRM) modelling technique to account for rock mass anisotropy and scale effects utilising the numerical software code, *3DEC*.
- Develop a new, robust methodology, that utilizes input from synthetic rock mass modelling, for the extraction of the spatial variation in parameters by highlighting possible areas - of any size or shape – that show unfavourable interactions with slope geometries in early stage projects, current operations and future pushbacks. According to (Read & Stacey, 2009), subsequent to the formulation of the geotechnical model and the population of this model with relevant data, the model is divided into geotechnical domains. The next step is then to subdivide these domains into design sectors incorporating failure modes utilising the conceptual failure model (strength and structural input). This new 3D geometrical analysis methodology will allow the geotechnical engineer to delineate design sectors much more accurately from a very early stage. Following an iterative process, the process enables the accurate identification of design sectors with potential risk, allowing focussed data acquisition and detailed geotechnical analysis. The early identification of risk allows for preventative controls to be put in place, enabling early risk mitigation. Alternatively, the accurate delineation of favourable design sectors allows the geotechnical engineer to optimise these sectors, unlocking significant value.
- Review data available from an early stage exploration project and operational mines, namely:
    - Heuningkranz Exploration Project, Northern Cape of South Africa
    - Sishen Mine, Northern Cape of South Africa

    - Kolomela Mine, Northern Cape of South Africa
    - Jwaneng Diamond Mine, Botswana

- Apply the new methodology to test its application in various geological settings and project stages. This thesis does not only present novel theoretical research and methodologies, but also shows how value can be unlocked by the practical application of these methodologies in different mines and project stages. At Sishen Mine, the application of these methodologies in an iterative way led to a slope optimisation initiative that was the major contributor to an increase in the mine's NPV of R10 billion from 2017 to 2018 (approximately 50.8 million tons of additional ore). Following the same methodologies, Kolomela Mine protected value by early risk mitigation of potential slope instability and unlocked additional value by accessing approximately 1 million tons of additional ore to date.

1.3. Format of the Thesis

Instead of including a dedicated Chapter to literature review, the thesis reviews the relevant references as part of each descriptive Section.

In his keynote address at the Slope Stability 2018 symposium held in Seville, Spain, J. Read (Read, 2018) discussed developments in open pit slope design since 2009. One of the clear advances in geotechnical engineering is the application of the Synthetic Rock Mass Model (SRM), initially developed by the Itasca Consulting Group, Inc. (Itasca). In a review of the SRM model for block caving studies performed by the Mass Mining Technology project (MMTII), (Hoek & Martin, 2010) noted that "the SRM approach has provided an outstanding set of tools which promise a far more realistic and reliable method of modelling rock mass behaviour than has been available in the past. At the very least this approach should enable us to calibrate traditional rock mass classification approaches used to estimate rock mass properties, but the approach also has the potential, in the long run, of replacing empirical approaches".

In order to advance this cutting-edge approach and its application in geotechnical engineering, Chapter 2 discusses the results of the first-time development of SRM's for anisotropic units in the Northern Cape of South Africa, on which the economics of large iron ore mines in the Northern Cape depend heavily. It introduces the novel notion of a "concept level" SRM for early-stage exploration projects wherein certain informed assumptions may be made, based on existing orebody knowledge and since SRM's are completely reliant on data provided by high quality, bench-scale structural mapping, which is not available on most early stage projects.

It is generally accepted that the definition and in-depth understanding of conceptual failure models and the role of structural geology are critical in slope design (Stead & Wolter, 2015). However, there appears to be a gap related to the *continuous* 3D geometrical analysis of slope geometries' interaction with structurally-controlled and/or anisotropic materials based on conceptual failure models informing design

sector definition, although certain advancements on kinematic analysis were found (Admassu & Shakoor, 2013). This thesis represents novel research to fully exploit the integration of structural geology with the slope design process and at the same time to make use of increasingly-emerging implicit 3D models built in leading-edge software such as LeapfrogGeo and Micromine. Chapter 3 introduces a new methodology that augments the use of 2D design sections by providing a rational and dynamic methodology to improve the definition of design sectors by utilising input from synthetic rock mass modelling. The results comprise practical inputs to the mine planning process from a very early stage. By applying this methodology as part of an iterative process, the slope design process may be improved significantly, particularly if the methodology is applied as early as possible to facilitate optimised designs and early risk mitigation.

Chapter 4 discusses how the new methodology improves the slope design process, according to the six main levels in development and execution of a mining project to facilitate expected project performance. It follows a risk-based approach to continuously improve mine plans – or the understanding and interrogation of existing mine plans - and their associated implementation risks, ultimately leading to increased investor confidence.

The crux of Chapters 5 and 6 is to test the application of the new methodology in various geological settings and project stages. Chapter 5 focusses on a conceptual level project, while Chapter 6 discusses the application of the methodology at three operational mines, namely Sishen Iron Ore Mine, Kolomela Iron Ore Mine and Jwaneng Diamond Mine. This Chapter also demonstrates firstly how early risk mitigation was successful, and secondly the realisation of significant value.

2. SYNTHETIC ROCK MASS MODELLING

2.1. Introduction

A rock mass consists of intact rock material intersected by sets of discontinuities (joints, faults, bedding planes, parting planes, etc.). The rock material has variable properties – strength, deformability, etc., and the discontinuities also have considerable variability – orientation, spacing, continuity, length, termination, shear strength etc. The statistical distributions of these properties have been well established. As a result, a discrete fracture network (DFN) is a way of representing the rock mass fabric as accurately as possible by stochastically generating fractures throughout a 3-D volume. This technique accounts for the spatial variability of different parameters: orientation, persistence and termination are each assigned a statistical distribution and a model is chosen for the generation of fractures in 3D space. Each stochastically generated DFN is a realistic "model" of the rock mass. However, because of the stochastic method of creating the models, each model will be somewhat different, i.e. there will be variability in the rock mass models.

Much of the early interest in the DFN approach was associated with modelling of groundwater flow through natural fracture systems (largely as part of nuclear waste isolation programmes) and for modelling fractured hydrocarbon reservoirs. DFN modelling has been well documented, e.g. (Dershowitz, et al., 1998); (Rogers, et al., 2009). Results discussed by (Elmo, et al., 2014), suggest that DFN models could effectively be used to define equivalent rock mass parameters to improve the predictability achieved by current geo-mechanical simulations and empirical rock mass classification schemes (Poulsen, et al., 2015). The DFN approach therefore represents an ideal numerical tool with which to synthesise realistic fracture network models from digitally and conventionally mapped data (Elmo, et al., 2014)

The crucial issue of the strength anisotropy and deformational behaviour of fractured rock masses, for design and stability assessment in rock engineering structures, is discussed by Bidgoli et al. (2014). The paper focuses on the limitations of laboratory testing that provides information about the strength and deformation behaviours of fractured rock masses. Sainsbury et al. (2008) pointed out that the most challenging aspects of design in moderately- to heavily-jointed rock masses relate to quantifying the impacts of in-situ joint fabric on rock mass behaviour. In addition, joint density and persistence must be considered relative to problem size or volume of interest, as rock mass properties can exhibit significant scale-dependence.

Recently, DFN's have been used for several purposes, including the investigation of slope stability, block caving and underground mining, tunnelling, groundwater hydrology, and geothermal and petroleum engineering. For instance, Perman et al. (2011) applied DFN in stress analysis of complex orebody geometry at the Malmberget Mine. Sainsbury et al. (2008) analysed caving behaviour and utilized a synthetic rock mass model. Elmo et al. (2008) examined the interaction between

block cave mining and a large overlying open pit, by using a finite element/discrete element modelling approach.

Banded Iron Formation (BIF), Shale (SH) and Tectonized Shale (SHT) in the Northern Cape of South Africa exhibit anisotropic behaviour on a rock mass scale (Mas Ivars, et al., 2008). It is not practical to explicitly model or to simulate bedding within large-scale numerical pit models, due to incomplete structural knowledge and the excessive computational requirements. Therefore, a straightforward, rigorous and generally applicable approach is to apply a Synthetic Rock Mass (SRM) methodology to characterise rock mass anisotropy (Mas Ivars, et al., 2007) (Pierce, et al., 2007). This approach was pioneered by Itasca and has been widely reported in the literature (Mas Ivars, et al., 2011). Consequently, equivalent continuum representation is required to ensure reasonable computation times for the realistic simulation of the effects of anisotropic rock mass strength and deformation behaviour on pit slope stability. The ubiquitous joint rock mass (UJRM) modelling technique in *3DEC* (Itasca Consulting Group, 2016) was developed by Itasca to account for rock mass anisotropy and scale effects. This simulates well-defined strength anisotropy due to embedded planes of weakness within a Mohr-Coulomb material. When used to simulate rock mass strength and deformational behaviour under unconfined compression, the UJRM model (Sainsbury et al., 2008) characterizes the progressive degradation of matrix cohesion and ubiquitous joint failure at various stages of loading.

2.2. Methodology

As stated before, the geometrical characteristics of in-situ jointing in BIF and shale found in the Northern Cape of South Africa can induce scale effects and anisotropy in rock mass behaviour. Therefore, an SRM methodology was utilised that allows for systematic and full rock-mass behaviour characterization, capturing the effect of scale and anisotropy in BIF and shale in a quantifiable manner (Mas Ivars et al, 2008). To this end, large scale, simulated triaxial tests were performed in *3DEC* using geometries that include an explicit or actual representation of 1) bedding planes and 2) near orthogonal jointing at a series of realistic spacings and persistences. The bedding plane dip angles (β angles) were varied from 0° to 90° (10° increments) with respect to the axial compression loading direction to provide measures of rock mass tensile strength (σ_t), unconfined compressive strength (σ_c) and compressive strength at several confinement levels (σ_{3i}, σ_{3ii}, etc) (Mas Ivars et al. 2008).

Mas Ivars et al. (2008) discuss this SRM standard suite of tests which were utilised for BIF and shale in the Northern Cape. The methodology will now be explained by the following steps:

i. Generation of a representative DFN based on available in-situ joint data.

   According to Mas Ivars et al. (2008), the in-situ joint fabric of any lithology can be described statistically by analysing the available joint data from

borehole logging and mapping. Afterwards, a representative Discrete, disc-shaped, Fracture Network can be calibrated to apparent fracture frequencies and orientation distributions. The DFN model encompasses statistical distributions for the fracture size and orientation, coupled to a density parameter. In practice, orientation distributions are not interpreted; rather, they simply are bootstrapped to available data, including an orientation bias correction. The fracture size distribution is chosen to be consistent with observations on a qualitative basis (information on this aspect is usually very poor). Then, the density parameter is calibrated in a two-step process:(1) DFNs with a tentative density term are generated in a Monte Carlo process, allowing the ratio between the density term and resulting fracture frequency (on borehole or scanline) to be defined; and (2) the density term is adjusted according to the ratio thus defined, resulting in a DFN realization calibrated both to the fracture frequencies, the orientation distributions and persistence observed.

Therefore, the DFN approach is a way of realistically representing the rock mass fabric, by stochastically generating fractures in a 3-D volume. This technique accounts for the spatial variability of various parameters, such as orientation, persistence and termination, each of which is assigned a statistical distribution in a series of model realizations.

ii. Generation of a large, 5 x 5 x 10-metre, intact rock sample, whose size is chosen based on the DFN characteristics and the scale of the engineering problem under consideration, and insertion of the DFN to obtain the generic large-scale cubic SRM sample.

A synthetic rock mass sample was created in *3DEC*. Bedding planes (or laminae) and orthogonal joint sets, with their actual spacings, were explicitly represented in the volume using DFN logic, while intact rock properties were applied for intervening volumes. The represented structure sets (bedding planes and joints) were selected from available mapping data in the various acQuire geotechnical databases.

iii. Model a series of SRM specimens at different orientations from the generic large-scale SRM sample.

This allows for the estimation of the spatial variability induced by the DFN in order to investigate the anisotropic strength of BIF and shale.

Since joints in the sample are defined by DFN logic and every sample shows a unique joint distribution, three different samples were tested for every bedding plane inclination, ranging from 0° to 90°. These three unique sample conditions satisfy the various structural geometrical assumptions.

The decision to utilise three samples was based on the outcome of running up to 6 iterations on Sishen BIF. The results are illustrated in Figure 1 and show that, for orientations where rock mass strength is more dependent on

bedding strength (more significant in terms of anisotropy due to weaker strength), running more than 3 iterations makes no difference in the average strength results.

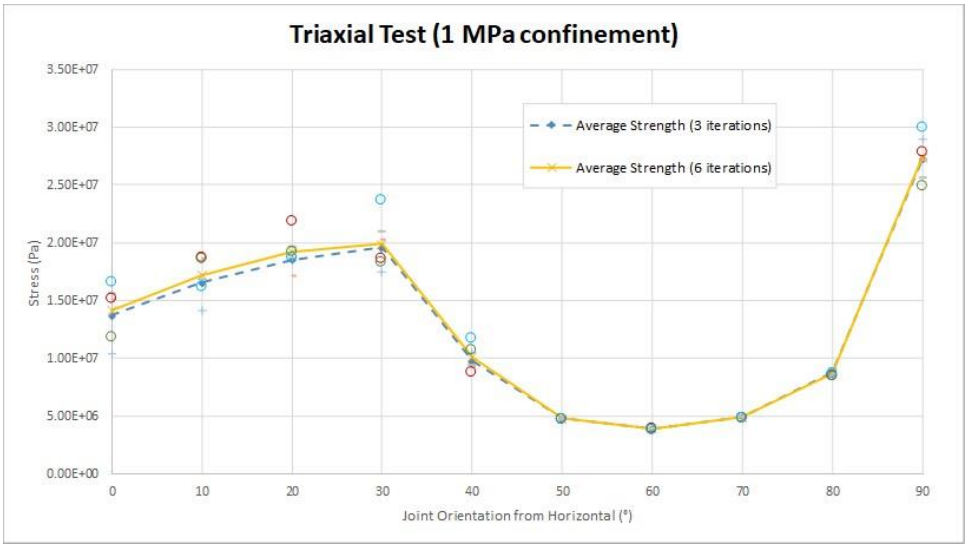


Figure 1 Average strength results for Sishen BIF for 3 and 6 iterations.

iv. Submitting the samples to numerical tests for confined compression.

In order to make test simulation times reasonable, the standard platen velocity-based testing procedure (Itasca, 2016) was used. A triaxial test is simulated where, after applying lateral confinement to the sample, small but continuous velocity is applied to the top and bottom of the sample until failure is reached.

A more rapid-loading methodology has been described by Mas Ivars et al (2008). This new technique, known as the 'full-strain' method, is based on the strain probe concept (Potyondy, 2005) used to apply a perturbation in the form of a full-strain tensor to all the particles in a spherical specimen. This approach assigns linearly varying (face to centre) axial velocities to all specimen particles such that they achieve a very small, defined degree of axial strain over a specified number of model calculation steps (e.g. one step). In this way, particle strains occur more rapidly, because fewer calculation steps are required. Small subsets of particles at the top and bottom regions of the specimen form the 'grips'. After each induced strain stage, the 'grip' particles are not allowed to displace, whereas the 'non-grip' (internal) particles are free to move until equilibrium is re-established, permitting the model to respond naturally. This process is repeated until the residual state is reached. The inherent rough nature of the walls of the periodically generated SRM does not allow the use of boundary walls to apply confinement to the sample. The constant confinement in the triaxial tests is achieved by applying the necessary force to the particles located within a skin-sleeve region surrounding the specimen. The skin sleeve is

elastic and softer than the rock mass sample, similar to the rubber membranes used in the laboratory, allowing for large deformations to occur. Using the 'full-strain' approach, it has been demonstrated that model run-times can be decreased by up to a factor of 10. The curve obtained with the full-strain method can be refined to a higher degree by increasing the number of steps over which the velocity is applied to the particles (e.g. ten steps rather than one). It is important to note that this is only valid when applying very small strain increments (e.g. 5e-5). The magnitude of the maximum applicable strain increment will depend on the strength and stiffness of the SRM specimen being tested. Parallel samples with an aspect ratio of 2:1 are used to minimize the frictional effects caused by boundary 'grip' particles.

v. Calibration of the continuum constitutive equivalent properties to the results from the application of the SRM numerical tests.

   A new technique to account for anisotropy and scale effects (as quantified through SRM testing) within large-scale continuum models has been developed by Sainsbury et al. (2008) (Sainsbury & Sainsbury, 2013). This technique allows large scale models to incorporate the influence of the in-situ joint fabric in rock mass behaviour, as well as other features such as major structures, adjacent excavations and surface topography.

   The behaviour produced by *3DEC*-simulated laboratory tests is ideally reflected in the rock mass response, which is achieved by calibrating UJRM continuum model behaviour to that of *3DEC* discontinuum models. The UJRM modelling approach provides a close match to the anisotropic curve derived from explicit DFN simulations of the joint fabric with *3DEC*.

   Additionally, calibrated UJRM properties are utilised to spatially analyse the interaction of anisotropic units with other geological features and pit geometry. The following Sections will describe the results for anisotropic units in the Northern Cape.

2.3. Synthetic Rock Mass Modelling for Sishen Mine

2.3.1. Background

The bulk of Anglo American Kumba Iron Ore's production comes from Sishen Mine, located in South Africa's Northern Cape Province near the mining town of Kathu (refer to Figure 2).

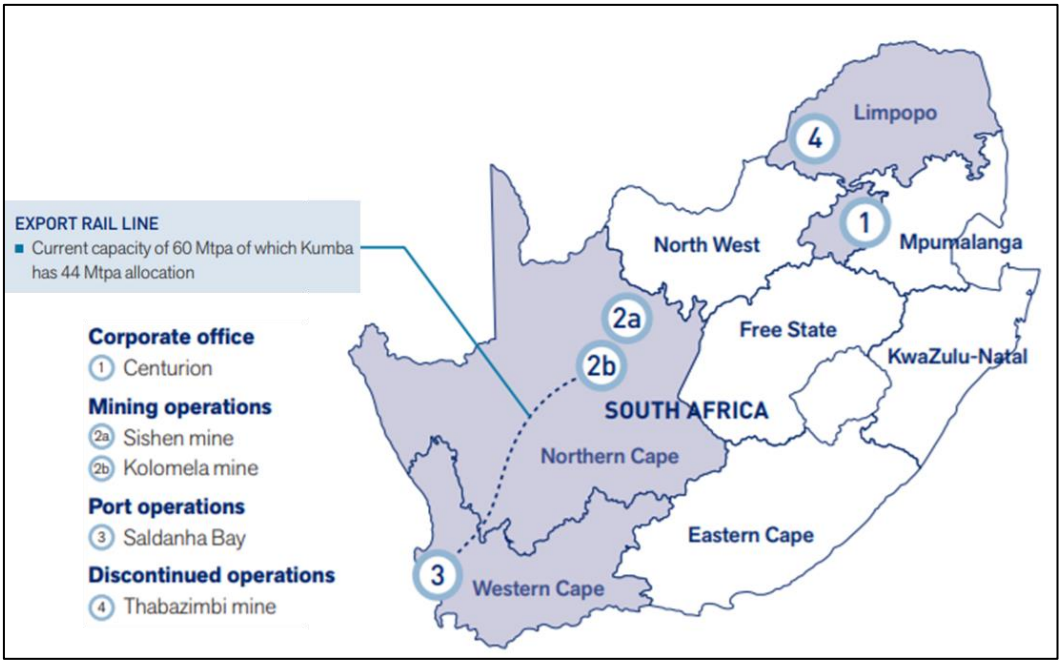


Figure 2 Locality map of Kumba Iron Ore operations *(Bester, et al., 2015)*

Opened in 1947, Sishen Mine is Kumba's flagship operation and one of the largest open pit mines in the world. It operates around-the-clock and its haematite iron ore is exported to clients around the world. All mining is done by open-cast methods, with ore transported to the beneficiation plant where it is crushed, screened and beneficiated. Sishen is the only haematite ore producer in the world to fully beneficiate its product, made possible through dense medium separation (DMS) and jig technology. The Jig Plant at Sishen Mine is the largest of its type in the world. Iron ore products, conforming to different chemical and physical specifications, are produced at this mine.

2.3.2. Geological setting of Sishen Mine

(Basson, et al., 2017) concisely describe the complex ore – geological structure relationships at Sishen Mine. The stratigraphy and tectonic evolution are summarised in the following Sections (Anthonissen, et al., 2016):

Stratigraphy of Sishen Mine

The stratigraphic succession for the Sishen area is illustrated in Figure 3.

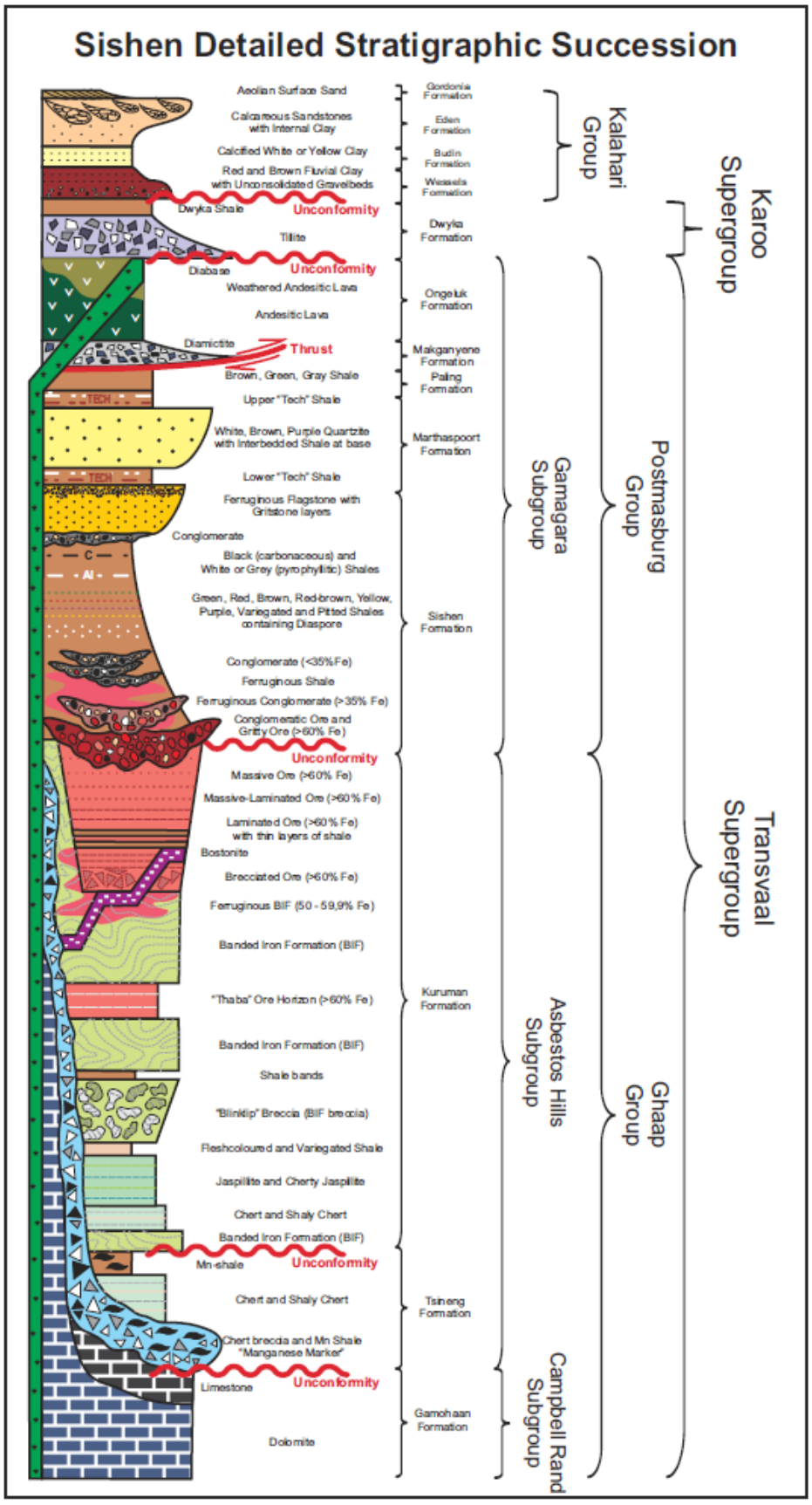


Figure 3 Detailed Sishen stratigraphic succession *(Venter & Deacon, 2017)*

Due to the stratigraphic succession including detailed geological terminology, the following was quoted from Basson, et al, 2017: "The Griqualand West Basin of the Transvaal Supergroup is preferentially preserved in the Northern Cape of South Africa. It consists of a basal carbonate platform sequence, which is conformably overlain by banded iron formation, in turn overlain by chemical and clastic sediments that are succeeded by Makganyene Formation diamictite and Ongeluk basalt and basaltic andesite. The sequence may be summarised as follows:

The base of the Ghaap Group (Transvaal Supergroup) comprises the *ca*. 2.6-2.43 Ga Campbellrand Subgroup, conformably overlying the Schmidtsdrif Subgroup. The proximal facies Campbellrand Subgroup dolomites were deposited on a carbonate platform, while more distal, deeper-water facies were deposited as carbonate turbidites (Beukes, 1986) (Sumner & Beukes, 2006). At Sishen Mine, carbonate and dolomite, which are commonly clastic and ferruginous, with local ankerite-rich chert beds (Beukes, 1983), are only observable in palaeosinkholes exposed during recent deep mining.

A siliceous chert breccia, the Wolhaarkop Breccia or Wolhaarkop Formation, unconformably overlies dolomite, is locally enriched in manganese and/or haematite and has a composition that suggests an exposed, relict, karstic topography or a solution-collapse breccia formed in a periodically-exposed shallow-water setting (Van Wyk, 1980) (Van Schalkwyk & Beukes, 1986) (Schalkwyk, 2005). The Wolhaarkop Formation grades upwards into undisturbed or partly brecciated and folded ironstones of the Manganore Formation (Van Schalkwyk & Beukes, 1986), occasionally interlayered with shale of the *ca.*2.52-2.43 Ga Asbestos Hills Subgroup (Beukes, 1983) (Van Schalkwyk & Beukes, 1986). The thickness of banded ironstone is typically >50 m in the vicinity of Sishen and forms the base of what is locally known as the Manganore Iron Formation of the Ghaap Group; a basal carbonaceous shale, overlain by interbedded ferruginous chert and shale, succeeded by banded ironstone that contains variably laminated and bedded heamatite (Van Schalkwyk & Beukes, 1986). The upper part of the Manganore Iron Formation consists of a series of ore horizons: "Thabazimbi"-type ore; laminated and massive ore; brecciated ore; conglomeratic and gritty ore and detrital ore, interlayered with BIF and shale.

The Gamagara / Mapedi Formation, which forms the base of the Palaeoproterozoic Olifantshoek Supergroup, has an age of *ca.* 2.05-1.83 Ga and overlies banded iron formation along an unconformable contact, representing approximately 380 Ma of uplift and erosion between *ca.* 2.43 Ga and 2.05 Ga. Conglomeratic ore directly overlies this unconformity and forms the base of the Olifantshoek Subgroup. Overlying shale, conglomerate and "grit" of the Gamagara / Mapedi Formation are highly variable in thickness or may be completely absent.

Flagstone occurs above variably-eroded lower Gamagara (i.e. grouped conglomerate, haematitic conglomerate and shale). The Marthaspoort quartzite, the most laterally-consistent unit in the area, is underlain by a thin, "lower tectonised shale", which is essentially a mylonite or proto-mylonite that is in direct contact

with the underlying flagstone. This sequence shows folding along N-S and N-E-trending axes and exhibits general dips of 7º-11º westwards, thickening from 25 m to 45 m over the extent of the mine. The quartzite member is overlain by a second, thin, tectonised shale unit or mylonite / proto-mylonite, known locally as "upper tectonised shale". The collection of these intervals straddles what is locally termed the Blackridge Thrust on Sishen Mine, although this is more accurately termed a tectonised erosional unconformity or tectonised unconformity (TU).

The Postmasburg Group of the Transvaal Supergroup occurs directly above the upper tectonised shale. Basalt or basaltic andesite of the Ongeluk Formation, occurs directly above the upper tectonised shale / mylonite. At Sishen Mine, Makganyene Formation diamictite and the Ongeluk Formation have been thrust eastwards, over the Gamagara Subgroup, primarily along sedimentary or lithological contacts and very low-angle thrusts.

Highly irregular pebble and sandstone units overly the Ongeluk Formation basalt / andesite and are relatively flat-lying and often interbedded. The pebble conglomerate or pebble layer is overlain by a thick clay layer, which in turn is overlain by a thick calcrete layer. Several diabase dykes transect Sishen Mine. These dykes are up to 80 m in width and primarily intrude into dolomite, chert, banded iron formation, ore, Gamagara shale and quartzite. Inversion of regional aeromagnetic data sets shows that dykes intruded into Ongeluk basalts / basaltic andesite along major N-S trending, partially inverted normal faults, that typically preserve downthrow to the west.

Structural Evolution

According to several authors, the area has undergone polyphase deformation (Van Schalkwyk & Beukes, 1986) (Stowe, 1986) (Hilliard, 1999) (Carney & Mienie, 2003) (Friese & Alchin, 2007) (Altermann & Hälbich, 1991) (Beukes & Smit, 1987) (Hälbich, et al., 1993). Obvious effects of deformation, particularly east-directed or east-verging deformation, is the N-S trending Ongeluk-Witwater periclinal syncline, which formed prior to Olifantshoek Supergroup deposition (Visser, 1944) (Beukes & Smit, 1987). The underlying Griqualand West units are very weakly affected by the Blackridge Thrust (effectively the tectonic unconformity at Sishen Mine). Each deformation phase in the area, from the development of the Ventersdorp Rift basin onwards also resulted in a suite of structures that were repeatedly reactivated. The persistence of these structures throughout the deformational history, and their interaction, are pivotal in both ore formation and ore preservation. The deformational history can be summarised as follows: (Humphreys & Van Bever Donker, 1987) (Humphreys, et al., 1988) (Hilliard, 1999)

2.79-2.35 Ga

- ~2.78-2.64 Ga: Ventersdorp rift basin initiation and subsidence: NE-SW trending normal faults, which formed graben boundaries;
- ~2.64-2.60 Ga: Extrusion and deposition of volcano-sedimentary Vryburg Formation and Ventersdorp lavas;
- ~2.60-2.52 Ga: Development of a carbonate platform, widespread marine transgression and conformable deposition of the Schmidtsdrif and Campbellrand Subgroup dolomites;
- ~2.52-2.465 Ga: Drowning of the carbonate platform and development of shelf deposits with shale and a thick sequence of Banded Iron Formation. Shallowing and reworking of BIF (Kuruman and Griquatown) and superposition of siliciclastic / BIF sequences (Koegas Subgroup);
- ~2.46-2.35 Ga: (Maremane Dome Area): Deposition of Mn-chert of the Wolhaarkop Formation, followed by deposition of the Asbestos Hills Sub-group (Manganore iron formation);

2.46-2.25 Ga

- ~ 2.46-2.35 Ga: Incipient break-up and rifting along N-S trending, predominantly W-dipping normal faults during a "second extensional stage" (Friese & Alchin, 2007) possibly "E1" or the "first extensional event" of (Dalstra & Rosière, 2008);
- ~2.35-2.25 Ga: The first phase of predominantly N-S trending folding (F_1), due to the E-verging "Kalahari Orogeny". (Altermann & Hälbich, 1991) cite the >2.24 Ga or pre-Makganyene development of the Uitkomst cataclasite as part of this event, which they attribute to a bedding-parallel thrust. Pre-existing, predominantly rift-related normal faults were inverted and underwent a minor component of strike-slip reactivation, while conjugate NE- and SE-trending, strike-slip faults formed. This orogeny caused uplift and erosion of underlying units, including the Ghaap Group, to form the Postmasburg Unconformity, which is central to the classic supergene Fe-enrichment model. The deposition of the Makganyene Formation, consisting of continental glacial deposits in the Lower Postmasburg Group, has a minimum age of 2.25 Ga and was facilitated by this event.

2.24-1.83 Ga

- ~2.24-1.83 Ga: Reactivation of faults related to both the N-S trending passive margin rift and the Ventersdorp Rift, causing deposition of the fault-controlled or fault-bounded, volcano-sedimentary / volcaniclastic Upper Postmasburg Group. Ongeluk lavas signify the peak of extrusion at *c.* ~2.22 Ga, via feeder dykes that exploited reactivated NNE- to NE-trending faults (Cornell & Schutte, 1996) (Friese & Alchin, 2007). Dykes locally recrystallized ores within the Manganore Iron Formation at Sishen Mine (Dalstra & Rosière, 2008). Deposition of clastic sediments in the form of

conglomerate, “grit”, quartzite and shale of the lower Olifantshoek Supergroup took place between ~2.05 Ga and 1.93 Ga, culminating in the deposition of the Gamagara / Mapedi Formation in a shallow-water rift environment (Beukes, 1983).

- The second extensional event or Eburnean / “E2” event described by (Dalstra & Rosière, 2008) occurred during or shortly after this period. Reactivated normal faults displaced or offset the lower Olifantshoek Supergroup. The formation of south-verging folds and thrusts, according to (Altermann & Hälbich, 1991), are the oldest post-Matsap event at 2.07-1.88 Ga;

1.83-1 Ga

- 1.83-1.73 Ga: The Kheis / Kheis-Koranna Orogeny, like the Kalahari Orogeny, showed eastward tectonic vergence, thrusting and folding (Stowe, 1986) (Beukes & Smit, 1987) (Altermann & Hälbich, 1991) (Hälbich, et al., 1993) (Hilliard, 1999). Rift-related structures of the Postmasburg Group and Olifantshoek Supergroup depositional settings were reactivated, F_2 folding and thin-skinned thrusting occurred along major unconformities and lithological contacts and F_1 folds were tightened co-axially. (Hilliard, 1999) states that Griqualand West Supergroup deformation is characterised by i) shearing along the contact with the Olifantshoek Supergroup; ii) shearing and rotation of bedding in the vicinity of major thrusts and iii) bedding sub-parallel simple shear in the Asbestos Hills and Koegas Subgroups. Seismic profiles show up to 17km of thickening within the Ventersdorp, Griqualand West and Olifantshoek Supergroups over a distance of 150 km, as well as Palaeoproterozoic (~ 1.8 Ga) folding and east-verging thrusting of Griqualand West and Olifantshoek Supergroups on major décollements (Tinker, et al., 2002). Based on the position of the two mylonites or proto-mylonites at Sishen enclosing the laterally-persistent quartzite member at Sishen Mine, the position of the Blackridge Thrust (viz. the tectonised erosional unconformity or TU) occurs at this level.
- ~ 1.35-1.0 Ga: The NNW-directed Lomanian (Namaqua-Natal) Orogeny caused deformation along the southern margin of the Kaapvaal Craton. Effects include: reactivation, segmentation and buckling of N-S trending normal and inverted normal faults; reactivation of 2.35-2.24 Ga Ne- and SE-trending conjugate strike-slip faults, usually with upthrow to the SE and SW, respectively and the development of ENE- to NE-trending F_3 folds. Broad F_2/F_3 fold interference patterns (Hilliard, 1999) or (Mortimer, 1995), who used and F_1/F_2 terminology) may be attributed to this. NW- to NNW-striking, oblique, dextral strike-slip faults, such as the Dagbreek Fault, are reactivated shear zones (Stowe, 1983). Koras Group sediments and volcano-sediments may have been deposited locally in pull-apart basins with margins controlled by this event (Hartnady, et al., 1985) (Thomas, et al., 1994).

The protracted deformation history would have had an effect not only on the exposure of BIF and the development of ore, but also the segmentation, variable preservation and redistribution, by erosion of ore. Furthermore, it is unlikely, in such a convoluted and protracted tectonic history, that there has been no fluid movement".

The Sishen iron ore deposit therefore essentially occurs in a sedimentary rock sequence (Basson, et al., 2017).

2.3.3. Banded Iron Formation (BIF)

In order to investigate the anisotropic strength of BIF, a synthetic rock mass sample of size 5 m × 5 m × 10 m was tested in *3DEC* under confined compression (triaxial test). Both bedding planes (or laminae) and orthogonal joint sets, with their actual spacings, were explicitly represented in the volume using DFN logic, while intact rock properties were applied for intervening volumes.

The same process was utilized for all BIF and shale synthetic rock mass samples and the results will be discussed in the following Sections.

The represented structure sets (bedding planes and joints) were selected from mapping data in the Sishen *acQuire* geotechnical database. Table 1 illustrates orientations used for BIF while Figure 4 shows stereonets generated from mapping data. Due to the highly jointed nature of BIF, joint sets are grouped into J1 (0° - 30°), J2 (30° - 60°) and J3 (60° - 90°).

Table 1 Structure set definition in BIF at Sishen Mine

SET	Dip (°)	Dip Direction (°)
Bedding Planes	18	273
J3 (60° - 90°) (Set 1)	88	254
J3 (60° - 90°) (Set 2)	78	196

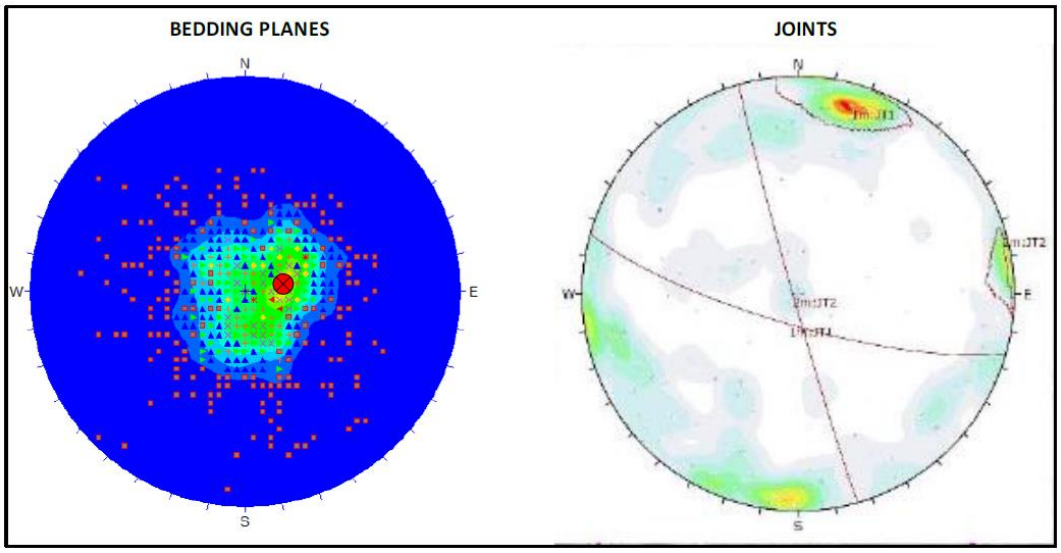


Figure 4 Stereonets for bedding planes (left) and orthogonal joints (right) in BIF at Sishen Mine.

Geometrical considerations for every set (bedding planes and joints) were also derived from pit mapping data in the Sishen *acQuire* geotechnical database. Figure 5 shows a spacing histogram and the median value for every set, while Figure 6 shows a persistency histogram for joints. Bedding planes are assumed to be fully persistent in all *3DEC* samples. The effect of this assumption is very important. If there are no rock bridges in the bedding (fully persistent), the strength of the rock mass when the inclination exceeds the bedding friction angle, will be given by the bedding strength. If there are rock bridges (which are known to exist), the rock mass strength would be a higher strength combination between bedding strength and intact strength. Therefore, the assumption of fully persistent bedding is conservative, but necessary as in some areas the bedding persistence will be large enough to cause stability problems in the pit (as observed in a design sector in the North Mine at Sishen).

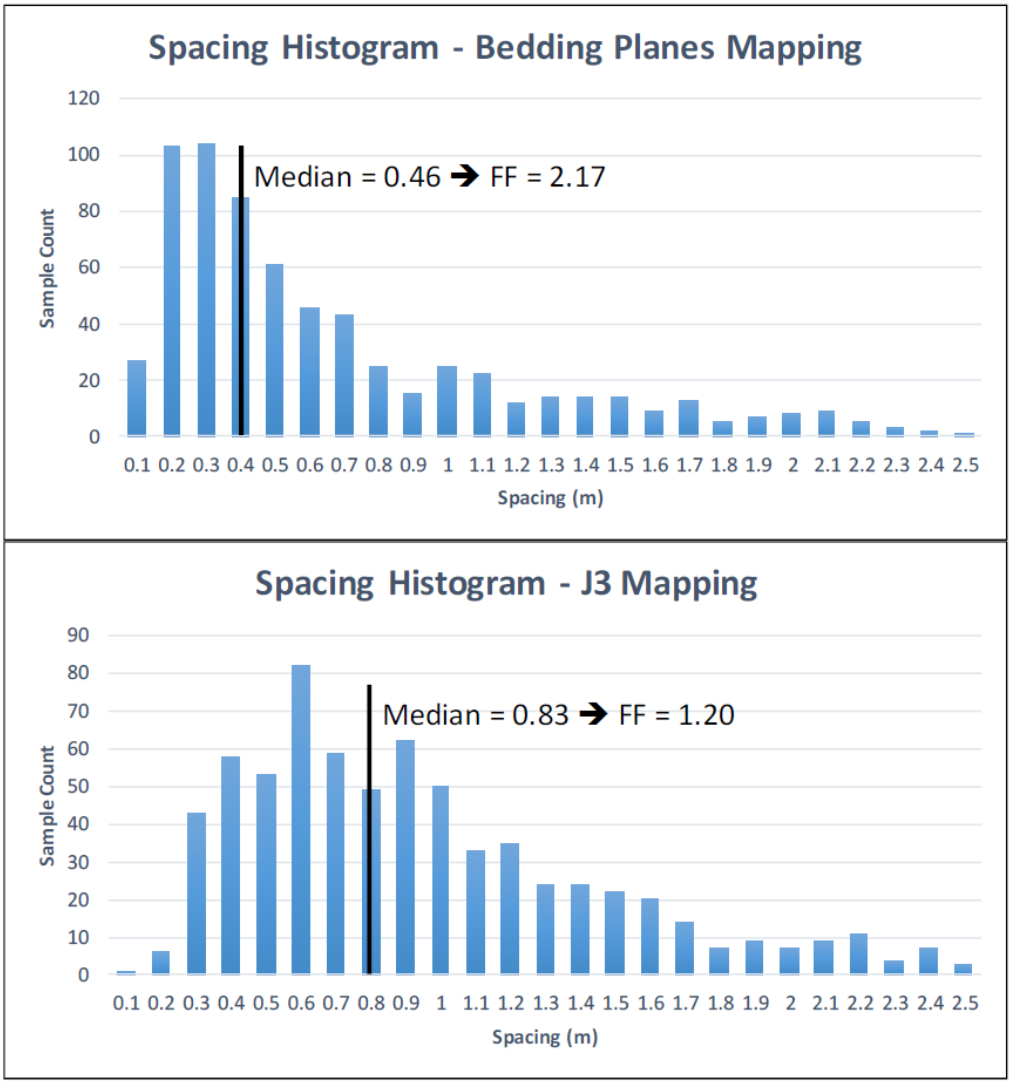


Figure 5 Spacing histogram (with median and equivalent Fracture Frequency FF) for bedding planes and orthogonal joints in BIF.

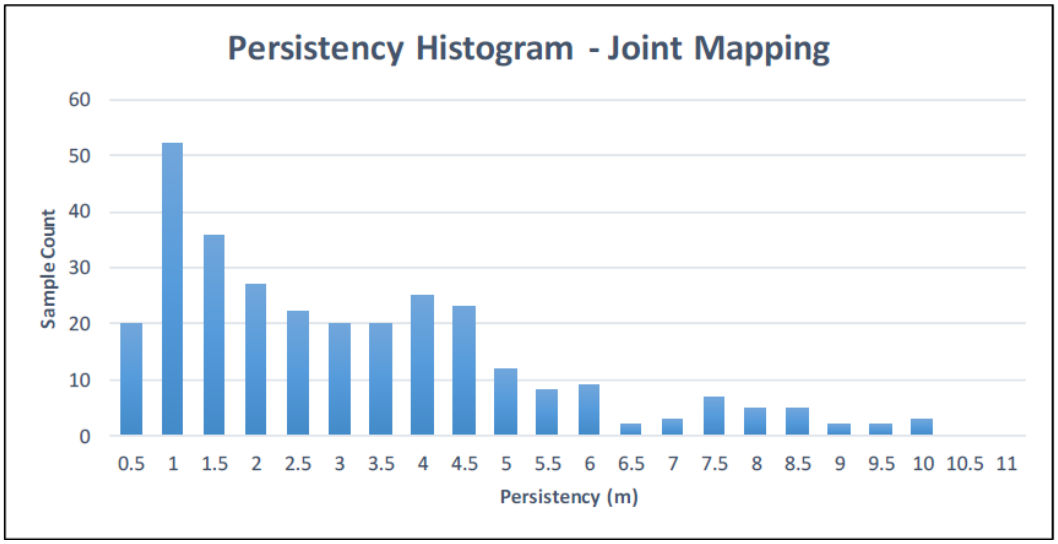


Figure 6 Persistency histogram for orthogonal joints in BIF.

Since joints in the sample are defined by DFN logic and every sample shows a unique joint distribution, three different samples were tested for every bedding plane inclination, ranging from 0° to 90°. These three unique sample conditions satisfy the various structural geometrical assumptions and are therefore explicit representations of the rock mass. Figure 7 shows one of these samples, which exhibits a 10° inclination for bedding planes.

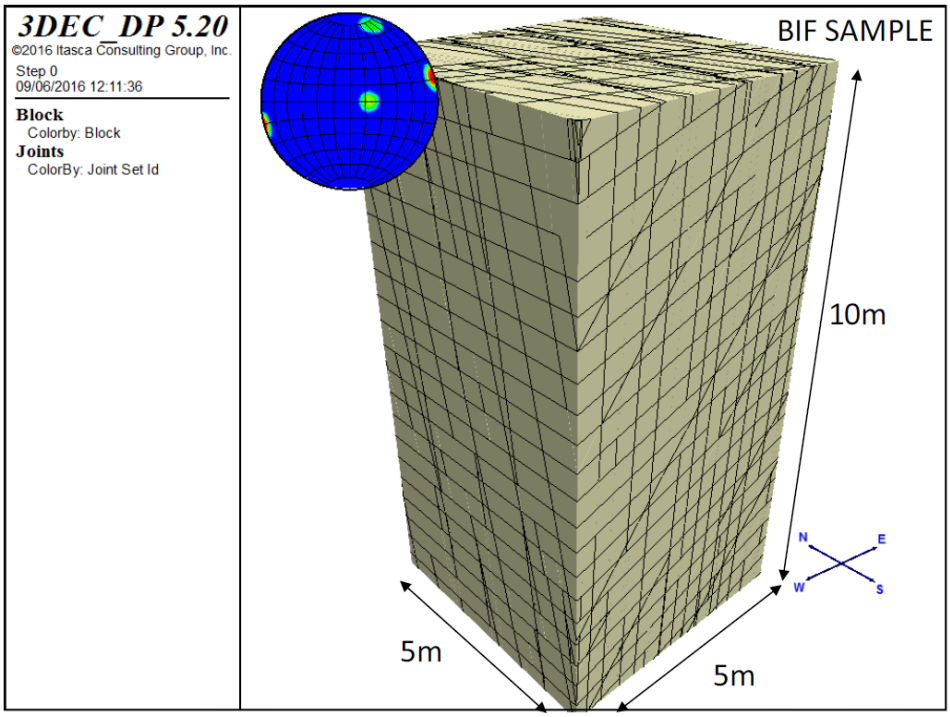


Figure 7 *3DEC* sample for BIF unit test with 10◦ inclination for bedding planes.

Intact rock material properties, assigned to the anisotropic rock mass in *3DEC* models, as well as the Mohr Coulomb (Labuz & Zang, 2012) properties for

structures, were obtained from the Sishen *acQuire* Geotechnical database (Refer to Table 2 and Table 3).

Table 2 Intact rock properties for BIF unit for explicit SRM test

	Density (kg/m^3)	Young's Modulus (GPa)	Poisson's Ratio	UCS (MPa)	GSI	m_i	Dilation (°)
Intact rock	3492	37.9	0.2	104	100	16	10

Table 3 Explicit structure properties for BIF unit SRM test

	Cohesion (kPa)	Friction (°)	Tensile Strength (kPa)	Dilation (°)
Structures (bedding and joints)	2.2	36	0	5

Explicit Joints Results

Numerical tests for confined compression were conducted by applying boundary conditions on these explicit models. Both the top and bottom of the model move with constant velocity in the *z*-direction (vertical), simulating model loading. The loading stress was estimated using a *FISH* function, by dividing the reaction forces on sample ends by the cross-Sectional area of the model. A FISH function is an embedded macro language in Itasca codes (Itasca Consulting Group, 2016). The mean values of the maximum principal stresses were monitored throughout the simulation. Figure 8 shows the strength result for a BIF sample with horizontal bedding planes. The strength is given by the stress at the selected "yield" point. There are two graphs that show the correct behaviour of the test. The right one shows the force (in N) applied at the top and bottom area (superimposed yellow and orange curves) of the sample per step. They are overlaid, which indicates a correct test with equal top and bottom forces applied (Max load ≈ 340 MN). The left graph shows the strength results with strain on the x-axis and stress on the y-axis.

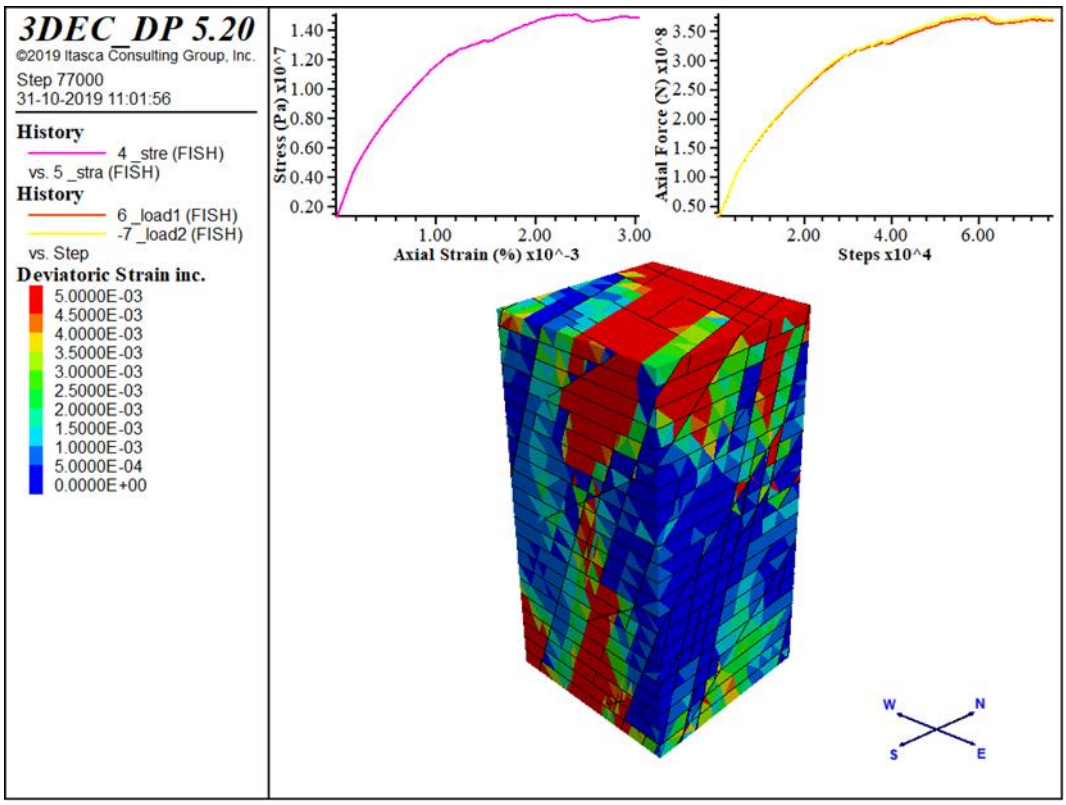


Figure 8 Strength results in Pa (magenta curve) for BIF unit test with explicit horizontal bedding planes. Comparative load results (yellow and orange curves) at both ends of the sample (in Newton).

Figure 9 presents the results of the numerical models for confined compressive tests on an anisotropic rock mass (1 MPa confinement). The maximum principal stress varies from approximately 5 MPa to 30 MPa, depending on the orientation the structure sets with respect the vertical loading orientation. The blue line represents the average value for every inclination, while colored crosses are values for each test.

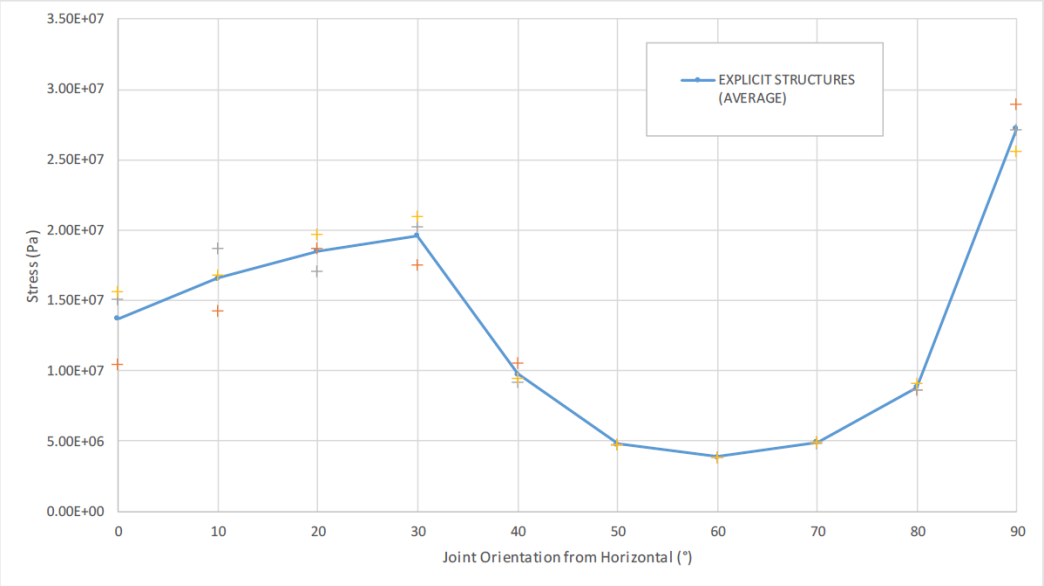


Figure 9 Strength results for the BIF unit for explicit tests at all analysed inclinations.

Implicit Joints Results – Calibration of Anisotropic Strength

In order to represent the anisotropic rock mass in a continuous model or to use the results to perform 3D geometrical analysis, all zones are assigned a ubiquitous joint model in the direction of bedding. These results will therefore be implicit as they represent all possible realisations of the joint network. The zone sizes in these samples are comparable to the smallest zones within the mine-scale numerical model.

Table 4 presents calibrated properties for the specimen rock mass. Ubiquitous joint properties are the same as in the explicit test. Calibrated properties were obtained by adjusting implicit results to the explicit average strength curve.

Table 4 Rock Mass properties, for BIF for implicit SRM test

	Young's Modulus (GPa)	Poisson's Ratio	Cohesion (kPa)	Friction (°)	Tensile Strength (kPa)	Dilation (°)
Rock Mass	18	0.25	1.1	45	0.2	10

Figure 10 illustrates the anisotropic strength response of the calibrated ubiquitous model, in comparison with explicit model results. The implicit result is somewhat conservative, except in the critical area of low strength, where a good correlation between the two curves is both critical and evident.

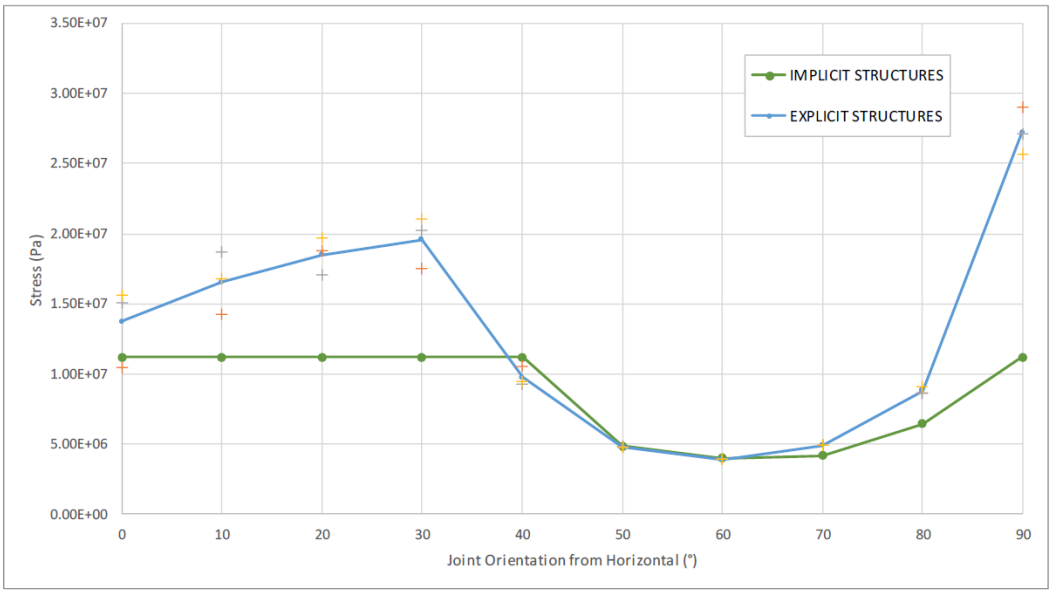


Figure 10 Comparison of results for BIF unit tests on anisotropic rock.

2.3.4. Shale (SH)

In presenting the results of the process for each rock type and mine/project, the same wording has been used deliberately. This is to ensure that the reader is not required to refer back to an earlier Section when viewing later results, i.e. descriptions and results appear together for each case.

Therefore, to investigate the anisotropic strength of the SH unit, *3DEC* was used to create a synthetic rock mass sample of the same size (5 m × 5 m × 10 m) to be tested under confined compression (triaxial test). As for the BIF, both bedding planes (or laminae) and the orthogonal joint sets with actual spacings were explicitly represented in the volume using DFN logic, and intact rock properties for zones between discontinuities. The structure set (bedding planes and joints) used for representation in this model is the same as that used for the BIF unit, and is based on the structural geological understanding at Sishen.

Geometrical considerations for every set (bedding planes and joints) in SH unit were analysed, based on mapping data available in the Sishen *acQuire* geotechnical database. Figure 11 illustrates the spacing histogram and the median value for every set.

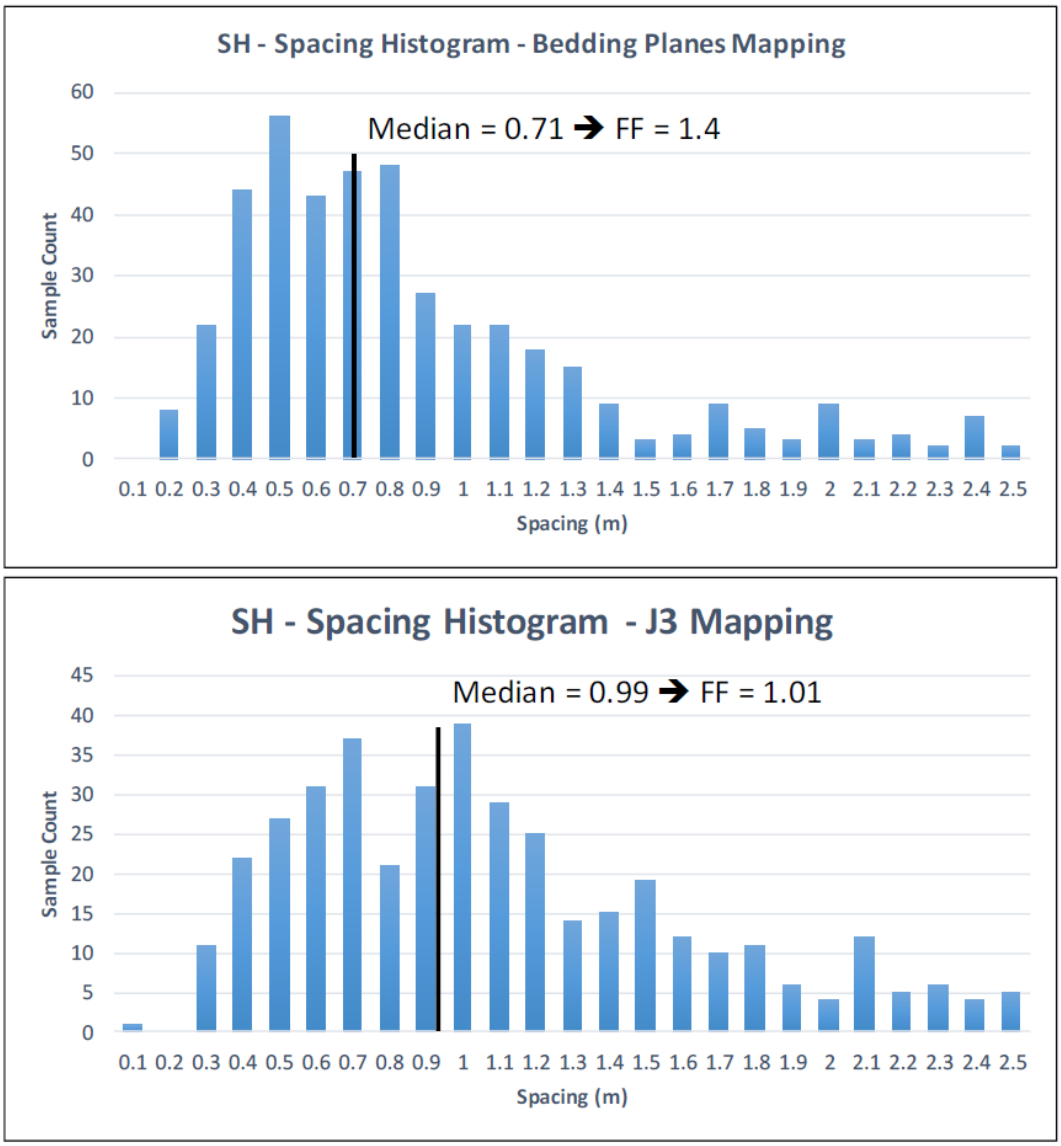


Figure 11 Spacing histogram (with median and equivalent Fracture Frequency FF) for bedding planes and orthogonal joints in the SH unit.

Figure 12 shows a persistency histogram for the joints. The bedding planes are assumed to have infinite persistence in all the samples.

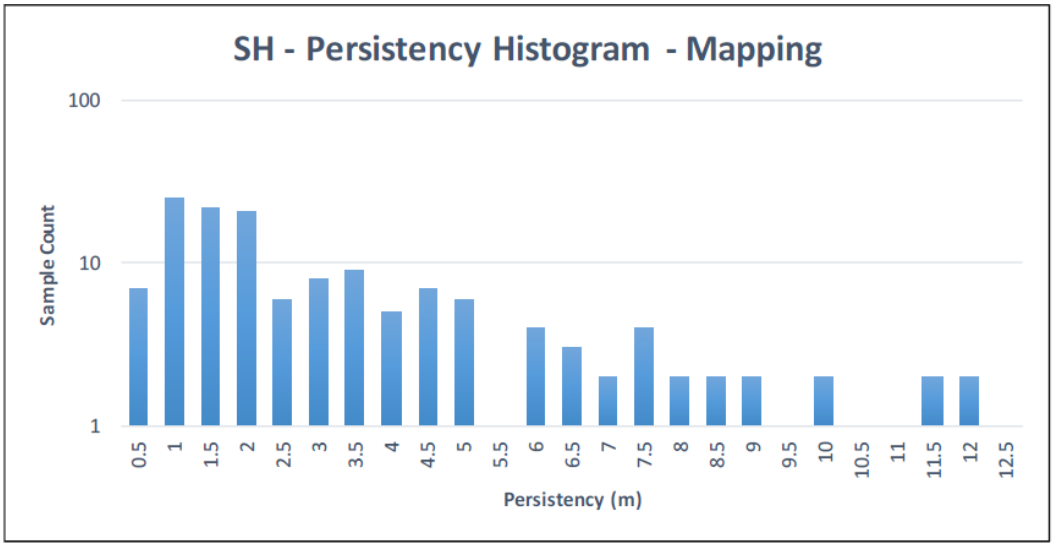


Figure 12 Persistency histogram for orthogonal joints in SH.

Since joints in the sample are defined by DFN logic, up to three different samples (i.e. joint distributions) were tested, at a variety of incremental inclinations. These three different samples satisfy structure geometrical assumptions but are spatially unique. Figure 13 shows one of these samples for the case with a 10º bedding plane inclination.

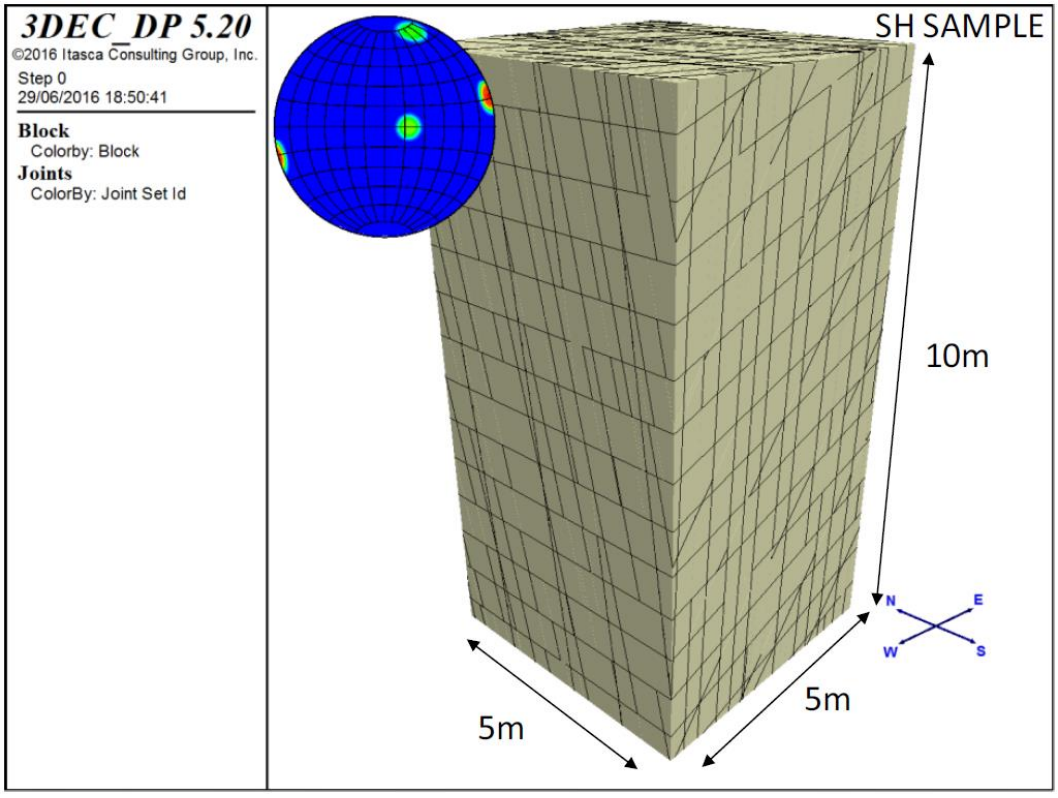


Figure 13 *3DEC* sample for the SH unit test with 10° inclination for bedding.

Material properties, for intact rock, utilized in *3DEC* simulations for the anisotropic rock mass are presented in Table 5. The structures' properties were obtained from the Sishen *acQuire* Geotechnical database and are presented in Table 6.

Table 5 Intact rock properties for SH for explicit SRM test

	Density (kg/m^3)	Young's Modulus (GPa)	Poisson's Ratio	UCS (MPa)	GSI	m_i	Dilation (°)
Intact rock	2708	51.4	0.2	28	100	8	10

Table 6 Explicit structure properties for the SH unit SRM test

	Cohesion (kPa)	Friction (°)	Tensile Strength (kPa)	Dilation (°)
Structures (bedding and joints)	1.9	28	0	5

Explicit Joints Results

Figure 14 presents the results of numerical models for the confined compressive tests on anisotropic rock masses at 1 MPa confinement. The value of the maximum principal stress varies from approximately 3 MPa to 10 MPa and depends on the orientation of loading relative to structure sets. Note that the blue line represents the average value for every inclination, while colored crosses represent the value for each test.

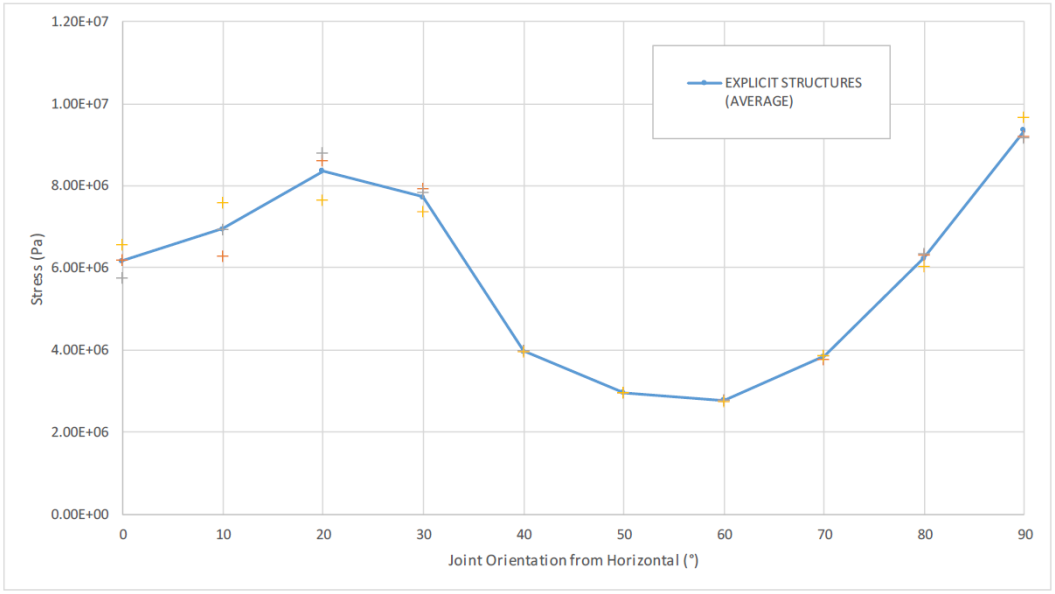


Figure 14 Strength results for SH for explicit tests, at all analysed inclinations.

Implicit Joints Results – Calibration of Anisotropic Strength

Table 7 presents the calibrated properties for the rock mass of the specimen. Ubiquitous joints' properties are the same as in the explicit test. These properties were obtained, in order to adjust the implicit results to the explicit average strength curve presented above.

Table 7 Rock mass properties for SH for the implicit SRM test

	Young's Modulus (GPa)	Poisson's Ratio	Cohesion (kPa)	Friction (°)	Tensile Strength (kPa)	Dilation (°)
Rock Mass	27.5	0.25	0.3	45	0.03	10

Figure 15 illustrates the anisotropic strength response of the calibrated ubiquitous model, in comparison with the explicit model results. The match is conservative (except for 0º inclination). However, a good correlation between the explicit and implicit models is obtained in the critical area of low strength.

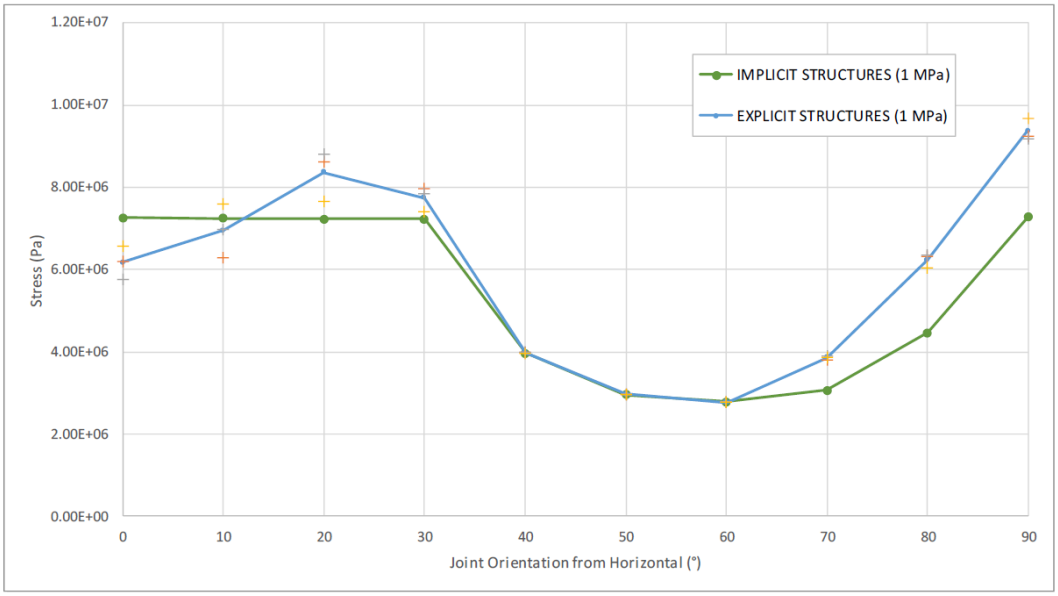


Figure 15 Comparison of numerical anisotropic strength results for implicit and explicit representations of joints in SH.

2.4. Synthetic Rock Mass Modelling for Kolomela Mine

2.4.1. Background

Kolomela Mine, formerly known as the Sishen South Project, is located approximately 9km from Postmasburg and approximately 80km south of Sishen Mine, in the Northern Cape Province of South Africa. Kolomela started production in 2011 producing primarily high-grade direct shipping ore (DSO) from several

separate deposits: Kapstevel North (KSN), Kapstevel South (KSS), Leeuwfontein (LF), Klipbankfontein (KF) and Ploegfontein (PF), of which KSN, LF and KF are presently mined.

The deposits consist of competent, massive ore, laminated ore and conglomeratic ore and the bulk of mineralisation comprises granular and microplaty haematite with specularite veining.

2.4.2. Geological setting of Kolomela Mine

The geological setting of Kolomela Mine is similar to that of Sishen Mine. (Basson, et al., 2018) summarise the stratigraphy and tectonic evolution of Kolomela Mine and this is quoted in Appendix 5.

2.4.3. Banded Iron Formation (BIF)

Following the same process as described above, the anisotropic strength of the BIF unit was investigated at Kolomela Mine. *3DEC* was used to create a synthetic rock mass sample, of size 5 m × 5 m × 10 m, to be tested under confined compression (triaxial test). Both bedding planes and orthogonal joint sets, with actual spacings, were explicitly represented in the volume using DFN logic, while intact rock properties were applied for intervening volumes.

The structure sets (bedding planes and joints) represented in this model were selected from mapping data informing the Kolomela structural geological model. Table 8 details the orientations used for BIF, and Figure 16 shows the stereonets generated from the mapping data.

Table 8 Structure sets definition in BIF for Kolomela Mine

SET	Dip (°)	Dip Direction (°)
Bedding Planes	29	243
J3 (60° - 90°) (Set 1)	89	089
J3 (60° - 90°) (Set 2)	89	164

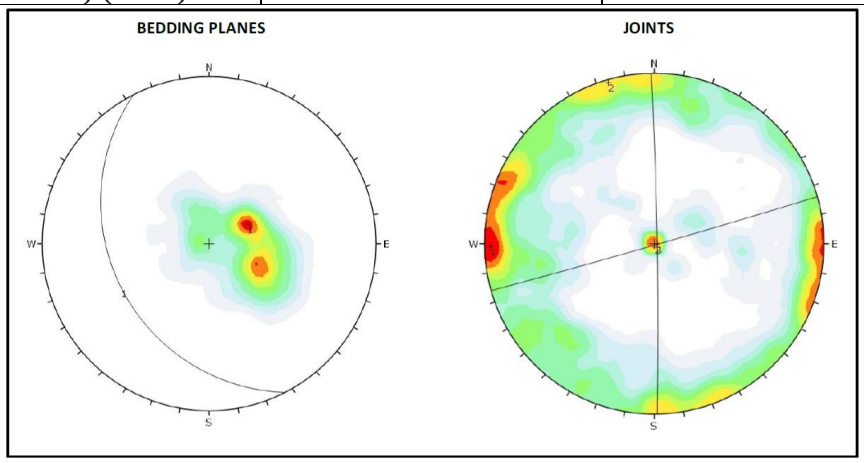


Figure 16 Stereonets for bedding planes and orthogonal joints in BIF at Kolomela Mine.

The Sishen BIF geometrical considerations (spacing and persistence) for bedding planes and joints were applied in the Kolomela analysis. Joints in samples were again defined by DFN logic and every sample was therefore unique, based on joint distribution. Three different samples were tested for every bedding plane inclination ranging from 0° to 90°. These three samples satisfy the structure geometrical assumptions but are spatially unique. Figure 17 shows one of these samples, for the case of a 29º inclination for bedding planes.

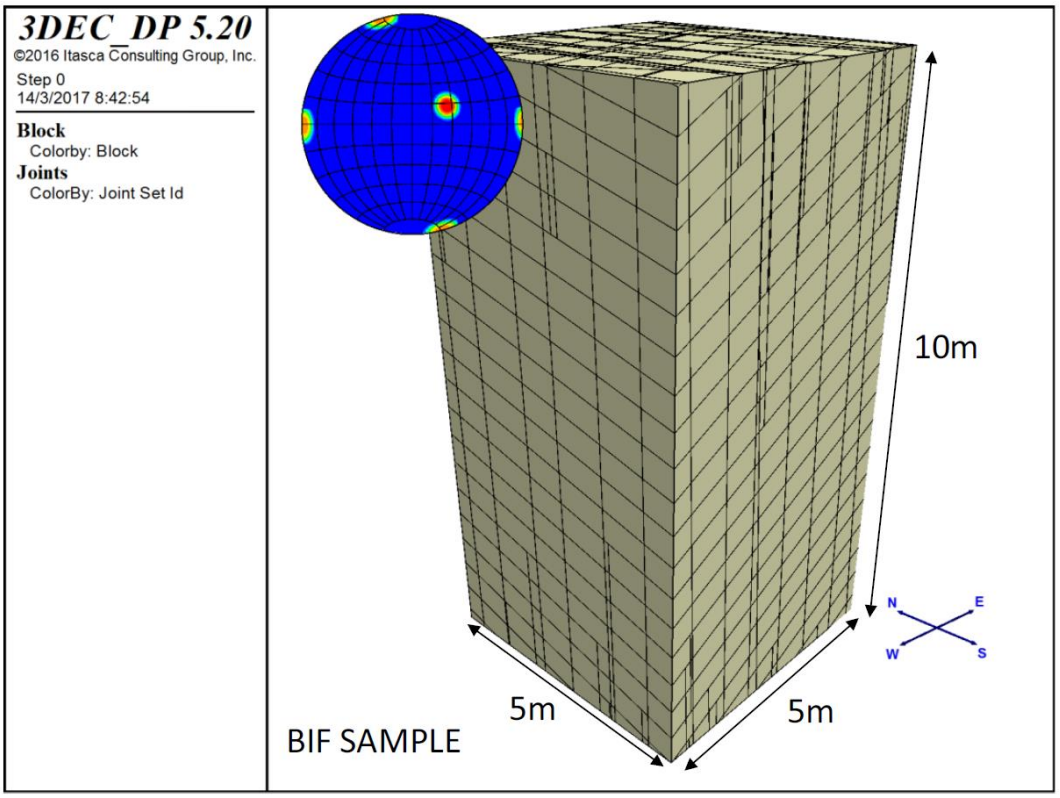


Figure 17 *3DEC* sample for Kolomela BIF test with 29° inclination for bedding planes.

Intact rock material properties, assigned to the anisotropic rock mass in *3DEC* models, as well as the Mohr Coulomb properties for joints, were obtained from the *acQuire* Geotechnical database (Refer to Tables 2 and 3).

Explicit Joint Results

Following the same methodology as described in the previous Section, numerical simulations of confined compressive tests were conducted in *3DEC*. Both the top and bottom of the model were moved with constant velocity in the *z*-direction (vertical) to apply loading to the model. While the model was being loaded, the loading stress was estimated using a *FISH* function that divides the reaction forces on the sample ends by the cross-sectional area of the model. The mean value of the maximum principal stresses in the *3DEC* model was monitored throughout the simulation. As an example, Figure 18 shows the strength result for a BIF sample with inclined bedding planes at 20°.

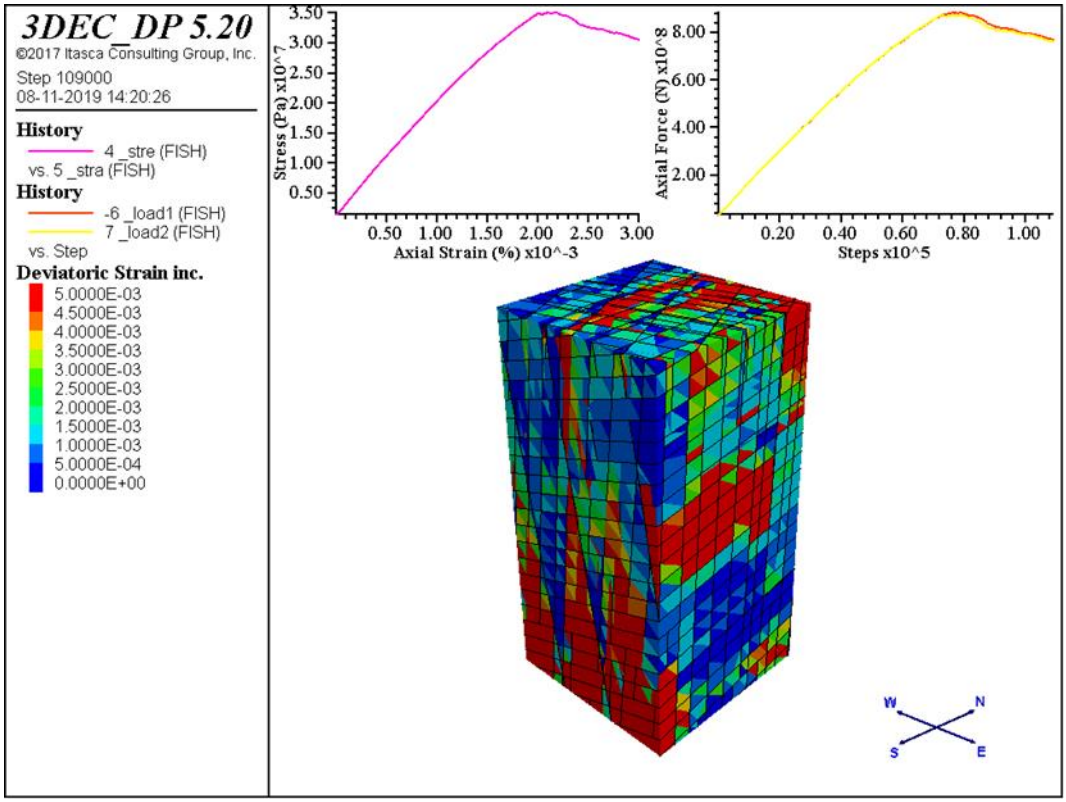


Figure 18 Strength results in Pa (magenta curve) for a BIF test at Kolomela Mine with explicit inclined bedding planes (20°). Comparative load results (superimposed yellow and orange curve) in both ends of the sample (in Newtons).

Figure 19 presents the results of the numerical models for the confined compressive tests on the anisotropic rock mass (1 MPa confinement). The value of the maximum principal stress varies from approximately 5 MPa to 45 MPa, depending on the orientation of joints relative to the loading direction. The blue line represents the average value for every inclination, while colored crosses represent values for each test.

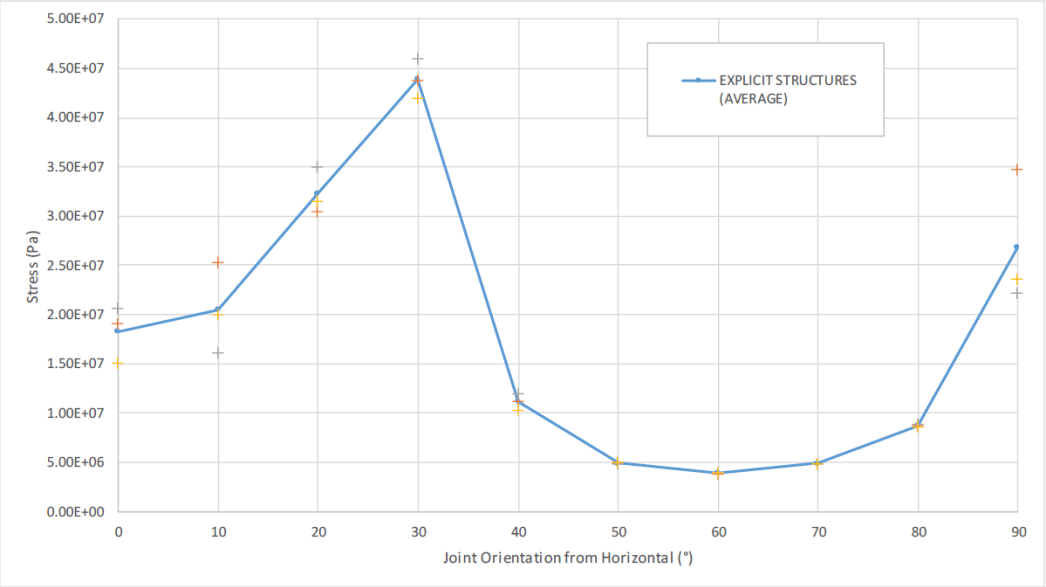


Figure 19 Strength results for BIF at Kolomela Mine for explicit tests at all analysed inclinations.

Strengths for 20° and 30° are higher than expected. This may be explained by the inclination of joints (almost vertical in both J3 sets), that produce a failure exclusively in the rock mass, since joints are constrained by boundary conditions at the top and bottom of the sample.

Implicit Joints Results – Calibration of Anisotropic Strength

In order to represent the anisotropic rock mass in a continuous model or to perform 3D geometrical analysis, BIF zones are assigned a ubiquitous joint model in the direction of bedding.

Table 9 presents the calibrated properties for the specimen rock mass. The ubiquitous joints' properties are the same as in the explicit test and calibrated properties were obtained by adjusting the implicit results to the explicit average strength curve presented above.

Table 9 Rock mass properties for BIF at Kolomela Mine for implicit SRM test

	Young's Modulus (GPa)	Poisson's Ratio	Cohesion (kPa)	Friction (°)	Tensile Strength (kPa)	Dilation (°)
Intact rock	18	0.25	1.1	45	0.2	10

Figure 20 illustrates the anisotropic strength response of the calibrated ubiquitous model, in comparison with the explicit model's results. The implicit behaviour has been adhered to, albeit with an upwards adjustment for pseudo-horizontal bedding planes (0° to 10°) and a conservative adjustment for bedding planes inclination

showing more strength (20° to 30°). For the remainder of the bedding plane inclinations, the implicit curve fits the explicit curve well.

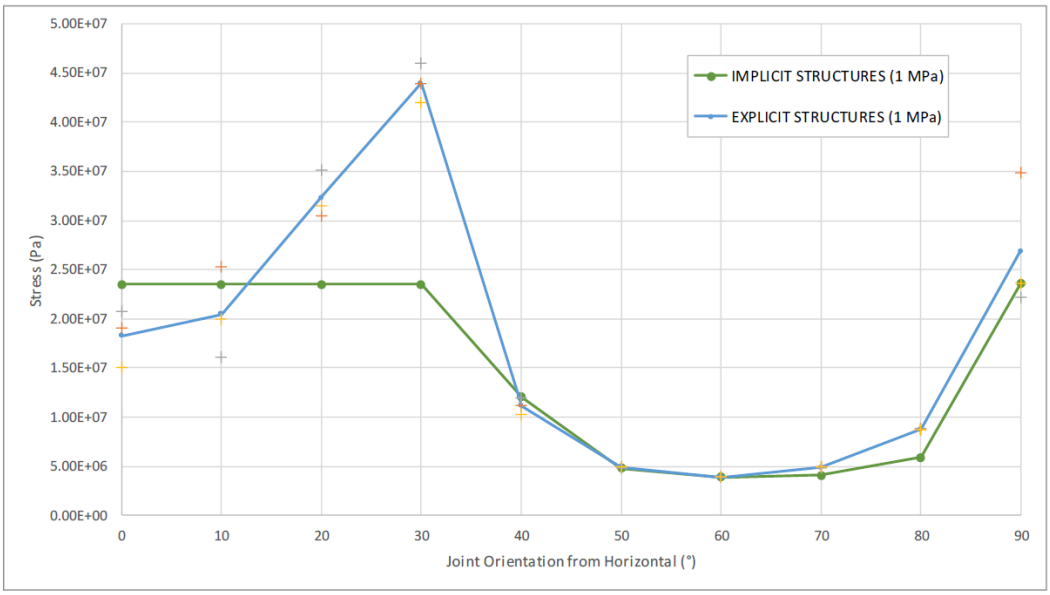


Figure 20 Comparison of results for BIF tests at Kolomela Mine on anisotropic rock mass.

2.4.4. Shale (SH)

To investigate the anisotropic strength of Shale units at Kolomela mine (Leeuwfontein, Klipbankfontein and Kapstevel North pits), *3DEC* was used to create a synthetic rock mass sample of size 5 m × 5 m × 10 m, to be tested under confined compression (triaxial test). Both bedding planes and orthogonal joint sets with actual spacings were explicitly represented in the volume using DFN logic and intact rock properties were used for intact zones.

The structure sets (bedding planes and joints) used for representation in these models were selected from data at all three of the abovementioned pits. Table 10 shows the orientations used and Figures 21-23 show the stereonets generated from structural data at every pit.

Table 10 Structure sets definition in Shale for different pits at Kolomela Mine

Pit	Set	Dip (º)	Dip Direction (º)
Leeuwfontein	Bedding planes	13	304
	J3 (Set 1)	90	285
	J3 (Set 2)	87	70
Klipbankfontein	Bedding planes	29	305
	J3 (Set 1)	85	354
	J3 (Set 2)	78	28
Kapstevel North	Bedding planes	25	145
	J3 (Set 1)	51	311
	J3 (Set 2)	53	20

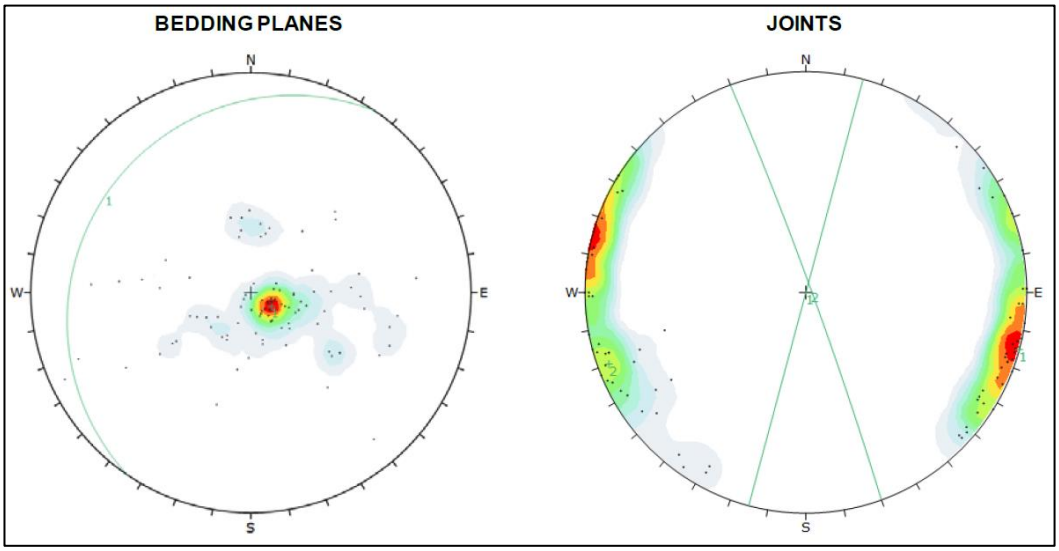


Figure 21 Stereonets for bedding planes and orthogonal joints in Leeuwfontein pit Shale.

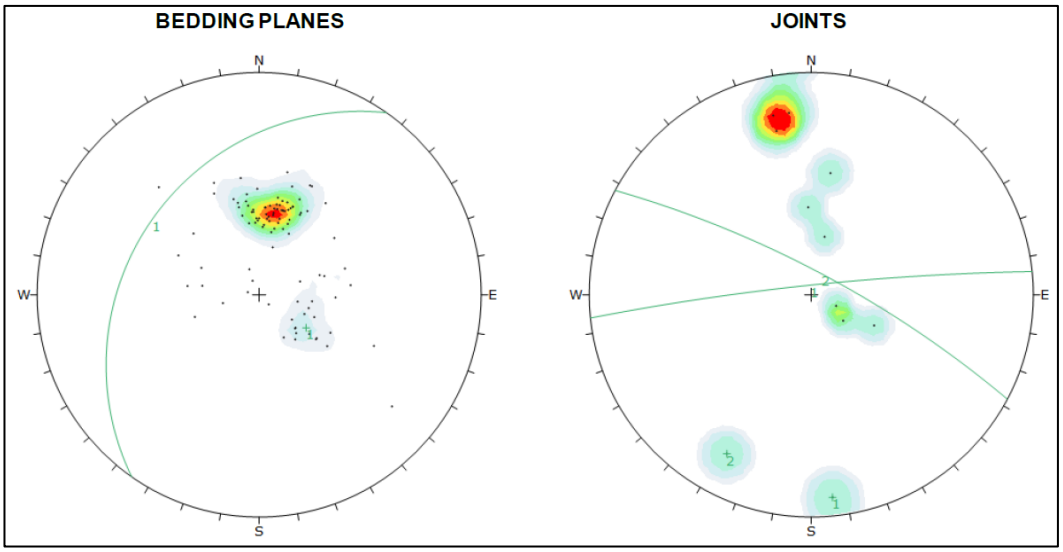


Figure 22 Stereonets for bedding planes and orthogonal joints in Klipbankfontein pit Shale.

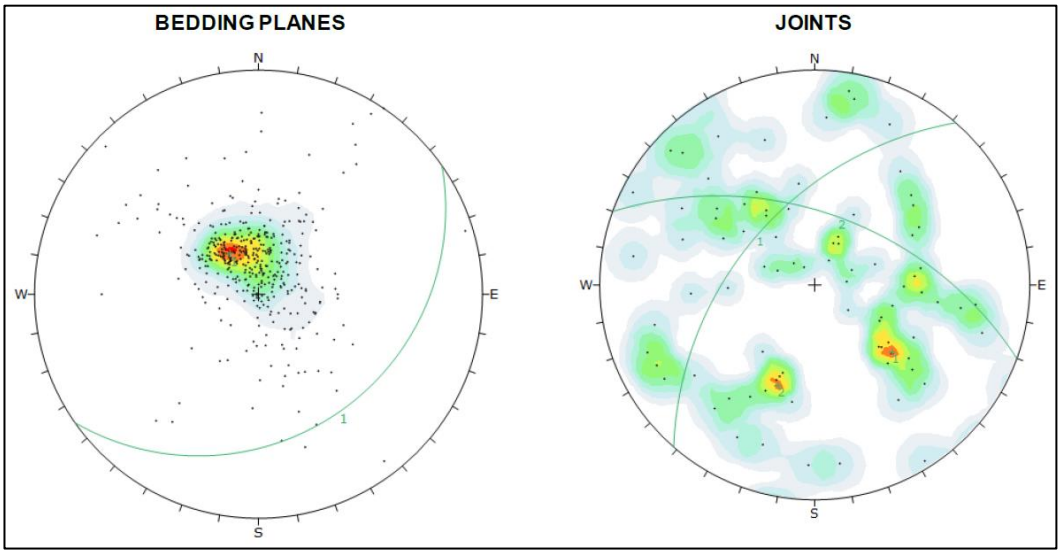


Figure 23 Stereonets for bedding planes and orthogonal joints in Kapstevel North Pit Shale.

Due to limited borehole data in shale at Kolomela, the whole dataset was combined to define bedding and joints spacings across all three pits. In addition, due to limited mapping data available for shale, and reasonably assuming that both operations are situated in the same stratigraphy, Sishen shale data were used to define persistence. Figure 24 illustrates the spacing histogram and median value for every set.

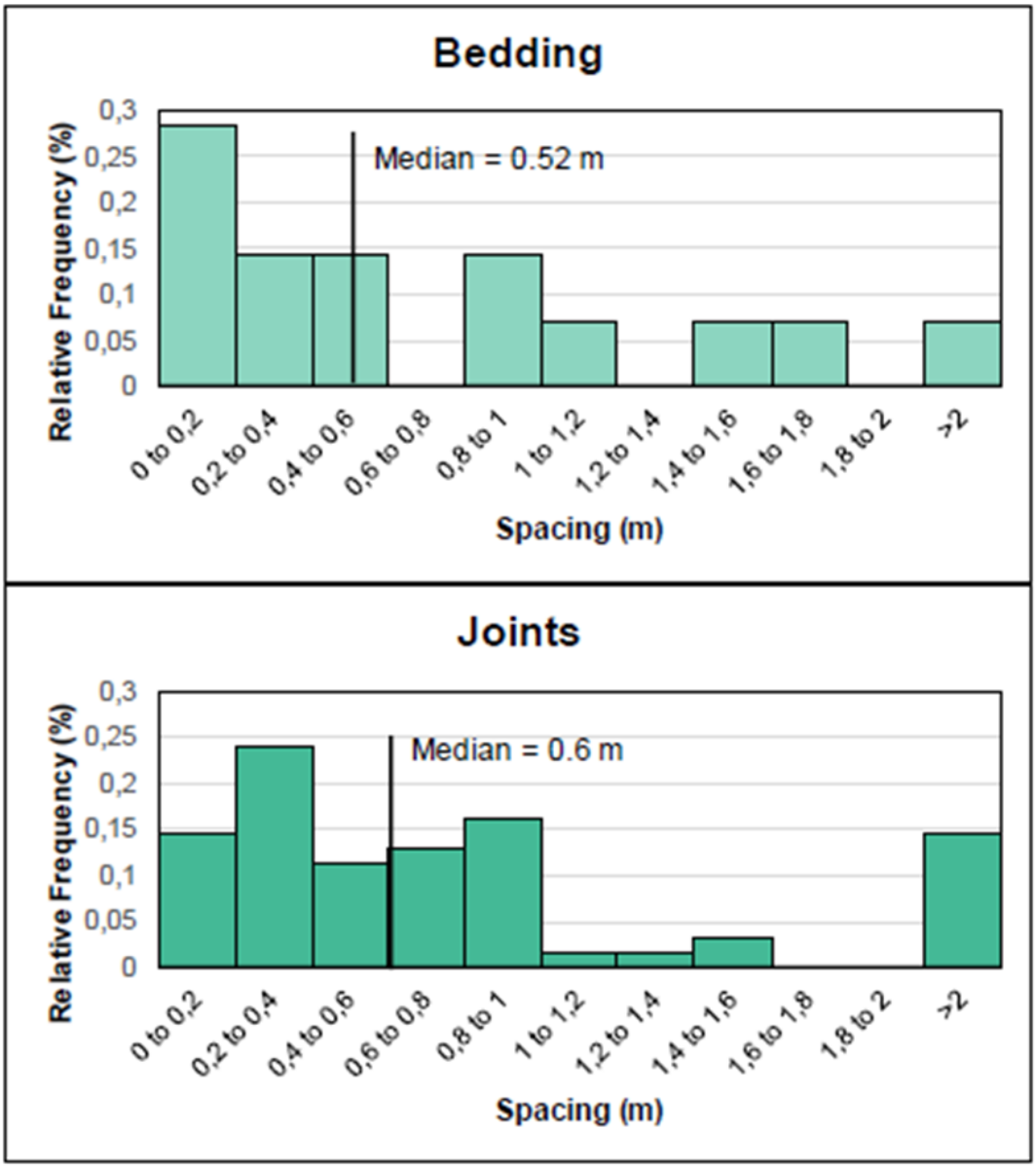


Figure 24 Spacing histogram for bedding planes and orthogonal joints in shale at Kolomela mine (Leeuwfontein, Klipbankfontein and Kapstevel North pits).

The joints in the sample are defined by DFN logic and every sample is unique based on the joint distribution; therefore, three different samples were tested for every bedding plane inclination ranging from 0° to 90°. These three, geometrically-unique samples satisfy the structure geometrical assumptions. Figure 25 shows the sample for Leeuwfontein shale for the original orientations (13º inclination for bedding planes).

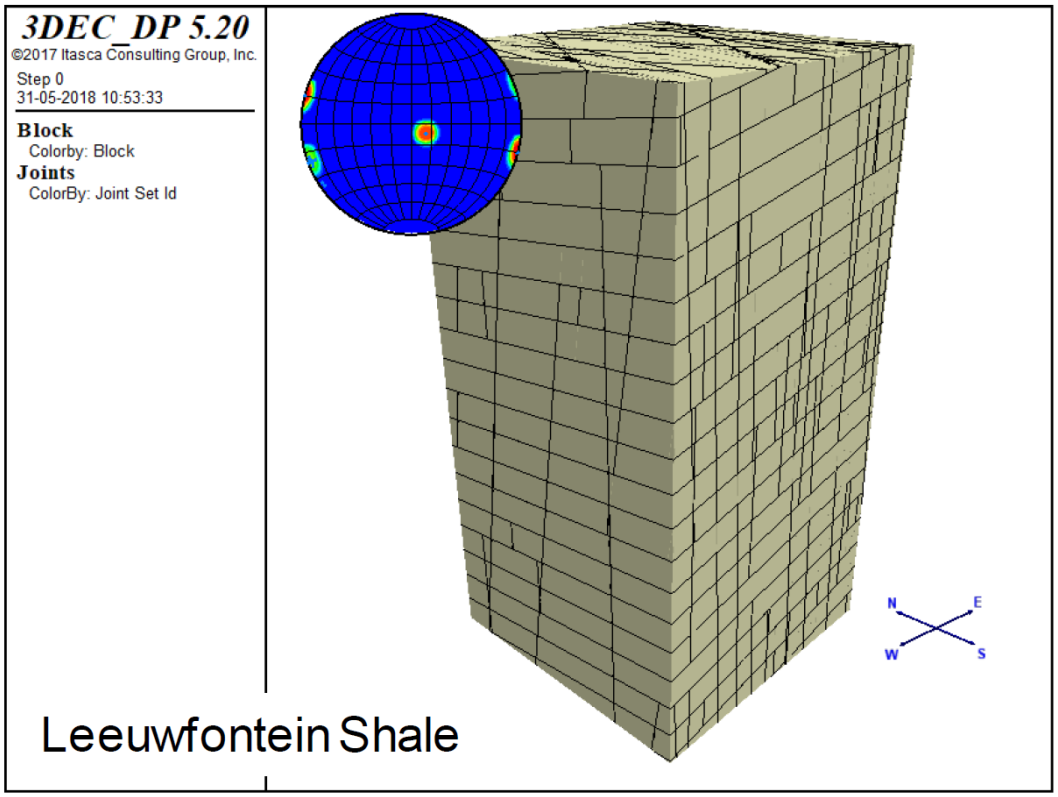


Figure 25 3DEC sample for Shale in the Leeuwfontein pit with 13º inclination for bedding planes (original orientation).

The intact rock material properties assigned to the anisotropic rock mass in the *3DEC* models are from the *acQuire* geotechnical database and are presented in Table 11. The Mohr-Coulomb (Labuz & Zang, 2012) properties for structures are the same as for Sishen and are represented in Table 6.

Table 11 Intact rock properties for Shale for the explicit SRM test

	Density (kg/m^3)	Young's Modulus (GPa)	Poisson's Ratio	UCS (MPa)	GSI	m_i	Dilation (°)
Intact Rock	2760	51.4	0.2	7.6	100	8	10

Explicit Joints Results

Figure 26 presents the numerical results for confined compressive tests on the anisotropic rock mass (1 MPa confinement) at Leeuwfontein pit. The value of the maximum principal stress varies from approximately 3 MPa to 8 MPa, depending on the orientation of the loading direction relative to the structure sets. Note that the blue line represents the average value for every inclination, while coloured crosses represent the values for every single test.

From the results, strength at an angle of 80° and 90° to the horizontal is lower than expected. At these orientations, the strength is usually comparable to that of horizontal bedding, but in Leeuwfontein's case, failure is predominantly structural (vs. rock mass) similar to 50° - 60°.

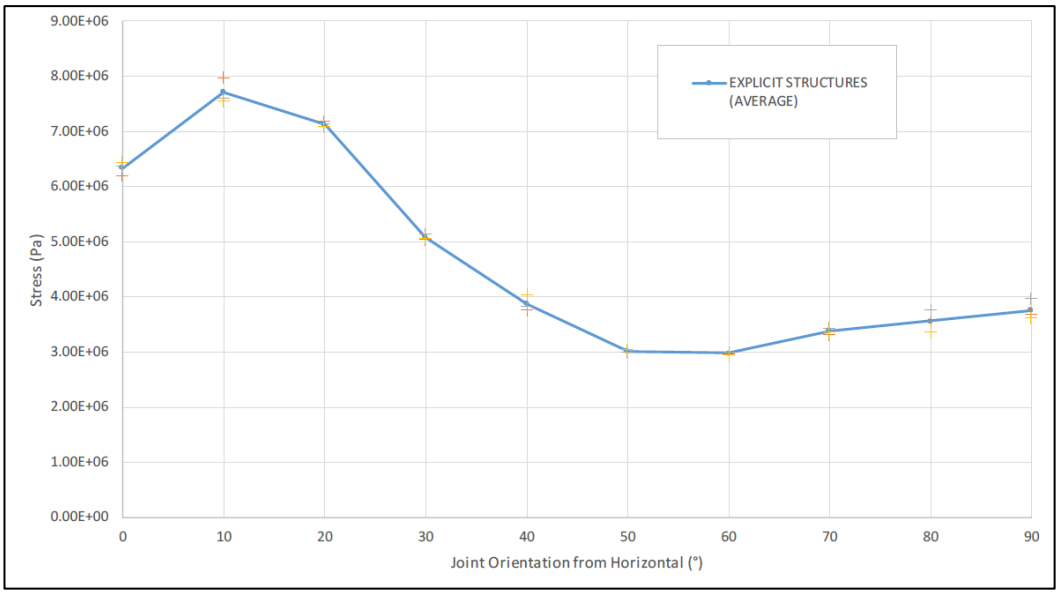


Figure 26 Strength results for Shale at Leeuwfontein pit for explicit tests at all analysed inclinations.

Figure 27 presents the numerical results for confined compressive tests on the anisotropic rock mass (1 MPa confinement) at Klipbankfontein pit. The value of the maximum principal stress varies from approximately 3 MPa to 5.5 MPa, depending on the orientation of the loading direction relative to the structure sets (note that the blue line represents the average value for every inclination, while coloured crosses represent the value for every single test). Klipbankfontein results indicate low strength, except bedding plane inclinations < 40°, where the strength is slightly higher.

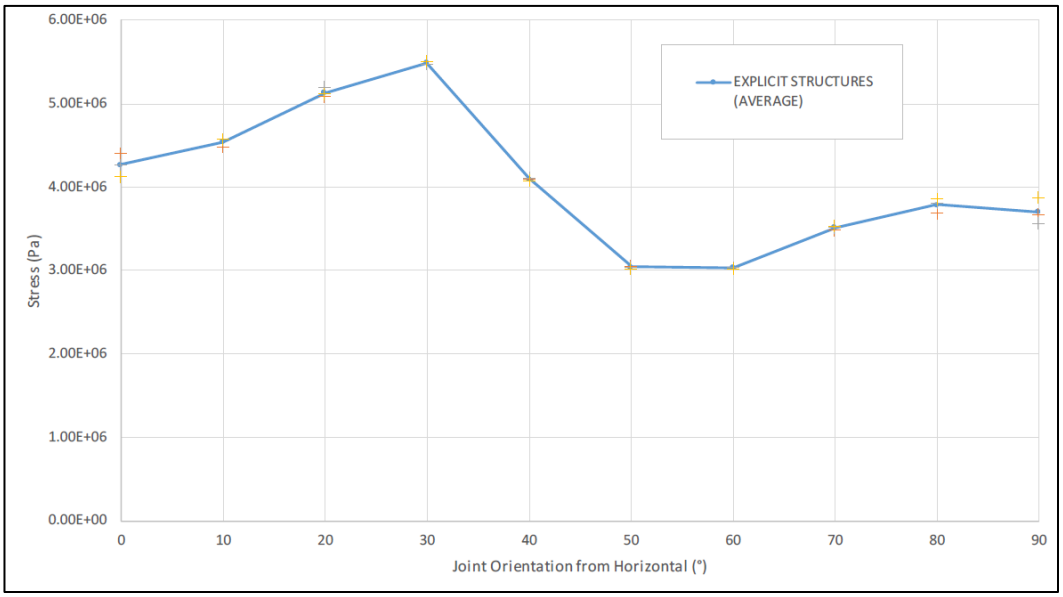


Figure 27 Strength results for Shale at Klipbankfontein pit for explicit discontinuity representation at various inclinations.

Figure 28 presents the numerical results for confined compressive tests on the anisotropic rock mass (1 MPa confinement) at Kapstevel North pit. The value of the maximum principal stress varies from approximately 3 MPa to 7.5 MPa, depending on the orientation of the loading direction relative to the structure sets. (Note that the blue line represents the average value for every inclination, while coloured crosses represent the value for every single test.)

In the Kapstevel North pit, the strength at 20° seems higher than expected. A plausible reason could be that the inclination of the joints results in failure exclusively in the rock mass since the joints are blocked by boundary conditions at the bottom and the top of the sample.

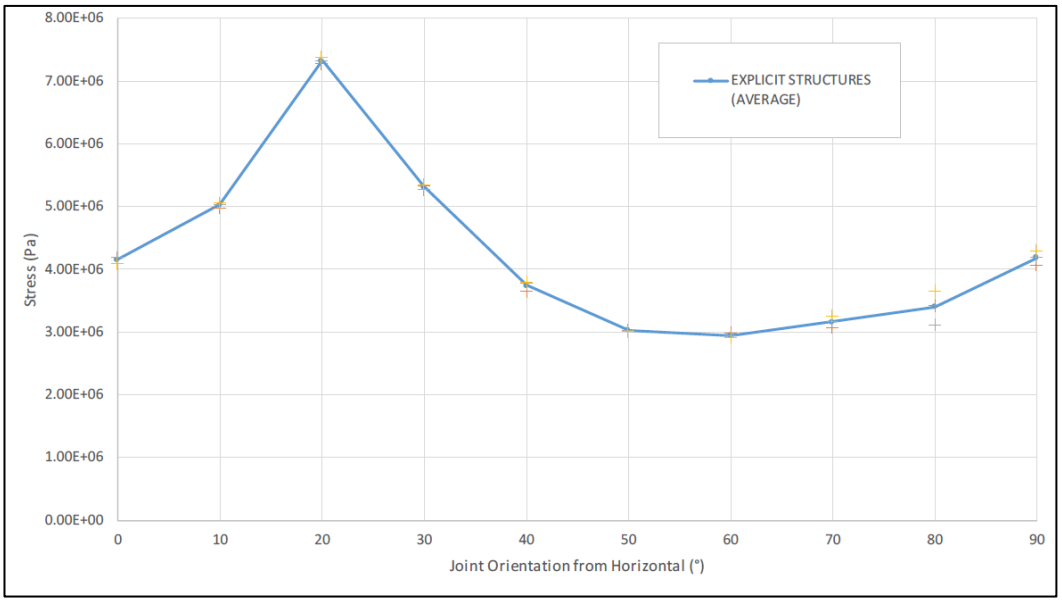


Figure 28 Strength results for Shale at Kapstevel North pit for explicit tests at all the analysed inclinations.

Implicit Joints Results

Table 12 presents the calibrated properties for the rock mass model for each pit. Calibrated properties were obtained by adjusting the implicit results to the explicit average strength curve presented before for each pit. The ubiquitous joints' properties are the same as in the explicit test.

Table 12 Rock mass properties for Shale material at the different Kolomela pits for implicit SRM tests.

Pit	Young's Modulus (GPa)	Poisson's Ratio	Cohesion (MPa)	Friction (°)	Tensile Strength (MPa)	Dilation (°)
Leeuwfontein	51.4	0.25	0.61	35	0.032	10
Klipbankfontein			0.61		0.032	
Kapstevel North			0.73		0.038	

Figures 29-31 illustrate the anisotropic strength response of the calibrated ubiquitous model, in comparison with explicit model results for each analysed pit. In each case, conservative adjustment was made for bedding plane inclinations showing higher strength (joint orientations from horizontal of 0° to 30°). For the rest of the bedding plane inclinations, the implicit curve fits well with the explicit curve.

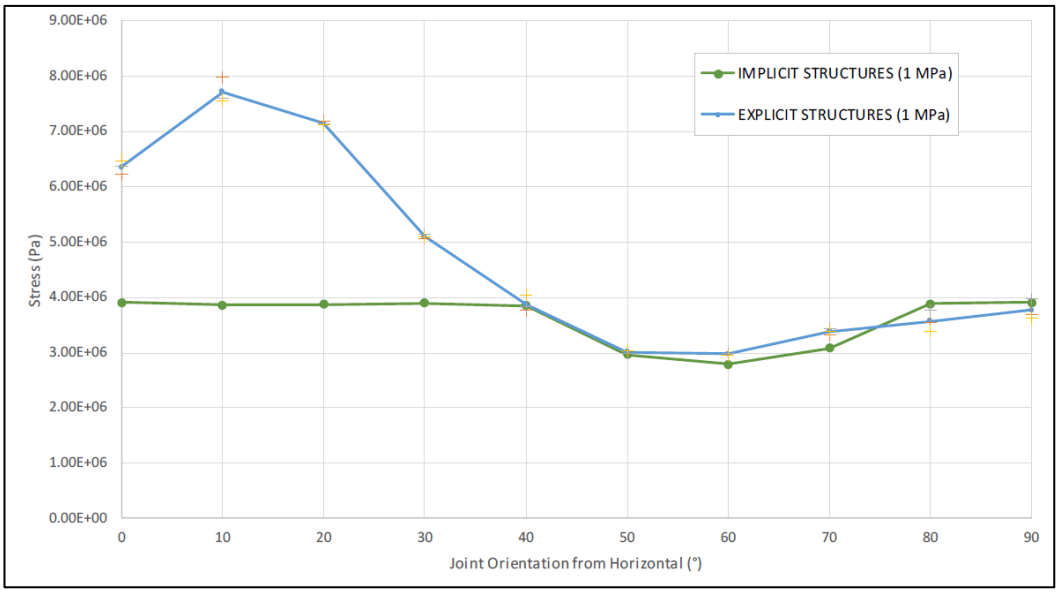


Figure 29 Comparison of results for Shale tests at Leeuwfontein pit on anisotropic rock mass.

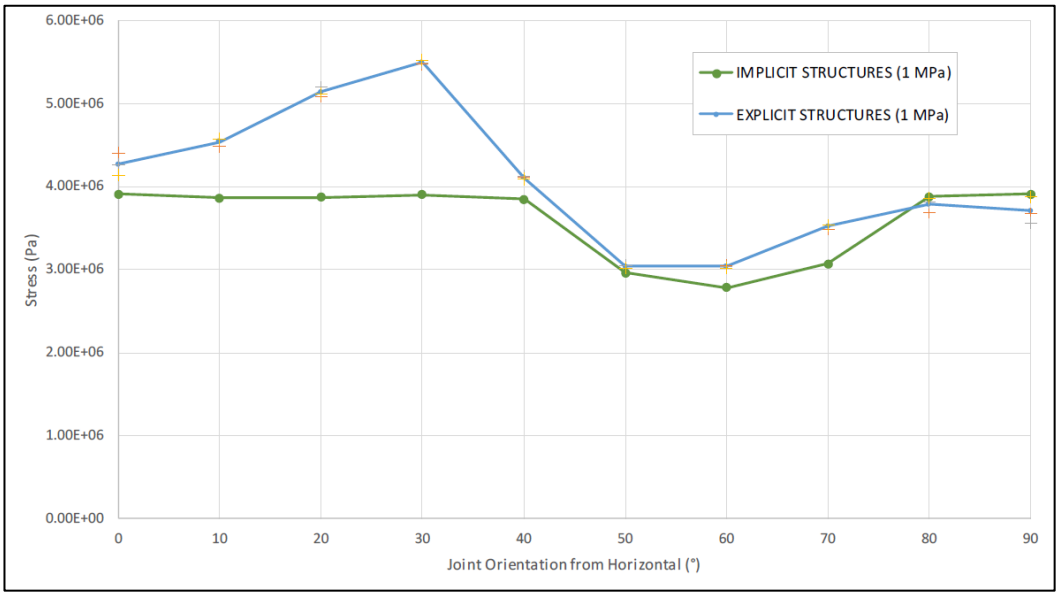


Figure 30 Comparison of results for Shale tests at Klipbankfontein pit on anisotropic rock mass.

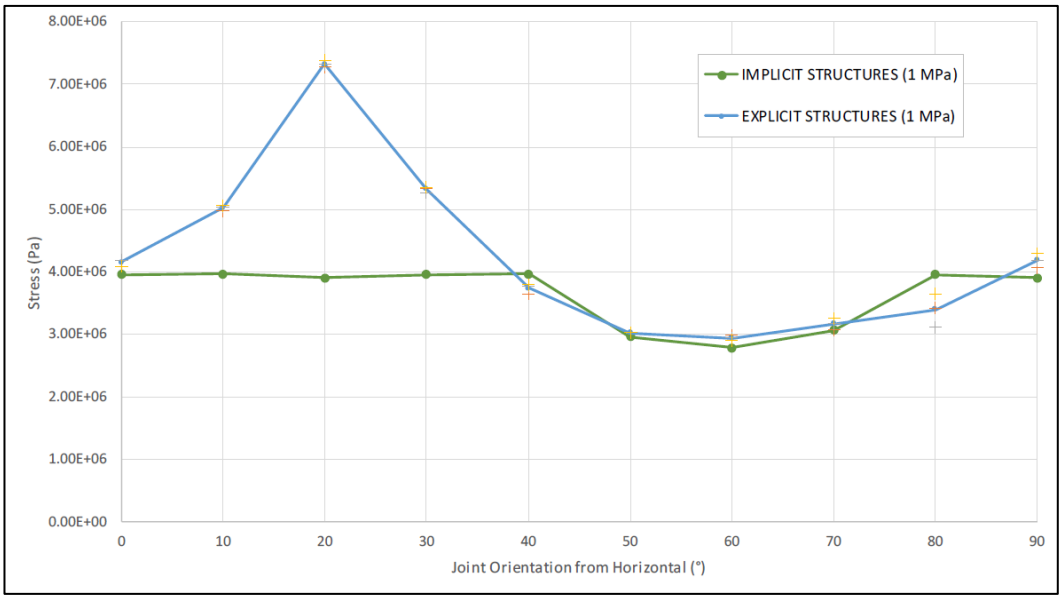


Figure 31 Comparison of results for Shale tests at Kapstevel North pit on anisotropic rock mass.

2.5. Synthetic Rock Mass Modelling (Conceptual) for the Heuningkranz Project

2.5.1. Background

The Heuningkranz Exploration Project is situated in the Postmasburg district of the Northern Cape Province of South Africa. This area is well known for iron and manganese-bearing lithologies that extend from Kathu to Postmasburg on a narrow north-south trending dolomitic dome termed the Maremane Anticline.

The Heuningkranz Project comprises one complete farm and one portion of a farm, totalling 3 426 hectares. The surface rights are owned by Sishen Iron Ore Company Pty Ltd, which is fully affiliated to Kumba Iron Ore Pty Ltd, a division of Anglo American (Figure 32).

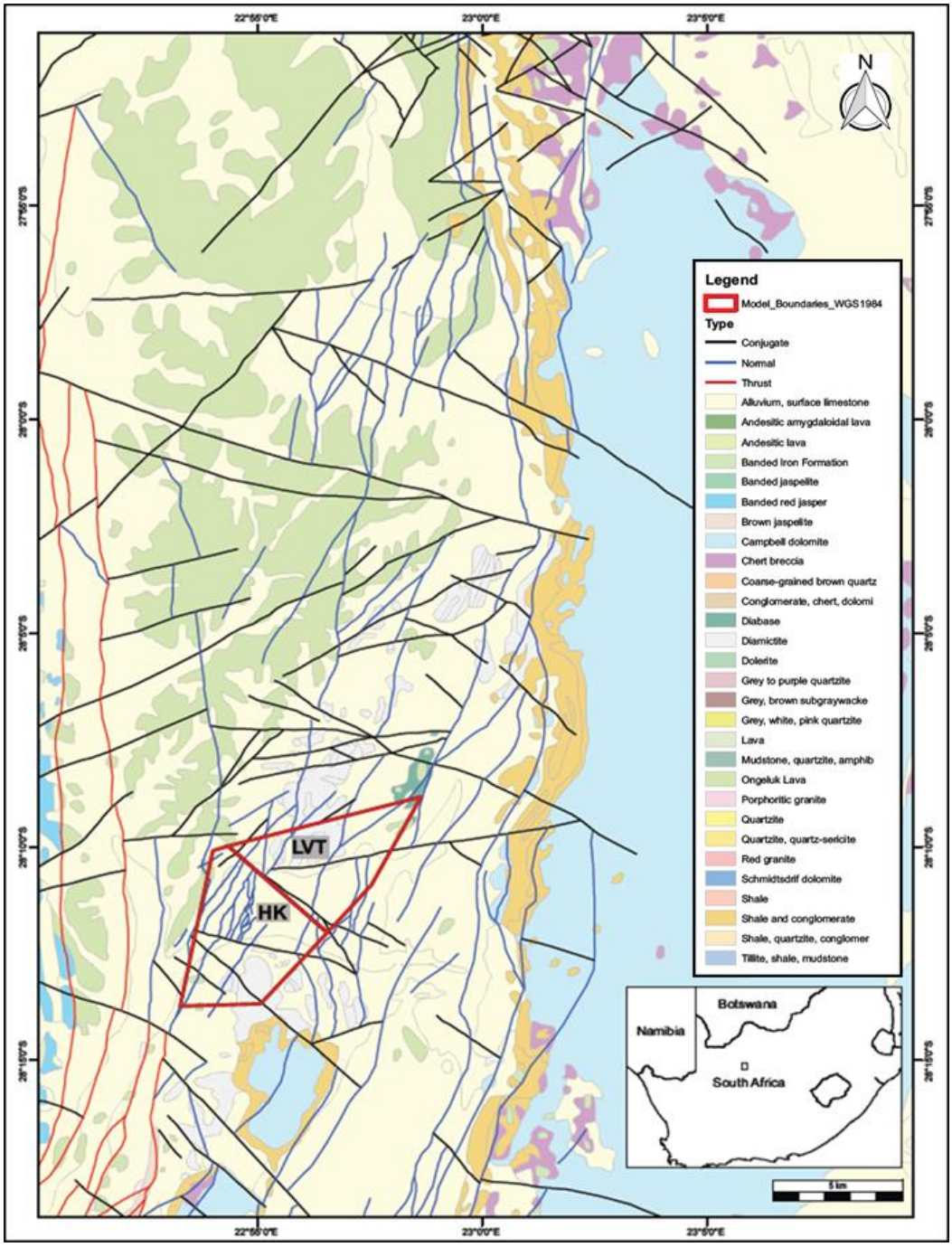


Figure 32 Location of Heuningkranz project on the Maremane Dome regional interpretation *(Kumba Iron Ore, 2019)*.

2.5.2. Geological Setting of Heuningkranz

The geological setting at the Heuningkranz Project is similar to that of Sishen and Kolomela and is described by (Koegelenberg & Basson, 2018). The Heuningkranz geological setting is summarised in Appendix 3.

Based on similar geological settings, the Banded Iron Formation (BIF) and Shale material at the Heuningkranz project is also expected to exhibit anisotropic behaviour on a rock mass scale. As this project is at the conceptual stage, no mapping information is available.

2.5.3. Banded Iron Formation (BIF)

In order to investigate the anisotropic strength of BIF at the Heuningkranz Project, the process described in previous Sections was again followed. *3DEC* was used to create a synthetic rock mass sample of size 5 m × 5 m × 10 m to be tested under confined compression (triaxial test). Both the bedding planes and the orthogonal joint sets with actual spacing were explicitly represented in the volume using DFN logic and intact rock properties were used for zones.

The structure sets (bedding planes and joints) used for representation in this model were derived from larger-scale structural trends from the concept-stage structural geological model (Creus, et al., 2017). Table 13 shows the orientations used for the BIF unit, while Figure 33 shows stereonets generated from the structural geological model.

Table 13 Structure sets definition in BIF

SET	Dip (°)	Dip Direction (°)
Bedding Planes	14	097
J3 (60° - 90°) (Set 1)	62	105
J3 (60° - 90°) (Set 2)	63	287

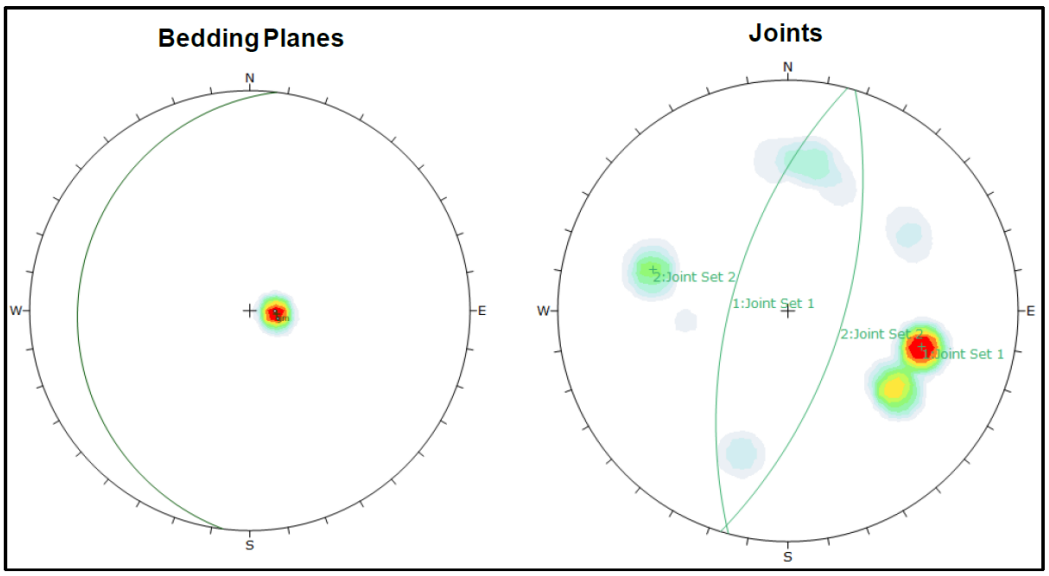


Figure 33 Stereo nets for bedding planes and orthogonal joints in BIF at the Heuningkranz Project. Note that the data is in mine grid (180° rotated).

Spacing data for every set (bedding planes and joints) were analyzed from Heuningkranz drillhole data extracted from the Heuningkranz *AcQuire* geotechnical database. Logging information is derived from geotechnical logging of core from exploration drilling. Figure 34 shows the spacing histograms for bedding and jointing.

Due to no mapping information being available at the conceptual stage of the project and keeping in mind that the goal is to develop a conceptual-stage synthetic rock mass model, the same persistence information for joints that occur at Sishen Mine was used for Heuningkranz. Bedding planes are assumed to have an infinite persistence in all the *3DEC* samples.

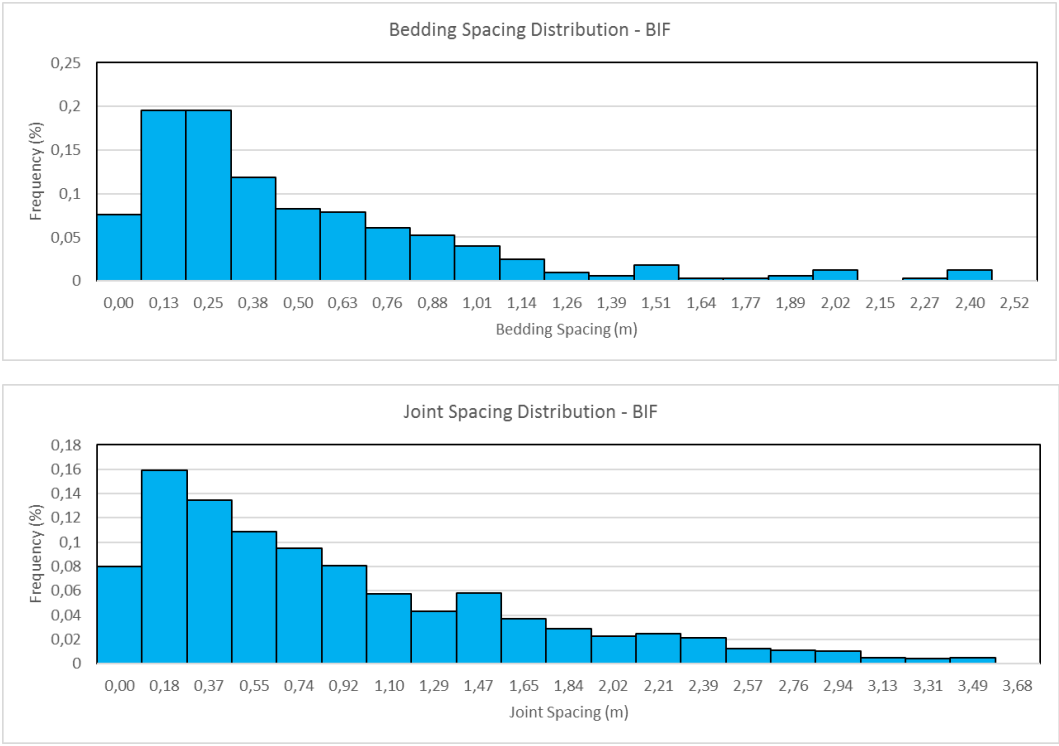


Figure 34 Spacing histograms for bedding planes and orthogonal joints in BIF at Heuningkranz.

Three geometrically unique samples have been tested for every bedding plane inclination ranging from 0° to 90°. Figure 35 shows one of these samples for the original orientations (14º inclination for bedding planes).

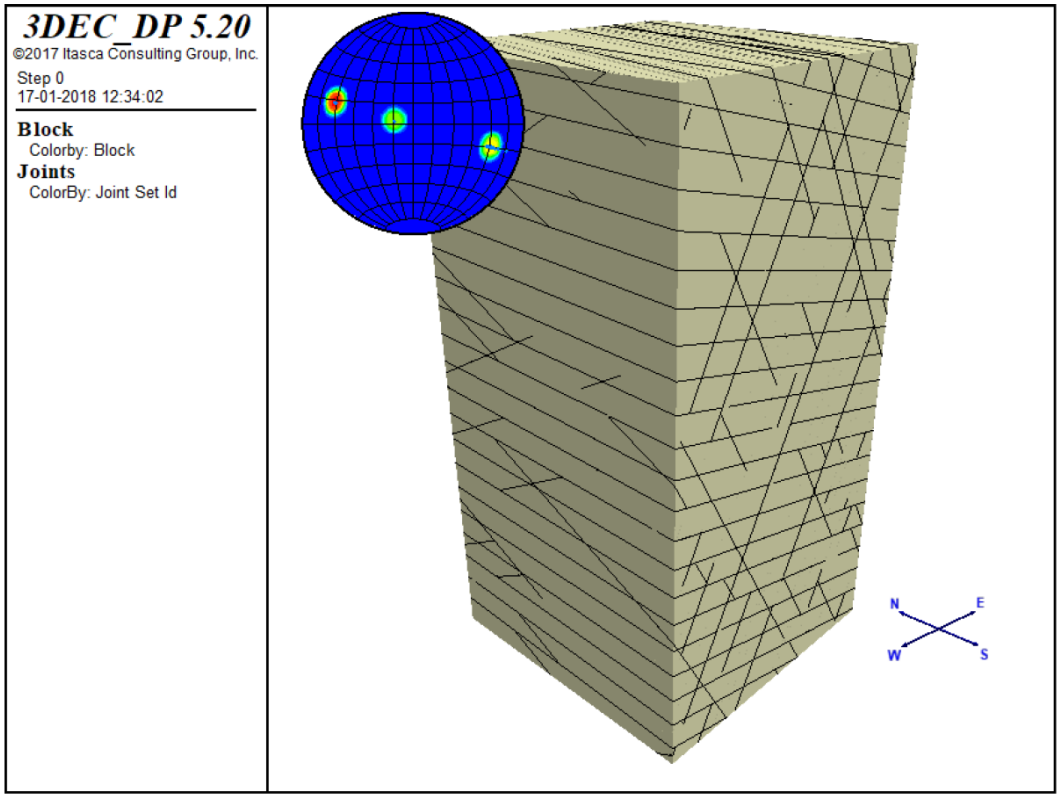


Figure 35 *3DEC* sample for a BIF test with 14º inclination for bedding planes (original orientation).

For the same reason discussed previously, intact rock material properties and Mohr Coulomb properties for structures were sourced from the Sishen *acQuire* database. These properties were assigned to the anisotropic rock mass in the *3DEC* models for analysis (Refer to Tables 2 and 3).

Explicit Joints Results

The numerical tests for confined compressive tests on the *3DEC* models were conducted by applying appropriate boundary conditions. Both ends of the model were moved with constant velocity in the *z*-direction (vertical) to apply loading to the model. While the model was being loaded, the loading stress was estimated using a *FISH* function by dividing the reaction forces on the sample ends by the cross-sectional area of the model. The mean value of the maximum principal stresses in the *3DEC* model was monitored throughout the simulation. As an example, Figure 36 shows the strength result for a BIF sample with inclined bedding planes (20°).

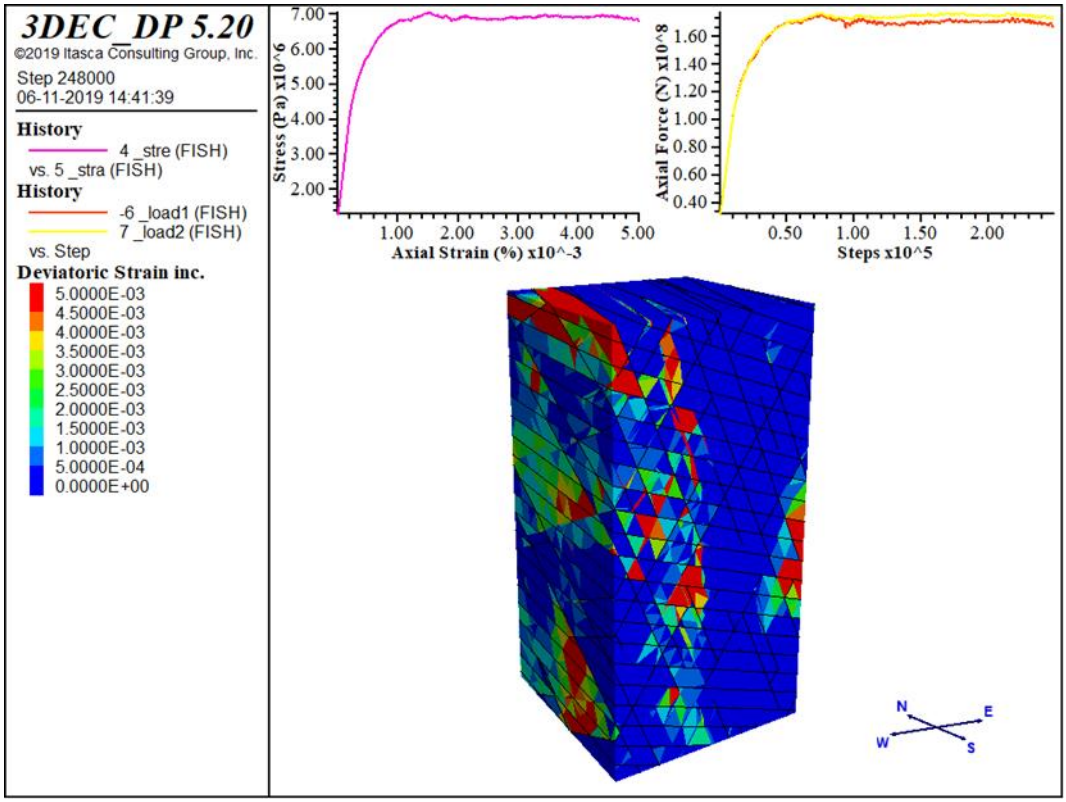


Figure 36 Strength results in Pa (magenta curve) for a BIF test for the Heuningkranz Project with explicit inclined bedding planes (20°). Comparative load results (superimposed yellow and orange curve) at both ends of the sample (in Newtons).

Figure 37 presents the results of numerical models for the confined compressive tests on the anisotropic rock mass (1 MPa confinement). The value of the maximum principal stress varies from approximately 4 MPa to 23 MPa, depending on the orientation of the loading direction relative to the structure sets.

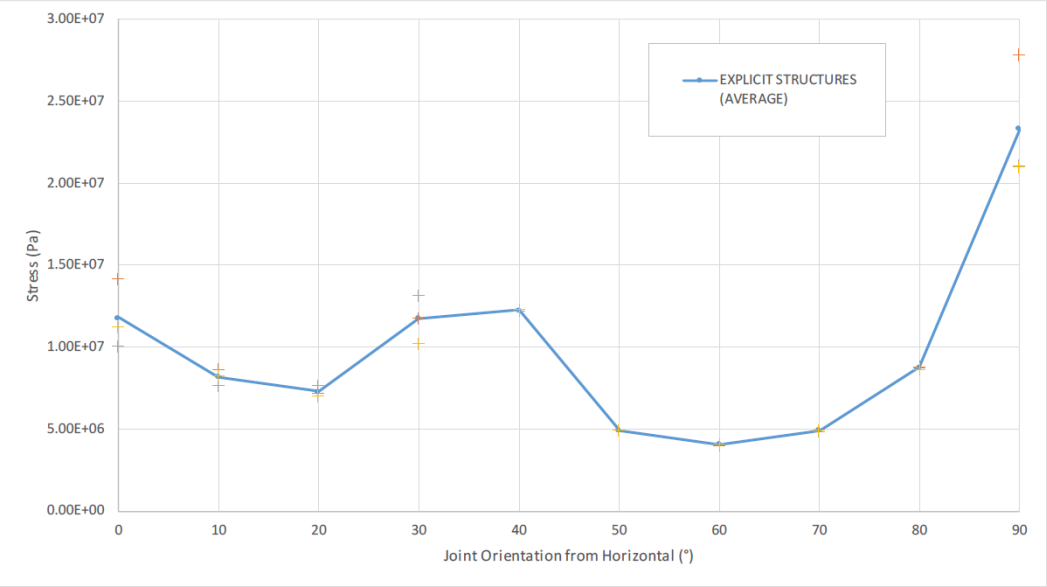


Figure 37 Strength results for BIF at the Heuningkranz Project for explicit tests at all the analysed inclinations.

Strength for 10° and 20° joint orientation from horizontal is lower than expected. A plausible explanation for this could be that the inclination of joints (approximately 60° in both J3 sets) and their persistence produce a failure based principally on structure.

Implicit Joints Results – Calibration of Anisotropic Strength

In order to represent the anisotropic rock mass in a continuous model or to perform early stage 3D geometrical analysis, BIF zones are assigned a ubiquitous joint model in the direction of bedding. Table 14 presents the calibrated properties for the rock mass of the specimen. Ubiquitous joints' properties are the same as in the explicit test. The calibrated properties were obtained by adjusting the implicit results to the explicit average strength curve presented above.

Table 14 Rock mass properties for BIF at the Heuningkranz Project for implicit SRM test

	Young's Modulus (GPa)	Poisson's Ratio	Cohesion (kPa)	Friction (°)	Tensile Strength (kPa)	Dilation (°)
Intact rock	37.9	0.25	0.55	45	0.11	10

Figure 38 illustrates the anisotropic strength response of the calibrated ubiquitous model, in comparison with explicit model results. Implicit behaviour has been fitted, with upwards adjustment for bedding planes, between 10° and 20° and conservative adjustment for the rest of bedding plane inclinations with higher strength.

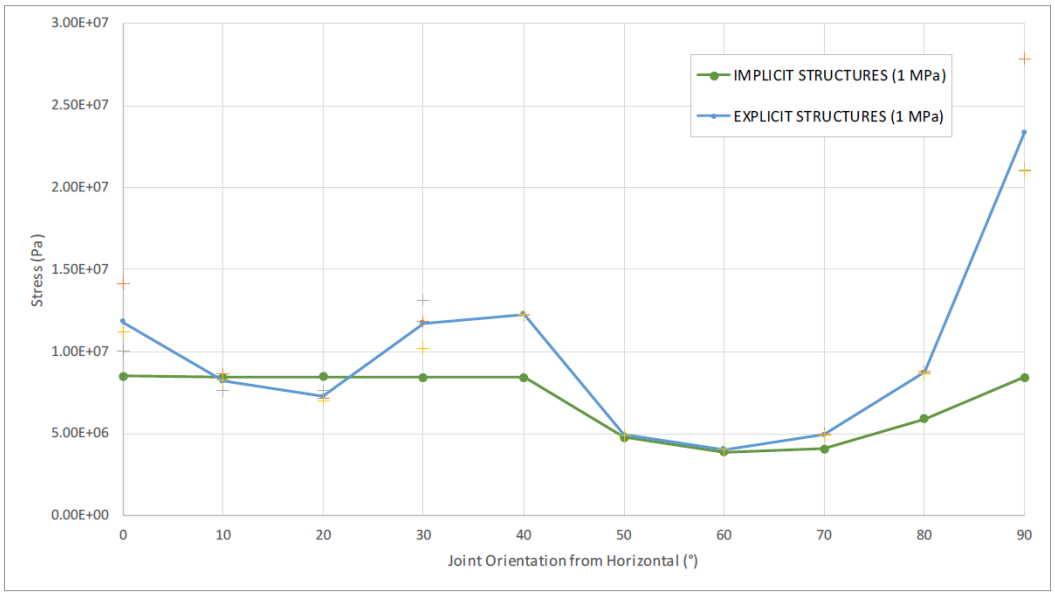


Figure 38 Comparison of results for BIF tests at the Heuningkranz Project on anisotropic rock mass.

2.5.4. Shale (SH)

Once more, following the same process to investigate the anisotropic strength of Shale at the Heuningkranz Project, *3DEC* was used to create a synthetic rock mass sample of size 5 m × 5 m × 10 m to be tested under confined compression (triaxial test). Both bedding planes and orthogonal joint sets with actual spacing were explicitly represented in the volume, using DFN logic and intact rock properties for zones.

The structure sets (bedding planes and joints) used for representation in this model were derived from larger-scale structural trends from the structural geological model (Creus, et al., 2017). Table 15 shows the orientations used for Shale, and Figure 39 shows the stereonets generated from the structural geological model.

Table 15 Structure sets definition in Shale

SET	Dip (°)	Dip Direction (°)
Bedding Planes	16	271
J3 (60° - 90°) (Set 1)	55	110
J3 (60° - 90°) (Set 2)	65	064

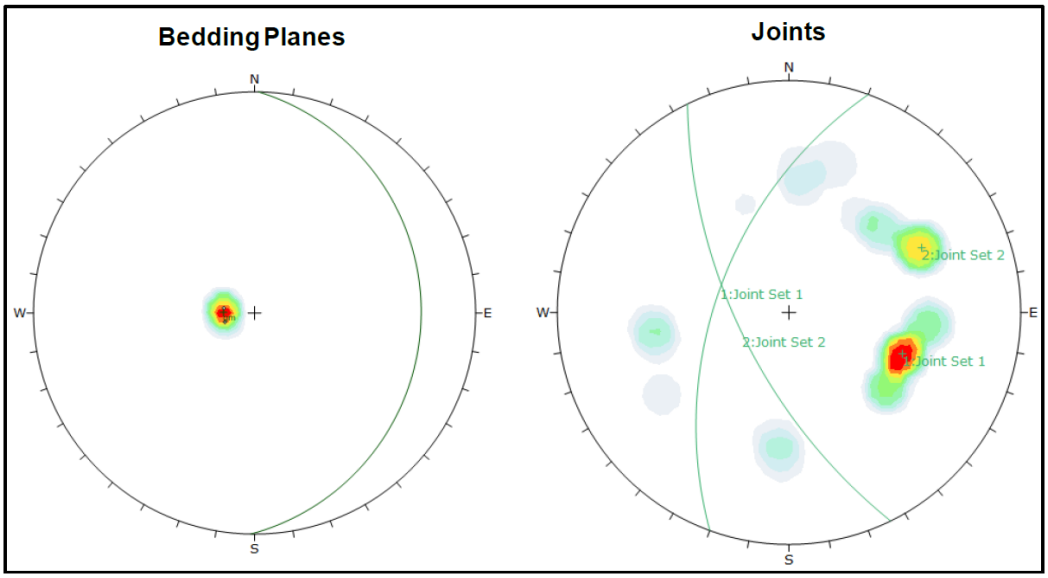
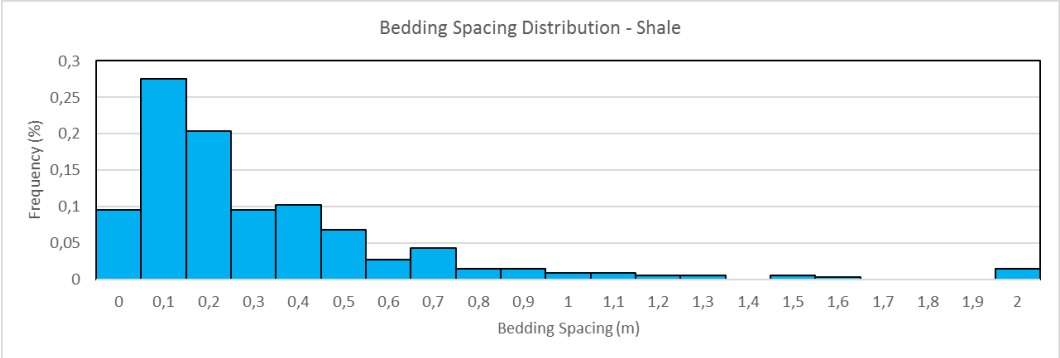


Figure 39 Stereonets for bedding planes and orthogonal joints in Shale at the Heuningkranz Project. Note that the data is in mine grid (180° rotated).

Shale spacing information for every set (bedding planes and joints) was analyzed from Heuningkranz borehole data extracted from the Heuningkranz *AcQuire* geotechnical database. Logging information is derived from geotechnical logging of exploration drillcore. Figure 40 shows the spacing histograms for every set.

Due to no mapping information being available at this conceptual stage and keeping in mind that one of the objectives is to develop a conceptual-stage synthetic rock mass model, the joint persistence recorded at Sishen Mine was used for Heuningkranz. Bedding planes are assumed to have an infinite persistence in all the *3DEC* samples.



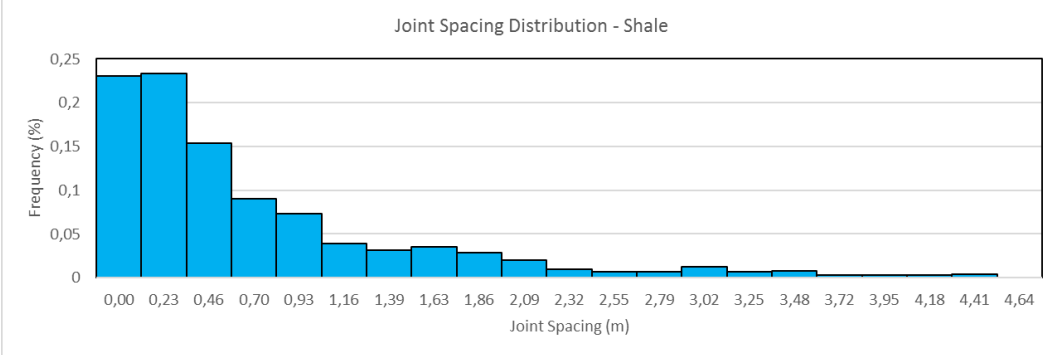


Figure 40 Spacing histograms for bedding planes and orthogonal joints in Shale at the Heuningkranz Project.

Three unique samples were tested for every bedding plane inclination ranging from 0° to 90°. Figure 41 shows one of these samples for the original orientations at 16º inclination for bedding planes.

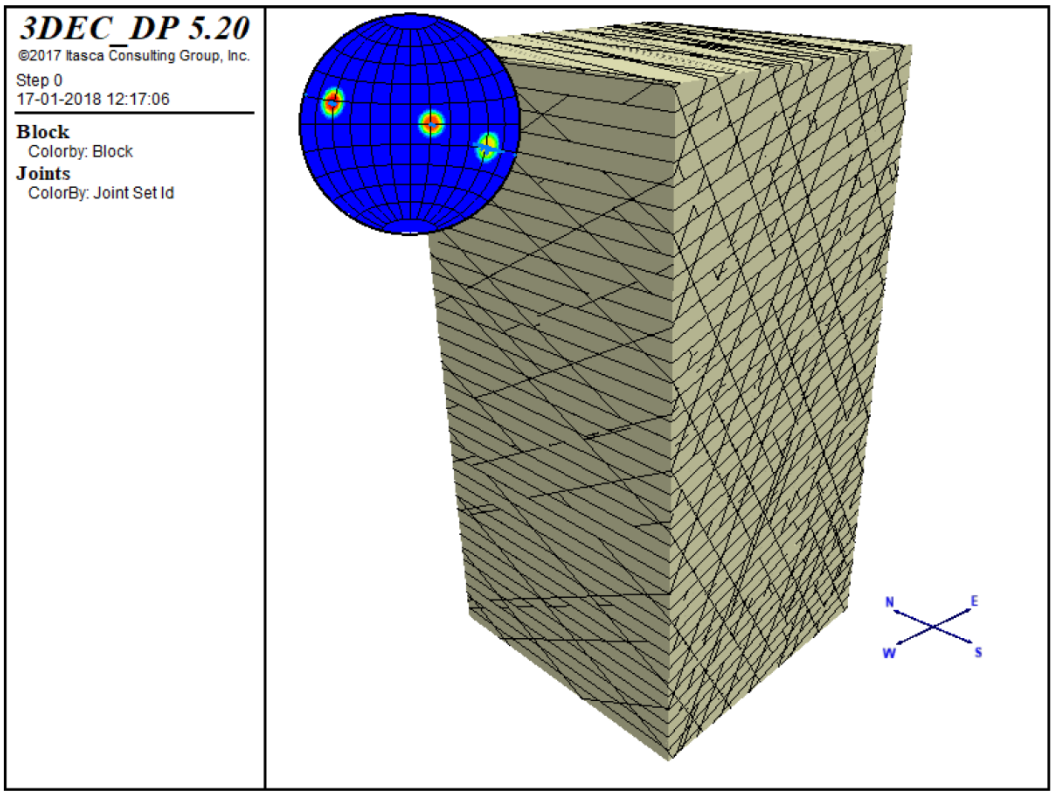


Figure 41 3DEC sample for a Shale test with 16º inclination for bedding planes (original orientation).

As for BIF, Shale intact rock material properties and Mohr Coulomb properties for structures were sourced from the Sishen *acQuire* database. These properties were assigned to the anisotropic rock mass in the *3DEC* models for analysis (Refer to Tables 5 and 6).

Explicit Joint Results

The numerical tests for confined compressive tests on *3DEC* models were conducted using the same methodology described above with the mean value of the maximum principal stresses in the *3DEC* model monitored throughout the simulation. As an example, Figure 42 shows the strength result for a Shale sample with steeply inclined bedding planes (90°).

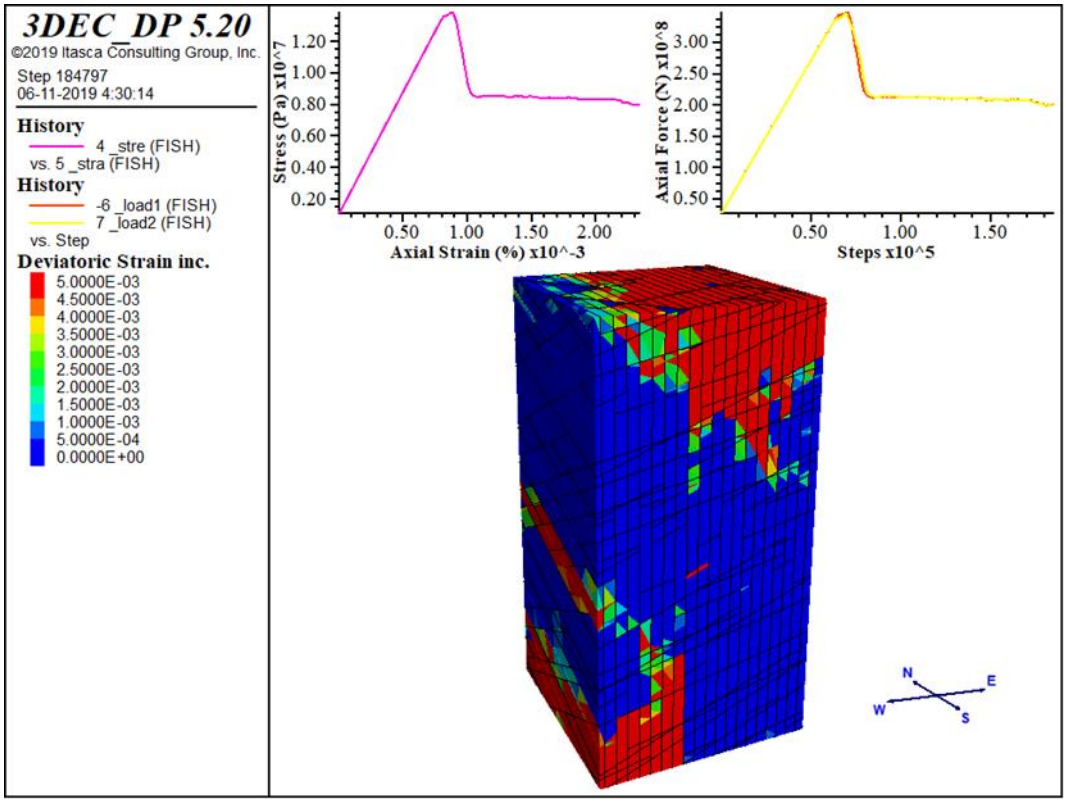


Figure 42 Strength results in Pa (magenta curve) for a Shale test at the Heuningkranz Project, with explicit vertical bedding planes (90°). Comparative load results (yellow and orange curve) at both ends (in Newtons).

Figure 43 presents the results of the numerical models for the confined compressive tests on the anisotropic rock mass (1 MPa confinement). The value of the maximum principal stress varies from approximately 3 MPa to 14 MPa, depending on the orientation of the loading direction relative to the structure sets. Note that the blue line represents the average value for every inclination, while colored crosses represent the values for every single test.

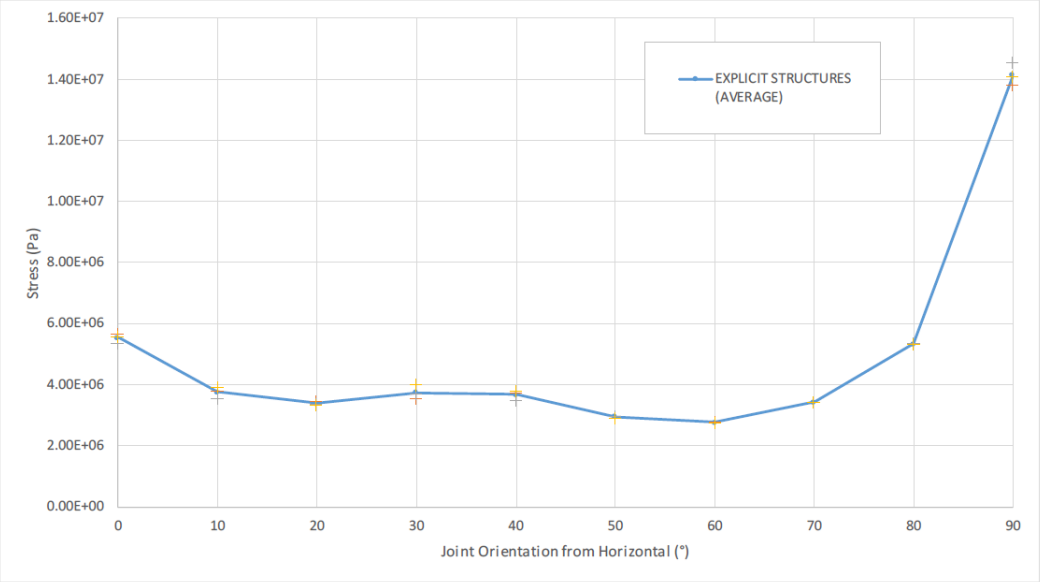


Figure 43 Strength results for the Shale unit at Heuningkranz Project for explicit tests at all analysed inclinations.

Strength for bedding planes at 10°, 20° and 30° are lower than expected. A plausible reason could be the lower spacings in both bedding planes and joints that produce failures principally along structures. Conversely, strength for vertical bedding planes seems higher than expected, possibly because of failure exclusively within the rock mass, since joints are constrained by boundary conditions at the bottom and top of the sample.

Implicit Joints Results – Calibration of Anisotropic Strength

Shale zones are assigned a ubiquitous joint model in the direction of bedding to represent the anisotropic rock mass in a continuous model.

Table 16 presents the calibrated properties for the rock mass of the specimen. The ubiquitous joints' properties are the same as in the explicit test. The calibrated properties were obtained by adjusting the implicit results to the explicit average strength curve presented above.

Table 16 Rock mass properties for Shale at the Heuningkranz Project for implicit SRM test

	Young's Modulus (GPa)	Poisson's Ratio	Cohesion (kPa)	Friction (°)	Tensile Strength (kPa)	Dilation (°)
Rock Mass	51.4	0.25	0.064	35	0.035	10

Figure 44 illustrates the anisotropic strength response of the calibrated ubiquitous model, in comparison to the explicit model results. In this case, implicit behaviour has been fitted by conservative adjustment to horizontal and vertical bedding

planes. For the rest of the bedding plane inclinations, the implicit curve fits very well with the explicit curve.

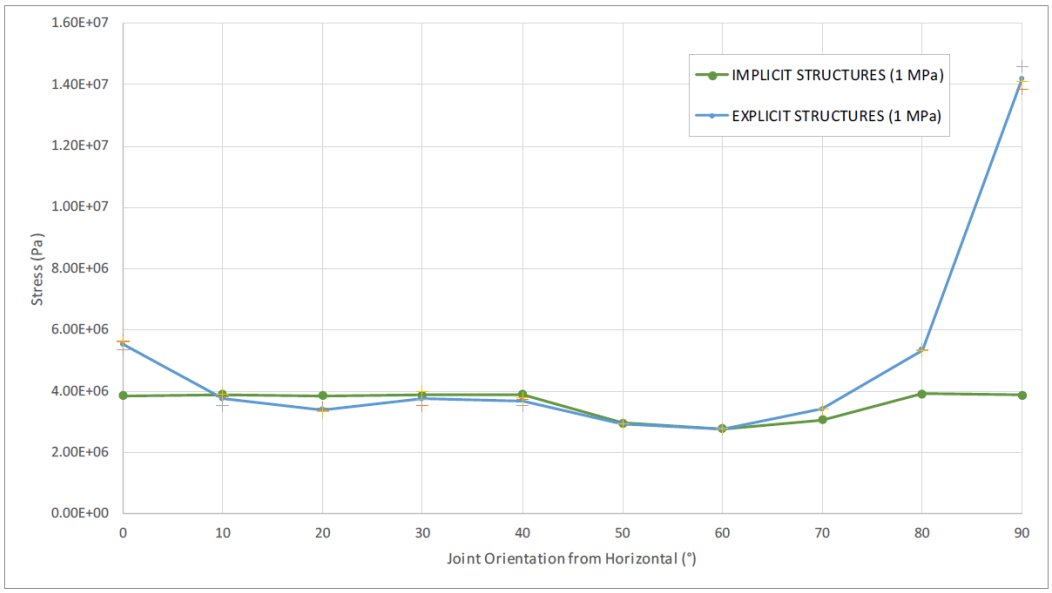


Figure 44 Comparison of results for Shale tests at the Heuningkranz Project on anisotropic rock mass.

2.6. Summary and Conclusions

The pioneering development of SRM's was undertaken for BIF and shale units in the Northern Cape of South Africa, as the most challenging aspects of slope design in moderately- to heavily-jointed rock masses relate to the impacts of in-situ joint fabric and scale effects on rock mass behaviour (Sainsbury, et al., 2008). Based on conceptual failure models, these units play a crucial role in the economics (e.g. stripping ratio) and geotechnical risk mitigation of mining iron ore reserves in the Northern Cape.

Figure 45 summarizes the results for BIF and the differences across operations and projects. Although the structural behaviour is the same for inclinations of between 40° and 80° from the horizontal (angle from perpendicular to the applied load), the remainder of inclinations, where failure is a combination of rock mass and structure, exhibit differences.

Kolomela Mine BIF was found to be the strongest and Heuningkranz Project BIF the weakest. These results are conceptually aligned with the geological and structural settings of the three areas as well as actual observations on Sishen and Kolomela. For instance, Heuningkranz is situated both close to the Kheis orogenic Front and on the flanks of the Wolhaarkop Dome. Based on geological information, the Heuningkranz project is structurally more complex and one would therefore expect BIF at Heuningkranz to be weaker than that at Sishen or Kolomela.

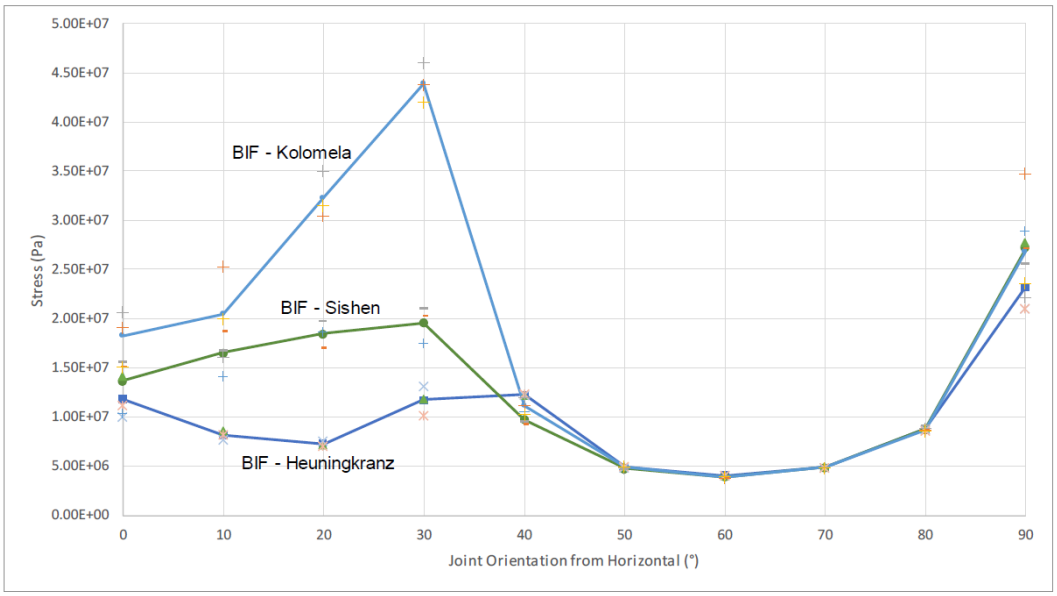


Figure 45 Comparison of results for BIF tests at Kumba operations in the Northern Cape.

Figure 46 shows the results for Shale at the operations and projects. Similar to BIF, the behaviour was found to be the same for inclinations between 50º and 60° from the horizontal, while the remainder of the inclinations, where failure should be due to a combination of rock mass and structure, exhibit differences. Shale at Sishen Mine was found to be the strongest and Heuningkranz Project shale the weakest. Once again, these results are conceptually aligned with actual observations at Sishen Mine and Kolomela Mine and the fact that the Heuningkranz project is tectonically more complex due to its closer proximity to the Kheiss Orogenic Front and on the flanks of the Wolhaarkop Dome.

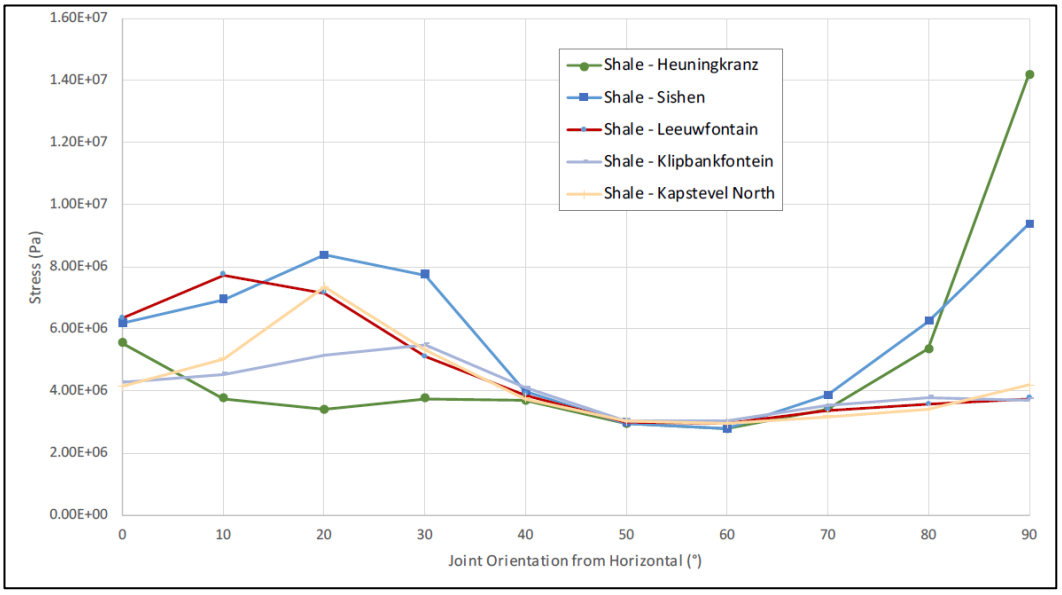


Figure 46 Comparison of results for Shale tests at Kumba operations in the Northern Cape.

Significantly, it is not possible to explicitly represent each of the aspects affecting the behaviour of a highly heterogeneous system, such as a large-scale rock mass. Moreover, uncertainty relating to key characteristics would remain, even upon termination of the mining operation. Important aspects that could influence rock mass behaviour and its reaction to mining, i.e., local geological units and their contacts, geological structures, zones of very weak or altered rock, deep weathering profiles, local changes in in-situ stresses, etc., are quantifiable at various levels of confidence depending on where the project is in its life cycle (e.g. a conceptual project like Heuningkranz vs. a full-scale mining operation at Sishen).

Bearing this in mind, expectations related to advanced numerical modeling should not go beyond investigating dominant behaviours and mechanisms, of the system being studied, under various well-constrained conditions of analysis. There are inherent limitations that should be considered when utilizing numerical models pertaining to volumes with high levels of complexity. The extent of a numerical model is not only limited by computer capacities. Although specific details are available for certain input parameters, it is necessary to impose a certain level of simplification upon representing or simulating a particular geometry.

With this objective in mind, and with the goal of elucidating the anisotropic behaviour of BIF and shale in the Northern Cape, the discrete fracture network (DFN) and synthetic rock mass (SRM) approaches were employed to capture the important effects that bedding has on the rock mass strength.

This produced good agreement with explicit behaviour and consequently, implicit properties may be used in 3D geometrical analysis and mine-scale numerical models. This work also supports Bidgoli & Jing's (2014) conclusions that in view of limited small-scale laboratory tests and the practical impossibility for proper controlling of large-scale in situ tests of large volumes of fractured rock masses, numerical modelling is probably the preferred method available at present for predicting the anisotropy of strength and deformability of fractured rocks. Correspondingly, the anisotropies of strength and deformability of fractured rocks are important issues for design and performance of geotechnical engineering projects, since the relative directions of in situ stresses (determining the loading directions), fracture system geometry (selecting the directional variation of stress distribution) and geotechnical engineering projects (such as choosing axis of tunnels relative to not only in situ stress directions but also orientations of dominating fracture sets; and their interaction with slope orientations) may have a significant impact on the safety and performance of the structures located in fractured rock masses (Bidgoli & Jing, 2014). Lastly, due to the directional dependence of strength and deformability of fractured rocks, proper site investigations, data capture and management for fracture system behaviours are crucial for design and performance/safety assessments of all engineering works in fractured rock masses (Bidgoli & Jing, 2014).

Following an iterative process, described in detail in Chapter 4, these models may also be tested and refined as new information becomes available during the life cycle of any project.

3. A NEW 3D GEOMETRICAL ANALYSIS METHODOLOGY

3.1. Introduction

According to Starfield & Cundall (1988), perspectives on modelling in rock mechanics have changed dramatically in the last quarter of the previous century, as modellers realised that data-limited problems require a very different modelling approach from that developed in, for example, electrical or aerospace engineering (Starfield & Cundall, 1988). This statement still rings true today. In the early stages of development of rock mechanics, studies relied on laboratory and field measurements, while mathematical or computational models were generally thought to be either irrelevant or inadequate. With the ongoing development of computer technology, significant focus and research are now aimed at improving 3D models to represent the geological setting and engineering characteristics as accurately as possible and based on all available or relevant data (Starfield & Cundall, 1988).

According to Grenon & Laflamme (2011), standard practice in geomechanical rock slope engineering for open-pit mines relies on the simplified representation of slope geometry, which does not take full advantage of the available topographical data. Mergili, et al., (2014) presented the results of an attempt to integrate a spatially-distributed three-dimensional limit equilibrium slope stability model of landslides in a raster GIS (Geographic Information System). A few authors including Lobatskaya et al. (2015) and Xie et al. (2004) described similar GIS based methods (also see Park, et al., 2016).

The importance of integrated structural stability analysis in open pit design is highlighted by Grenon & Hadjigeorgiou (2010). This article traces the evolution of tools used for limit equilibrium analysis and design of rock slopes susceptible to wedge-type failure. These contributions highlight a focus on capturing and representing structural information accurately to provide a more realistic prediction of the stability of natural and man-made excavations (also see Vatcher, et al., 2016).

From this introductory literature review, there appears to be a gap related to the 3D geometrical analysis of slope geometries' interaction with structurally-controlled and/or anisotropic materials, based on conceptual failure models. Definition and in-depth understanding of conceptual failure models and the role of structural geology are critical in slope design. This is highlighted in a critical review of rock slope failure mechanisms by (Stead & Wolter, 2015).

Therefore, a new methodology was developed during this research that enables a comprehensive 3D analysis of the interaction of lithological contacts and complex geological features (faults, anisotropic behaviour from bedding or foliation), with slope geometry. For the first time, this study describes how to fully exploit the integration of modern, smooth, implicitly built, radial basis function derived surfaces and solids in geological/structural geological modelling as critical inputs

to slope design. Utilising input from advanced Synthetic Rock Mass modelling, this dynamic methodology greatly improves the definition of design sectors, as inputs to the mine planning process in operational mines as well as early stage projects.

The new methodology will be described in detail in the following Sections and can be summarised by the following high-level steps aligned with the slope design process (Read & Stacey, 2009):

- Develop / refine the geotechnical model (geological / structural / rock mass / hydrogeological models)
- Define Geotechnical Domains.
- Derive orientation data (dataset can include both measured and modelled data).
- Perform interpolation for dip and dip direction.
- Assign dip and dip direction to slope design surface triangle centroids.
- Calculate apparent dip.
- Grid and project onto design surface.
- Perform binning to produce maps utilising input from Synthetic Rock Mass modelling or available information according to the conceptual failure model.
- Utilise maps to define design sectors. In order to illustrate this, the following practical example from a mine is described. An area in which a slope must be designed (Sishen North Mine) consists of the following domains (Figure 47):
    - Calcrete (CC)
    - Clay (CL), pebble layers (PEB) and weathered lava (LAW)
    - Lava (LAV)
    - Banded Iron Formation (BIF).

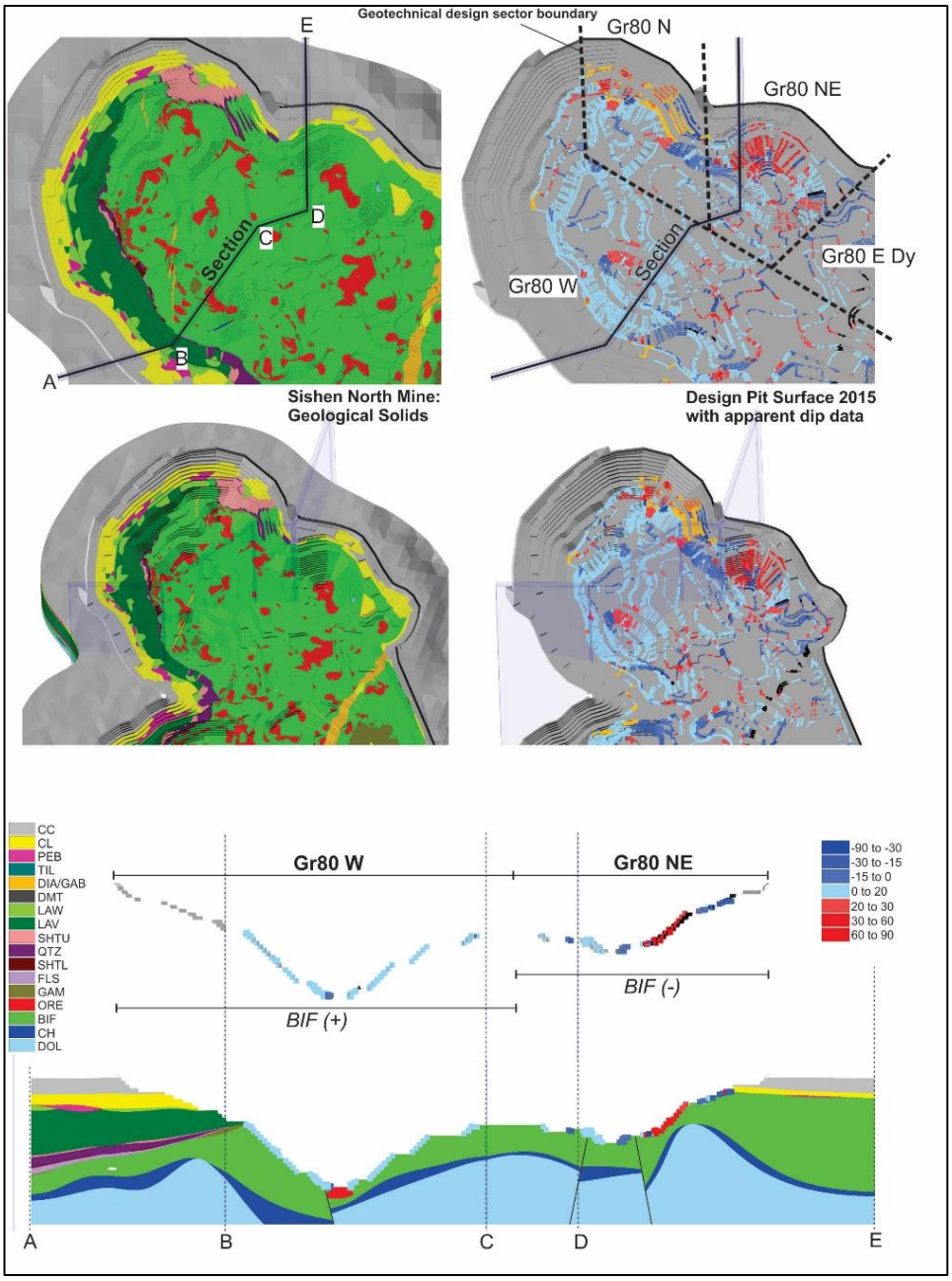


Figure 47 Illustration of geotechnical design sectors.

Depending on the orientations of slopes planned in the area and taking into account the conceptual failure model, the resultant slope can include either favourable (BIF+) or unfavourable (BIF-) anisotropic material such as Banded Iron Formation resulting in the subdivision of the area in design sectors. The overall slope angle and the slope configuration in the specific design sector therefore depends on this interaction, e.g. unfavourable BIF = single bench configuration at 45 degrees (GR80NE) vs. favourable BIF = double bench configuration at 50 degrees (GR80W).

- Follow an iterative, risk-based approach to address design sectors of concern, by implementing focused data acquisition programs, rigorous stability and risk assessments and subsequent mitigation actions for early stage projects through to operational mines.

3.2. Development of the Methodology

Following synthetic rock mass analysis (SRMA), a methodology was developed to augment the use of vertical two-dimensional (2D) design sections by applying and analysing SRMA results in three dimensions (3D), without sectional constraints. This seeks to develop a more accurate methodology for the extraction of spatial variation in parameters while at the same time obviating several limitations of pre-ordained, typically wedge-shaped design sectors and their central, vertical sections.

The methodology aims to improve design sector classification by highlighting possible areas - of any size or shape – that show unfavourable interaction with slope geometries in future pushbacks or on final faces, thereby resulting in a more robust and practical suite of sector-specific design parameters as inputs for mine design.

The geometry around instability events may also be utilised to investigate other volumes with comparable structural interactions with slope geometry. This allows for focussed data acquisition, such as mapping, dedicated geotechnical drilling with downhole Optical/Acoustic Televiewers and more rigorous stability analysis to further improve the geotechnical model. Any plane of anisotropy is amenable to this analysis (viz. bedding, foliation, faults).

In order to perform stability analyses for any project, a conceptual failure model should be derived. As in the example illustrated in Figure 48, rock mass failure could only occur in softer rock masses (calcrete), whereas rock mass failure is unlikely within rock masses such as Banded Iron Formation and related anisotropic units. A structurally-controlled, stepped path failure mechanism (interaction between faults, bedding, joints and rock bridges) is therefore anticipated for BIF. The step path failure mechanism can be further complicated by weak geological contacts (weak BIF / Gabbro contact).

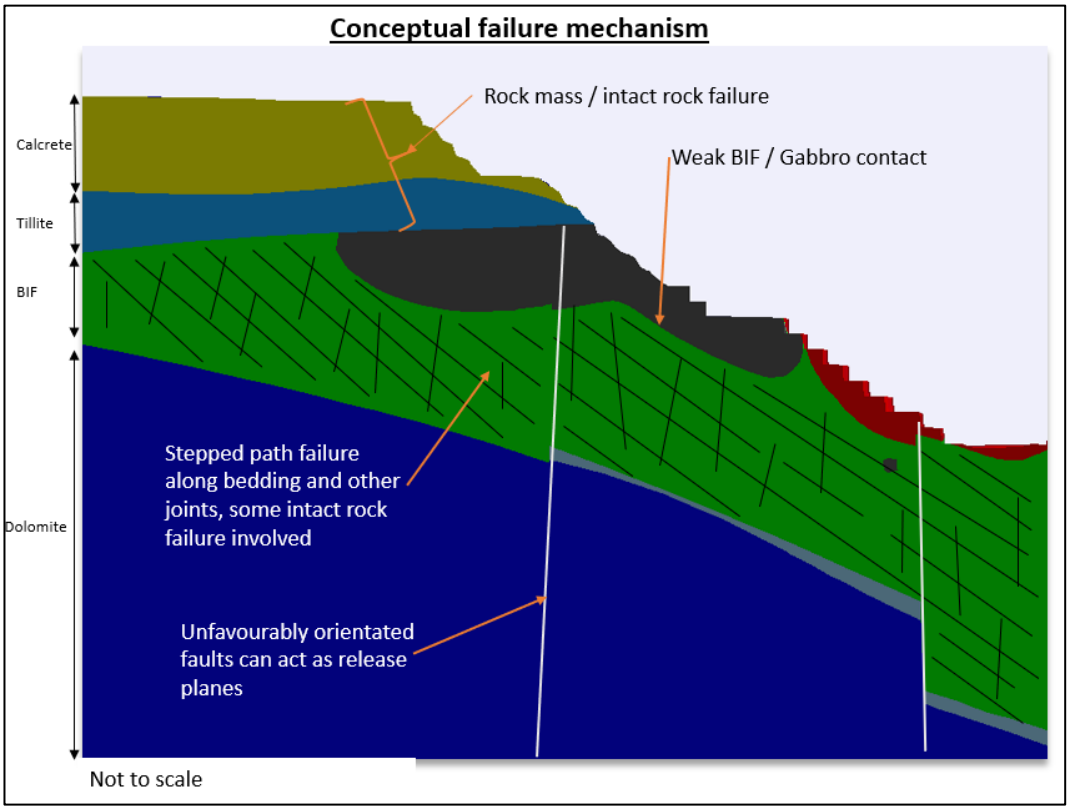


Figure 48 An example of a conceptual failure model.

Due to the nature of some orebodies, pit geometries may be complex with mining progressing in several phases or pushbacks, each with their own unique geometry. This may lead to multiple permutations of pit geometries interacting with geological features in each geotechnical domain and where unfavorable, these interactions may be the ultimate drivers of stability or instability according to the conceptual failure model.

3.3. Calculation of Apparent Dip

Explicitly-modelled surfaces (built in Surpac, Gemcom and Datamine) using Delauney triangulation, or explicit individual triangle assembly, cannot accurately represent the true geometry of geological contacts or fault surfaces. In contrast, surfaces that are built using any of the radial basis functions (RBFs), employed in packages such as Leapfrog and Micromine, are smoother and more geologically-realistic. In geological modelling, the orebody and associated lithologies are represented by triangles that are connected to form a surface (wireframe). Each triangle on these surfaces is defined by three vertices. Collections of triangles are therefore planar approximations of a smooth surface since graphics software packages and hardware devices operate more efficiently utilising triangles.

The interaction of a geological plane (e.g. foliation, bedding or contact) with a vertical surface will result in a calculable apparent dip (AD) (Figure 49), as long as the plane is not exactly perpendicular to the vertical surface, which is a rare condition.

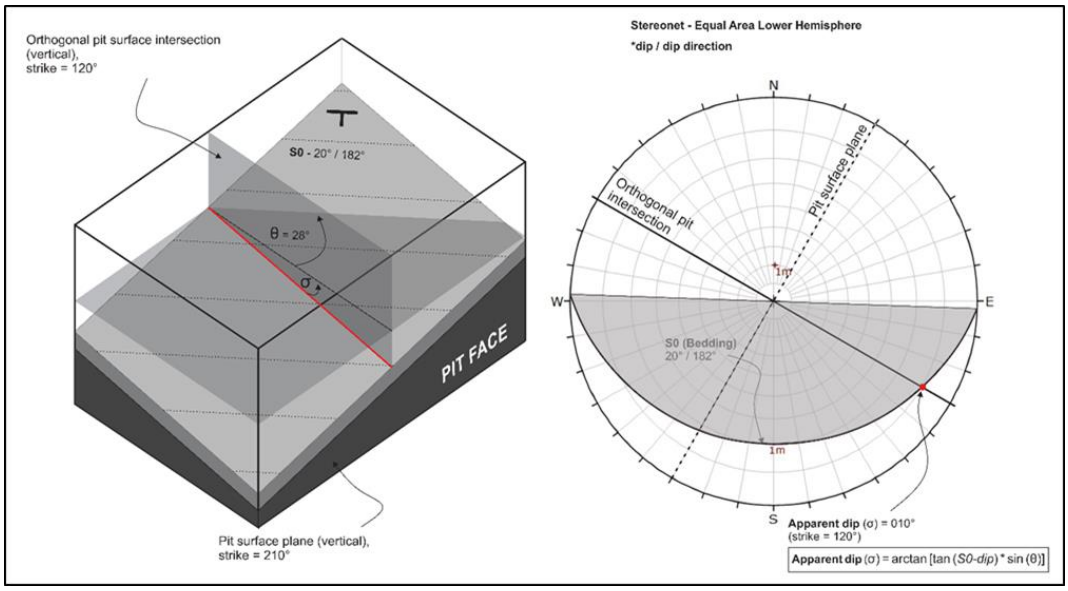


Figure 49 Stereonet illustrating the principal of apparent dip calculation *(Bester, et al., 2015).*

In the establishment of this interaction, a design surface is preferred over an actual mining surface, as mining surfaces progressively lose their bench and face definition and even high-resolution laser scans of mining faces may be problematic to use in the following calculations (Creus, et al., 2019).

In the case of analysed anisotropic units (BIF and SH) found in the Northern Cape, these units occur within the block-faulted footwall to the primary orebodies. Utilising *Micromine*, triangle orientations were extracted from wireframes representing lithological contacts, essentially the uppermost limit of 3D volumes or closed wireframes, in order to quantify and qualify the geometry (dip direction / dip) of lithological contacts in 3D space. Areas or volumes where these were in direct contact with erosional or tectonic unconformities were excluded, as this violates one of the basic assumptions of the analysis. Otherwise, triangle orientations were reasonably assumed to be parallel or sub-parallel to bedding within their respective volumes and structural domains. This can be tested by comparing recorded bedding readings, from in-pit mapping, with surface-extracted triangle orientations in the same area. Each sub-set of triangle orientations, in the form of dip direction and dip, was assigned to separate structural domains (*viz.* fault-bounded blocks). Triangles on the sides of these blocks, which would provide anomalously steep dips, where they are against steep or vertical bounding faults, were removed from the analysis.

Gridding and contouring of this data show the spatial variation in the true dip of lithological contacts. Depending on the project stage and if available, it is also advisable to integrate mapping data or actual dip direction and dip data from oriented drill core into triangle orientation files prior to gridding and contouring. In order to fully undertake the analysis and to account for changes in orientations of actual mining surfaces or a design layout relative to bedding in any given area, it is necessary to calculate the *apparent dip* of bedding.

Gridded triangle orientations, i.e. true lithological dip directions and dips, were assigned to these pit surfaces using a nearest-neighbour algorithm. The distance from which this projection is performed from off-(pit)-surface data varies, but it is advisable to refer to the thickness, lateral extent and internal coherence of the unit from which data is taken and, by default, through which data will be extrapolated. It was found that using true dip data within 20-50 m of the pit surface was acceptable for Sishen, Kolomela and Heuningkranz geology. The calculation to determine AD is given in equation 1 and illustrated in Figure 50.

Equation 1 $AD = arctan\{cos(XS - TDD)\} \times tan(TD)$

where:

AD	=	apparent dip
TD	=	true dip
XS	=	azimuth of design surface triangle centroid
TDD	=	true dip direction

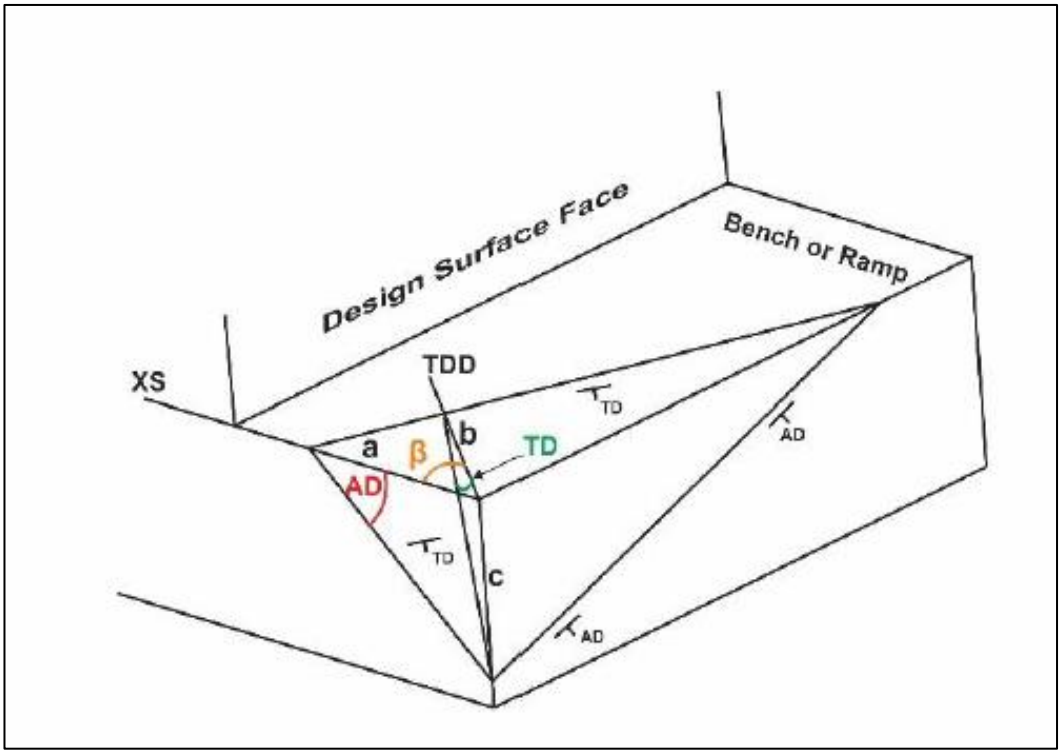


Figure 50 Calculating apparent dip *(Creus, et al., 2019)*

The schematic in Figure 50 shows the calculation of AD, whereby the three triangles need to be related by trigonometry as in the following equations:

Equation 2 $\tan AD = \frac{c}{a}$ *or* $c = a \times \tan AD$

Equation 3 $\tan TD = \frac{c}{b}$ *or* $c = b \times \tan TD$

Equation 4 $\cos \beta = \frac{b}{a}$ *or* $b = a \times \cos \beta$

β is the angle difference between the azimuth of a design surface triangle centroid and the dip direction of the plane of interest at that design surface centroid.

Thus, equation 2 = equation 3 and therefore:

Equation 5 $a \times \tan AD = b \times \tan TD$

Substitute equation 5 into equation 4 and simplify:

Equation 6 $a \times \tan AD = a \times \cos \beta \times \tan TD$

$AD = \arctan(\cos \beta \times \tan TD)$

Part of recent developments in geological modelling is the use of form surfaces. Form surfaces, or structural iso surfaces, are explicit 3D representations of the variation of a single feature in 3D space, e.g. contacts, bedding and foliation. Form surfaces are useful for several reasons. They show the dominant trend of the dominant fabric potentially interacting with the slope and are continuous. They also provide a representation of orientation of the dominant plane of anisotropy for 3D geometrical analysis and geotechnical stability analysis. As such, form surfaces are an explicit, interpreted representation of a feature in wireframe format, which may be utilised to perform apparent dip analyses as well as imported and viewed in any mainstream 3D software package (Creus, et al., 2019).

The methodology is therefore versatile and can be utilised in a variety of mining environments wherein any plane of anisotropy or geological feature are amenable to this analysis.

3.4. Contouring and Binning of AD Results

The next step is to contour and bin the AD results to show various scenarios according to a project's conceptual failure model. This new methodology allows for AD to be contoured and binned to show a range of relative orientations visualising the interaction of slope geometries with geological features. Apparent dips are only displayed where certain units / features intersect the design pit. This was achieved by clipping modelled lithological volumes against the design pit to show where units under investigation daylight on the design pit surface.

For early stage projects, binning and contouring can simply display inward or outward dipping attitudes to guide early design sector definition. In this case, bins

are defined to show apparent dips into the face (0° to -90°) and out of the face (0° to 90°).

For more advanced projects, these relative orientations may be re-phrased to represent the results of advanced SRM analysis. The ranges of the bins are based on results obtained from the strength curve of the anisotropic strength response of the calibrated ubiquitous model described in the previous Section (refer to Figure 51.)

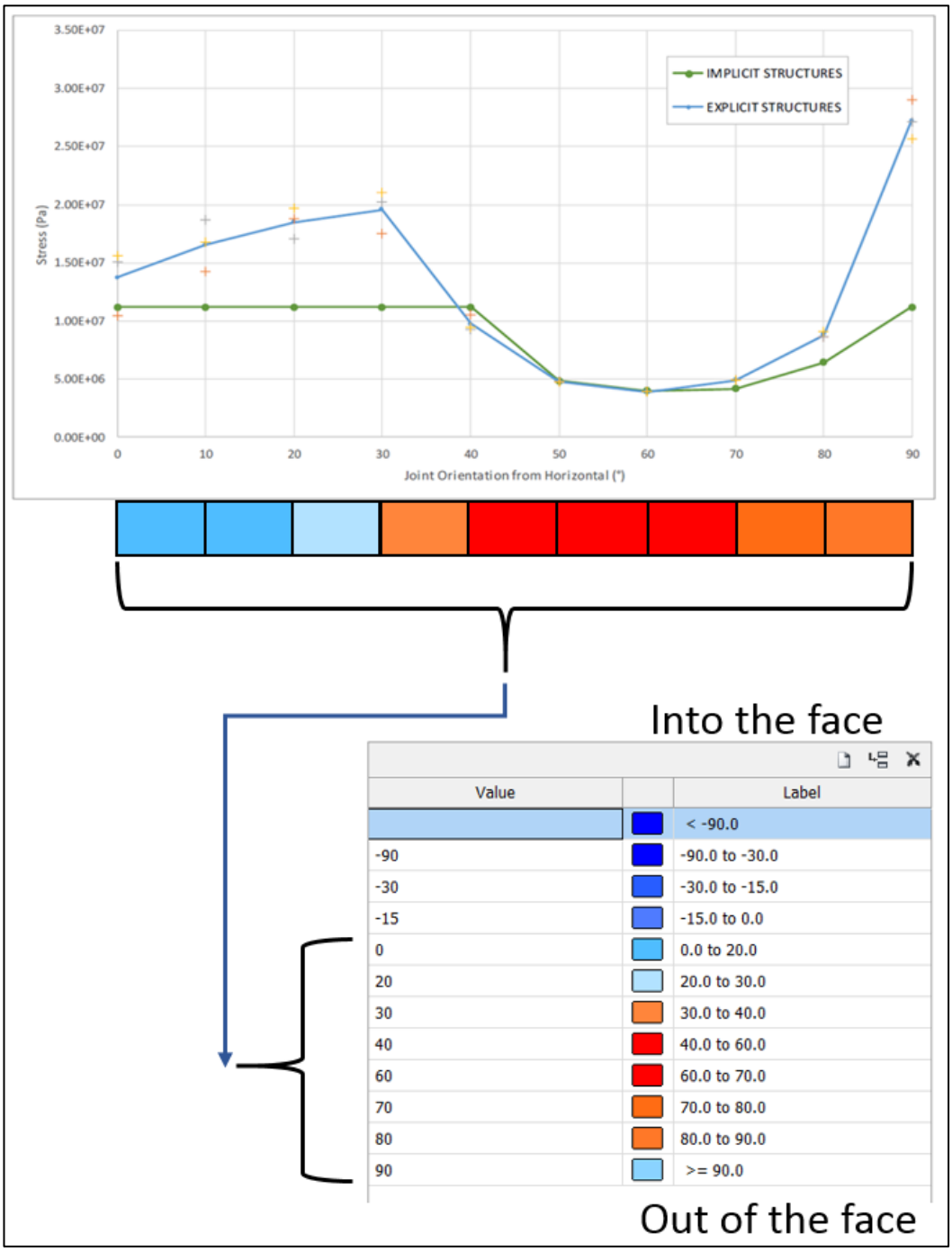


Figure 51 Ranges of bins are based on results obtained from the strength curve of the anisotropic strength response from SRM modelling.

Figure 52 is an example at Sishen Mine of gridded (utilising Inverse Distance Power gridding) and colour-coded BIF and SH according to the BIF and SH anisotropic strength response curves obtained from SRM analyses. 12 dip angle bins, between -90° and +90° were used in this example. Areas that are orange and red are of particular concern due to the unfavourable interaction of anisotropic materials and the planned pit geometry.

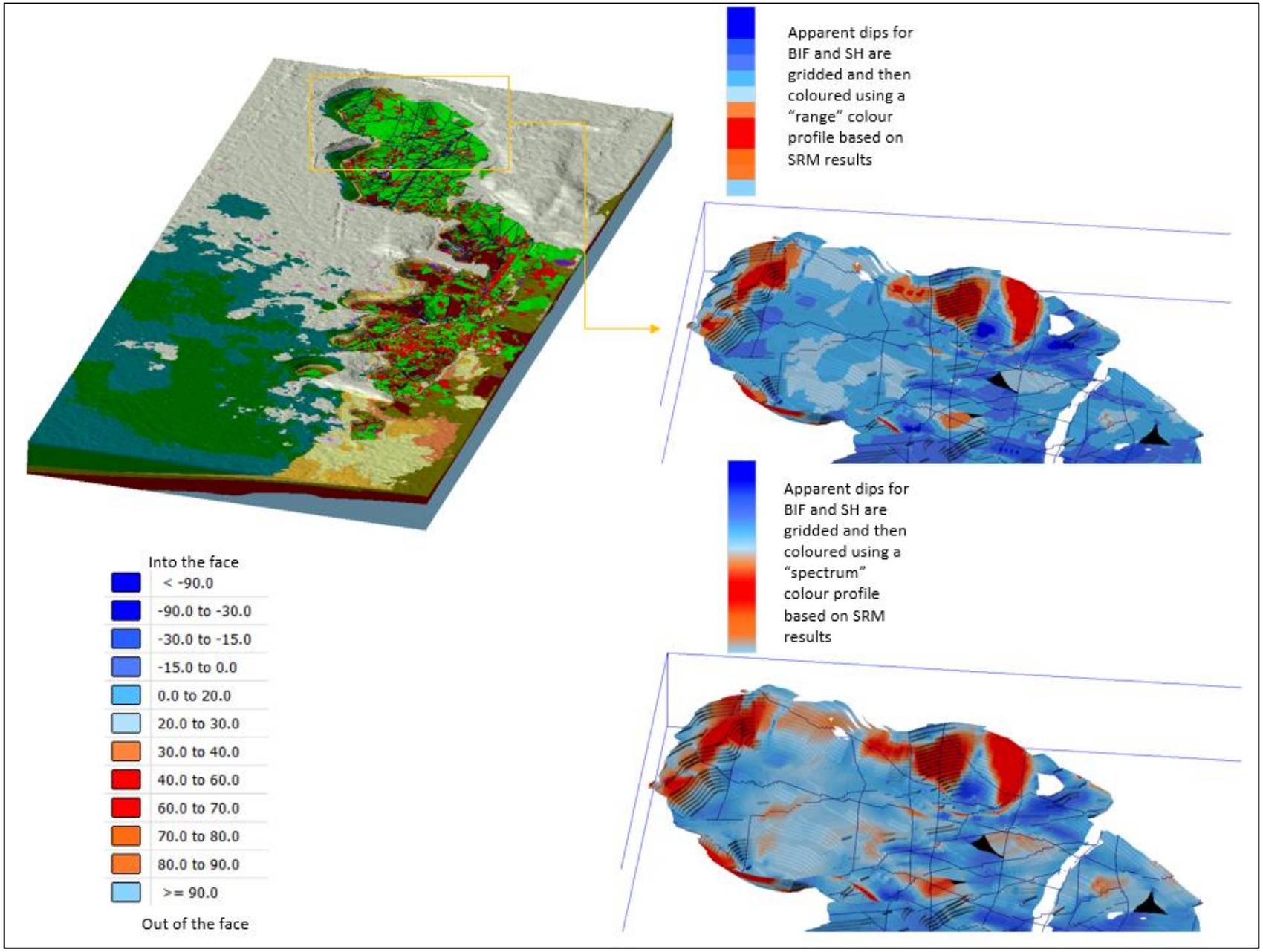


Figure 52 Example of results of obtained for Sishen Mine utilising SRM input for BIF and shale.

The methodology is versatile and should SRM analysis not be available, it can also be used for example to indicate areas where certain critical friction angles are exceeded or where orientation conditions are met for potential planar sliding, e.g.

Equation 7 $\omega > AD > \phi$

Where: ω = *slope angle*

AD = *apparent dip*

Φ = *friction angle*

3.5. Applying the New Methodology at Different Stages of a Project's Life Cycle

It is generally recognized that the quality and quantity of data is defined by the design objectives and functional requirements of the analysis and design tools. (Read & Stacey, 2009) developed guidelines for open pit slope design and suggested that different levels of effort, with associated levels of confidence, are required in data collection from the early conceptual to the late operations stage of a mining project. Data availability can therefore significantly vary for the different stages of the life cycle of a project and will have a major influence on reaching a satisfactory engineering design to mitigate geotechnical risk caused by geological uncertainty. The new methodology, described in the preceding Sections, can be applied throughout the life cycle of a project, although the confidence in results will be dependent on the accuracy, coverage and density of input data.

3.5.1. Early-Stage Projects (Limited Data)

For early stage projects, only a geological model, based on drillhole information, is normally available. In some cases, limited surface mapping informs or partially informs these models.

Figure 53 illustrates the steps to follow for early stage projects or future pushbacks where dense datasets are not yet available.

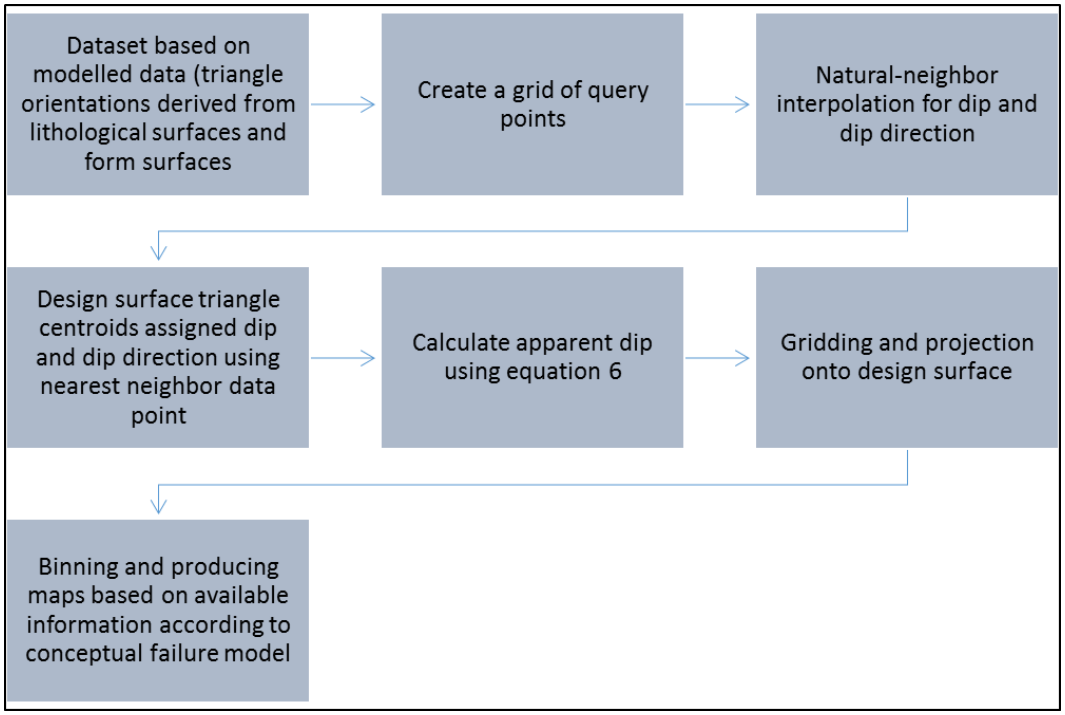


Figure 53 Flowchart illustrating the process of applying the 3D geometrical analysis methodology with a limited dataset.

In Figure 53, "modelled data" refers to triangle orientations that are extracted from contacts and form surfaces, which are in turn modelled from logging data. This allows for the interpretation of lithological logging to be incorporated into the analysis.

Results from using the new methodology at an early stage informs the definition of design sectors and should guide focussed geotechnical data acquisition to continuously improve confidence in the geotechnical model following an iterative process described in detail in the following Chapter.

3.5.2. Operational Stage Project (Denser Data Sets)

In advanced projects or operations, denser data sets, which include pit mapping, are available to inform and confirm most aspects of the geotechnical model, thereby resulting in increased confidence. This includes outputs from geological and geotechnical mapping, infill drilling and ongoing reconciliation processes, which are referred as "measured data" herein. Figure 54 illustrates the process where denser datasets are available.

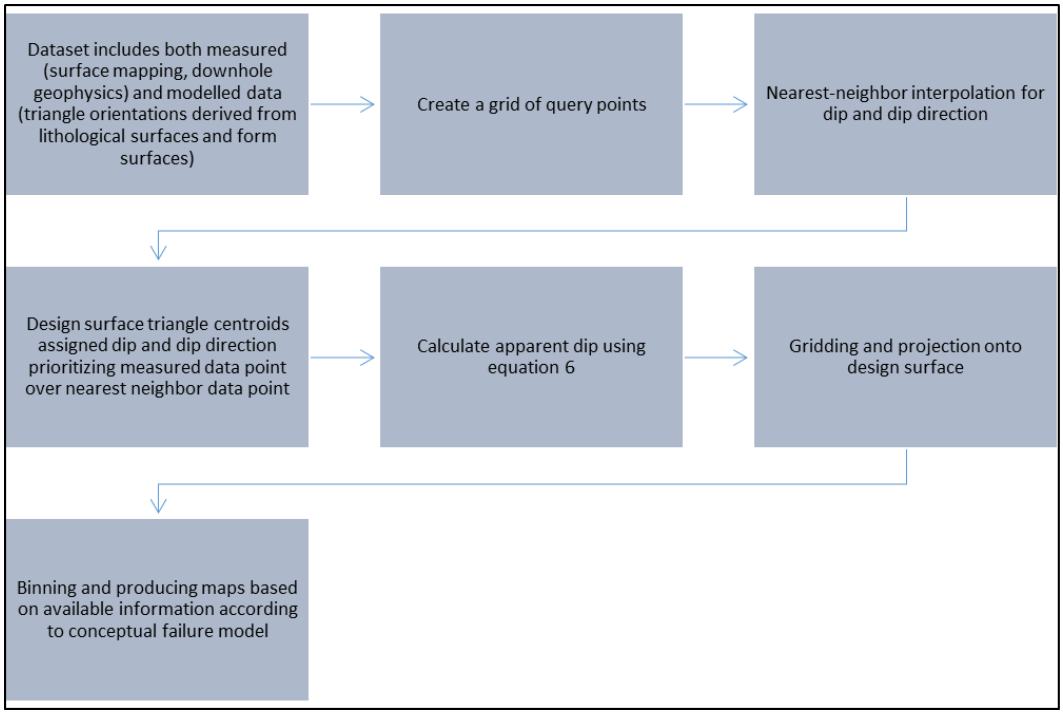


Figure 54 Flowchart illustrating the process of applying the 3D geometrical analysis methodology with a dense dataset.

The difference between the two processes (Figure 53 vs. Figure 54), is that the point data derived from modelled surfaces ("modelled data") are imported separately from measured data. The logic for this approach is that it is simpler to establish the projection distance for each dataset, to determine which data point will be assigned to a particular grid point. If a measured data point occurs within a set distance from a query point, that value is assigned, otherwise the nearest neighbour from either dataset is assigned. In effect, measured data are prioritised over modelled data within a set distance from a query point.

There are several advantages to this new approach, *a priori* extents and shapes of specific design sectors are minimised or completely avoided; design sectors are more rationally defined from early stages according to the structural analysis and reliance on average or median dips on central sections of simplistic, wedge-shaped design sectors is precluded. The definition of design sectors will now be discussed in more detail.

3.6. The Definition of Geotechnical Design Sectors

Incorporating data obtained from following the process described above, as well as utilising various strength models according to the conceptual failure models (with regards to lithological layers), unique geotechnical design sectors may be defined.

Design sectors are first identified and grouped according to lithology or a collection of lithologies with similar strength properties. If required (i.e. for anisotropic

layers), these sectors are gridded with calculated apparent dips on the design pit surface (see previous Sections) to constrain further possible design "sub"-sectors.

To illustrate this principle, a design sector was created for grouped BIF and SH and populated with apparent dips (refer to Figure 55). Importantly, apparent dip orientations that denote a low strength area are considered as separate design "sub"-sectors. Interaction with faults and weak contacts according to the conceptual failure model is also considered during this process.

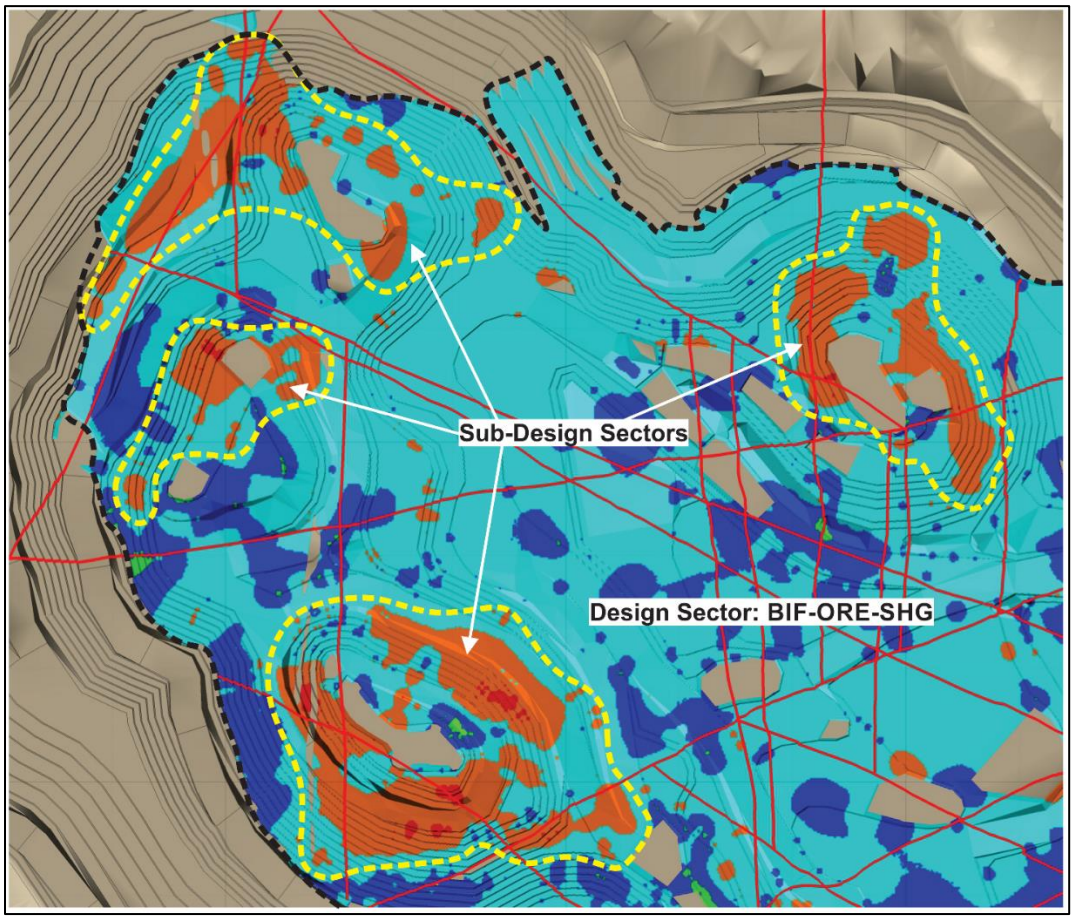


Figure 55 Example of Geotechnical Design Sectors *(Bester, et al., 2015)*

Design sectors are then digitised (in this case using Micromine) to create wireframes of each individual design sector.

Once completed, the geotechnical block model (discussed in detail in the next Chapter) may be constrained with these individual design sector solids and populated with sector-specific geotechnical design parameters, including berm width and stack angle for use in mine design optimisation, scenario analysis and practical pit layout construction.

3.7. Summary and Conclusions

Any plane of anisotropy or geological feature is amenable to this analysis. This novel methodology of analysing the interaction of lithological contacts, representative bedding isosurfaces and complex geological features with slope geometry fully exploits the integration of smooth, implicitly-built radial basis function (RBF)-derived surfaces and solids as critical inputs to slope design. It augments the use of 2D design by providing a rational and dynamic methodology to improving the definition of design sectors, as inputs to the mine planning process from a very early stage. This is particularly important where the main plane(s) of anisotropy show significant changes in dip direction, which may justify domain subdivision. This technique also overcomes the situation wherein certain parts of the pit inevitably show a dramatic change in orientation with respect to strike or dip direction within a domain or sector, which have historically been addressed by more traditional means (*viz.* average or median dips).

The methodology may be utilised in early-stage projects when only modelled data, derived from geological models, are available. In certain instances, this may be augmented by downhole data from oriented drill core, or from dense – or closely-spaced – readings derived from OTV/ATV analysis. Improved and early design sector classification highlights possible areas - of any size or shape – that show unfavourable interaction with slope geometries, thereby resulting in a more robust and practical suite of sector-specific design parameters as inputs for mine design. The results also allow for more downstream, focussed data acquisition, including dedicated geotechnical drilling, to further improve dynamic geotechnical models.

In more advanced projects, a greater array of usually denser data sets is available to inform all aspects of the geotechnical model, thereby resulting in increased confidence in the results obtained from applying the methodology. During operations, instability events and slope performance reconciliation may also be plotted with respect to AD or derived SRM maps, to elucidate failures or to investigate other volumes with comparable interactions between structural features and either current pit geometries, pushbacks or final/planned slope geometries.

By applying this methodology as part of an iterative process, the slope design process can be improved significantly, especially if applied as early as possible to facilitate optimised designs and early risk mitigation.

4. THE SLOPE DESIGN PROCESS

4.1. Introduction

The slope design process, developed over the past 25 years, is widely utilized in a relatively standard format (Figure 56) (Read & Stacey, 2009). Data from geological, structural, rock mass and hydrogeological models are used to formulate and populate geotechnical models. Based on these parameters, the volume of interest is divided into geotechnical domains. Structural and rock strength information are key inputs to define the conceptual failure model(s) within these geotechnical domains. Subdivision of domains into design sectors should typically result in practical slope designs for volumes that contain structurally-controlled and/or anisotropic materials (Read & Stacey, 2009).

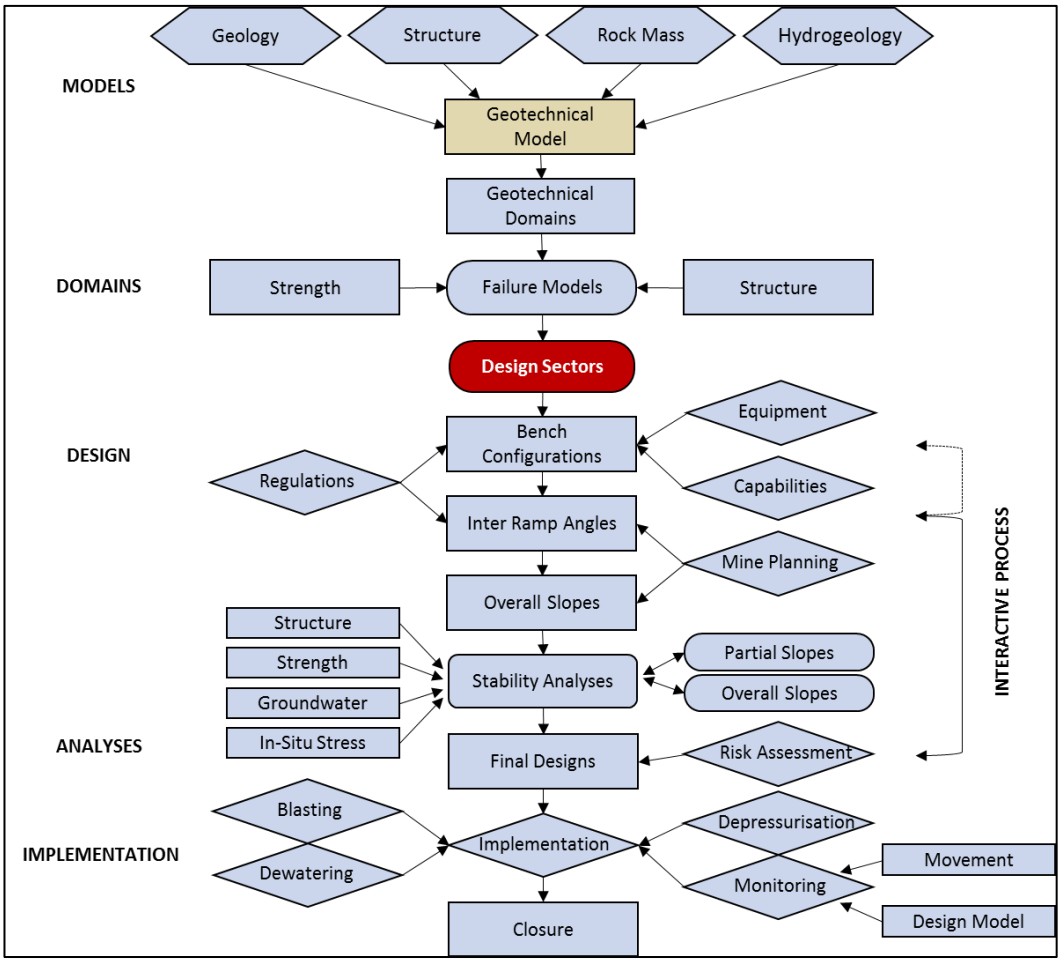


Figure 56 The slope design process (*Read and Stacey, 2009*)

According to Read and Stacey (2009), certain degrees of safety, economic and financial risk have always been implicit in mining operations. In open pit mines, slope instability is one of the major sources of risk, largely due to data uncertainty, as well as the generally modest levels of stability accepted for designs. With the increasing requirements for management to be involved in the decision-making

process for slope designs, risk quantification is necessary. The objective of risk-based design is to provide management with quantitative information for:

- Defining acceptable risk in terms of safety and economics;
- Assessing relative risk levels for different slope configurations;
- Benchmarking risks against industry norms and the corporate mission statement.

Steffen (1997) addresses the methodology of introducing risk into the open pit mine planning. Recommendations are put forward for achieving a risk balance between mineral resource estimate and slope design. Subsequently, Steffen (2007) stated that mine planning is a typical engineering design function that integrates the disciplines of geology, metallurgy, geotechnics, mining and economics. Slope angles are a key economic and risk parameter in open pits.

Since the objective of mining is to maximize the value, steepening slope angles to their safe limits is always a priority. This is a clear case of evaluating risk against reward, where risk is not the failure of the slope, but the consequences of a failure.

4.2. Applying the New Methodology to Improve the Slope Design Process

In order to reach this goal of optimal and safe extraction (risk vs. reward) of the mineral reserve, mining needs to be progressively more predictable (Vorster, 2001). Satisfactory engineering design mitigating geotechnical risk caused by geological uncertainty involves a design process (Stacey, 2009). According to (Hill, 1983), as discussed by (Bieniawski, 1988), the design process is "a sequence of events within which the design develops logically, and a process that provides a work plan in the planning of a design programme" (also see Bieniawski, 1989, 1991, 1992 and 1993). (Stacey, 2009) compared this engineering design process with the strategic planning approach described by (Ilbury & Sunter, 2005) and found a remarkable correlation. This was found to be not surprising, since engineering design is a strategic up-front issue, and front-end loading in a project is critical to achieve the expected project performance (Stacey, 2009). Based on the close correlation between the strategic conversation and engineering design processes, (Stacey, 2009) proposes a circular design process, rather than a linear process.

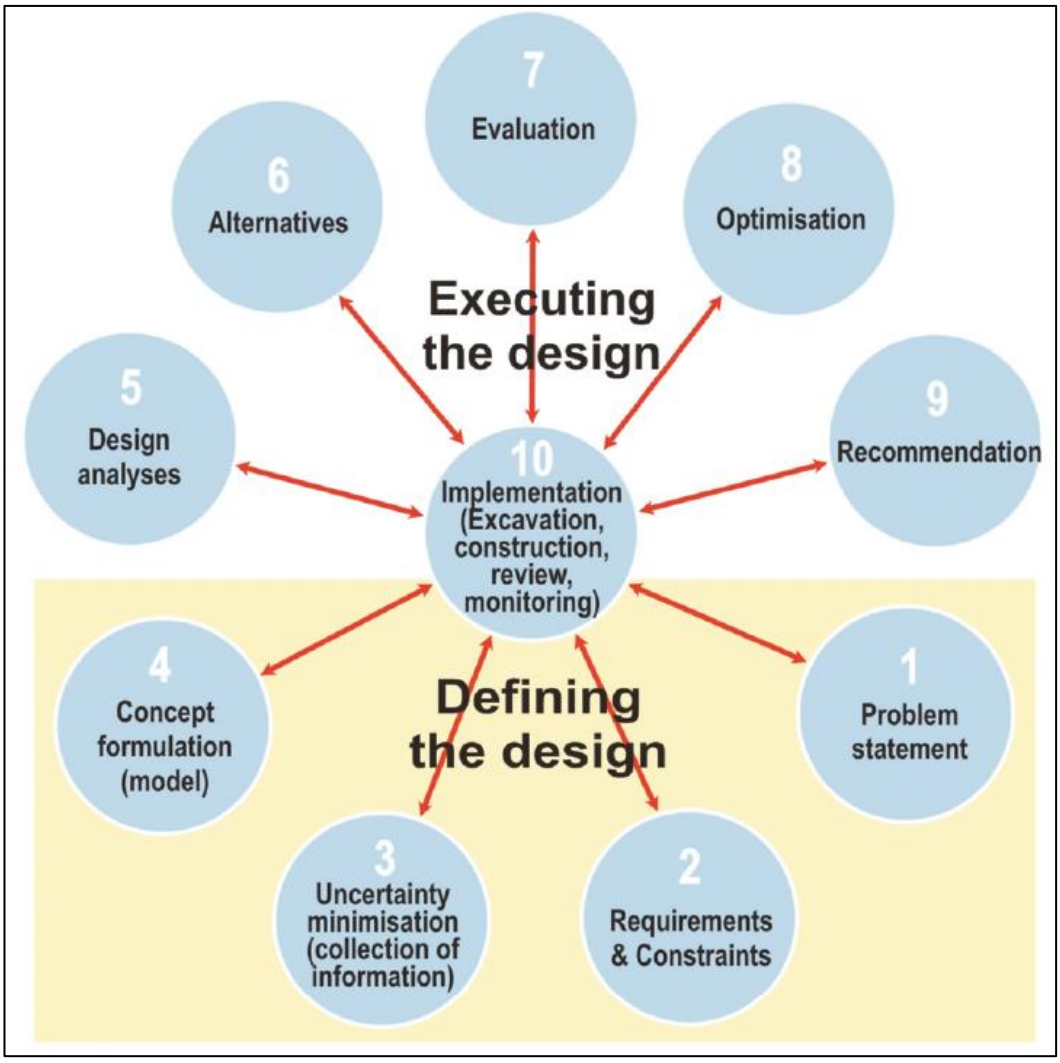


Figure 57 The engineering circle or wheel of design *(Stacey, 2009)*

The "circle of design" (Figure 57) better reflects the importance of review and monitoring in the two phases of successful design and implementation – defining the design and executing the design (Stacey, 2009).

Based on these principles, the methodology discussed in the previous Chapter can be incorporated in the slope design process from early stage projects through to operational mines' planning cycles to achieve expected project performance. Appendix 1: Examples of a Mine Planning Cycle (annual or bi-annual) and a more Detailed Process Jointly Performed by the Mine Planning and Geotechnical Engineering Functions. shows examples of a mine planning cycle (annual or bi-annual) as well as a more detailed process jointly performed by the mine planning and geotechnical engineering functions.

According to Read & Stacey (2009), there are six main levels in the development and execution of a mining project in which slope design input is required. Details on suggested levels of confidence in geotechnical information can be found in Table

17. The steps in the process illustrated in Figure 58 during project phases will now be discussed.

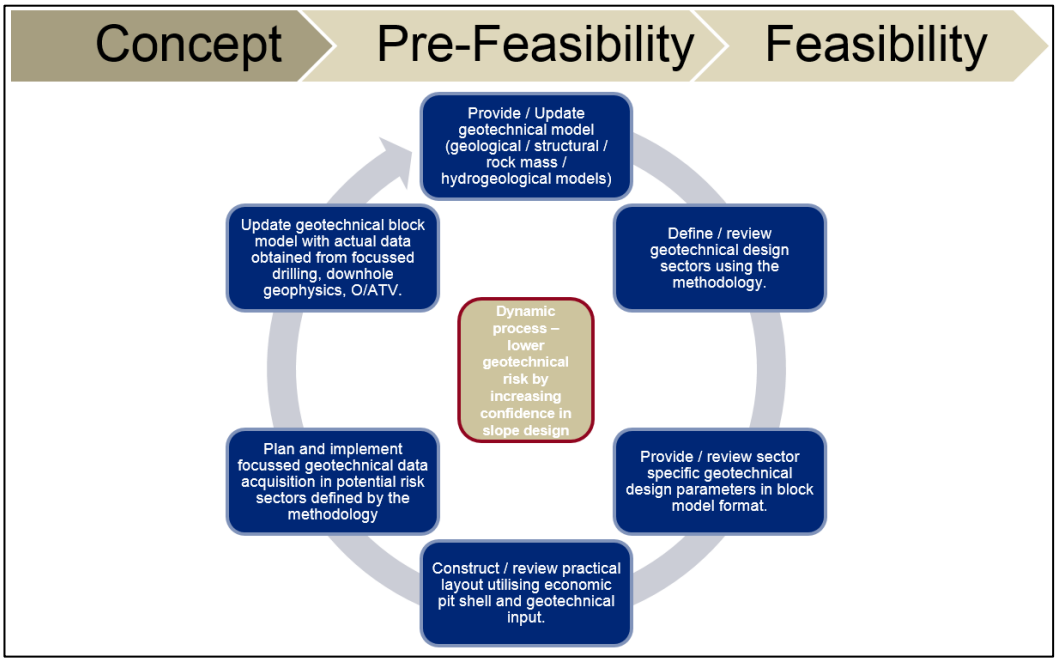


Figure 58 The methodology improves the slope design process during early project stages.

4.2.1. Concept stage

The objective of this stage is to look for fatal flaws and to refine investigation with new data. The major drivers of the project should be identified if possible (Read & Stacey, 2009).

Provide a Geological/Structural/Rock Mass/Hydrogeological Model

Concept stage geological-, structural- and hydrogeological models are available to inform the geotechnical model. Geotechnical data acquisition should start as early as possible in the exploration program to inform the rock mass model. This includes geotechnical logging and point load testing of exploration core for rock mass characterisation of all lithologies. This would typically include:

- Collar data
- Material recovery
- RQD
- Geotechnical zone data
- Discontinuity data (joint spacing / fracture frequency /joint characteristics)
- Structural features
- Rock strength data

A laboratory testing program should also be initiated to inform input parameters for slope stability analysis as the design of safe and economically viable slopes can be significantly influenced by the quality and quantity of collected data (Fillion & Hadjigeorgiou, 2017).

According to Read & Stacey (2009), data uncertainty leads directly to unreliability and possible poor pit slope performance. Increased Fall of Ground risk could therefore be a direct consequence of geotechnical data uncertainty. In order to address this risk, target levels for the four aspects informing the geotechnical model were suggested by Read & Stacey (2009) and are represented in Table 17.

Table 17 Suggested target levels of data confidence *(Read & Stacey, 2009)*

Target levels	Conceptual	Pre-Feasibility	Feasibility	Design and construction	Operations
Geology	>50%	50-70%	65-85%	80-90%	>90%
Structural	>20%	40-50%	45-70%	60-75%	>75%
Hydrogeological	>20%	30-50%	40-65%	60-75%	>75%
Rock Mass	>30%	46-65%	60-75%	70-80%	>80%
Geotechnical	>30%	40-60%	50-75%	65-85%	>80%

Addressing confidence in the rock mass model, Fillion (2018) describes how small sampling theory can be used to determine the minimum number of specimens to reach targeted levels of confidence from 30 to >80% for normally and lognormally distributed data.

Fillion (2018) demonstrated, by utilising small sampling theory, that the number of test results has a significant impact on the decision process through project stages and identifies the need for additional data to adhere to design stage reliability criteria. The sequence of testing of the rock core samples is also shown to have an important role in defining appropriate sampling and testing strategies. Due to the potential spatial correlation of the test results, a sampling strategy that maximises the distance between the sampling points can minimise the influence of the testing sequence. The proposed method can easily be applied to analyse any series of laboratory testing data. Probably its greater potential is as a tool for reviewing the ongoing database of a project and justify if further data collection is necessary according to suggested levels of confidence (Fillion & Hadjigeorgiou, 2017).

Furthermore, to inform the concept stage rock mass model for projects that exhibit anisotropy, a generally applicable approach is to apply a Synthetic Rock Mass (SRM) methodology to characterise rock mass anisotropy. This technique was discussed in detail in Chapter 2 and accounts for the spatial variability of various parameters, such as orientation, persistence and termination, each of which is assigned a statistical distribution in a series of model realizations.

Although no mapping information is available in early stage projects, core logging information can inform discontinuity spacing and orientation data that can be determined from a well constrained 3D geological and structural model.

Conservative assumptions regarding persistence can be made based on existing knowledge. The synthetic rock mass (SRM) approach can therefore be utilised to capture the important effects anisotropy has on the rock mass strength as it is not possible to explicitly represent each of the aspects affecting the behaviour of a highly heterogeneous system, such as that of a large-scale rock mass.

Therefore, utilising said approach provides conceptual level stage implicit results that can be obtained by adjusting the implicit results to the explicit average strength curve derived from SRM analyses. These implicit properties can be used in 3D geometrical analysis and should be refined as the project advances through its life cycle and more information becomes available.

Early Definition of Geotechnical Design Sectors using the 3D Geometrical Analysis Methodology

The next step is to define geotechnical domains based on lithological units. Lithological units with similar characteristics may be classed together as geotechnical domains. Considering geological structure and the conceptual failure model at this stage, geotechnical design sectors can then be identified utilising the 3D geometrical analysis methodology discussed in Chapter 3. To account for the interaction of slope orientation with geological features in geologically complex (anisotropic) environments, a pit layout is required. Even if a practical layout is not yet available, the 3D geometrical analysis methodology can be applied to economic shells derived from programs like Whittle. This can provide a coarse estimation of where one can expect favourable vs. unfavourable interaction of anisotropic units with future pit slope orientations. Utilising the 3D geometrical analysis methodology, Figure 59 shows an example of a Whittle shell draped with geology as well as indicating areas where a pre-concept level geological interpretation shows favourable (dipping away) vs. unfavourable (dipping into) interaction of bedding planes with future slope orientations.

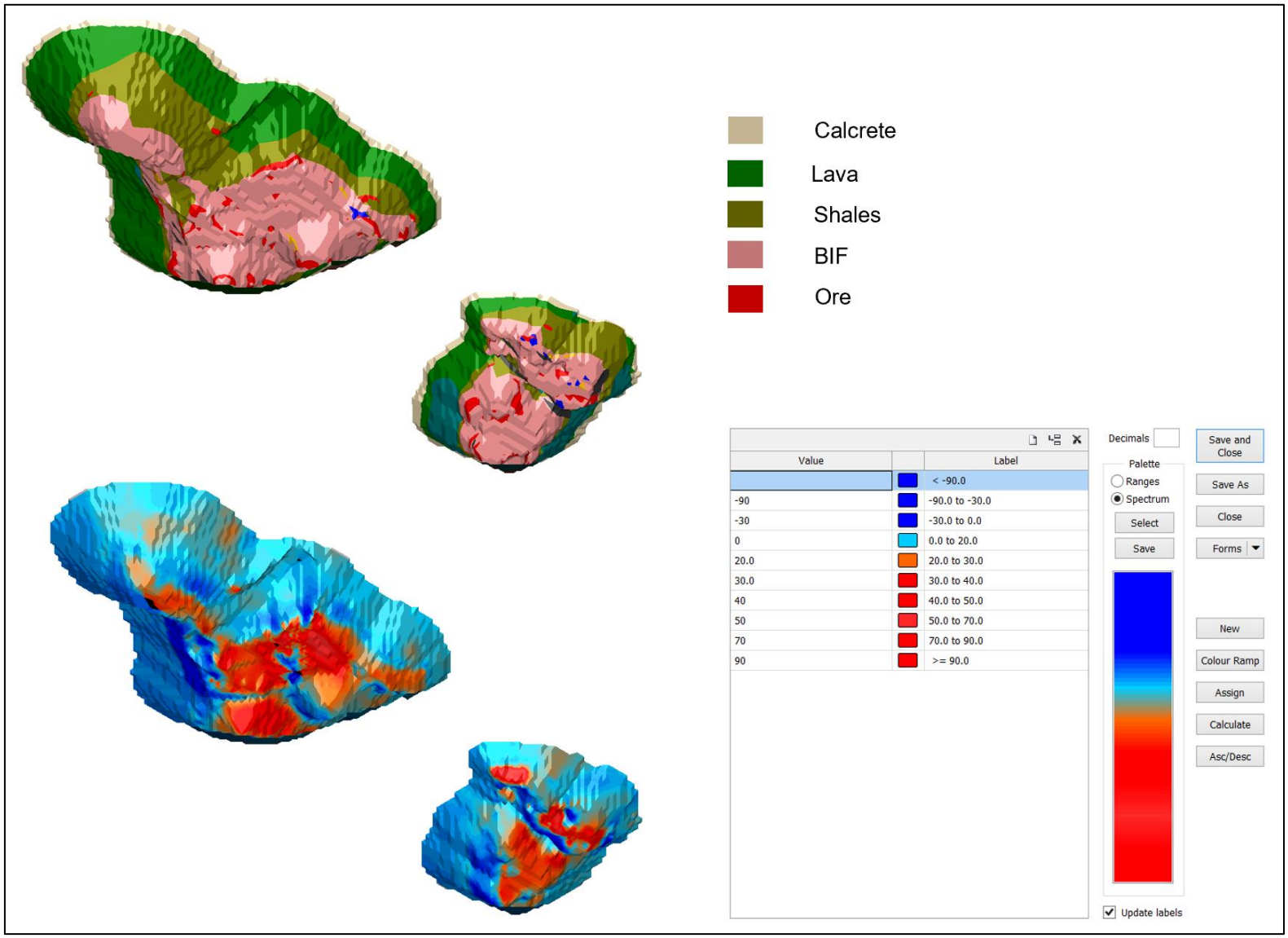


Figure 59 Example of Whittle shell draped with geology (top) and apparent dip (bottom). Apparent dip was binned and contoured to show favourable (dipping away, 0 to -90 degrees, blue) vs. unfavourable (dipping into, 0 to 90 degrees, red) interaction of bedding planes with future slope orientations.

Utilising this information, early stage geotechnical design sectors can be delineated based on conceptual failure models.

Provide Geotechnical Design Parameters in Block Model Format

Utilising the available geological model, the next step is to populate a geotechnical block model with specific design parameters, i.e. bench height, face angle, inter ramp angle, bench width etc. This is done per design sector based on conceptual stage geotechnical design input for use in the construction of a practical pit layout. Practical aspects related to the geotechnical block model as the main output from the geotechnical engineering function will be discussed in detail later in this Chapter.

Practical Pit Layout Construction

Initial practical layouts can be constructed rapidly utilising available tools like Trimble Top Design (Trimble Inc., 2019) that reads geotechnical design input directly from the geotechnical block model. Once a practical pit is available, the 3D geometrical analysis can be run again on the layout to determine favourable and unfavourable areas and to review design sectors (Figure 60).

Additionally, at this very early stage, results from the 3D geometrical analysis can inform practical considerations such as ramp placement to ensure ramps are in the most favourable areas where possible.

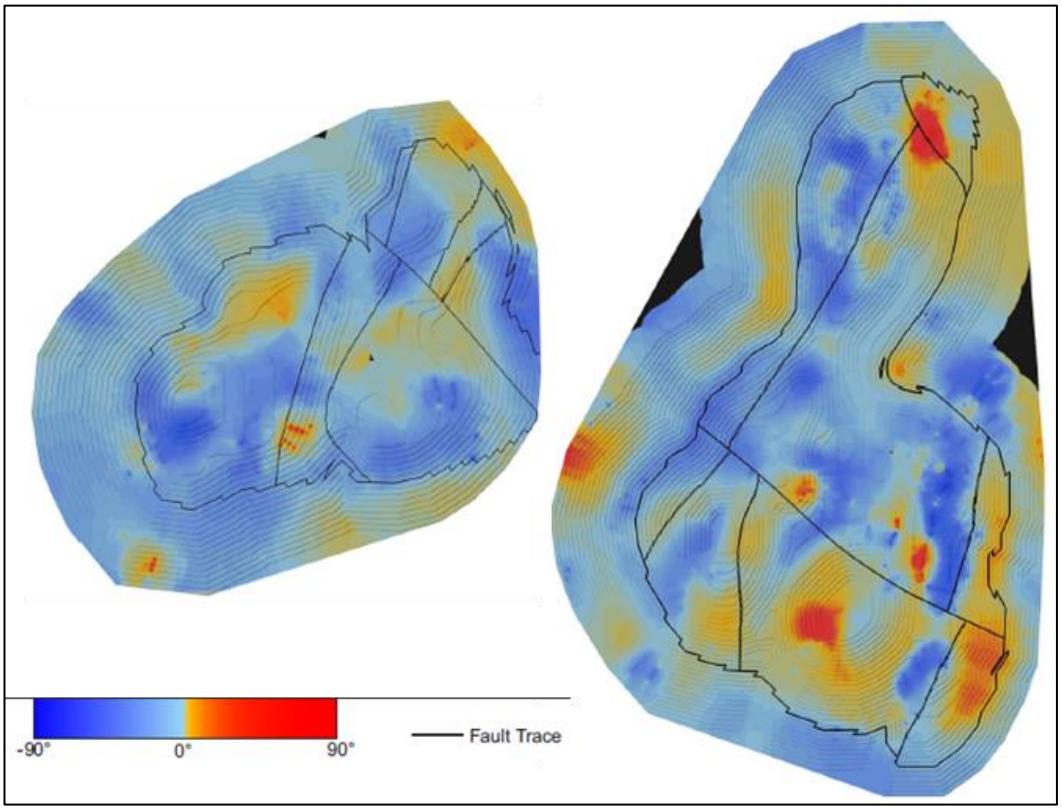


Figure 60 Example of apparent dip analysis on early stage pit layout {Note that layout has no ramps yet and apparent dips only contoured to show dipping into the pit (red) and dipping out of the pit (blue)}.

Geotechnical Data Acquisition

The next step is to plan and implement continued geotechnical data acquisition campaigns utilising the 3D geometrical analysis results, focussing on areas showing unfavourable interaction between geological features and slope orientation. This includes dedicated geotechnical drilling with downhole surveys (OTV/ATV) to determine orientations and further develop the geological, structural and rock mass models as discussed earlier. Figure 61 is an example of a downhole survey log for an optical televiewer.

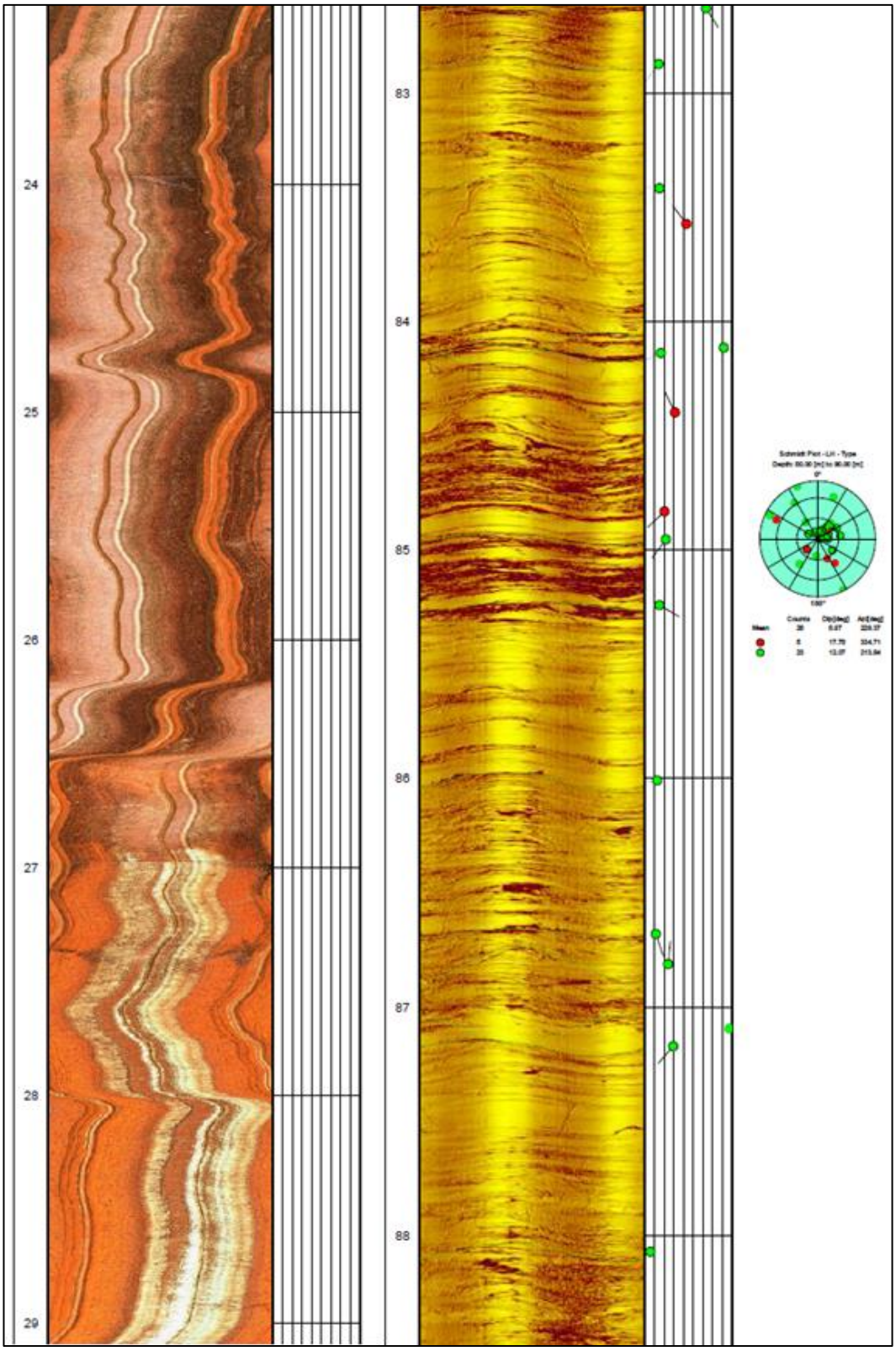


Figure 61 Example of downhole survey log (OTV) showing 23 – 29 m interval on the left and 83 – 88m interval on the right. Joints and bedding are interpreted from the log with, in this example, green and red pins each with dip and dip direction.

As previously stated, the focus at concept stage is to refine models with new data to address the 3 key contributors to geotechnical data uncertainty by focussing data acquisition programs initially in areas that show possible unfavourable interaction indicated by the 3D geometrical analysis (Read & Stacey, 2009):

- Geological uncertainty

This includes uncertainty regarding geometries and relationships between lithologies and structures (focussed geotechnical drilling with Optical /Acoustic Tele viewer).

- Parameter uncertainty

Typically, uncertainties associated with values adopted for rock mass and hydrogeological model parameters {Utilising small sampling theory as described by Fillion, (2018) to reach targeted levels of confidence}.

- Model uncertainty

Uncertainty associated with the selection process of stability analysis tools and the different types of slope stability analysis methods available. Model uncertainty exists if there is a possibility of obtaining an incorrect result even if exact values are available for input parameters. Continued data acquisition improves confidence and understanding of conceptual failure models leading to the application of the correct analysis methods and tools.

Update Geotechnical Model with New Data

Once new information is obtained, apparent dip maps and the geotechnical block model can be updated with actual data.

Data collection (front end loading in a project) is the first step in the design process, and the outcome of geotechnical analysis will be influenced by the quality of the input data. The effort in collecting good, sufficient and reliable data is justified given the increased access to sophisticated and powerful computational tools for the design process (Fillion & Hadjigeorgiou, 2017).

From here, a circular design process should be followed to achieve the expected project stage gate criteria and suggested levels of confidence. This is to reduce geotechnical risk by increasing the confidence in the slope design through focussed data acquisition.

The importance of water and its associated environmental impact due to mining activities are also critical for all operations and projects. In future it will most probably be one of the key drivers determining whether a project develops into the implementation stage or not. Therefore, early stage project front end loading (following a circular process) of hydrogeological parameters and associated environmental aspects are vital to ensure an effective and efficient dewatering system (Bester, et al., 2013).

4.2.2. Pre-Feasibility Stage

The objective of this stage is to ensure a robust business case exists before proceeding to the next stage. This stage does not look to optimise the project, capital or operating plan. The stage will test major operating options to establish a robust case. The major drivers of the project need to be identified (Read & Stacey, 2009).

4.2.3. Feasibility Stage

The objective of this stage is to determine the best operating configuration and to refine it for capital and operating costs and revenues. This stage refines data and assumptions following the circular process suggested to enable the corporation to report reserves (Read & Stacey, 2009).

4.2.4. Design and Construction Stage

The objective of this stage is to construct the project on time and within budget and to transfer skills to operations staff from construction staff. Pre-stripping would fall into this stage. Developing the necessary action plans by discipline or function in enough detail to assure a smooth implementation from commencement of construction until early operations (Read & Stacey, 2009).

4.2.5. Operations

The objective of this stage is to execute mine production plans to the most efficient level possible including health, safety and loss prevention while maximising return on investment. For the geotechnical engineering discipline, this stage involves using pit phase implementation as a test of what to expect when the final walls are achieved, based on present material interpretation and current procedures and practices for loading and blasting (Read & Stacey, 2009). The steps in the process illustrated in Figure 62 during implementation, will now be discussed.

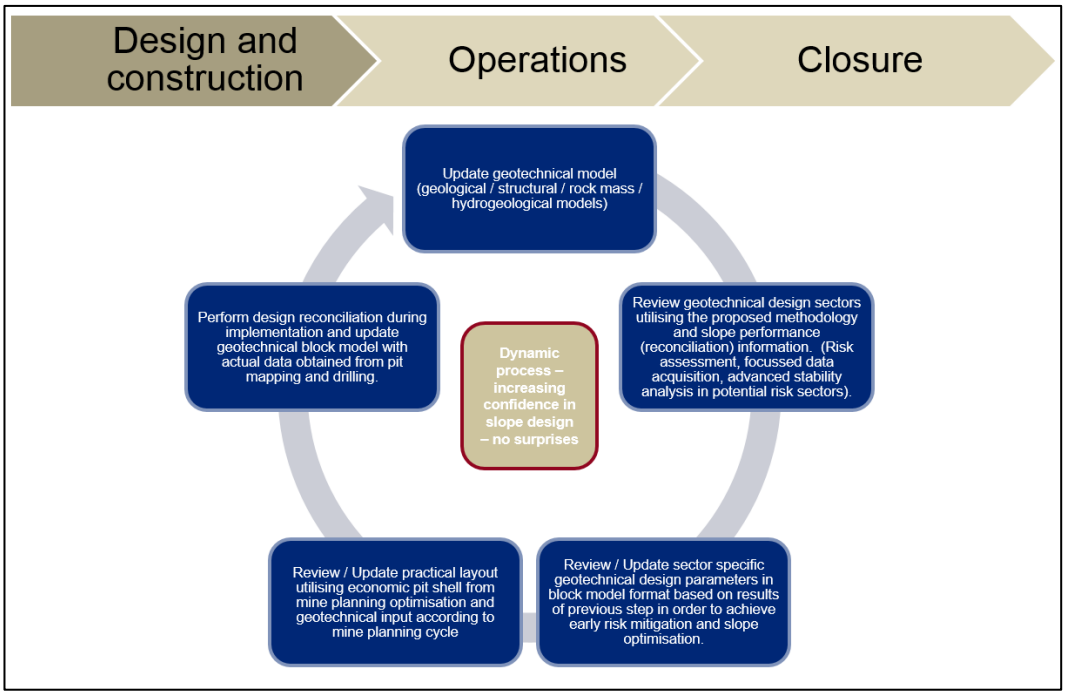


Figure 62 The methodology improves the slope design process during implementation.

Update the Geological/Structural/Rock Mass/Hydrogeological Models

To reiterate, continued collection of geo-mechanical data to inform the rock mass model during mine development may contribute to reducing the uncertainty associated with the geotechnical properties informing the slope design (reaching suggested levels of confidence).

Fillion (2018) showed that the variability of the input data can be significantly different from one project stage to another, resulting either in a wider or in a narrower factor of safety (FoS) distribution once the operational stage is reached. Effectively, she found that in some cases, a wider distribution for the FoS values was obtained at subsequent stages, which implies that data variability may be larger at more advanced project stages. This supports the generally accepted concept that collecting additional data may sufficiently reduce the uncertainty associated with data variability to support decisions on optimising slope designs. Further conclusions reached by Fillion (2018) include the following:

- the minimum number of specimens for lognormally distributed data is higher than for data normally distributed to reach targeted confidence levels,
- The decision to test more specimens or not should be made with the knowledge of the confidence level in the data. Based on the conceptual failure model, it may be acceptable / justifiable to accept a lower confidence interval for available samples – resulting in a slightly reduced lower limit instead of incurring costs of more testing. Therefore, if the confidence level is lower than the target, in some cases this may be acceptable / justifiable

based on a sensitivity analyses to determine if the resulting wider confidence interval of the parameter is critical for stability analysis.

- Applying subject area expertise to all aspects of hypothesis testing is crucial. Engineering judgement about the plausibility of the results needs to be applied. Geotechnical knowledge should transform statistics from numbers into meaningful, trustworthy findings.

Similarly, data obtained from operational drilling campaigns (in-fill drilling), dedicated geotechnical drilling and mapping campaigns should be used to update the geological and structural aspects of the geotechnical model.

Regarding hydrogeology, a structured approach according to engineering design principles (circular process) is suggested for the design and implementation of mine dewatering systems (Figure 63) (Bester, et al., 2013) . Although not illustrated, the validation of the design (reconciliation) is equally important.

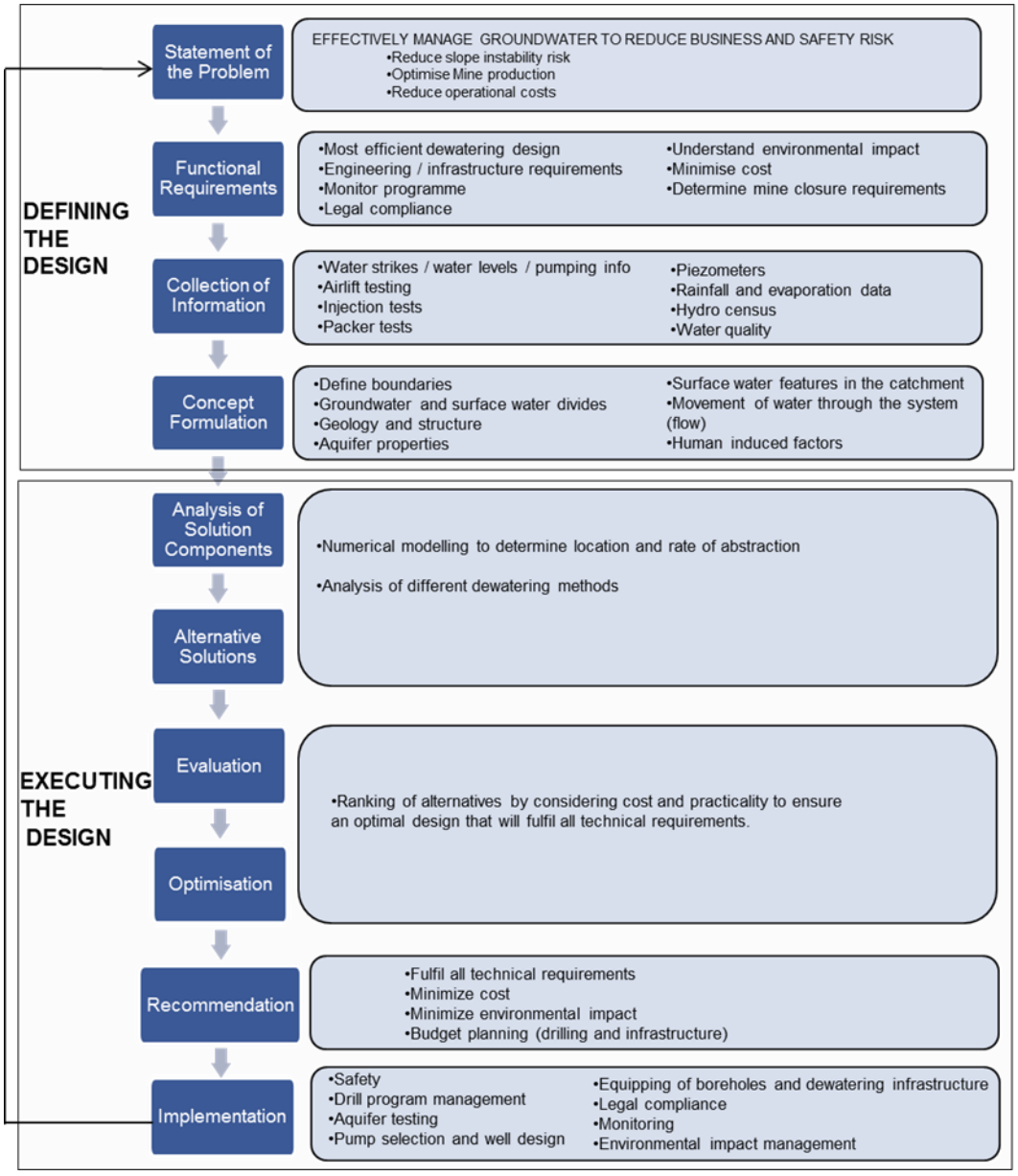


Figure 63 A summary of the design process for mine dewatering according to engineering design principles *(Bester, et al., 2013)*

Review Geotechnical Design Sectors

The next step is to review geotechnical design sectors by performing a 3D geometrical analysis based on the latest available data from the geotechnical model as discussed in the previous Section.

Review Sector-Specific Geotechnical Design Parameters in Block Model

Format

Based on latest information and geotechnical risk assessments, input parameters in the geotechnical block model as input to the mine planning process need to be reviewed with the goals of achieving early risk mitigation and optimised slopes.

Review Practical Layout According to the Mine Planning Cycle.

Stability analyses on the latest pit layout is conducted during this step. The use of vertical 2D design sections is optimised due to the improved establishment of the sizes and geometries of design sectors by using the 3D geometrical analysis from early project stages, based on well-constrained 3D models and the input obtained from synthetic rock mass modelling. Once mine schedules are available, geotechnical and mine dewatering risk assessments are conducted. Based on the conceptual failure model, design sectors of concern highlighted by the 3D geometrical analysis, informs the risk assessments leading to further focussed data acquisition and advanced 3D stability analysis to achieve early risk mitigation as well as slope optimisation in favourable design sectors with lower risk.

Perform Design Reconciliation

Due to the risk associated with inherently variable properties and characteristics of natural materials, (Bester, et al., 2018) discuss the importance of design reconciliation during mining implementation by summarising key aspects of slope design reconciliation, i.e. mine to design including mine residue deposits (slope geometry), blast design reconciliation (face conditions), rock mass response to mining, groundwater response and structural analysis.

(Russell, 2017) discusses face mapping as a simple but invaluable means of geological or geotechnical data acquisition whereby intact rock properties, rock mass properties, discontinuity properties and structural orientation can be assessed. Although traditionally done via direct contact with the mapping face through techniques such as line mapping or window mapping, remote face mapping using various digital techniques has become increasingly popular in recent years.

Face mapping systems that use a point cloud generated by a terrestrial laser scanner in conjunction with a concurrent scanner generated photographic overlay represent a rapid and practical means of collecting the raw data required for geotechnical face mapping in the open pit mining environment (Figure 64) (Bester, et al., 2018).

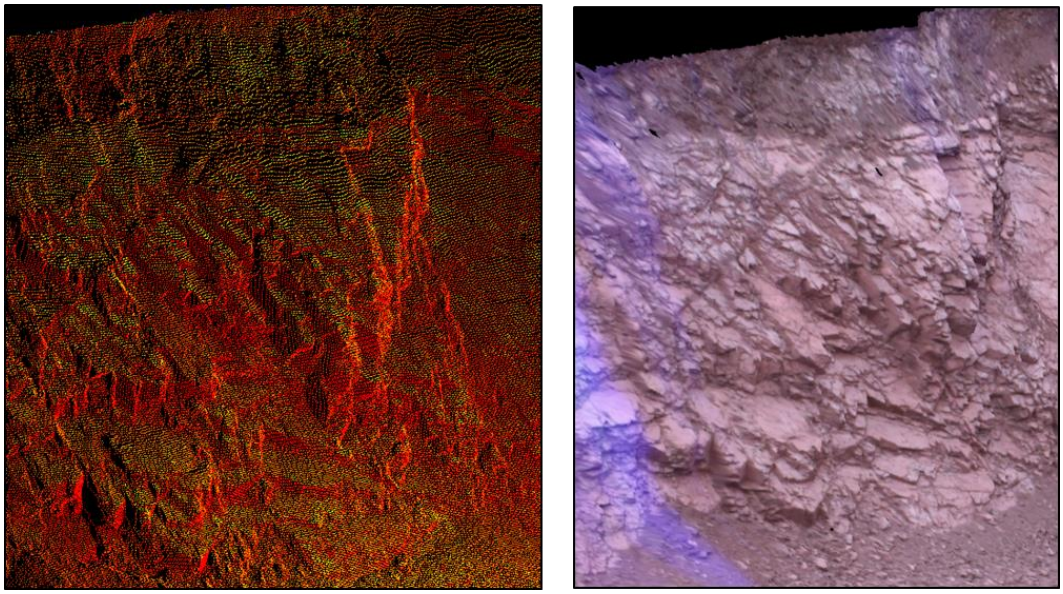


Figure 64 Raw high-density scanner point cloud (Left) versus point cloud with concurrent photographic overlay (Right) *(Bester, et al., 2018)*.

Digital face mapping systems are generally incorporated into the point cloud processing software released with terrestrial laser scanner systems produced by various manufacturers.

Utilising digital face mapping systems, various rock mass and structural parameters can be captured remotely, without the practical constraints and safety aspects associated with approaching pit faces during manual face mapping exercises. Built in functionality of point cloud processing software such as I-Site Studio (Maptek Pty Ltd, 2018) allows for accurate orientation measurements as well as for the capture of parameters such as discontinuity spacing and persistency (Figure 65) (Bester, et al., 2018).

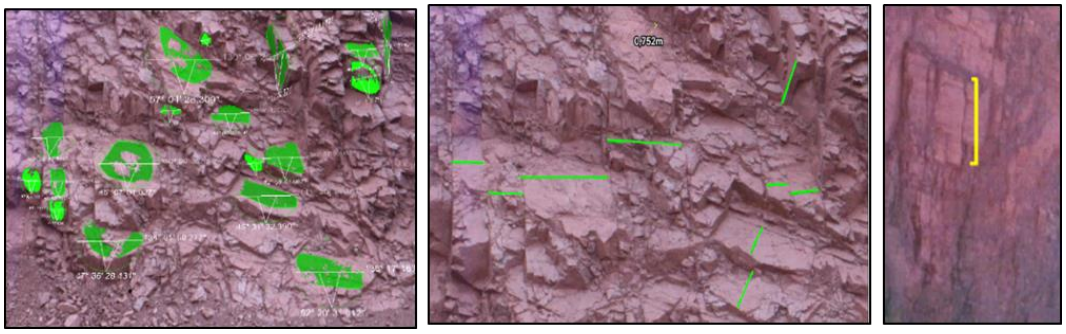


Figure 65 Orientation, Spacing and Persistency measurements taken using the geotechnical and CAD functionalities of I-Site Studio *(Bester, et al., 2018)*.

These parameters are not only essential in performing kinematic analysis and rock mass characterisation, but also to continuously (circular process) refine the synthetic rock mass models discussed in Chapter 2 as input to 3D geometrical analysis of slope-structure interaction. Geotechnical mapping combined with

Discrete Fracture Network (DFN) analysis is currently the only way to accurately determine specifically the persistence of discontinuities that has a critical influence on rock mass behaviour.

Slope reconciliation programs should provide the information needed to progressively validate and refine the geotechnical models, in particular the underlying geological model (Read & Stacey, 2009). This should incorporate all scale components including bench scale, inter ramp and overall slopes. This information should be reviewed periodically, usually according to the mine planning cycle. Reconciling actual geology and structure vs. the model that was used to conduct slope stability analysis and risk assessment, need to be checked against design criteria and the conceptual failure model in order to inform risk assessment of the lower levels of the slope.

A geological model that incorporates large scale structures, an interpretation of geological contacts, and inferred bedding orientations are key inputs to inform the geotechnical model utilised throughout the various stages of the geotechnical design process. The structural model itself will inherently contain inferences with a relatively high level of uncertainty as structural assumptions regarding a large volume of rock are made on small and sometimes sparsely distributed data points such as geological boreholes. One of the primary roles of geotechnical face mapping within the design and reconciliation process is to ground proof and inform the inferred structural models with measured field orientation data. Figure 66 gives an example of inferred bedding orientations (red and blue) projected onto a design pit versus laser scanner face mapping measured orientations (green arrows), taken from the exposed area of the pit (Bester, et al., 2018).

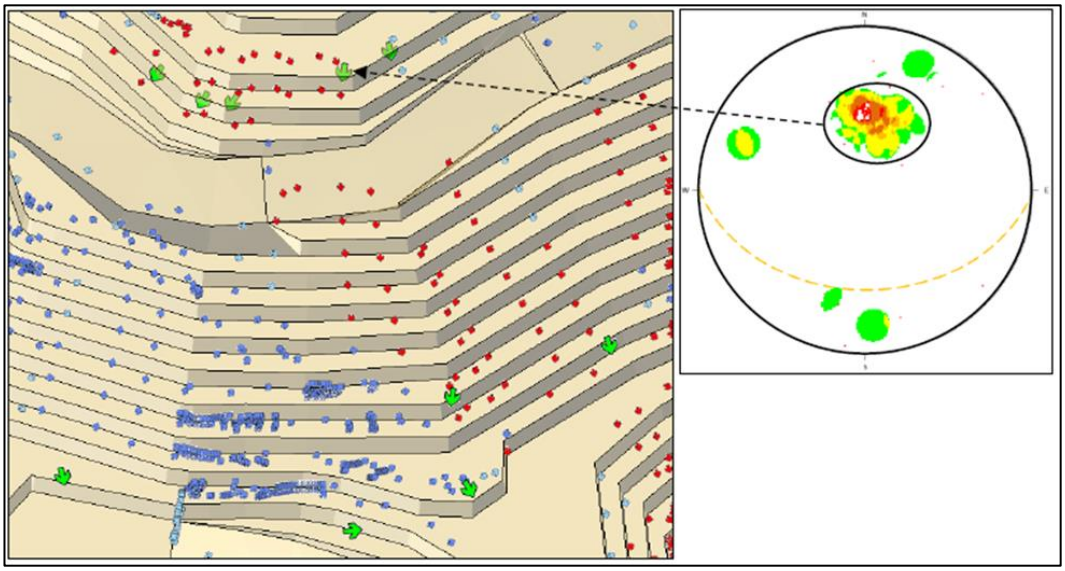


Figure 66 Example of an overlay of actual mapped (Green arrows) and inferred bedding orientation measurements from the geological model (Red and Blue Arrows) *(Bester, et al., 2018).*

With respect to the slope design process, delineation of a particular design sector and accurate analysis of the stability of design slopes therein, is heavily dependent on the available structural data. Following on from design and stability analysis, effective implementation of the design is reliant on prevailing structural conditions, particularly in an anisotropic rock mass. The actual structural information provided by face mapping to progressively supplement and inform an inferred structural model (Figure 61), increases model confidence, thereby increasing confidence in the slope design and stability. As with most aspects of the design process, this is iterative. As a pit is mined out, faces are mapped which feeds into the structural model, which in turn informs future slope design and geotechnical risk assessment.

Figure 67 illustrates an example of reconciliation between inferred bedding orientation data points and actual measured values. In this example bedding dip direction values for inferred data points within 100m of each mapping face centroid have been compared with the measured bedding dip direction from the mapping face in question.

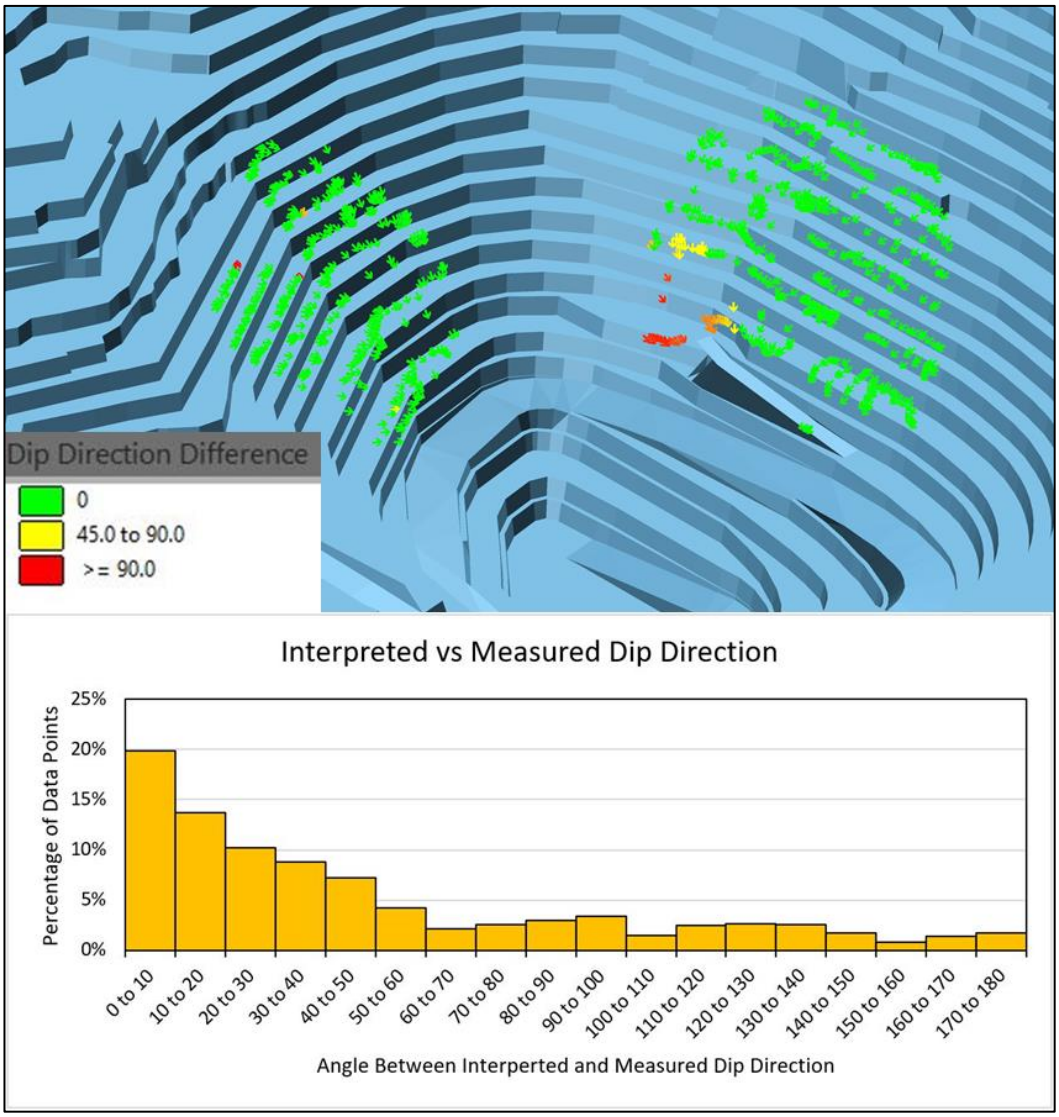


Figure 67 Example of conformance between actual measured dip direction and inferred dip direction based on lithological contacts (Inferred data points within 100m of mapping face centroids). Example face centroids – above, Distribution in deviation for model wide face mapping data – below *(Bester, et al., 2018).*

Similarly, Figure 68 shows an example of a measured fault position from a mapped pit high wall versus interpreted fault positions from the site's structural model. Smaller scale faults mapped with similar orientation than larger scale faults in the structural model, is good indication of the accuracy and therefore confidence in the structural model.

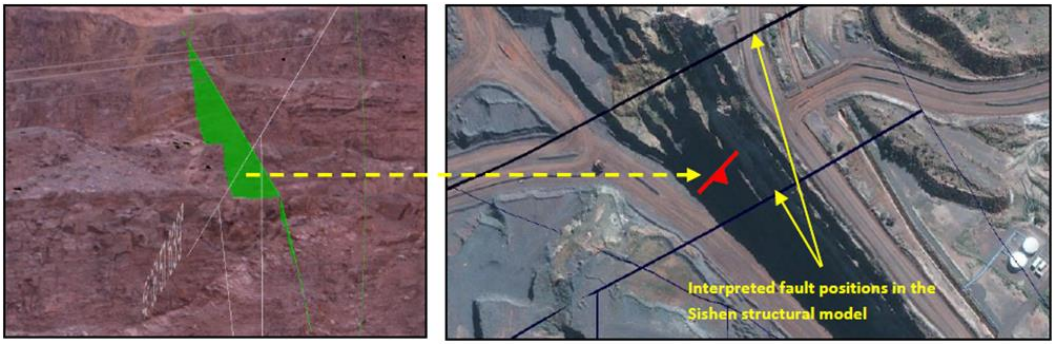


Figure 68 Example of inferred faults versus a measured fault location in an exposed portion of a high wall *(Bester, et al., 2018).*

By following the circular process discussed earlier, confidence in a predominantly interpreted structural model can be progressively improved by comparison with actual mapping data acquired during deployment of the pit.

Accordingly, the geotechnical design process is iterative and slope design and geotechnical risk assessment need to be reviewed based on available data according to the mine planning cycle. Geotechnical face mapping is an excellent means of rapidly acquiring structural, kinematic and rock mass data required to inform and update existing geotechnical models and designs. As high wall faces are exposed during mining, face mapping allows for the immediate comparison of actual geotechnical conditions with those predicted from available information prior to exposure.

This type of reconciliation may be relevant for reviewing slope designs, assessing current and potential future geotechnical hazards and informing blast designs.

Overall, geotechnical face mapping is considered an invaluable tool in the slope design reconciliation process.

4.2.6. Mine Closure

This stage is focused on the physical and chemical stability of materials and effluent products of mining activity to ensure care of human health and environment. Furthermore, it focusses on the sustainable usage of land post mining activity and the mitigation of social effects in communities when operations cease. (Read & Stacey, 2009).

The role of geotechnical and hydrogeological aspects in mine closure will remain critical in any successful closure project. The 3D geometrical analysis methodology improves the definition of design sectors leading to more accurate closure considerations per design sector. Therefore, a similar, iterative approach (refer to Figure 69) is suggested for geotechnical and hydrogeological input to mine closure planning with the aim of continuously improving confidence in estimating closure risk and the cost of associated controls throughout the life of a mining project.

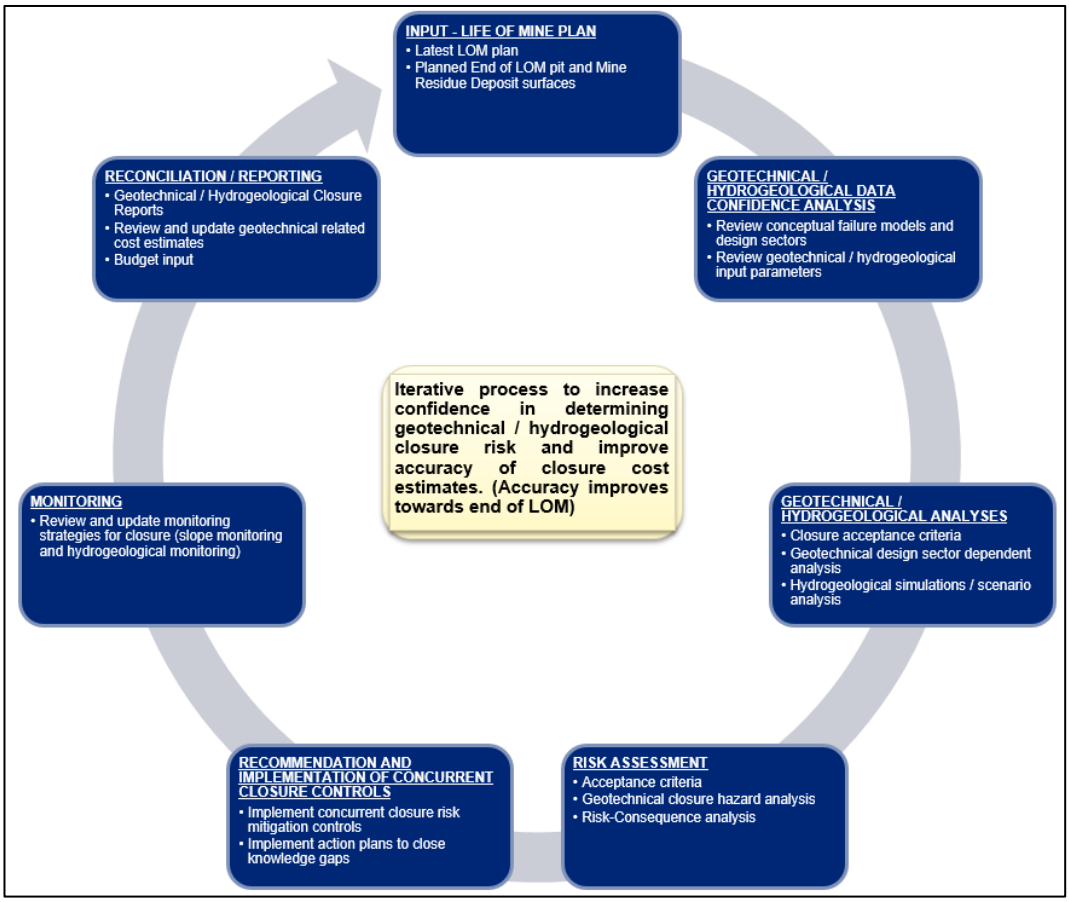


Figure 69 Suggested approach for geotechnical and hydrogeological input to mine closure according to the mine planning cycle.

4.3. The Geotechnical Block Model as the Main Output from the Geotechnical Engineering Function

(Bye, 2003) discussed the development of a computerised 3D, geotechnical model containing geotechnical parameters, namely RMR, UCS, FF/m and RQD. The research focussed on the practical application of the 3D geotechnical model through the development of both a fragmentation and slope design model with the aim of providing an engineering tool to optimise mining and processing performance. The research enabled detailed geotechnical information to be available in three dimensions that can be readily accessed and interpreted, thus providing a powerful planning and financial tool from which production optimisations, feasibility studies and planning initiatives can be implemented (Bye, 2003).

To support the iterative process discussed earlier, the development of a geotechnical block model as the main output of the geotechnical engineering function, is essential to facilitate a dynamic model that can be continuously updated with new information. It also enables seamless outputs to clients, e.g. mine planning and

blasting operations with the main goal of early risk mitigation and slope optimisation.

The development of a geotechnical block model is described in the high-level steps listed below.

4.3.1. The Geological Wireframe Model and Geological Block Model

The geological model (computerised 3D wireframe model resulting from interpreted geoscientific data) is a key input to inform the geotechnical model utilised throughout the various stages of the geotechnical design process. (Ronald, 2017) discusses a list of fundamental considerations for the successful creation of a robust and useful geological model:

- What will the model be used for? (fit for purpose)
- Understand the deposit /area geology
- Incorporate all (trusted) data
- Get to know fundamental data
- Think regionally first, then model down to deposit scale
- Start with a structural "skeleton"
- Keep it as simple as it needs to be
- Don't forget the waste! (critical from a geotechnical client perspective)
- Reconcile shapes in 3D

The geological wireframe model is subsequently utilised to create a block model that will be used for grade estimation. Aspects considered during this process include optimum estimation of block size, sub-blocking, sequenced assignment of material types (segments / zones / domains), interpolation of relevant *in situ* geological characteristics per domain per material type. The aim is ultimately to provide a validated geological block model for resource reporting with clearly stated assumptions and approach followed, and subsequent input to mine planning for reserve reporting.

4.3.2. Creating a Geotechnical Block Model

Typically, the geological block sizes required for grade estimation are smaller than what is practical for geotechnical engineering and mine planning purposes. The next step therefore is to "up block" the geological block model to a site specific smallest mining unit (SMU). Figure 70 illustrates the Sishen geotechnical block model derived from the geological block model as an example. The SMU of a mine is typically a function of bench height, equipment size and blast block sizes. Fields not required can be deleted from the model to improve computational ease of use. Alternatively, a block model can be created directly from the wireframe model stipulating required block sizes based on the site-specific SMU.

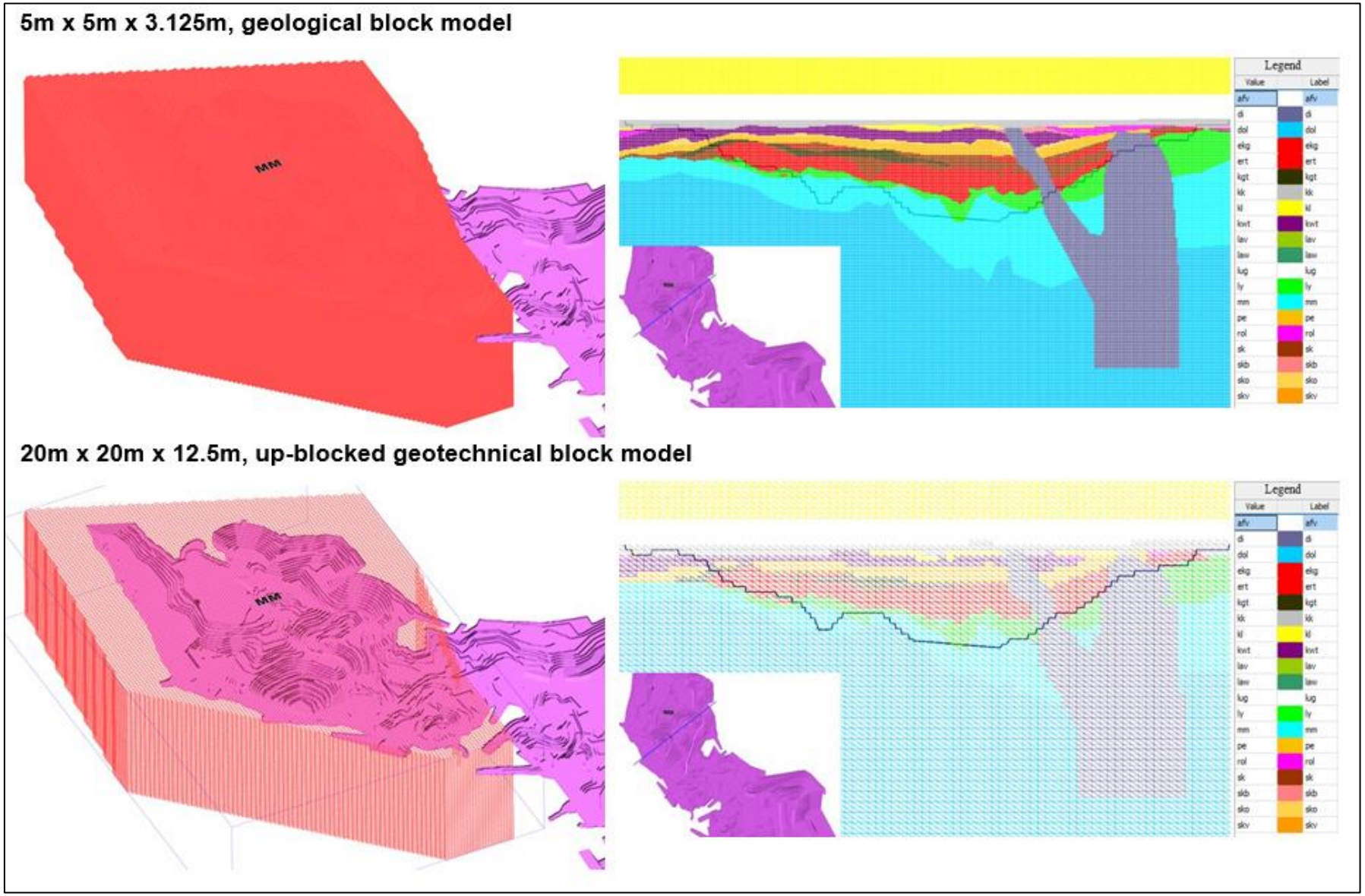


Figure 70 An illustration of the Sishen geotechnical block model (below) up-blocked from the geological block model (above) with a cross Section through both models.

4.3.3. Assign Geotechnical Attributes and Design Parameters to the Geotechnical Block Model

The next step is to create attribute fields for each block in the model. These attribute fields typically can be numerical, text or calculated fields. Suggested attribute fields for a geotechnical block model include the following:

- Spatial attribute fields

These include x-, y- and z-coordinates and fields describing the block size, e.g. 20m x 20m x 12.5m in the case of Sishen Mine according to the SMU.

- Lithology code

This field contains geological codes for the different material types.

- Segment code

A segment code should be used if different lithologies with similar mechanical properties are grouped together, e.g. the pebble layer and weathered lava are grouped together with clay at Sishen Mine.

- Density (in situ)

This field is carried over from the geological block model for input in slope stability analysis as well as to perform tonnage calculations using the block model.

- Design sector

This field contains the name of a specific design sector following the methodology described in Section 3.4. Unique geotechnical design sectors can be defined incorporating data obtained from apparent dip maps and utilising various strength models (including anisotropic strength envelopes from SRM's) according to the conceptual failure models. The geotechnical block model may then be constrained with these individual design sector solids and populated with sector-specific geotechnical design parameters. This allows the engineer to prescribe specific design parameters for all the blocks in the model within each design sector. This allows flexibility to have different designs in the same lithologies based on slope orientation interaction with geological features. Most of the latest available slope design software, e.g. Micromine, Trimble Top Design, Deswik, Surpac, Datamine, Vulcan have automated pit layout construction tools that read relevant parameters from the block model. These tools have vastly improved the time it takes to construct pits, allowing more time for option analysis and layout optimisation.

- Pit layout design parameter fields

The following slope design parameters should be populated in the geotechnical block model (refer to Figure 71 as an example):

    - Bench height

Usually standard on a mine, except where different satellite pits are mined with different size equipment (10-18m are common in most large open pits).

- Face angle

An effective bench face angle principally aims to undercut as few of the structurally formed planes, wedges or blocks as possible (Read & Stacey, 2009).

- Inter ramp angle
- Berm width

The berm width is a calculated field using equation 7.

Equation 7: Berm Width = Bench Height / tan (Slope Angle)

- Configuration

This field stipulates what bench configuration should be followed, e.g. single bench or double bench configuration.

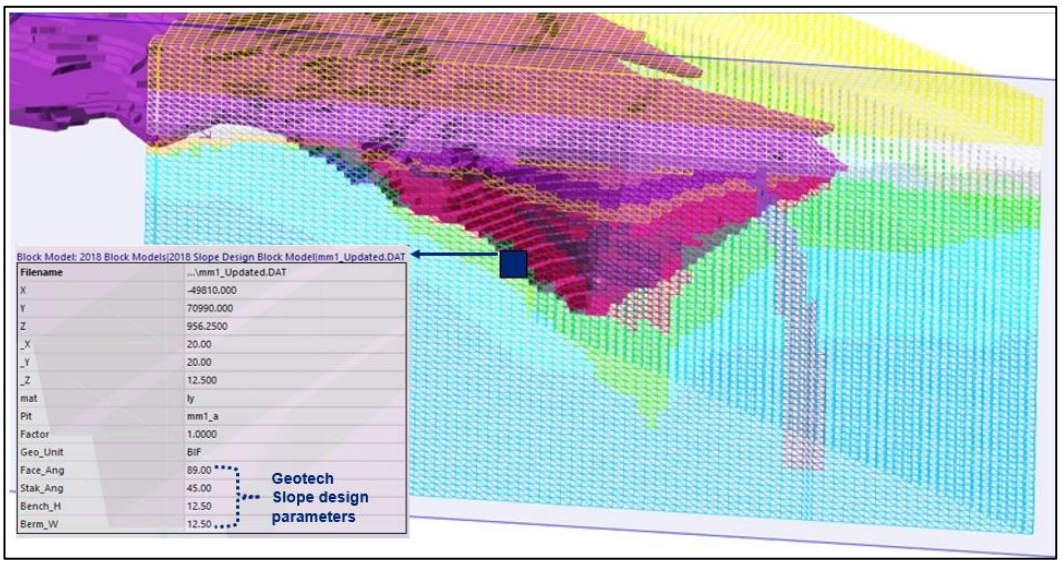


Figure 71 The Sishen geotechnical block model intersected with the pit layout indicating a BIF block with its slope design parameters.

- Rock Quality Designation (RQD)

The most basic form of rock mass classification is the Rock Quality Designation (RQD) first introduced by (Deere, et al., 1967). The system rates borehole core based on the sum of core pieces longer than 10 cm in a core run, expressed as a percentage of the total core run length. In spite of the suggestion by (Pells, et al., 2017), it is suggested that this parameter should be captured as a minimum on all available exploration core from the onset of exploration.

- Rock Mass Characterisation value (GSI / RMR / Q / MRMR)

This field should contain the value from various empirical rock mass rating systems in use such as the RMR (Bieniawski, 1989), MRMR (Laubscher, 1994) and Q (Barton, et al., 1974) systems (Barton & Grimstad, 2014).

The GSI system was initially developed to allow for easy determination of rating values using the GSI chart, whereby a GSI rating is determined by visual comparison of the rock mass structure and discontinuity surface conditions with a set of descriptive values.

Another method of deriving the GSI from measured input data utilised by Kumba Iron Ore operations was proposed by (Hoek, et al., 2013). The GSI is derived using the RQD and the Joint Condition rating from the RMR System (Bieniawski, 1989) through the following formula.

Equation 8: GSI = (1.5 x Joint Condition) + (RQD / 2)

- Uniaxial Compressive Strength (UCS)

Uniaxial compression of rock samples prepared from drill core is probably the most widely performed test on rock (Read & Stacey, 2009). It is used to determine the uniaxial compressive strength (unconfined), σ_c, Young's modulus, E, and Poisson's ratio, υ.

- Discontinuity Spacing or Fracture frequency (FF)

Equation 9: Discontinuity Spacing = 1 / FF

In the most general sense, discontinuity spacing represents the distance between individual discontinuities within a rock mass (Priest, 1993). Discontinuities delineate the boundaries between individual rock blocks. The spacing, persistency and relative orientation of the discontinuities play a major role in the freedom of individual blocks within the rock-mass to move and rotate (Marinos, et al., 2005). Block size and the spacing of discontinuities are key factors in most of the major rock mass classification systems that are used in quantifying rock mass strength as input parameters for slope stability analysis.

- Blastibility Index (BI)

Several empirical rock mass rating systems were developed to deal with rock mass variables in engineering design, e.g. RMR (Bieniawski, 1989), MRMR (Laubscher, 1994) and Q (Barton, et al., 1974) amongst others. The rock mass ratings derived from these systems allow semi-quantitative estimates for engineering design. This concept has been extended by (Lilly, 1986) to include rock mass blastibility (Bye, 2003).

The Blastibility Index (BI) was developed by (Lilly, 1986) with the purpose to develop a tool for the characterisation of a rock mass in terms of ease of breakage by means of blasting. Site specific correlations can then be established between the blast energy factor and the BI.

According to (Bye, 2003), the BI incorporates easily recognisable rock mass parameters, which are significant in affecting blast performance and muck pile diggability. Diggability refers to the ease with which an excavator can load a blasted muck pile.

The calculation of the BI for this attribute field in the geotechnical block model is detailed in equation 10 and the various BI parameters are calculated from the tables and equations below. (Lilly, 1986) noted that the index is heavily weighted towards the nature and orientation of the planes of weakness in the rock mass, as these planes generally control the post blast block size (Bye, 2003).

Equation 10: BI = 0.5 x (JPS+RMD+JPO+RDI+S)

Where:

BI	=	Blastibility Index
JPS	=	Joint Plane Spacing
RMD	=	Rock Mass Description
JPO	=	Joint Plane Orientation
RDI	=	Rock Density Influence
S	=	Rock Strength

- Joint Plane Spacing (JPS)

The joint plane spacing parameter refers to all discontinuities in the rock mass and includes mining induced fractures. The inherent rock mass block sizes, which are bounded by discontinuities, give the engineer a good indication of the post blast fragmentation size. Table 18 details the weighting placed on the degree of jointing when calculating the BI.

Table 18: Joint Plane Spacing (JPS)

	Description	**Rating**
1	Close (<0.1m)	10
2	Intermediate (0.1 to 1m)	20
3	Wide (>1m)	50

- Rock Mass Description (RMD)

The rock mass description is the parameter used to give a general description of the global rock mass conditions (Table 19). This assessment of the global rock mass is extremely important as the fragment size distribution of a totally massive rock will be dependent on the generation of blast induced fractures whereas the fragmentation of a friable rock mass will be dictated by the inherent jointing (Bye, 2003).

Table 19: Rock Mass Description (RMD) *(Lilly, 1992)*

	Description	Rating
1	Powdery / Friable	10
2	Blocky	20
3	Totally Massive	50

- Joint Plane Orientation (JPO)

The orientations of the dominant joint sets in relation to the free blast face plays a major role in blast performance. Planes dipping in the direction of the free face can result in blocky fragmentation and rough floors while horizontal bedding poses few blasting problems. Based on apparent dip maps, pits can be zoned according to dominant joint orientations. Table 20 describes the BI rating for various joint plane orientations in relation to the free face of the blast.

Table 20: Joint Plane Orientation (JPO)

	Description	Rating
1	Horizontal	10
2	Dip out of face	20
3	Strike normal to face	30
4	Dip into face	40

- Rock Density Influence (RDI)

RDI expresses the influence the density of the rock has on the BI as evident in equation 11. A heavier rock mass requires more explosive energy to move the rock so that it can be efficiently loaded. This parameter has a less significant weighting in the BI equation when compared to the influence of jointing (Bye, 2003).

Equation 11: RDI = (Density (g/cm^3) x 25) - 50

- Rock Strength (S)

It follows that the harder the inherent properties of the rock, the greater the explosive energy required to generate the design fragmentation. The uniaxial compressive strength (UCS) values are obtained from laboratory testing, point load testing or Schmidt hammer testing. Equation 12 formulates the calculation of the rock strength rating for the BI (Bye, 2003).

Equation 12: S = (UCS (in MPa) x 0.05)

The five BI parameters described above are then added together and multiplied by 0.5 to derive the BI (Eq. 10). As with other rock mass rating systems, the BI has gained widespread acceptance as a useful blasting tool since it was published in 1986. The BI provides the quantitative link between the in-situ rock mass

conditions and blast design parameters. Site specific correlation can be developed to relate the BI to blast design parameters, such as energy factor (Lilly, 1992).

The blast powder factor can be defined as quantity of explosives used, per unit volume of rock, measured in kg/m^3. There are several different explosive formulations available in the market and depending on which one is used, the energy delivered by the powder factor will vary. For this reason, the relative weight strength (RWS) of the explosive is obtained. The RWS is the strength of the explosive, as a percentage, in comparison to ammonium nitrate fuel oil (ANFO) explosives. ANFO is widely used in the mining industry and is therefore used as a standard for comparison of explosive energies. To ensure consistency, for comparison of blast powder factors, the energy factor is used. The energy factor is determined by multiplying the powder factor by the RWS of the explosive (Bye, 2003).

Some of the latest blast design software packages, e.g. Maptek BlastLogic, are also capable of reading relevant geotechnical input parameters discussed above from a geotechnical block model in order to ensure safe and efficient blasting operations.

- Priority (real data vs. modelled / surface proxy vs. median background in domain) is the next suggested attribute field for a geotechnical block model.
- dip
- dip direction
- Geotechnical confidence rating

The concept behind a geotechnical confidence rating should address the four aspects of the geotechnical model based on the amount of data points in a defined geotechnical design sector. It should therefore be a combined rating addressing:

    - Geological confidence - typically how many data points support the accuracy of geological contacts.
    - Structural confidence - information supporting the interpretation of the structural network and fabric. A fault confidence rating table utilised in Kumba Iron Ore operations can be found in Appendix 2 as an example.
    - Rock mass confidence - the confidence associated with geotechnical input parameters for stability analysis as was discussed earlier.
    - Hydrogeological confidence – monitoring points supporting water related input parameters in slope stability analysis.

The aim of this parameter is therefore to inform geotechnical risk assessment (fault tree analysis) based on the principle that higher geotechnical data confidence relates to higher reliability in slope design and lower geotechnical risk.

4.3.4. Interpolation and Population of the Geotechnical Block Model

The last step is to populate the block model cells utilising an appropriate interpolation method subsequent to a geostatistical analysis and testing of the model to verify the chosen interpolation method.

(Bye, 2003) discusses this process in detail for the Sandsloot Open Pit Mine and concludes that geotechnical engineering is well served by adopting geostatistics and the development of geotechnical models. Geostatistics deals with spatial data, i.e. data for which each value is associated with a location in space. In such analysis it is assumed that there is some connection between location and data value. From known sample points, geostatistical analysis can be used to predict spatial distributions of properties over large areas or volumes (Bye, 2003).

Care must be taken in considering appropriate methods, as most methods were developed for grade estimates, which are additive properties whereas geotechnical parameters are non-additive.

4.4. Summary and Conclusion

This Chapter discussed how the new methodology improves the slope design process by consequently improving the understanding of mine plans and their associated implementation risks, ultimately leading to increased investor confidence.

The methodology can be incorporated in the slope design process from early stage projects through to operational mines' planning cycles.

It follows a risk-based approach as the resulting focused data acquisition, rigorous stability analysis and risk assessment in areas of concern mitigates risk from early project stages (Stacey, 2009) to operational mines (future pushbacks).

It therefore addresses the fact that slope instability is one of the major sources of risk in open pit mining, largely due to data uncertainties.

5. APPLICATION OF THE DESIGN PROCESS, SYNTHETIC ROCK MASS MODELS AND 3D GEOMETRICAL ANALYSIS METHODOLOGY TO CASE STUDIES IN PROJECT PHASE

5.1. Conceptual Stage Project – Heuningkranz Project

5.1.1. Introduction

As described in Chapter 2, Heuningkranz is an exploration project situated in the Postmasburg district of the Northern Cape Province of South Africa. Its BIF and Shale SRM development was discussed in that Section.

5.1.2. Discussion of results: Application of 3D Geometrical Analysis Methodology

The exploration program is designed to delineate the mineralization and to increase the reliability of the geological and structural model to an indicated resources status, allowing an effective economic evaluation of the resource.

This is achieved by following a phased exploration approach to adhere to the Anglo-American stage (concept through to feasibility) gate criteria in terms of geological confidence (Mineral Resource status). Heuningkranz is being extensively explored to the highest standards in line with Exploration Drilling Standards (including QA/QC Protocols) as well as other applicable standards (SAMREC and SAMVAL codes).

In terms of geotechnical engineering, stage gate criteria are also specified for different aspects of geotechnical engineering (aligned with international guidelines, e.g. (Read & Stacey, 2009)). These include:

- Data acquisition
- Specific open pit / underground requirements
- Mine Residue Deposits
- Containment facilities
- General site infrastructure and facilities.

With the aim of potential open pit mining, the primary aim of geotechnical data acquisition is to start as early as possible following the process described in Chapter 4 to provide sufficient and relevant information for all the components of the geotechnical model, including geo-mechanical properties of the rock (rock mass model).

Geotechnical logging of exploration core is performed in accordance with a standardised protocol and is essential to provide a database for stability analyses and slope design. This early stage geotechnical logging is done on exploration holes to achieve substantial coverage of the modelled area.

Logging aspects include, material recovery, RQD, definition of geotechnical zones, jointing, joint spacing, joint orientation, joint surface conditions and ground water conditions. Point load testing is also performed to derive strength characteristics for all lithologies. Laboratory testing is also performed. A specific sequence for data acquisition is followed aligned with the exploration process as illustrated in Figure 72 below.

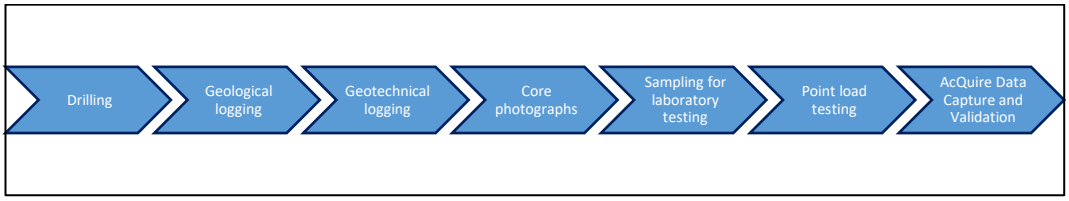


Figure 72 Geotechnical logging sequence

Data from the Heuningkranz *acQuire* database as well as orientation data from the geological model were used to develop conceptual level SRM models for the anisotropic units as was discussed in Chapter 2.

In order to illustrate how the 3D geometrical analysis methodology can be applied using the input from the SRM analysis of anisotropic units (BIF and shale) at an early stage project, the analysis was done on a pre-concept pit layout without ramps (Figure 73). Initial slope angles were based on inter ramp angles utilised at Sishen and Kolomela.

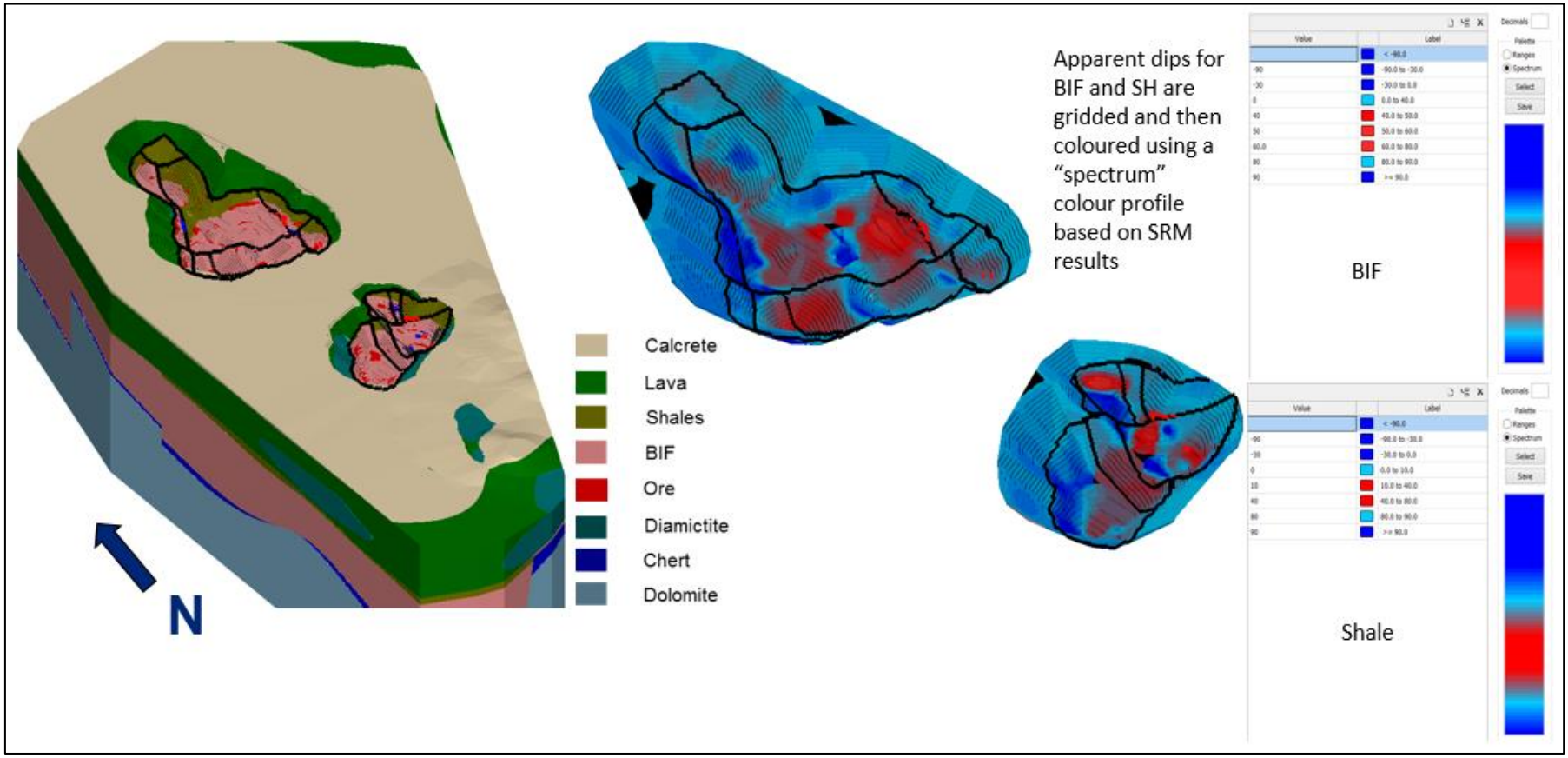


Figure 73 Results of early stage 3D geometrical analysis based on SRM strength envelope results.

Potential risks identified based on the 3D geometrical analysis

Based on the results obtained from the geometrical analysis and observations from extensive core logging, a significantly weak zone was identified above the ore zone. Thicknesses vary, with weak shale present on a tectonic unconformity. Consequently, elevated geotechnical risk may be the result, depending on the continuity and orientation (dipping into the pit) of these thrusted shales and its interaction with slope geometry and faults.

The results also clearly indicate that unfavourably orientated BIF and shale will mainly be exposed on the eastern slopes of planned pit designs. This early stage information improves the planning process as ramp and waste dump designs can be optimally positioned.

Defining Early Stage Design Sectors

The next step following the proposed methodology, was to delineate concept level design sectors based on results obtained from the 3D geometrical analysis (Figure 74).

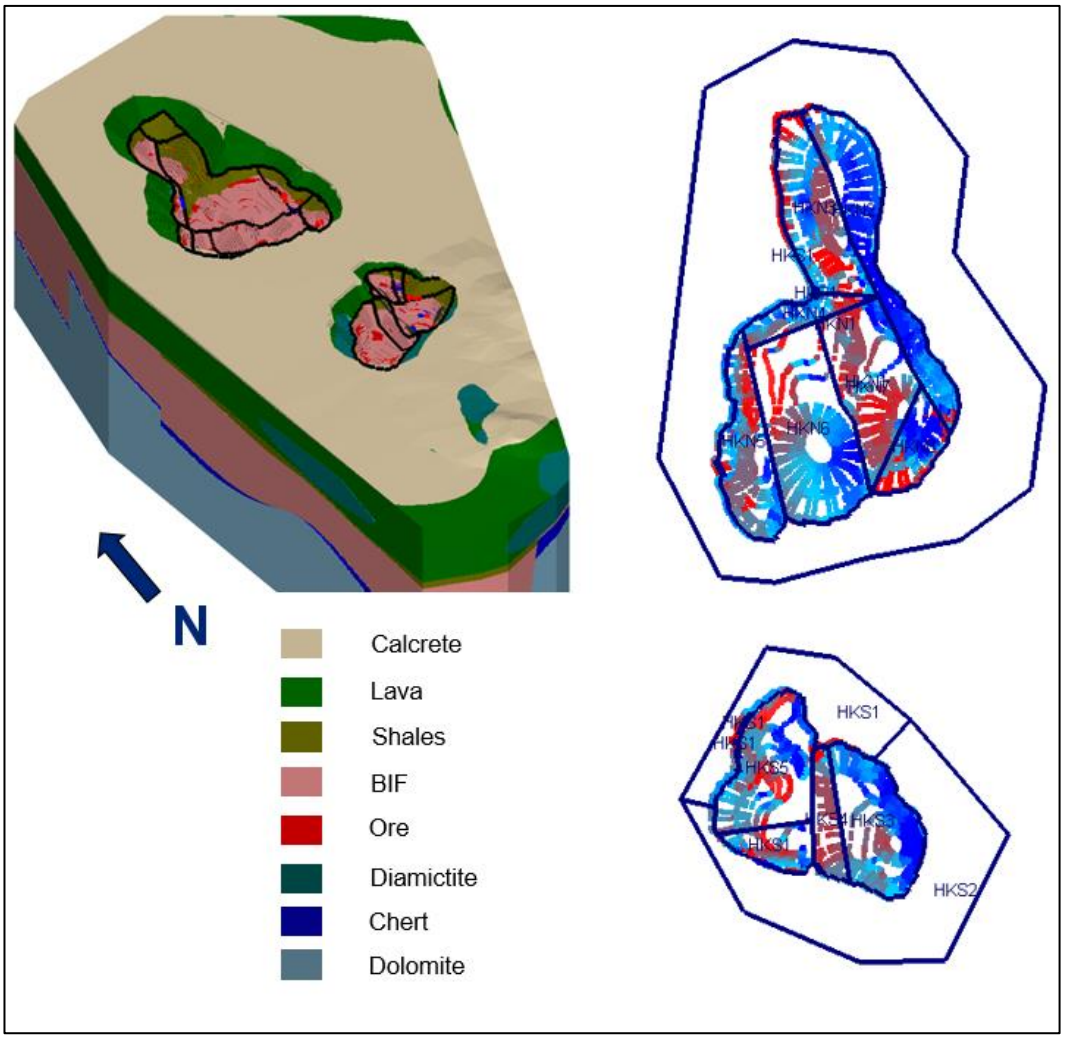


Figure 74 Concept level design sectors were delineated based on 3D geometrical analysis.

Design sectors closer to surface were delineated using the lower lava contact on the design surface that will consist of homogenous lava and calcrete. Lower design sectors mainly in BIF and shale (anisotropic units), were delineated based on potential favourable and unfavourable interaction with slope geometries.

Provide Sector Specific Design Parameters in Block Model Format

Design sectors were digitised utilising Micromine to create wireframes of each individual sector. This allows the geotechnical block model to be constrained with each sector in order to populate sector specific geotechnical design parameters in the attribute fields discussed in Chapter 4. Conceptual level design parameters for this project were based on slope angles utilised at Sishen and Kolomela.

Construct Practical Layout Utilising Economic Shell and Geotechnical Input

The geotechnical block model was made available to the Mine Planning Department to construct practical pit layouts to be utilised for further evaluation of the project. As was discussed in Chapter 4, front end loading of this project from a

geotechnical point of view, will greatly assist in achieving the objectives of the project stage, i.e. to highlight potential fatal flaws and to refine further investigations with new data (Read & Stacey, 2009).

Planning and Implementation of Focussed Geotechnical Data Acquisition

In order to achieve study phase objectives and based on the 3D geometrical analysis results, dedicated geotechnical drill holes were planned (Figure 75) and included in the exploration budget. At the time of writing this thesis, eight holes were completed and drilled into the dolomite.

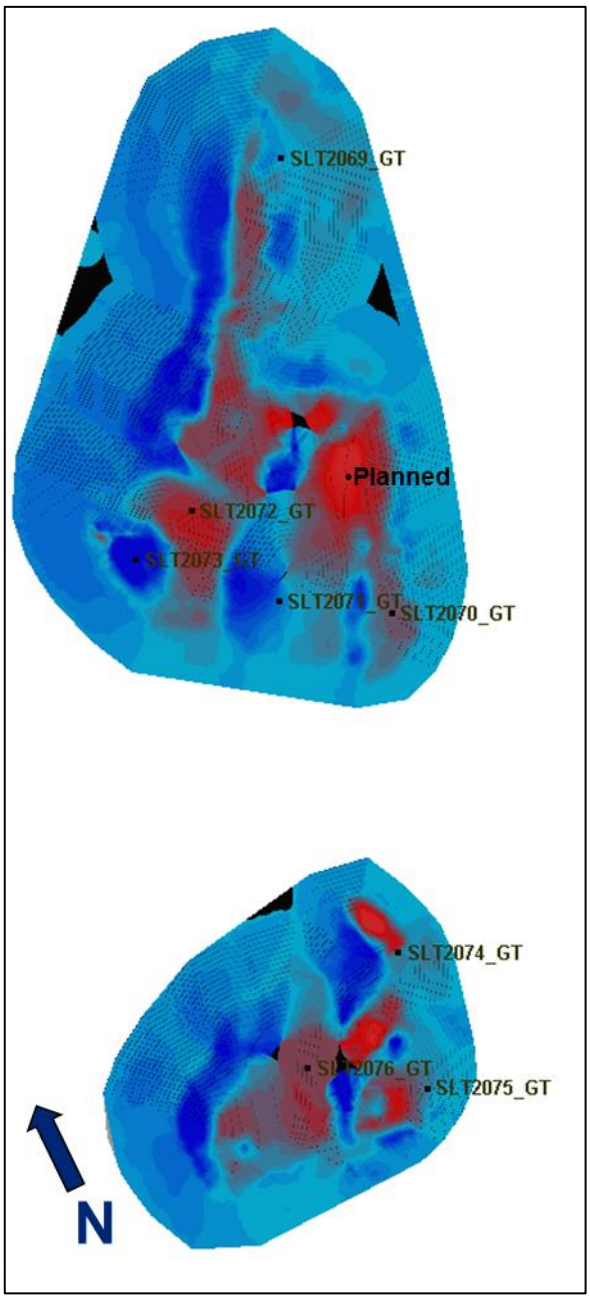


Figure 75 Plan of dedicated geotechnical drill holes targeting potential unfavourable areas.

The holes were drilled at an inclination of 70º targeting potential unfavourable areas utilising the correct split tube wireline equipment.

Data obtained from geotechnical logging and downhole surveys were then included in the project's *acQuire* geological and geotechnical databases to be included in the subsequent model updates following the suggested iterative process.

5.2. Summary and Conclusions

This Chapter introduced the novel notion of a "concept level" SRM for early-stage exploration projects wherein certain informed assumptions were made, based on existing knowledge and since SRM's are completely reliant on data provided by high quality, bench-scale structural mapping, which is not available on most early stage projects.

Utilising the input from the SRM analysis, the new 3D geometrical analysis methodology was successfully applied at the Heuningkranz project resulting in the definition of early stage design sectors. A geotechnical block model was developed, constrained with design sectors and populated with geotechnical design parameters as input in the mine planning process. Early stage focussed geotechnical data acquisition was also planned and implemented based on results obtained from the 3D geometrical analysis. New data was included in the geological and geotechnical databases to inform model updates following the suggested iterative process.

The application of the new methodology at the Heuningkranz exploration project showed how early front-end loading of a project utilising the suggested iterative process, greatly improves the design process to achieve the objectives of the project stage, i.e. to look for fatal flaws and to refine the investigation with new data (Read & Stacey, 2009). From a geotechnical engineering point of view, this was achieved as focussed data acquisition targets potential risk areas early on to allow for optimised ramp and waste dump placement leading to improved slope designs. It therefore increases the confidence in one of the major drivers of this project, viz. the strip ratio that is vital to the economic viability of the project.

6. APPLICATION OF THE DESIGN PROCESS, SYNTHETIC ROCK MASS MODELS AND 3D GEOMETRICAL ANALYSIS METHODOLOGY TO CASE STUDIES IN THE OPERATIONAL PHASE

6.1. Sishen Mine

6.1.1. Introduction

SRM development for Sishen Mine was discussed in Chapter 2, followed by a detailed description of the new 3D geometrical analysis methodology. These methods were further described in the context of the slope design process, following an iterative approach. The application of this approach to an existing pit will now be discussed.

6.1.2. Discussion of results: Application of synthetic rock mass models and 3D geometrical analysis methodology

The resolution and density of data at Sishen Mine and the availability of a fully-constrained 3D model, to the original pre-mining surface, allowed for high confidence input to SRM development of anisotropic units. Following the process described in Chapter 4, the SRM results were used to spatially analyse mine layouts at Sishen, which is mined in a series of pushbacks or phases towards the final pit boundary. Subsequent to performing 3D geometrical analysis and defining design sectors, two design sectors of concern were highlighted. The first design sector is in an active pit (GR35) and the second in a future pushback (GR80) (refer to Figure 76).

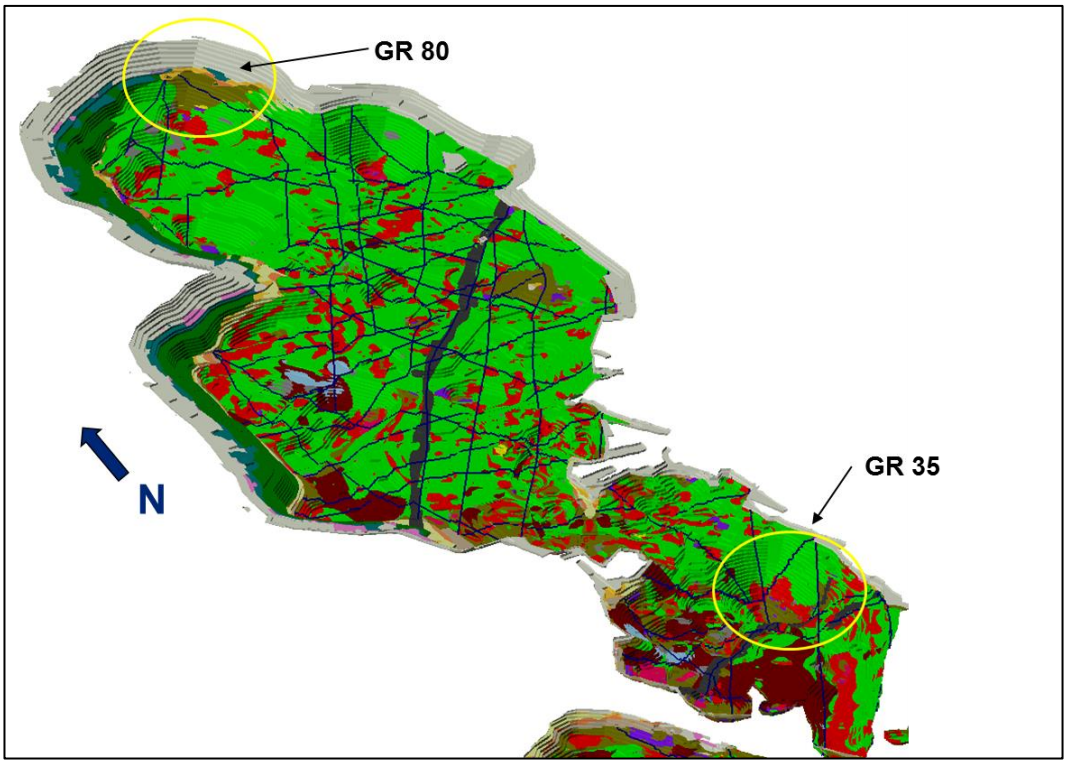


Figure 76 Location of GR35 and GR80 areas of Sishen Mine.

Although 2D analysis results of these areas adhered to acceptance criteria for probability of failure (PoF), it was deemed necessary to conduct more rigorous 3D stability analyses in the areas to improve the confidence in the design. To achieve this, the *3DEC* numerical code was used which has been specifically developed to study three-dimensional rock mechanics problems involving large numbers of explicit structures that divide a rock mass into blocks. Within *3DEC*, slip, separation and rotation along explicit structures can occur while the individual blocks can deform and yield. A mesh consisting of cubic elements of varying sizes was constructed to provide the overall slope geometry. The cubic element size in the areas of interest has been reduced to the bench height (12 m). The mesh has been refined further to 6 metres in some areas of interest (at 150 m depth below surface) to better represent key weak components.

The geological wireframe model was directly imported in *3DEC* in DXF format and every element assigned to a geotechnical unit based on lithology and geo-mechanical properties. Table 21 shows the geotechnical units with a description.

Table 21 Geotechnical units at Sishen Mine

Code Assigned	Unit name	Description
CC	Calcrete	Calcrete
CL-PEB	Clay	Clay, weathered lava and pebblestone
LAV	Lava	Andesitic lava
QTZ	Quartzite	Quartzite, flagstone
CGT	Conglomerate	Conglomerates
HEM	Ore	Haematite Ore
BIF	BIF	Banded Iron Formation
SH	Shale	Shale and Floor shale
MN-CH	Manganese Marker	Chert Breccia, Manganese Marker
DOL	Dolomite	Dolomite
DI	Dyke	Diabase

The Hoek and Brown failure criterion (Hoek & Marinos, 2007) was used for all materials with isotropic behaviour. The input parameters needed for this failure criterion are σ_{ci}, GSI and m_i. The values used in all the analyses were obtained from the Sishen geotechnical database and are presented in Table 22. A summary of the Sishen geotechnical database can be found in Appendix 4.

Table 22 Geo-mechanical properties for isotropic geotechnical units at Sishen Mine.

Code assigned	Unit name	UCS		GSI		m_i
		Mean (MPa)	St. Dev.	Mean	St. Dev.	
CC	Calcrete	68	47	57	10	17
LAV	Lava	133	67	64	9	18
QTZ	Quartzite	195	105	49	12	20
CGT	Conglomerate	90	84	52	9	22
HEM	Ore	202	147	52	10	7
MN	Manganese Marker	236	124	57	12	14
DOL	Dolomite	167	75	60	10	23
DI	Diabase	202	75	53	12	16

Rock mass behaviour was considered to be elastic – perfectly plastic. Final values used in the *3DEC* models were the average minus one standard deviation, as it is considered that failure occurs preferentially through the weaker rock mass components (see (Renani, et al., 2018)).

Material showing soil behaviour (CL) was simulated using the Mohr-Coulomb failure criterion (Labuz & Zang, 2012). The properties for clay are based on a back

analysis of a test slope failure in the northern part of Sishen mine. Parameters used in the numerical models for clay are presented in Table 23.

Table 23 Geo-mechanical properties for clay materials at Sishen Mine.

Material	Cohesion (kPa)	Friction (º)	σ_t (kPa)
Clay	71	22	7

Elastic moduli for the isotropic rock materials were based on the Hoek and Diederichs (Hoek & Diederichs, 2006) formulation as in equation 13:

Equation 13
$$E_m(GPa) = E_i \times \left(0.02 + \frac{\left(1-\frac{D}{2}\right)}{1+e^{\frac{60+15.D-GSI}{11}}}\right)$$

Where:

D = Hoek Damage Factor

GSI = Geological Strength Index

E_i = Intact rock modulus

The intact rock modulus (E_i) was obtained from the modulus ratio (MR). E_i is calculated as:

Equation 14
$$E_i\ (MPa) = MR \times \sigma_{ci}(MPa)$$

Finally, Poisson's ratio is defined as:

Equation 15
$$v = 0.32 - 1.5\frac{GSI}{1000}$$

Geological structures were explicitly included in the *3DEC* analyses. Their behaviour is represented by a linear Mohr-Coulomb failure criterion and the residual values are $c_{res} = 0$ (cohesion) and $\phi_{res} = \phi_{peak}$ (friction). The shear strength parameters of the structures and lithological contacts are presented in Table 24.

Table 24 Geo-mechanical properties for faults and contacts at Sishen Mine.

Geological Feature	Cohesion (kPa)	Friction (º)	σ_t (kPa)
Faults	10.0	33	1.0
Lithological contact	10.0	33	1.0

The major fault in GR35 pit was modelled as a material using the same properties as in Table 24 with an approximate width of 60m. The tectonic unconformity in GR 80 was also modelled explicitly. UCS and GSI parameters obtained from an area where the tectonic unconformity was exposed, were used to estimate the shear

strength. Based on a confinement stress of 1 MPa, Mohr-Coulomb strength parameters were derived for the tectonic unconformity as presented in Table 25.

Table 25 Geo-mechanical properties for the tectonic unconformity in GR 80.

Geological Feature	Cohesion (kPa)	Friction (°)	σ_t (kPa)
Tectonic unconformity	95.0	17	9.5

The Hoek damage factor (D) has been used to reduce the rock mass properties close to the surface of the pit (Hoek & Marinos, 2007). Blast damage has been observed to decrease away from the rock wall or pit floor. The values assigned for the damage factor also changes with depth from 1 to 0 as is illustrated in Figures 77-78.

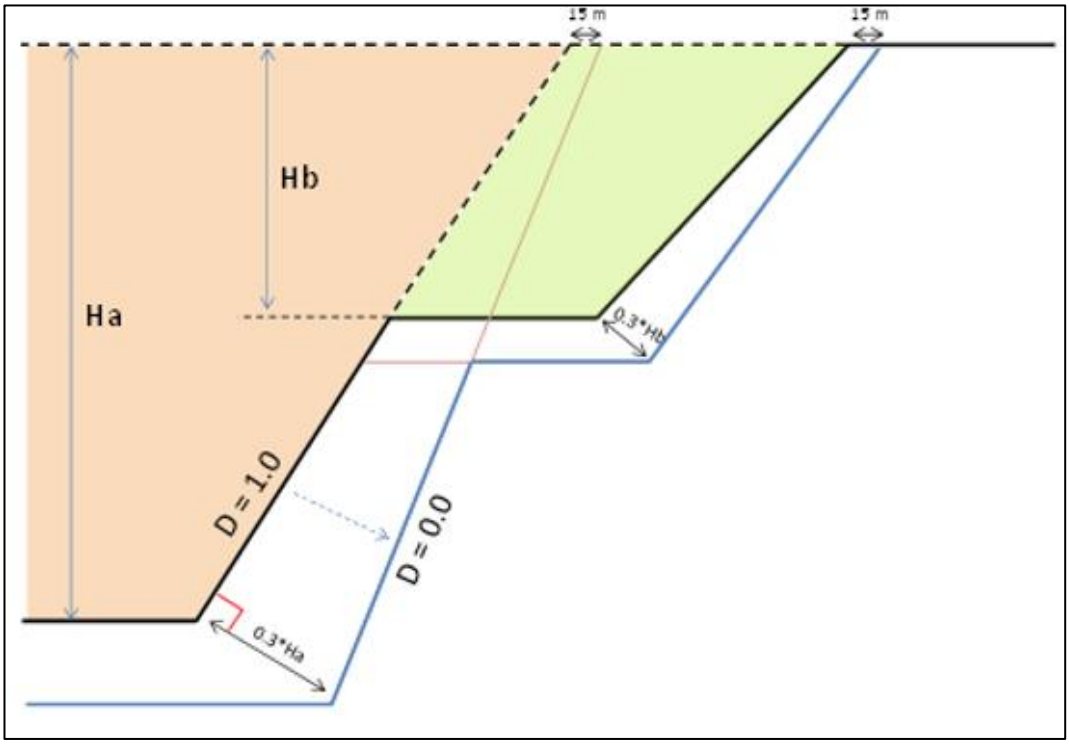


Figure 77 Conceptual definition of the area influenced by blast damage (D) – Ha and Hb refers to slope height.

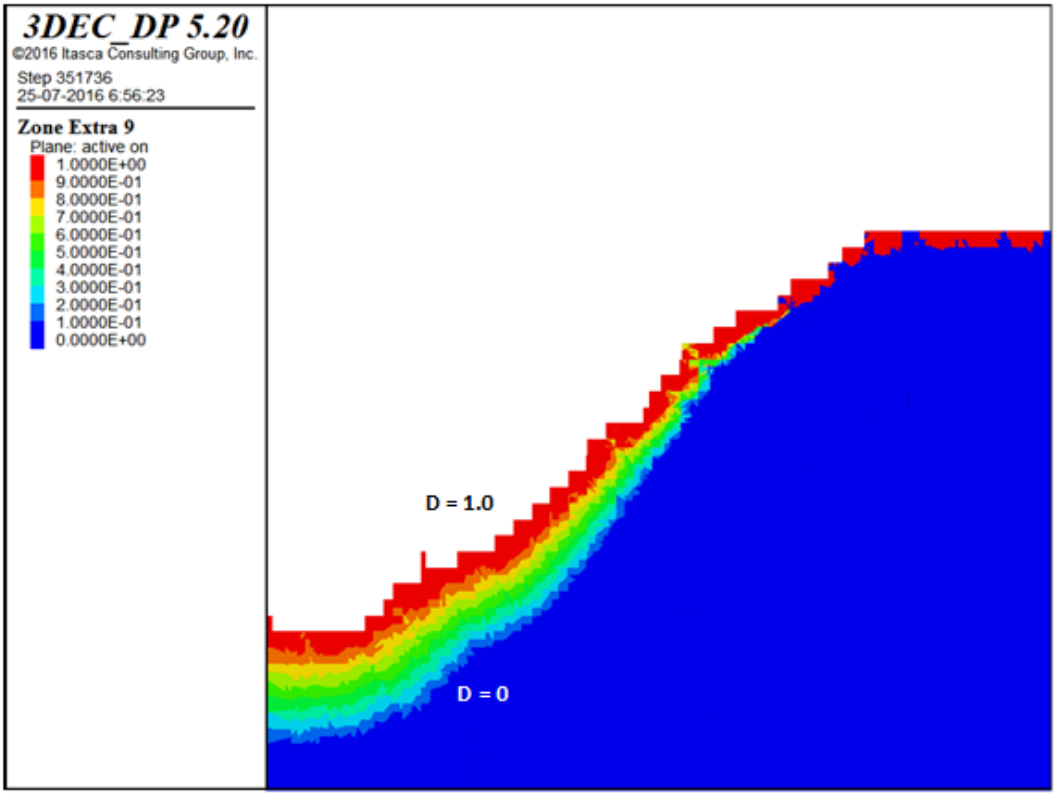


Figure 78 *3DEC* Section with damage factor applied in depth, from 1 on surface to 0 in depth.

In terms of in-situ stress, lithostatic stresses, meaning the horizontal and vertical stress components were assumed to be equal, i.e. k_h (E-W) = k_h (N-S) = σ_v. The vertical stress is given by the product of depth, gravity and material density.

Due to the fact that the pits in question are dewatered, no pore pressures were simulated in the numerical models. However, sensitivity analyses considering pore pressure were conducted.

GR 35 Analysis

The GR 35 area in the central part of the mine, shows unfavourably-orientated BIF and shale dipping into the pit potentially interacting with faults and a diabase dyke once exposed as mining progresses (Figure 79).

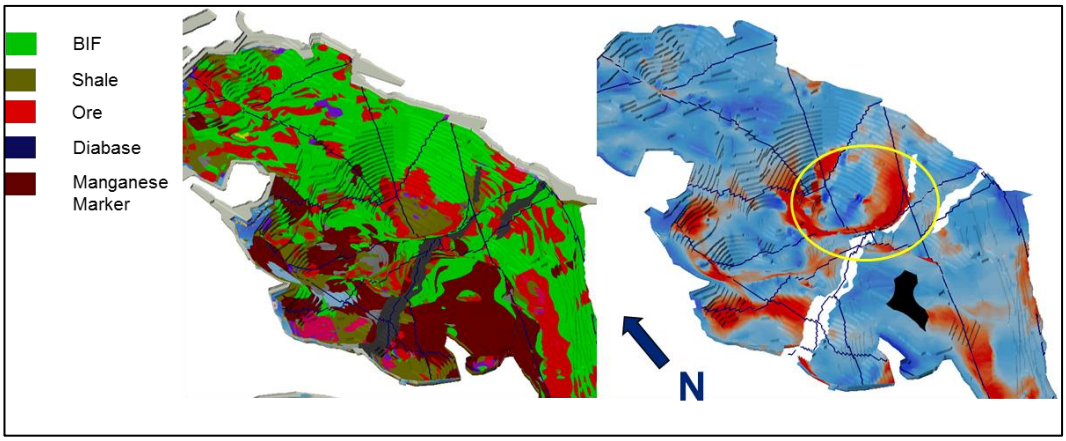


Figure 79 Area of concern in the central part of Sishen Mine (GR35)

Faults in the area of interest were modelled explicitly and the largest fault (locally named the Sloep Fault) was modelled as a fractured material due to the occurrence of sympathetic faults with a width of 60 metres (Figure 80).

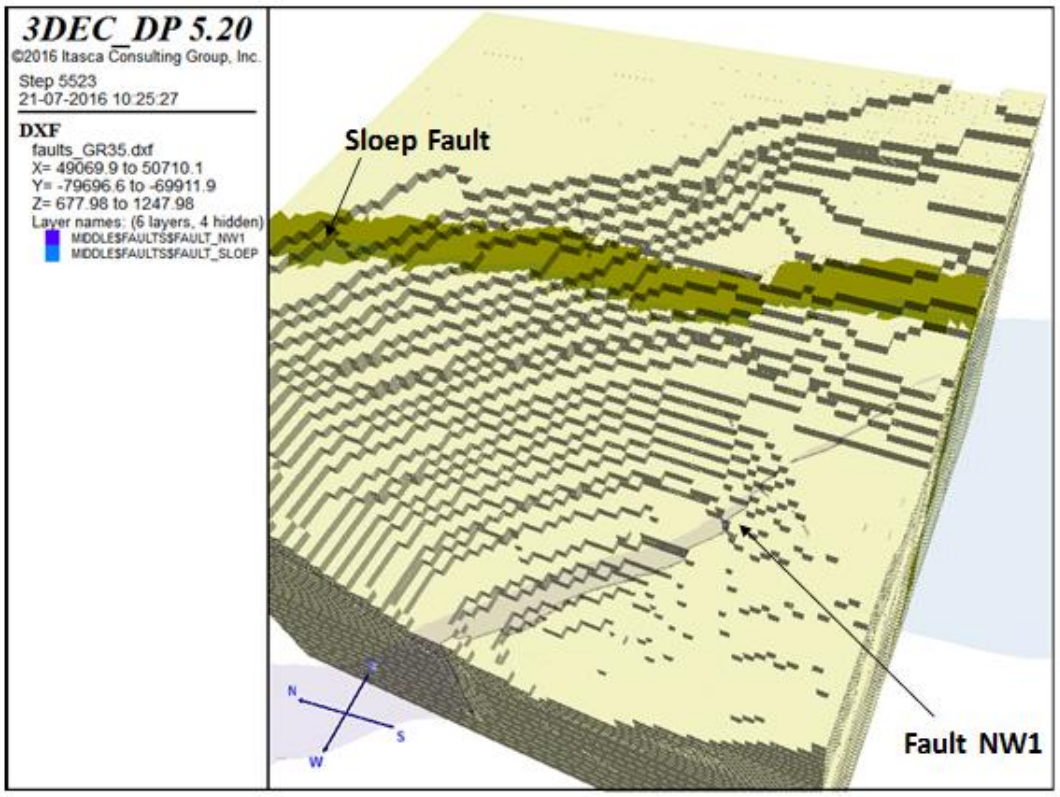


Figure 80 Fault NW1 was modelled explicitly and the Slope Fault modelled as a zone of weak material.

Most of the final pit boundary in the area consists of BIF, with shale and ore present towards the bottom of the pit. Furthermore, these lithologies may interact with the Sloep Fault intersected by a diabase dyke (refer to Figure 81).

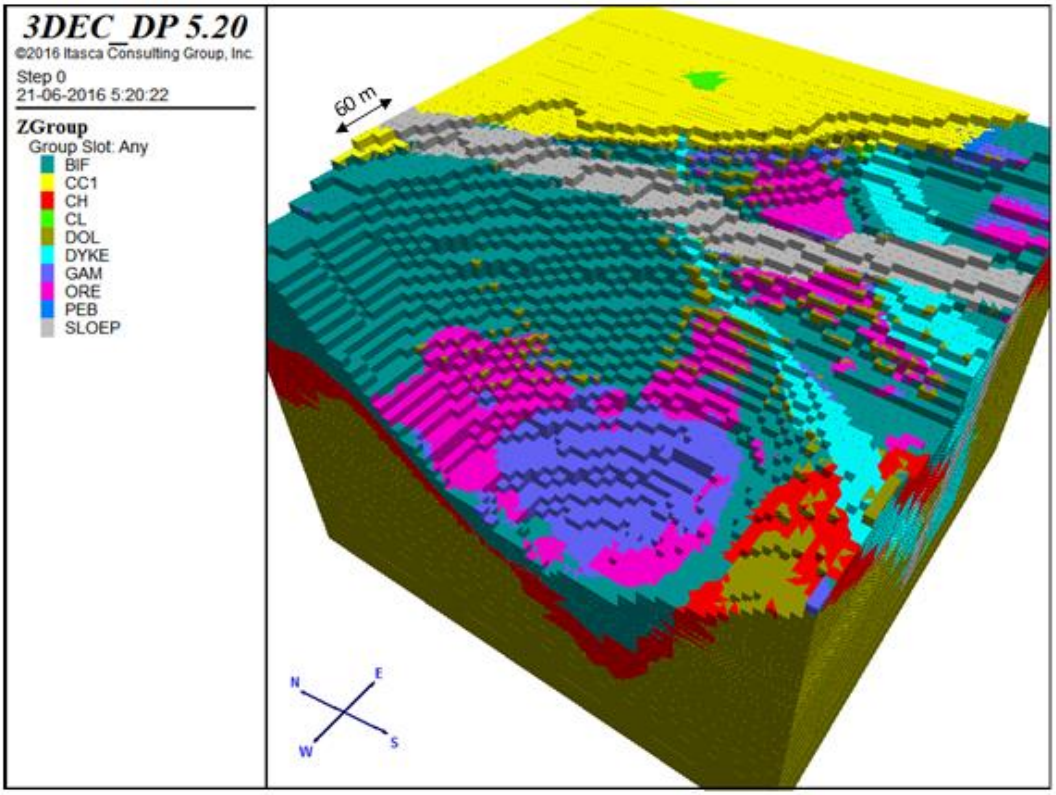


Figure 81 Lithologies in the GR35 numerical model.

Based on observations in the pit, it was also decided to model certain contacts explicitly to account for weakness, i.e. the BIF-dyke and BIF-Chert contacts. Figure 82 shows the numerical model with these considerations.

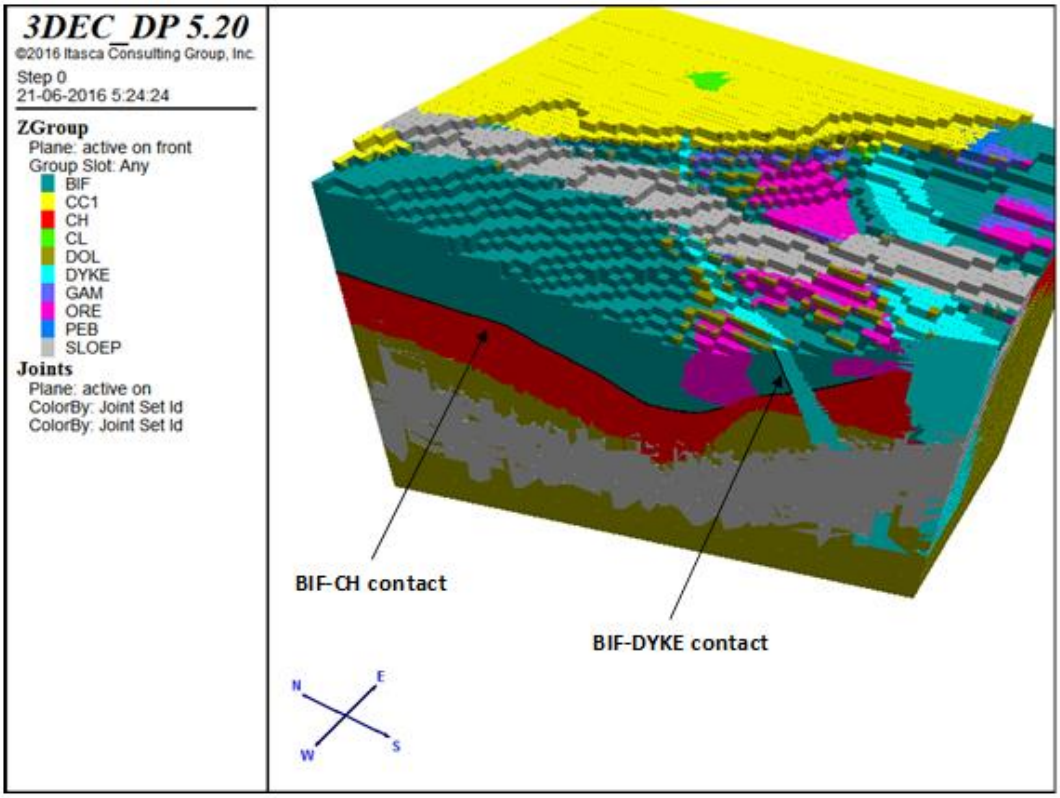


Figure 82 BIF-CH and BIF-dyke lithological contacts explicitly represented in the numerical model.

BIF and shale material at Sishen Mine exhibit anisotropic behaviour. The dip and dip direction of these units have been assigned to every zone and strength properties utilised were obtained from the SRM analysis described in Chapter 2 (Figure 83).

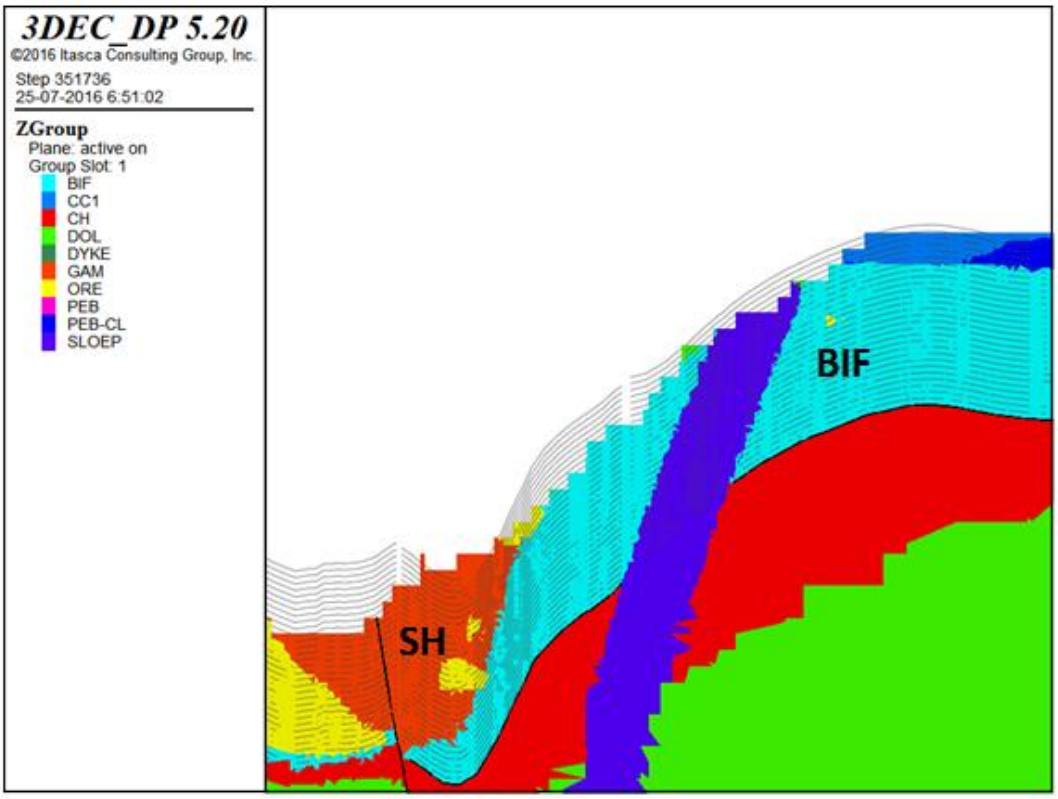


Figure 83 A Section showing anisotropy orientations in BIF and shale.

GR 35 results

The numerical model is analysed in terms of numerical velocity (Itasca Consulting Group, 2016). An unstable condition is assumed in the model when after a significant number of calculation steps, the numerical velocity remains above a certain value (different in each model). Figure 84 illustrates the definition of stable vs. unstable in terms of numerical velocities.

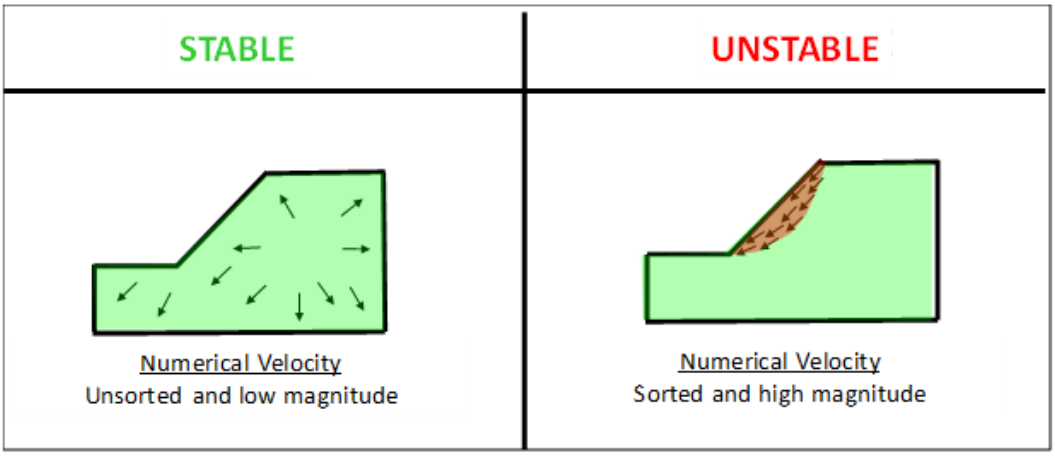


Figure 84 Definition of stable vs. unstable behaviour in terms of numerical velocities.

The stability analyses were conducted utilising the shear strength reduction method to quantify the factor of safety. In this approach, all the geo-mechanical strength elements (of rock mass, anisotropy, structures) are reduced and the stability evaluated under each new condition. Figure 85 shows the results of the analysis for GR 35.

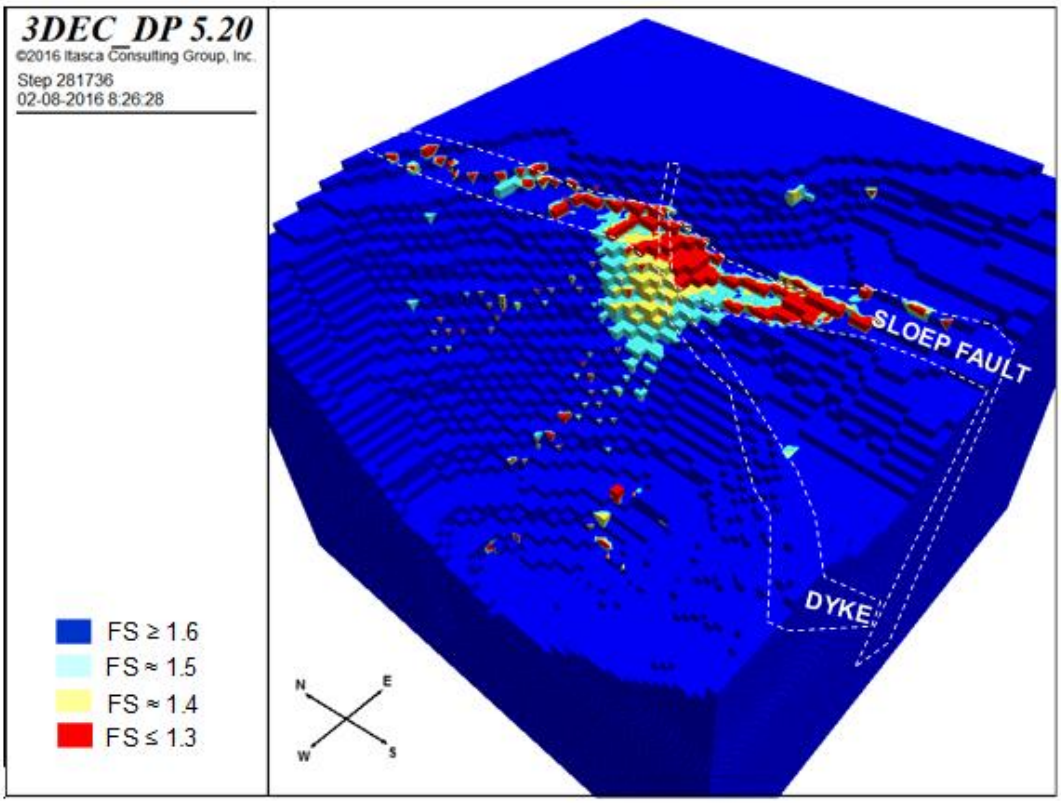


Figure 85 Factor of safety results for the GR 35 analysis.

The results indicate areas on a bench scale with a factor of safety lower than 1.3, associated with the fractured material of the Sloep Fault. Furthermore, there is a sector (inter-ramp scale) with factor of safety between 1.4 and 1.5 with a height of approximately 7 benches (84 metres) in the Slope Fault material as well as BIF material, following the anisotropy orientation (sub-parallel to the slope). Figure 86 shows a Section in this area.

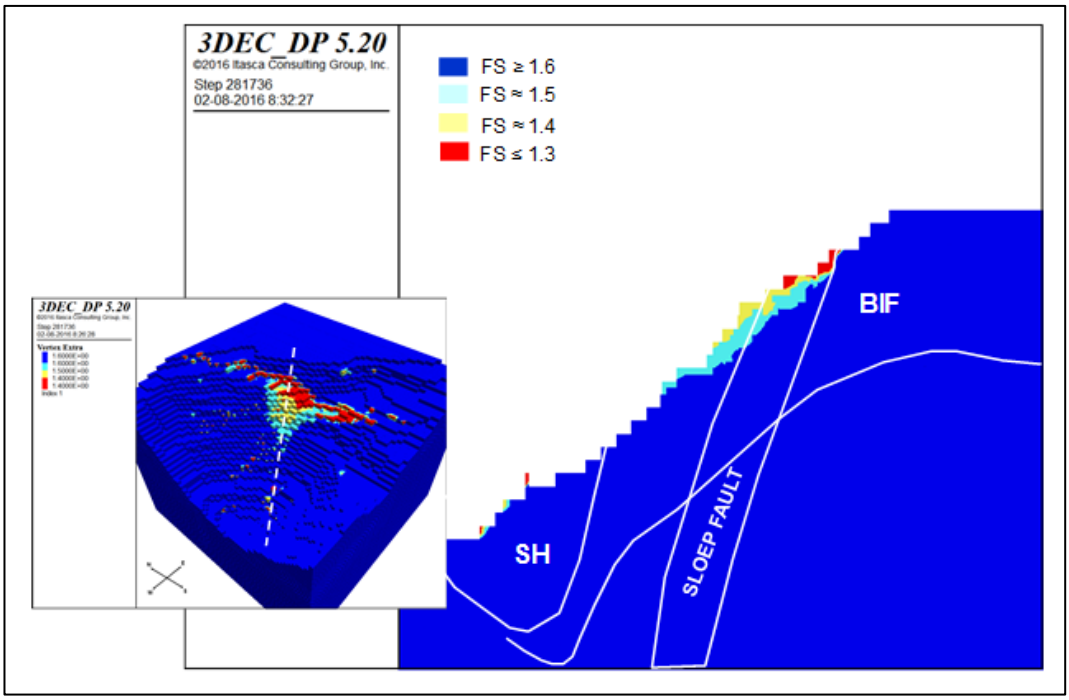


Figure 86 Section in GR 35 showing the factor of safety results.

Figure 87 shows displacement magnitudes and velocity vectors (black arrows) for the unstable condition (decreasing material properties to have a factor of safety < 1.0) where mechanics of movement are appreciated.

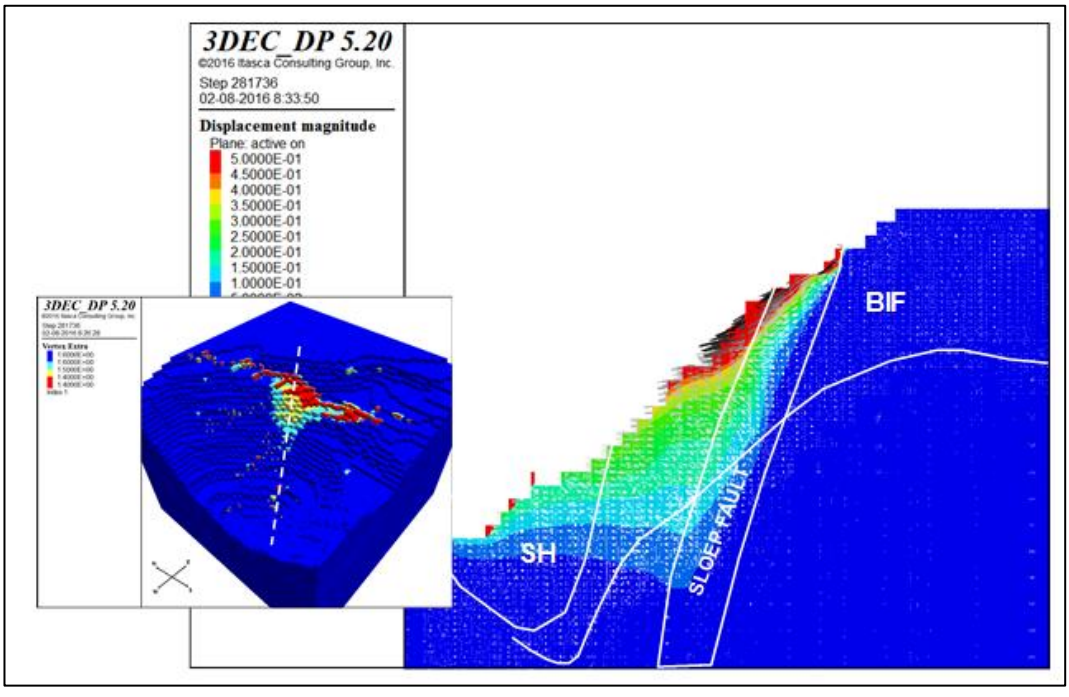


Figure 87 Section in GR 35 showing displacement magnitudes.

Taking into account that the probability of failure for bench scale of up to 30% is acceptable according to industry standards (Read & Stacey, 2009), bench scale

failures where BIF dips into the pit (unfavourable interaction) in GR35 are expected and do occur. However, these failures can be managed by limit blasting techniques and pit wall control as well as various operational geotechnical controls, e.g. operational risk assessments, safe declaration procedures and standoff rules.

3DEC analysis results for GR 35 therefore indicated acceptable risk levels for larger scale instability in the potential risk area highlighted by the apparent dip analysis. The confinement aspect of the convex nature of the pit was deemed a major contributing aspect towards stability of the slope.

By applying the new 3D geometrical analysis methodology as part of the suggested iterative slope design process, the GR35 example is a case in point where more advanced stability analysis based on apparent dip maps increased the confidence in the slope design, therefore decreasing geotechnical risk. At the time of writing this thesis, only two levels of the pit remained, with advanced slope stability monitoring systems confirming expected slope performance.

GR 80 Analysis

The second potential risk area identified by the 3D geometrical analysis, is located in a future pushback in the northern part of the pit (Figure 88).

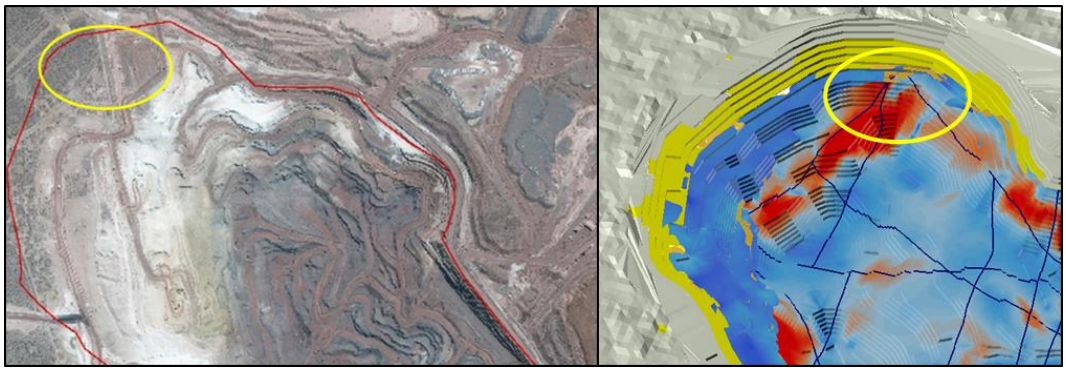


Figure 88 Area of concern (GR80) in future pushback in northern part of Sishen Mine.

Based on the 3D geometrical analysis, the area shows unfavourably-orientated BIF and shale dipping into the pit, as well as faults that could act as release planes according to the conceptual failure model. Furthermore, the shale is underlain by a tectonic unconformity. Following the methodology suggested in the previous Chapters, more rigorous analysis and focussed data acquisition were deemed necessary in this area, to achieve value protection through early risk mitigation.

Focussed data acquisition

Two dedicated geotechnical core drill holes were planned and drilled in the area of concern. A downhole survey was also performed, resulting in the confirmation of both an unfavourably-orientated geology and the position of the tectonic unconformity. The red arrows in Figure 89 indicate shale dipping into the pit.

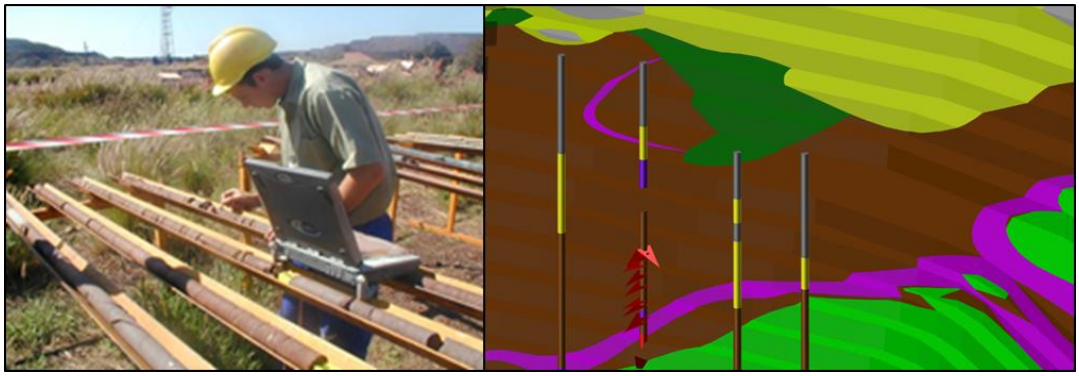


Figure 89 Geotechnical drilling to confirm bedding orientation and tectonic unconformity

Geotechnical logging of drill holes furthermore indicated localised ferruginisation of shales, which needs to be accounted for in the stability analysis of this area.

A model of the area was constructed in *3DEC* for stability analysis, with strength properties obtained from the Sishen a*cQquire* geotechnical database as described earlier. Principal faults and a tectonic unconformity were modelled explicitly as is illustrated in Figure 90.

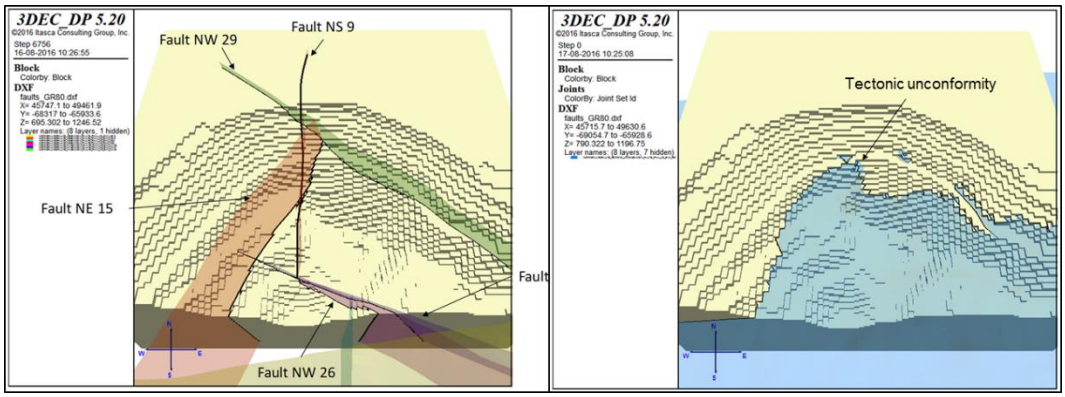


Figure 90 GR 80 faults and tectonic unconformity modelled in *3DEC*.

Similar to GR 35, BIF and shale in GR 80 exhibit anisotropic behaviour and play a critical role in stability at Sishen Mine. The dip and dip direction of these units have been assigned to every zone and strength properties utilised were obtained from the SRM analysis described in Chapter 2 (Figure 91).

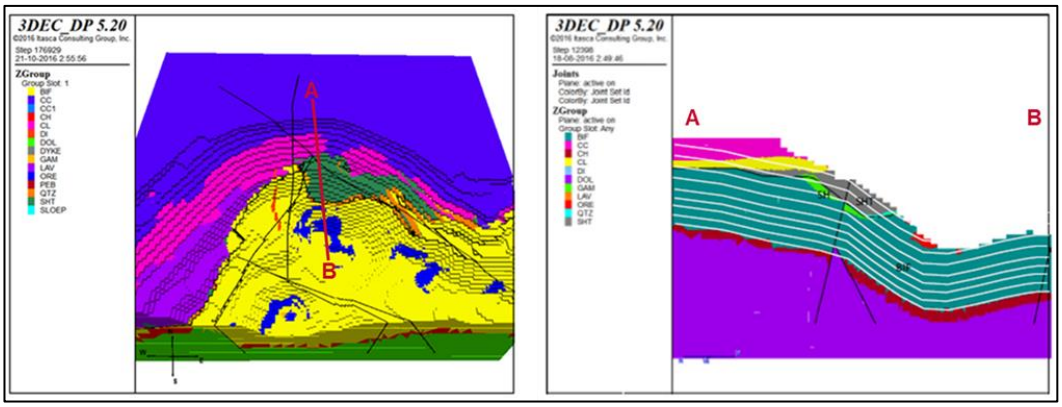


Figure 91 Plan view and Section of *3DEC* numerical model

GR 80 Analysis Results

Analyses of various scenarios were completed. In the first analysis, the factor of safety ranged between 1.0 and 1.6. Figure 92 shows the results of this analysis.

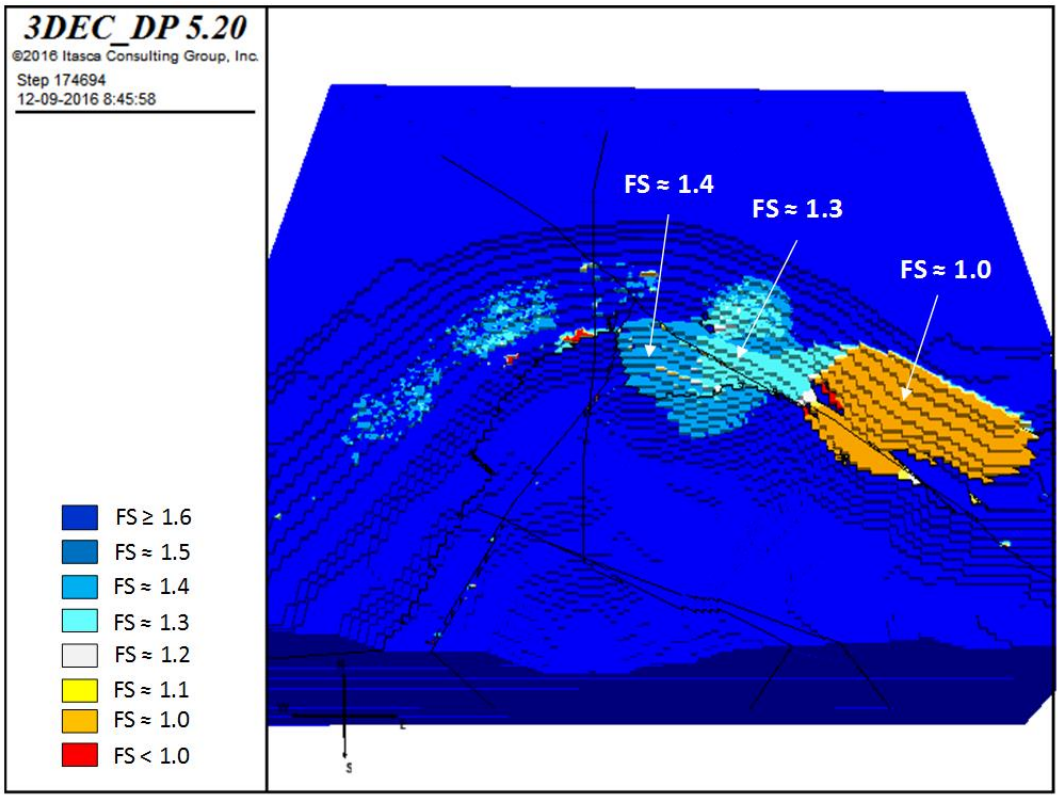


Figure 92 Factor of safety results for the GR80 stability analysis.

Results show a large area with a factor of safety of approximately 1.0. This implies that the area is geo-mechanically stable but in a limit condition. The main reasons for this potential instability are the location and orientation of the tectonic unconformity, which is sub-parallel to the slope, daylighting in the face, as illustrated in Figure 93.

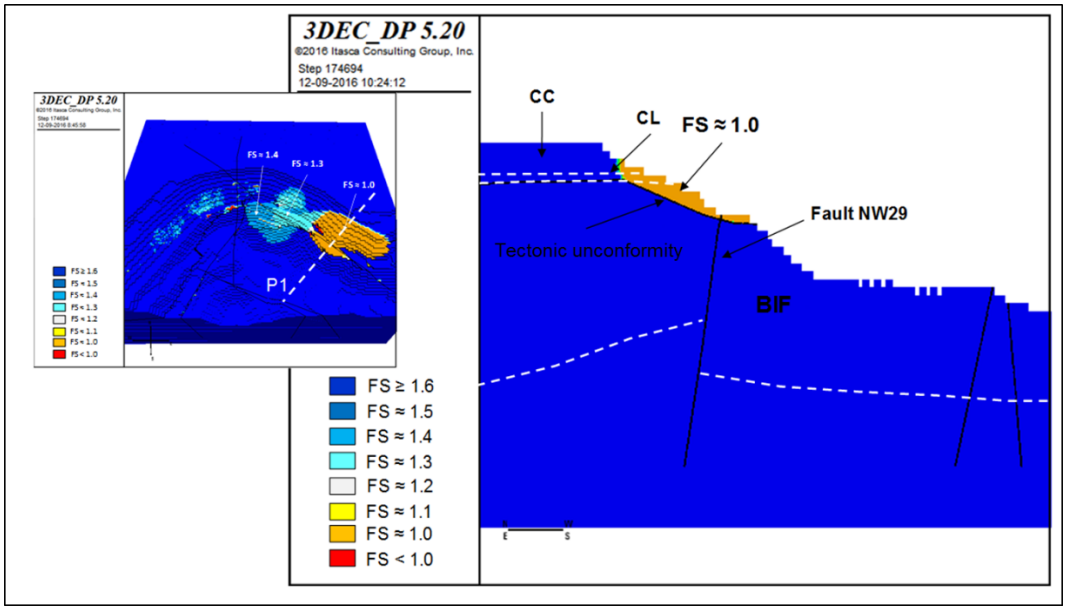


Figure 93 Section in GR 80 showing the influence of the tectonic unconformity

Figure 94 shows the velocity vectors for the potential unstable situation where potential sliding on the tectonic unconformity could occur.

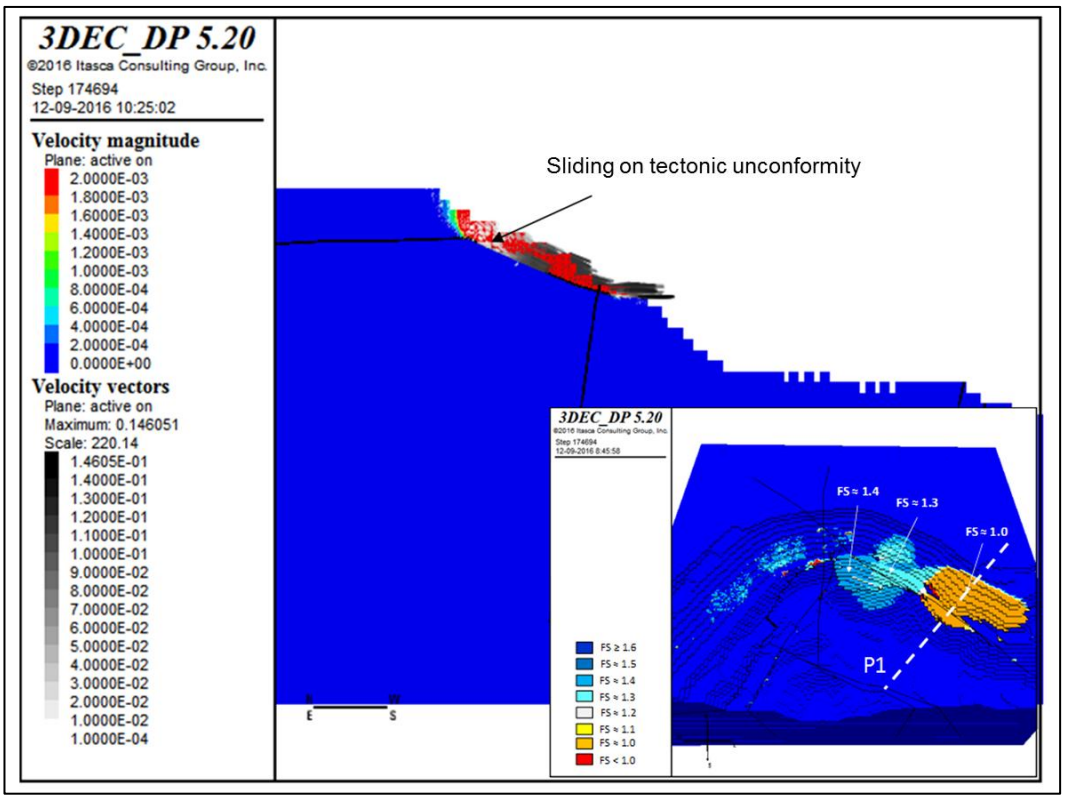


Figure 94 Section in GR 80 showing mechanics of potential movement.

Towards the north in the area under investigation (factor of safety of 1.3 - 1.4), the stability is influenced by the location and orientation of the tectonic unconformity as well as the anisotropy orientation of BIF and shale materials (Figure 95).

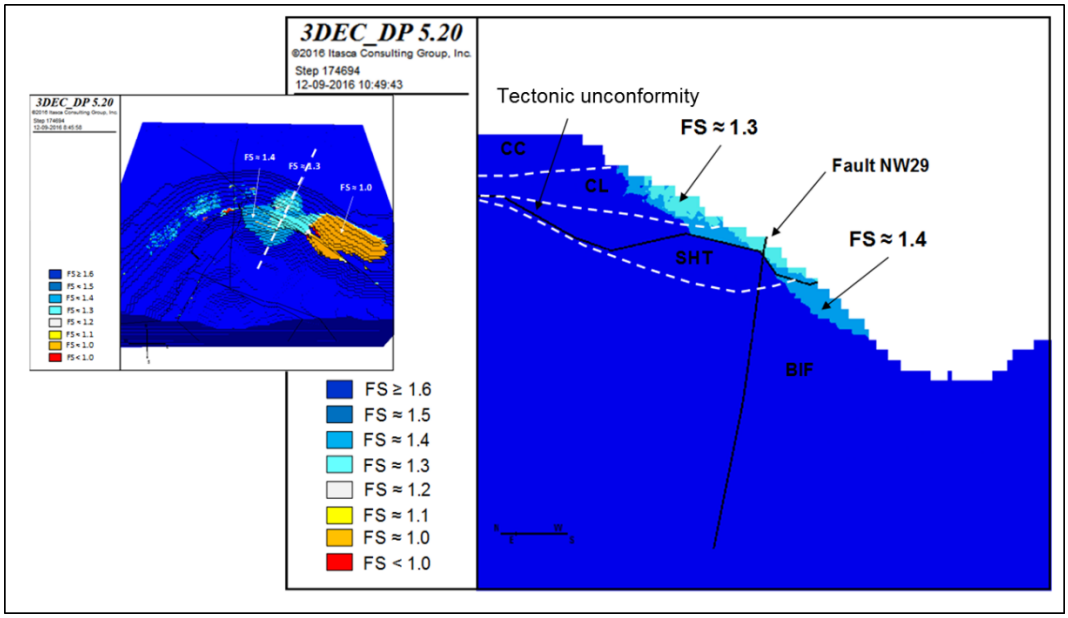


Figure 95 Section in GR 80 showing the area with factor of safety of 1.3 – 1.4.

To improve understanding of the potential complex interaction of several aspects influencing stability, various sensitivity analyses were conducted.

The first analysis was done by adjusting the friction angle of the tectonic unconformity. This parameter was increased from $\phi = 17$ to $\phi = 33^{o}$. The second analysis was done by adjusting the residual cohesion of the tectonic unconformity by increasing $c_{res} = c_{peak} = 0$ kPa to 95 kPa. The results for both analyses are shown in Figure 96.

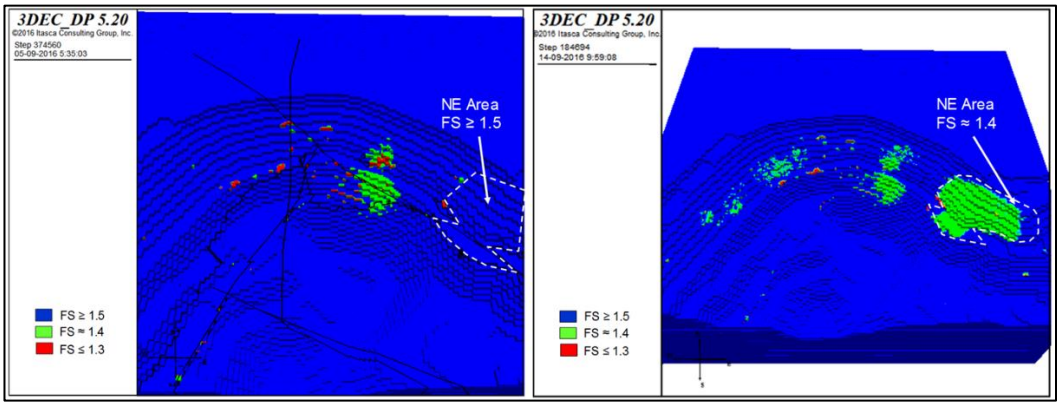


Figure 96 Factor of safety results for GR80 sensitivity analyses (increased friction angle left and increased residual cohesion right).

In both cases, the factor of safety in all areas increases significantly, i.e. equal to or greater than 1.4 and equal or greater than 1.5.

For the third sensitivity analysis, the cohesions on all faults were reduced from c = 10 kPa to c = 0 kPa. The results are shown in Figure 97.

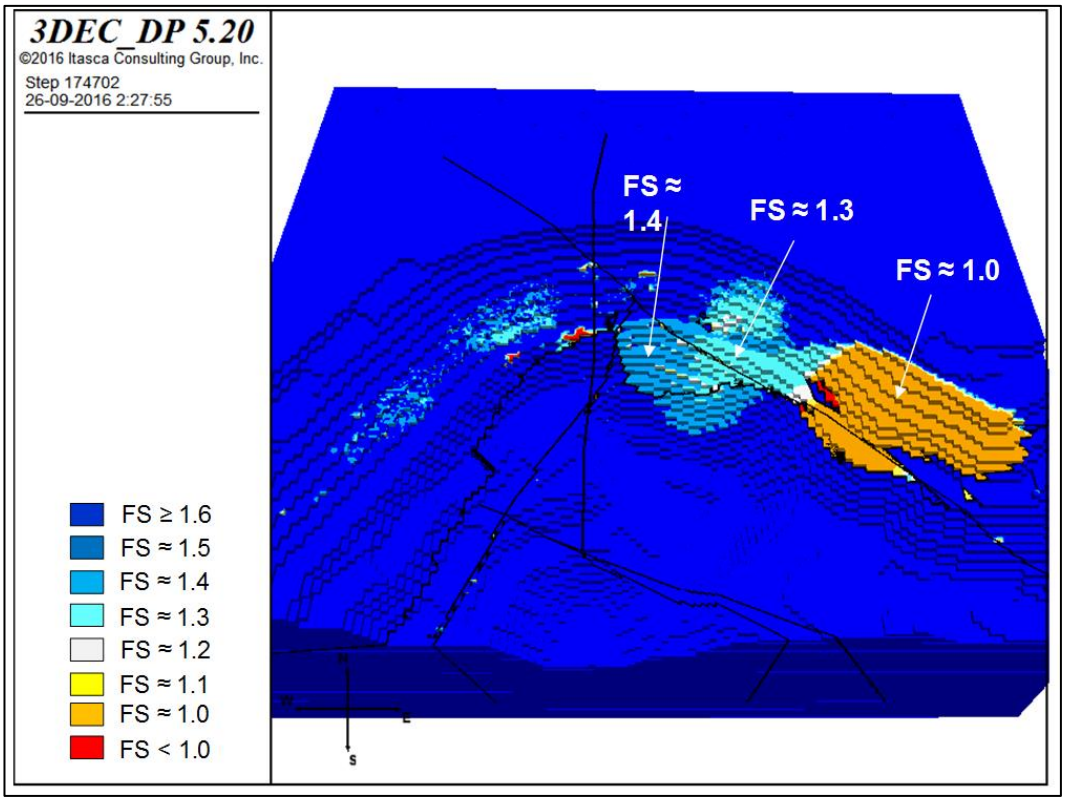


Figure 97 Factor of safety results for GR 80 sensitivity analysis with decreased cohesion on faults.

The factor of safety results obtained are similar to the original results, indicating that slope stability is more sensitive to the strength of the tectonic unconformity than that of the faults.

It should be noted at this stage that all previous analyses were performed with no pore pressure in any of the zones. Therefore, for the third and fourth sensitivity analysis, two hydrogeological conditions were analysed.

For the third analysis, a near surface aquifer in calcrete (CC) and clay (CL) materials was considered in which pore pressures were applied only in the zones and structures inside these lithologies. The rationale behind this is that Sishen Mine has an extensive dewatering program with current water levels already drawn down in excess of 100m below the current pit floor, and that only the surface aquifer in the Kalahari formation (Calcrete and clay) can be considered. The pore pressures were allowed to develop in the *3DEC* model as a product of the depth, water density and gravitational acceleration. The results are shown in Figure 98.

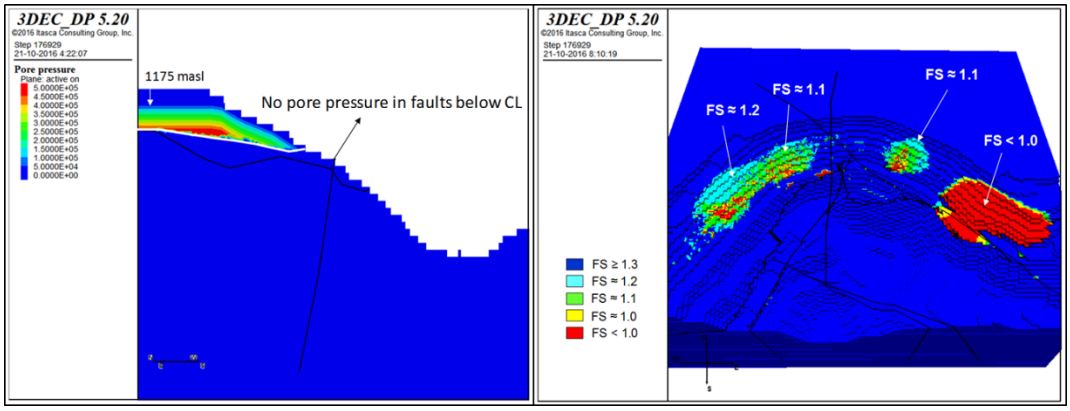


Figure 98 Factor of safety results for GR 80 sensitivity analysis with pore pressure applied in the surface aquifer.

Results indicate that the factor of safety decreases significantly in the areas with pore pressure, ranging from FS = 1.1 – 1.2 to FS < 1.0.

The fourth sensitivity analysis was performed considering the near surface aquifer with pore pressures also applied in all structures (faults and tectonic unconformity). This scenario considers a hydrogeological connection through structures where surface water infiltrates along said structures. This is justified by the Sishen groundwater numerical model and practical experience that Sishen is essentially a fractured aquifer where dewatering infrastructure targets water bearing structures. The results are shown in Figure 99.

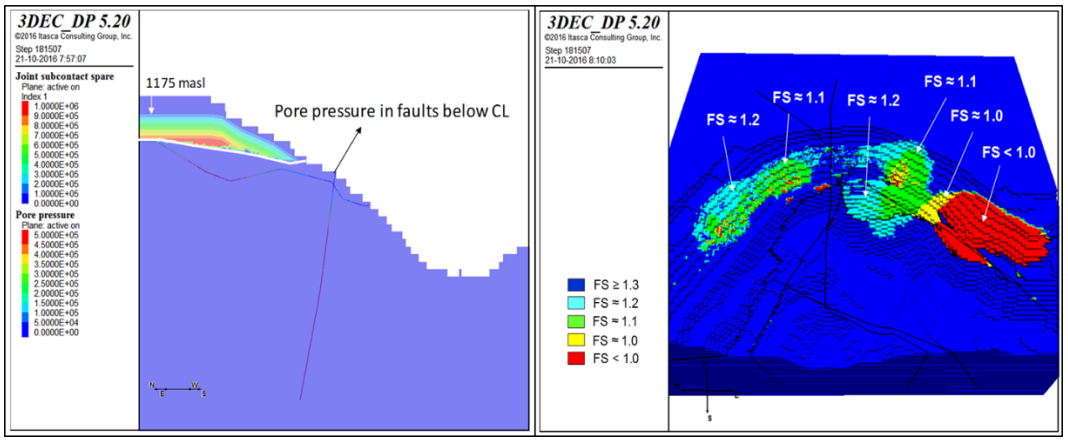


Figure 99 Factor of safety results for GR 80 sensitivity analysis with pore pressure applied in the surface aquifer as well as structures.

Results are similar to the previous analysis, but areas lower down also showed a significant reduction in factor of safety. This is attributed to a decrease in strength of the tectonic unconformity due to pore pressure.

To summarise, by varying strength properties of large-scale faults, the tectonic unconformity, phreatic levels and pore pressures, the results indicated that stability will be most sensitive to the strength and orientation of the tectonic unconformity as well as increased pore pressures in the rock mass and structures.

Risk Mitigation

The geotechnical risk management process at Sishen Mine employs controls at all levels, from slope design to implementation (Figure 100).

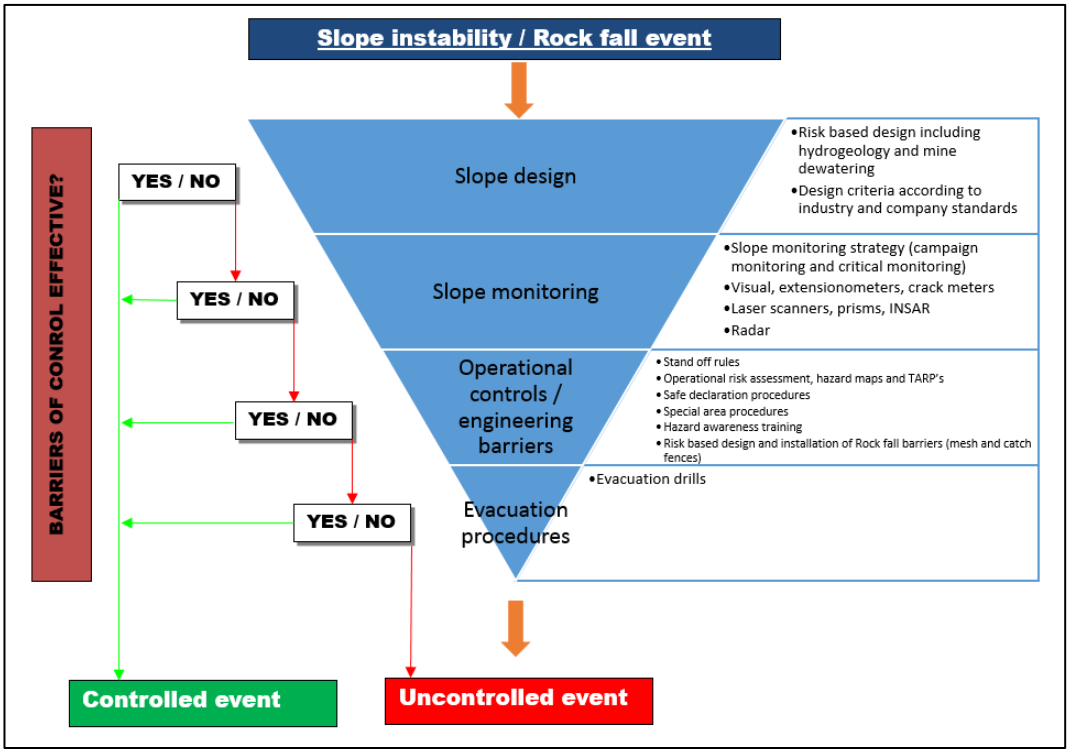


Figure 100 The geotechnical management process employs critical controls at all levels – from design to implementation.

The slope in question does not carry critical infrastructure, therefore to adhere to corporate and industry-accepted criteria and based on the new information obtained, advanced stability assessment and the subsequent risk assessment, the following mitigation actions were implemented:

- Extension of the depressurisation project

Sishen Mine's dewatering strategy, until recently, was focussed on dewatering the deep, fractured aquifer in BIF and Chert Breccia overlying the dolomite. The shallow Kalahari formation aquifer became a focus area for depressurisation, due to the increased rate of mining and instability in an area south of the study area. Piezometer monitoring drill holes and a series of shallow drill holes were established and equipped with solar-powered pumps to depressurize the Kalahari aquifer (Figure 101).



Figure 101 Location of solar powered depressurisation holes with discharge into lined storm water canal.

Based on the successful drawdown achieved (Figure 102) and the sensitivity to pore pressures in the rock mass and structures highlighted by *3DEC* analysis, the network is being expanded to cover the future pushback area as well as the western slope.

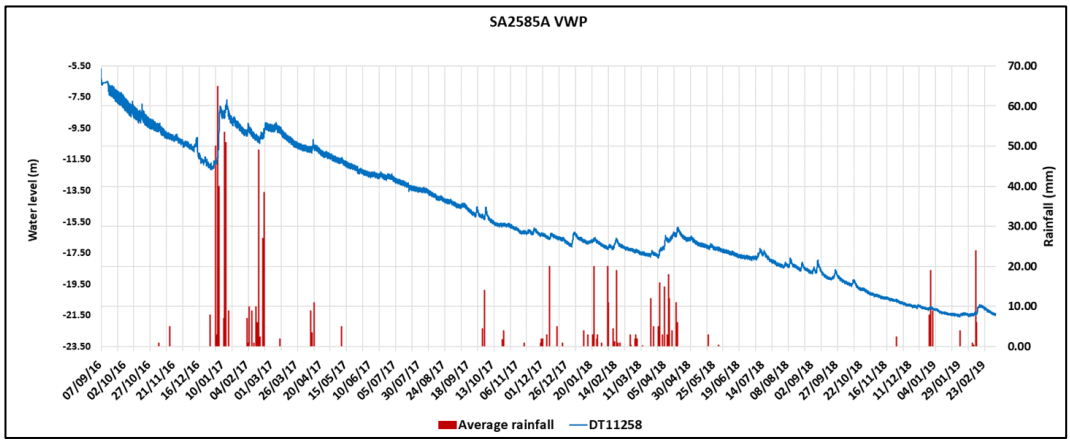


Figure 102 Depressurisation results achieved (note the quick response to rainfall).

- Economic risk mitigation

Based on the mine planning schedule, further mitigation actions are planned for the period in which mining will take place in the area in question, ensuring adequate stockpile levels and access to alternative exposed ore should instability occur.

- Slope stability monitoring

Sishen Mine utilises appropriate slope monitoring technologies in order to manage slope instability and will therefore employ strategic and critical / tactical monitoring in the area in question.

- Pit wall control and mine to design reconciliation

Limit blasting techniques (pre-split and trims) will be employed in the area in question with a robust process in place to reconcile actual performance against the slope design (geometry and face conditions).

- Operational controls

All operational controls to be in place including continuous risk assessments, hazard maps and trigger action response plans, safe declaration procedures and stand-off / exclusion zone procedures.

6.1.3. Summary and Conclusions

The Sishen Mine case study is a case in point that adhering to the methodology described in this thesis will consequently improve the understanding of the way mine plans interact with the underlying geology and their associated implementation risks through a dynamic geotechnical model. Ultimately it leads to increased investor confidence by unlocking maximum value without compromising the geotechnical risk profile of the mine.

Following the methodologies and processes described in this contribution facilitated the unlocking of value that increased Sishen Mine's NPV with approximately R10 billion (approx. US$ 720 000 000) from 2017 to 2018. This will be discussed in detail in Chapter 7.

6.2. Kolomela Mine

6.2.1. Introduction

The application of these methodologies and processes at Kolomela Mine will now be discussed to further illustrate its versatility for various orebodies.

6.2.2. Discussion of results: Application of 3D geometrical analysis methodology

Fully-constrained 3D models, to the original pre-mining surface, were available for all pits at Kolomela Mine. SRM results were used to spatially analyse pit layouts, which are (similar to Sishen Mine) mined in a series of pushbacks or phases towards the final pit boundary. Subsequent to performing 3D geometrical analysis, certain areas of concern were highlighted.

Leeuwfontein Pit North

The main geological features of this area include a paleo-sinkhole structure at the north-eastern extent of the pit, basically an ore-filled circular depression. A series of NE-SW-trending "longitudinal" normal faults which have contributed to the formation of a central, synclinal "keel"; and predominantly NW-SE trending, sub-vertical, strike-slip faults that segment and offset these longitudinal faults (Anthonissen & Basson, 2017). Figure 103 shows the results of the 3D geometrical analysis.

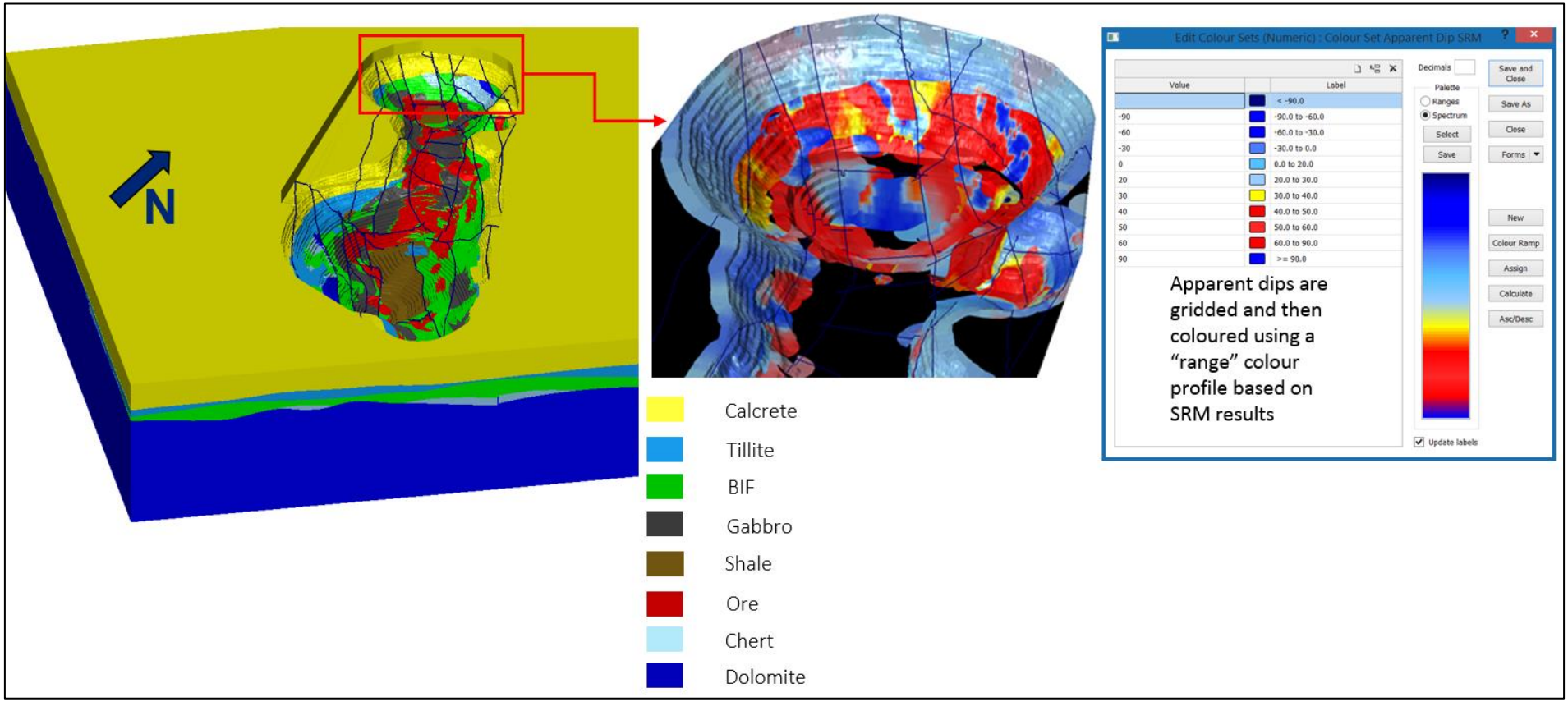


Figure 103 Results of the 3D geometrical analysis of Leeuwfontein Pit at Kolomela Mine.

The 3D geometrical analysis indicated that unfavourable interaction (dipping into the pit) can be expected all around this area. This is due to the fact that the area is a paleo sinkhole that preserved the ore. Unfavourably dipping BIF is successfully controlled at Kolomela Mine with limit blasting techniques to achieve acceptable catchment capacity and acceptable rock fall risk. However, a highly friable carboniferous shale was exposed on the dolomite / chert contact on the eastern side (Figure 104) of the pit.

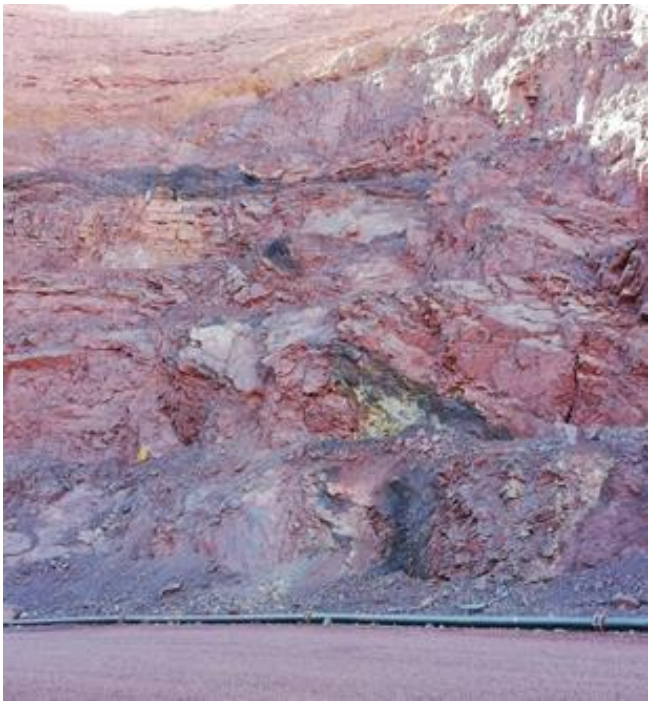


Figure 104 Carboniferous shale exposed on the north-eastern side of the Leeuwfontein Pit.

The analysis also indicated that this contact will be exposed in a fault block on the northern face leading to bench / double bench scale failures due to its orientation (Figure 105).

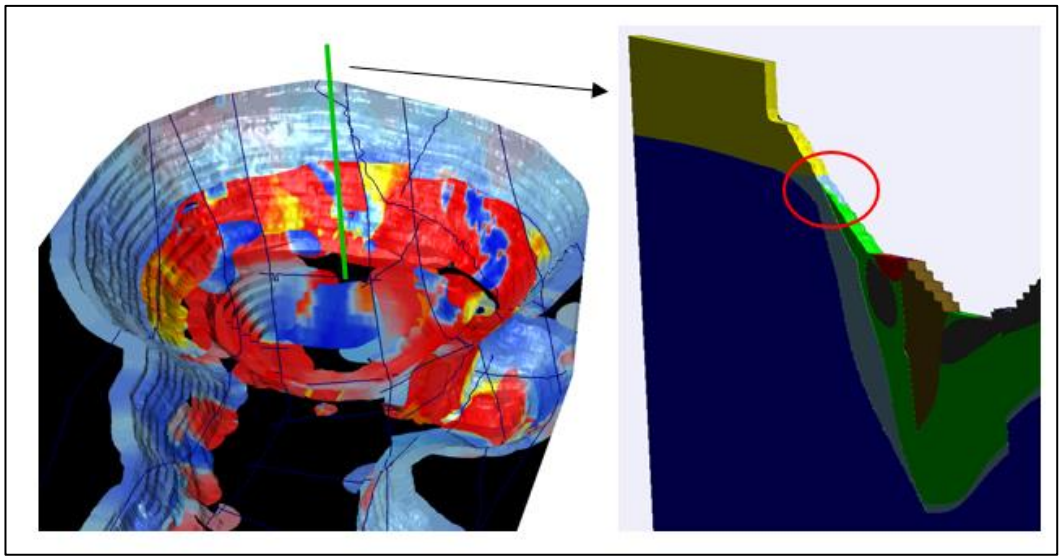


Figure 105 Model with Section illustrating Dolomite / Chert contact exposed in the face in northern fault block.

Stability analysis and risk assessment were conducted (stability analysis attached as Appendix 7) with results indicating that the overall slope adhered to company and industry acceptability criteria. Since a PoF of up to 30% for smaller scale instability is acceptable and taking into account that the slope in question does not carry any infrastructure, the expected risk of smaller scale instability was deemed acceptable based on the application of best practice geotechnical controls at all levels.

When mining of the area exposed the contact, instability did occur. All instability events were successfully managed with no adverse incidents to date. Figure 106 shows the slope stability radar image during instability triggering the successful evacuation of the area.

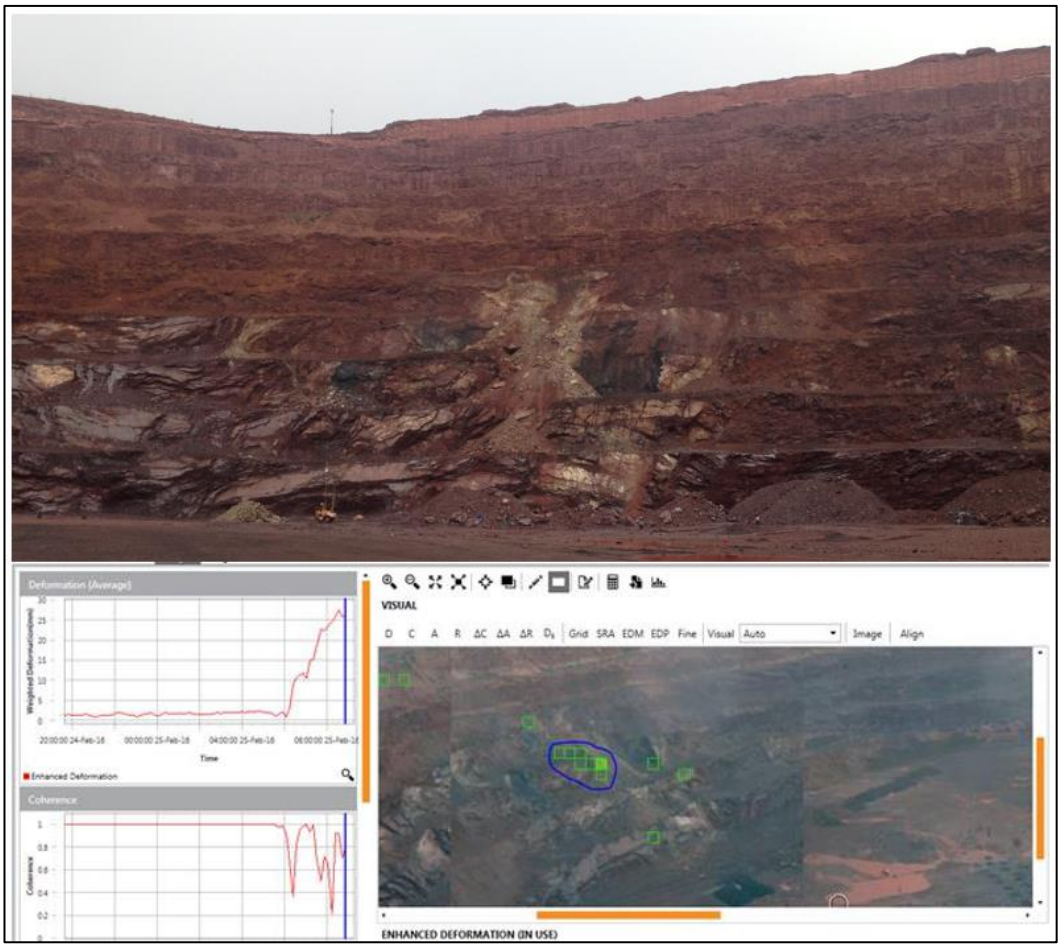


Figure 106 Image (above) and radar image (below) of instability event in the Leeuwfontein Pit.

Subsequent remediation of the area included loading out of failed material to the contact and the installation of wire mesh to manage rock fall risk due to the loss of catchment capacity (Figure 107).

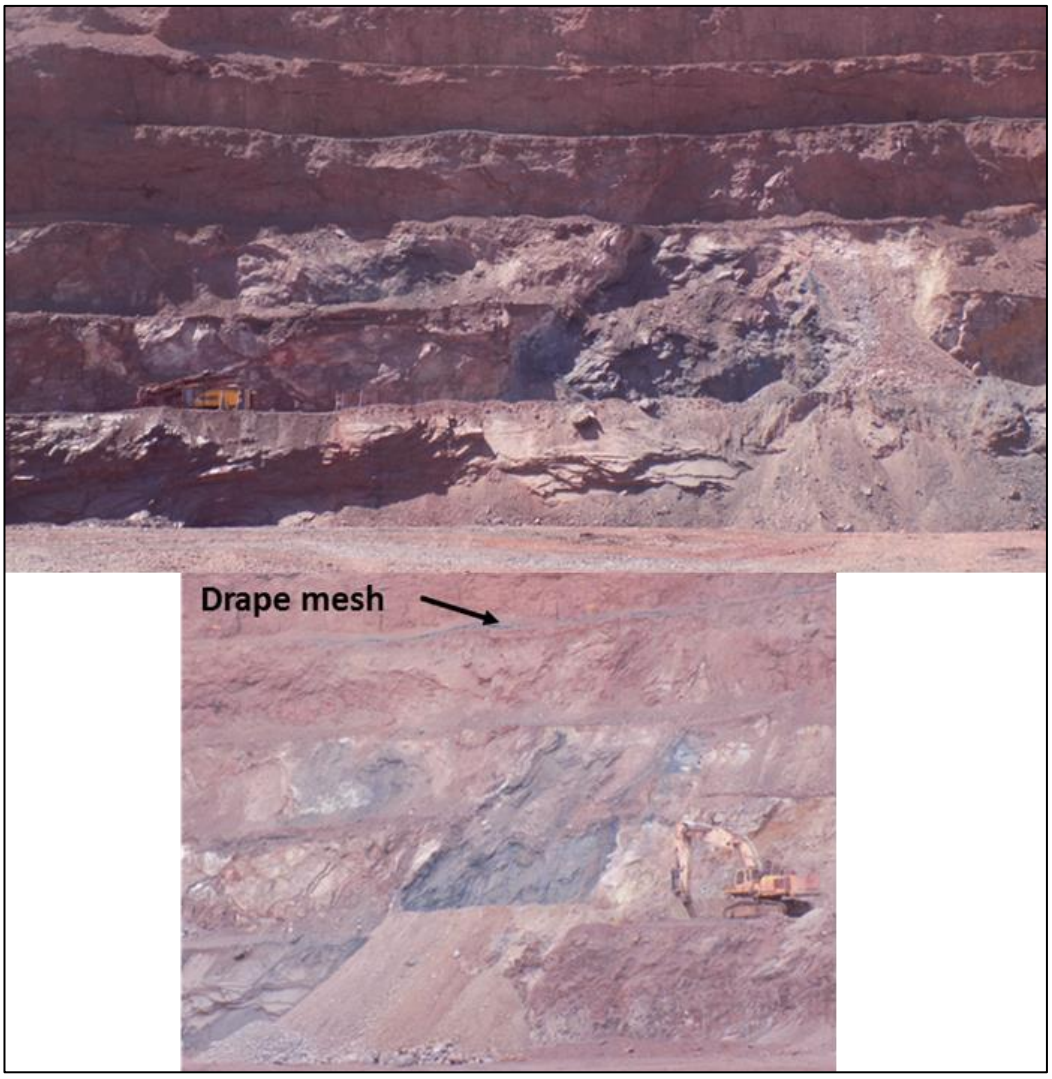


Figure 107 Remediation of failure in the Leeuwfontein Pit at Kolomela Mine (note the installation of drape mesh).

However, the fact remained that only limited boreholes were available adjacent to the ore body in this area informing the geological model. This was due to financial constraints during the exploration phase of the then Welgevonden Project. Although geological uncertainty is accounted for in the fault tree analysis during geotechnical risk assessment, it was still deemed necessary to perform further focussed data acquisition to increase confidence in the geological model of this area. This was mainly due to uncertainty and associated geotechnical risk regarding the possible daylighting of this weak contact lower down in the slope.

Focussed Geotechnical Data Acquisition

Dedicated geotechnical core drilling was planned in the north of Leeuwfontein Pit and drilling integrated with mine planning and execution in 2016. The holes were planned to be drilled in phases, first at an angle of 55 degrees, the second phase at an angle of 70 degrees, and lastly vertical. Figure 108 illustrates the positions of the

holes in plan and the orientation of each phase. The different inclined holes were drilled from the same positions into the slope indicated in Figure 107.

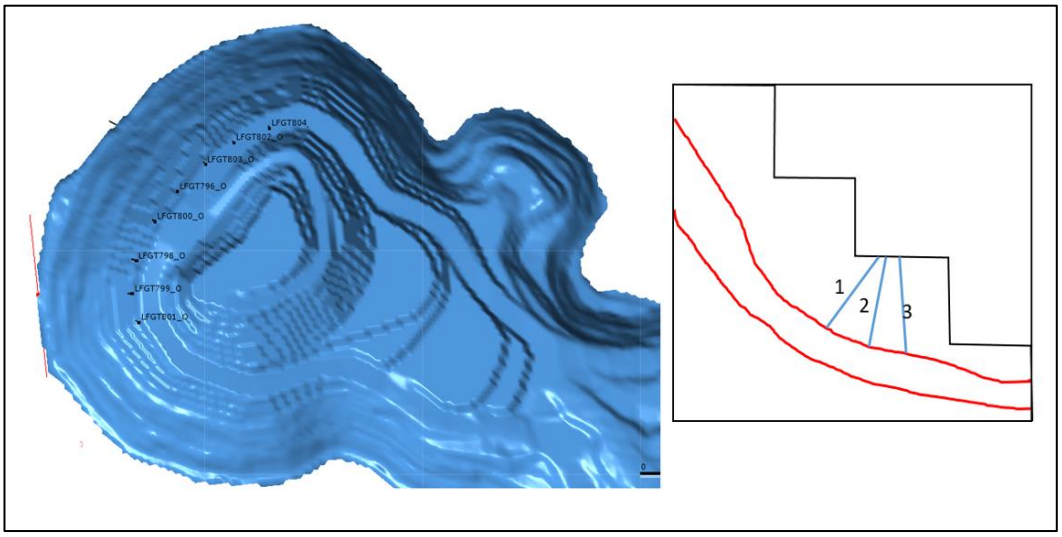


Figure 108 Plan of geotechnical drill holes and an illustration of inclinations drilled.

During the first phase, eight holes at an inclination of 55° were completed to an average depth of 120m. Eight phase 2 holes were then drilled at an angle of 70° with an average depth of 140m. All the holes targeted the chert / dolomite contact.

All holes were logged and included in the geological and geotechnical *acQuire* databases to inform the next geological model update according to the mine planning cycle.

Based on the information obtained from logging, only two phase 3 vertical holes were drilled.

Logging information and the subsequent 2017 geological model update confirmed that the weak chert / dolomite contact did not daylight in the slope, leading to improved confidence in the slope design.

Although the drilling campaign described here could be deemed expensive, the information obtained greatly improved confidence in the slope design by addressing geological uncertainty. The Leeuwfontein Pit example is another case in point where by following the methodology described in this thesis, led to the early identification of geotechnical risk and the successful management thereof. This is therefore an example of how value was protected by following the suggested methodology.

6.2.3. Summary and conclusions

The Kolomela Mine case study is another case in point that adhering to the methodology described in this thesis will consequently improve the understanding of the way mine plans interact with the underlying geology and their associated

implementation risks through a dynamic geotechnical model. This results in the unlocking of maximum value without compromising the geotechnical risk profile of the mine.

Following the methodologies and processes described in this contribution facilitated the unlocking of value to a total of approximately US$ 51 mil at Kolomela Mine. This will be discussed in more detail in Chapter 7.

At the time of writing this thesis, the Leeuwfontein North Pit was mined out. Pit backfilling has commenced with significant operational savings due to shorter hauling distances. This was done without any FoG related accidents due to the effective management of geotechnical risk and through effective collaboration by the Geotechnical Engineering, Mine Planning and Mining Operations Departments.

6.3. Jwaneng Mine

6.3.1. Introduction

Jwaneng Mine is situated in the Republic of Botswana approximately 160 km to the west of the capital city of Gaborone and has been operating since 1982 (Figure 109).



Figure 109 Locality map of Jwaneng Mine *(Debswana Diamond Company (Pty) Ltd, 2015).*

The mine operates utilising a split shell pushback approach and is currently mining what is locally called Cut 7 on the west and Cut 8 on the east. The mine is the largest contributor to the national economy of Botswana and is the world's richest diamond mine by value. The importance of this mine to Botswana cannot therefore be over-emphasized and has significantly contributed to the growth and development of Botswana (Gabanakgosi, et al., 2018).

6.3.2. Geological Setting of Jwaneng Mine

A summary of the geological setting of Jwaneng Mine is provided by (Basson, et al., 2016) and a representative geological Section is illustrated in Figure 110.

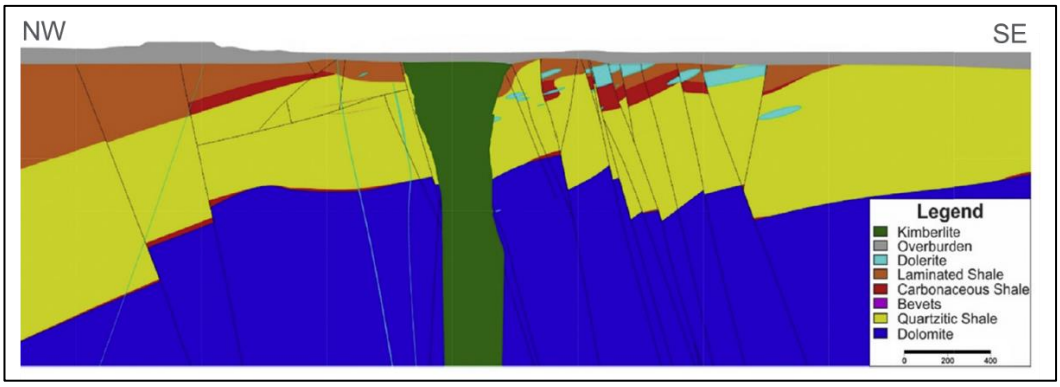


Figure 110 Cross-Section of the centre of the pit. Jwaneng kimberlites are inferred to occur within, or close to the edge of a horst-like structure *(Creus, et al., 2018).*

Stratigraphy

Jwaneng Mine is in the Okavango and Shakwe Zone(s) (Carney, et al., 1994), covered by Palaeoproterozoic (circa 2300-2100 Ma) sediments of the Griqualand West Supergroup of southern Africa. The base of the sequence consists of the c. 2.552 Ga Malmani dolomite. The contact between the Malmani Subgroup and the Rooihoogte/Duitschland Formation has been delineated in several very deep drillholes. The overlying (Middle) Rooihoogte/Duitschland Formation consists of laminated sandstone, mudstone, greywacke and black shale. The upper and lower portions of the (Middle) Rooihoogte/Duitschland Formation are subdivided into quartzitic shale (QS2) and carbonaceous shale (CS2). A chert pebble conglomerate, consisting of angular to rounded chert clasts in a gritty matrix, separates the upper part of the Rooihoogte/Duitschland Formation from its lower part, representing an 80 Ma hiatus in the depositional history. This unit is termed the Bevets Conglomerate (BVT) on Jwaneng Mine, although (Coetzee, 2001) found that the base of the Duitschland Formation near Thabazimbi (South Africa) is occupied by a "flat" chert-pebble conglomerate, which is termed the Bevets or Bevetts Conglomerate at this location. The upper part of the Rooihoogte or Duitschland Formation consists of fine-grained to medium grained, poorly-sorted argillaceous quartzite, greywacke, subgreywacke and silty mudstone. Quartzitic shale (QS1) is succeeded by a diachronous, transgressive (erosional) surface. Above this erosional surface, the 2.264 Ga Timeball Hill (or Lower Ditlhojana) Formation consists of deep marine laminated sandstone, mudstone, greywacke and black shale interbedded with thin, mafic tuff bands. The upper part of the Timeball Hill (or Upper Ditlhojana) Formation consists of laminated sandstone and black, laminated shale (LS). The 2.184 Ga Boshoek Formation, which overlies the upper Timeball Hill Formation, consists of felsic volcanics and graphitic or carbonaceous shale with sandstone intercalations. Together with the Upper Timeball Hill Formation, these comprise the laminated shale unit (LS). The Kalahari Sequence or Group consists of calcrete, sand and scree, which includes alluvial material of unspecified or undocumented origin. The lower part of the Kalahari Group in the area of interest

consists of calcrete or caliche, which comprises calcium carbonate-cemented surficial gravel, sand, clay and silt.

Deformation Events

The deformation sequence and geometry in 3D reveal an early compressional deformation (D) event directed towards a bearing of 350° or almost due north (Figure 111).

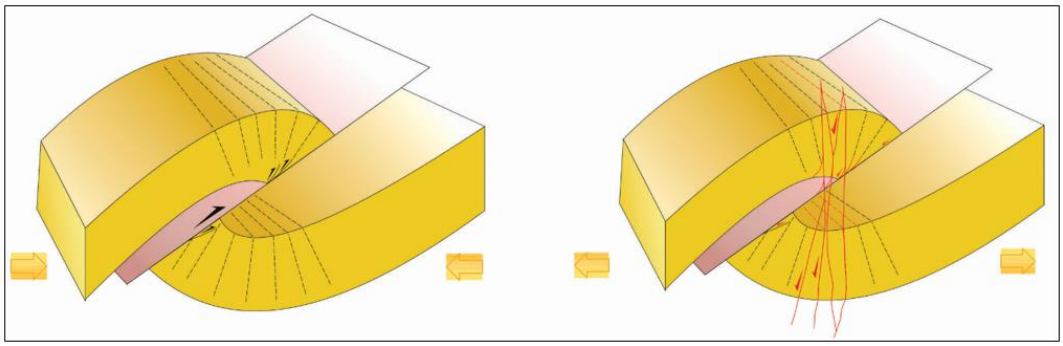


Figure 111 Schematic of the deformation events at Jwaneng Mine: D_1 compression forming breached folds and low-angle thrusts (left); D_2 extension exploiting fanning axial planar cleavage (right) *(Basson, et al., 2016).*

This event is expressed by a series of mesoscale folds and associated low-angle thrusts that show strike extents on the order of 100m. Thrusts merge laterally and down-dip into bedding, expressing "distributed" strain throughout the sequence. This early compressional event was defined by (Dietvorst, 1988) in the Ramotswa-Lobatse area, 120 km ESE of Jwaneng. In that study, regional folding around NE- to ENE-trending, gently plunging (0°-20°) open folds preceded extension and the development of normal faults. A similarly oriented compressional event is evident in the Thabazimbi area in South Africa, approximately 250 km to the east of Jwaneng Mine. At Thabazimbi, a maximum age of thrusting is constrained by a quartzporphyry age of 2054 ± 4 Ma (essentially Bushveld Complex age), from the basal unconformity of the Waterberg Group (Dorland, et al., 2006). The Ramotswa-Lobatse area shows large-scale, normal faulting that sub-divides the Transvaal Supergroup into blocks showing characteristic dips and F_1 fold axis orientations (Dietvorst, 1988). Based on (Dietvorst, 1988), an overview of deformation in the Thabazimbi area, and mapping performed at Jwaneng Mine, regional NE- and ENE-trending faults exploited axial planar cleavage around D_1 anticlines and synclines. In effect, the orientations of D_2/D_3 are controlled by the macrostructural "fabric" imposed on the sequence due to early development of this fold-and-thrust belt. The geometry resulting from this sequence of deformation events is a series of NW-dipping, NE-SW elongated, fault-bounded, wedge-shaped blocks. These define structural domains, each with a characteristic average bedding dip, determined from robust datasets. Relatively minor E-W trending faults within these blocks may subdivide the geology into rhomboid-shaped blocks.

6.3.3. Discussion of Results: Application of 3D Geometrical Analysis Methodology

(Basson, et al., 2016) describes the application of the 3D geometrical analysis methodology discussed in Chapter 3 for assessing the interaction of dominant bedding planes within anisotropic materials (laminated, quartzitic and carbonaceous shales of the Griqualand West Supergroup at Jwaneng Mine) with a design pit.

Applying the Methodology

Standard mapping data, downhole oriented bedding from A/OTV logs and well-constrained, high-confidence 3D models, which are built using implicit modelling techniques, form the basis for the analysis. Based on well-constrained mapping and oriented geotechnical drilling, lithological contacts are predominantly parallel to bedding in their related volume(s), except for volumes that have tectonic or erosional unconformities against their upper limits. Apparent dips of a given lithology, at either an existing or planned pit surface, may therefore be derived from a combination of the dip and dip direction of individual triangles on finely-triangulated lithological surfaces (*viz*. sedimentary contact orientations represent bedding orientations), with the dip direction of individual triangles on pit surfaces, on a pre-defined grid basis. The relationship between the orientation of contacts and the orientation of bedding may be tested via stereonet analysis. This produces an *apparent dip* value that represents the continuous variation in the interaction of the main plane of anisotropy with the pit surface or design surface. Several steps are adopted in Micromine to create apparent dip maps:

- Extraction of triangle orientations (dip and dip direction) from wireframed or triangulated surfaces from the Jwaneng geological model, assigned to structural domains (*viz.* fault-bounded blocks). Surfaces of specific lithological contacts are proven and/or reasonably assumed to be parallel or sub-parallel to bedding within their respective structural domains, thereby providing a "proxy" to bedding orientation;
- Erosional or tectonic unconformities, which violate one of the basic assumptions of the analysis, are filtered out;
- Data from triangles on the sides of fault-bounded blocks, which would provide anomalously steep dips against steep or vertical bounding faults, are filtered out;
- Using a nearest-neighbour algorithm, all surface orientation data, with respect to each structural domain, are assigned to a pit or design. The proximity over which this projection is done from off-(pit)-surface varies, but it is usually advisable to refer to the thickness, lateral extent, and internal coherence of the unit from which data are taken and, by default, through which data will be extrapolated. It was found that using true dip data within a vertical distance of 20m–50m of the pit surface was acceptable;

- Lastly, an apparent dip is calculated by spatially coinciding, on a grid basis, the proxy to bedding surface orientation (dip and dip direction) with face orientation of the design pit;
- Apparent dips are displayed only where units intersect the design pit. This was achieved by clipping modelled lithological volumes against the design pit, to show where they daylight on the design pit;
- Areas on ramps and berms are filtered out;
- Apparent dips are re-gridded using an inverse distance interpolator to give an accurate representation of the *spatial variation in apparent dip for each anisotropic lithological unit, within each fault-bounded block.* Ranges may be arbitrary, or plots could show individual units with ranges or bins based on various critical friction angles.

Definition of Geotechnical Design Sectors

By incorporating data obtained from apparent dip maps and utilizing various strength models according to conceptual failure models (with respect to lithological layers), geotechnical design sectors may be defined (Refer to table 26 for lithological codes).

Table 26 Explanation of lithological codes at Jwaneng Mine.

Lithological Code	Lithology
Sand	Aeolian sand
Calc	Calcrete
LS	Laminated shale
CS	Carbonaceous shale
QS	Quartzitic shale
BVT	Bevets Conglomerate
DM	Dolomitic marble (dolomite)
DOL	Dolerite
SY	Syenite
KIM	Kimberlite

Design sectors are first identified and grouped according to lithologies with similar strength properties, i.e. Hoek-Brown strength parameters (UCS, GSI, Mi, and D) as illustrated in Figure 112.

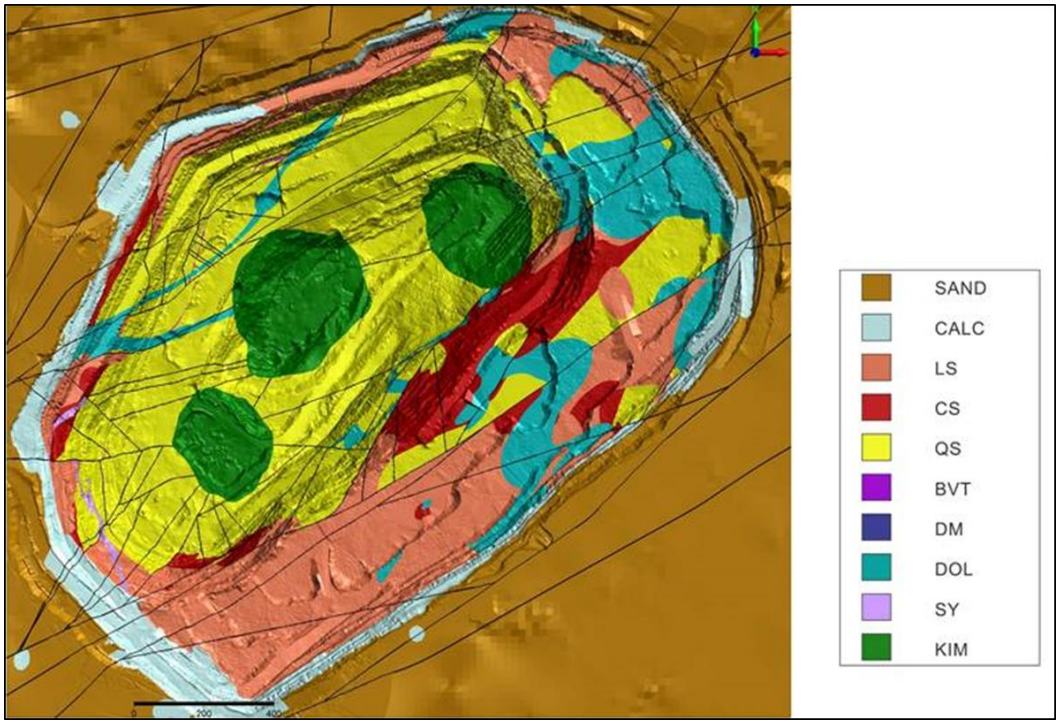


Figure 112 3D geological model clipped to design pit surface showing daylighting or intersecting country rock lithologies *(Basson, et al., 2016)*.

For instance, quartzitic shale is very different from laminated shale or carbonaceous shale at Jwaneng. Zones where the apparent dip of bedding is into the design pit, but importantly, with apparent dips regularly exceeding 37°, are considered for the delineation of separate design subsectors (Figure 113-114).

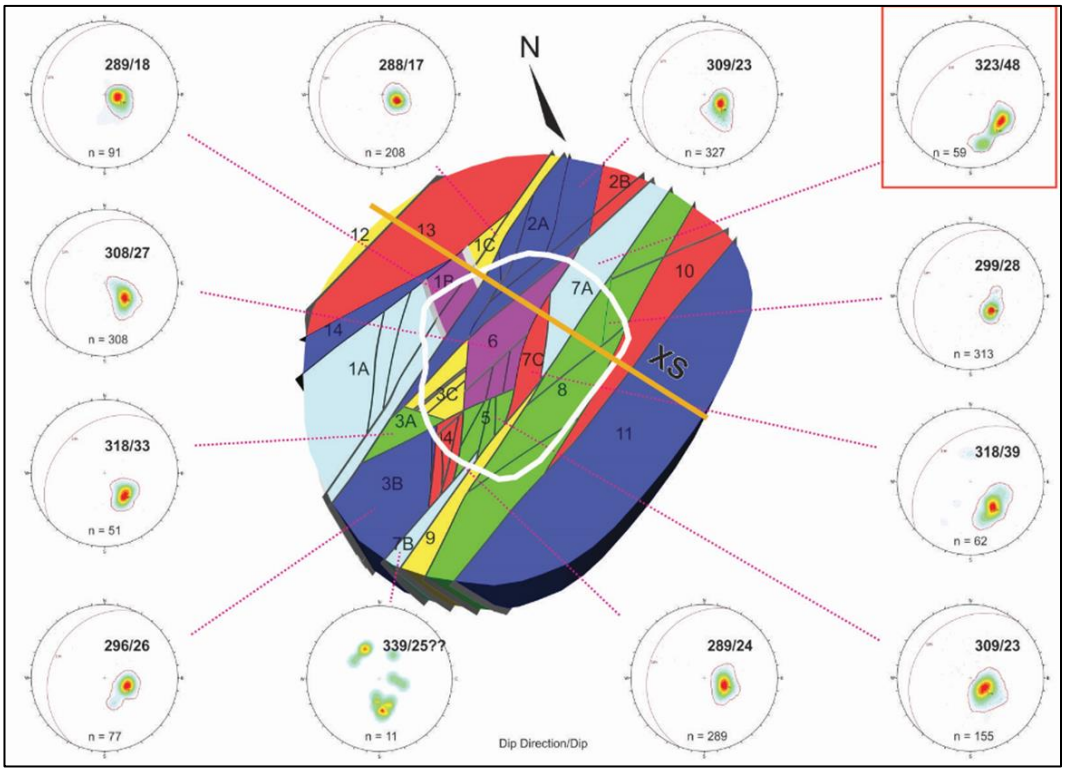


Figure 113 Sub-domaining of bedding readings from pit mapping into fault-bounded blocks. Anomalously steeper dips from Domain 7A are highlighted *(Basson, et al., 2016).*

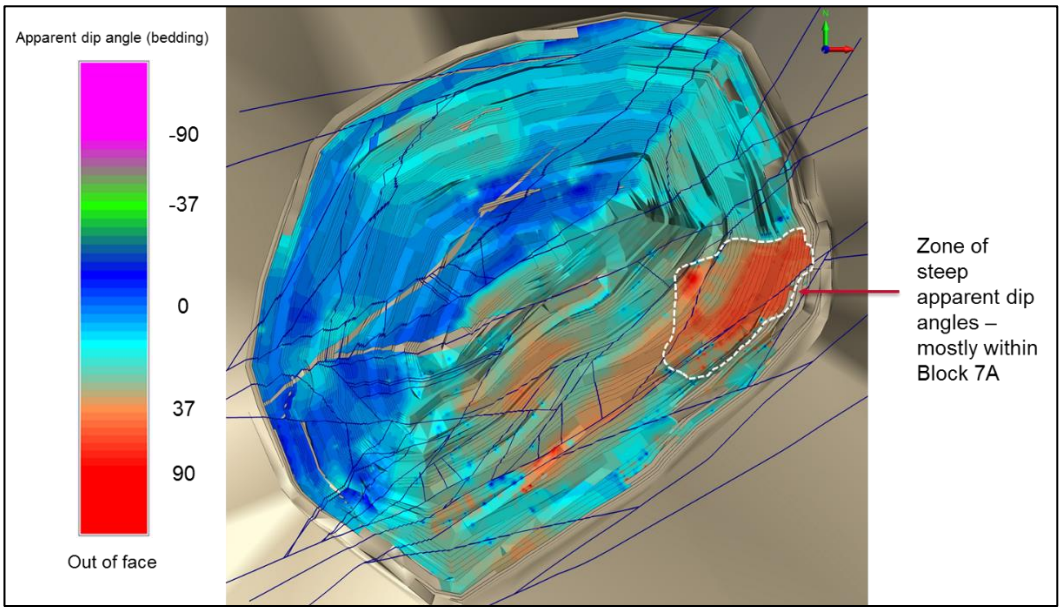


Figure 114 Contoured plot of apparent dip for QS, CS, LS (dolomite and sill is excluded), binned according to average friction angle (37 deg) and sense of dip (into vs. out of face). The plot highlights a zone of relatively steeper bedding, compared to the underlying design surface, within Domain 7A and trending NE-SW through Domains 8 and 9 *(Basson, et al., 2016).*

Conversely, large areas where the apparent dip is more favourable (viz. away from the pit centre or into the pit face), may be delineated, which provides opportunity for optimising the design. This methodology allows for a significantly improved definition of design sectors without using averages or median dips of planes of bedding or other planes of anisotropy for a whole domain or sector. When combined with strength and failure criteria, this allows for the early subdivision of domains into practical design sectors as individual 3D volumes.

When utilized early in the mine design process, this methodology optimizes (viz. usually reduces) the required number of 2D design sections that need to be analysed. Time and expense required to perform the iterative process of geotechnical stability analysis and risk assessment is also optimized and reduced.

A case in point is the NE Corner of the pit at Jwaneng Mine. An apparent dip analysis highlighted potentially problematic blocks (Block 7A and 8A), which appeared to show steeper bedding dips compared to adjacent blocks (an additional 8°-10°), based on an average within a DIPs stereonet window (Figure 115).

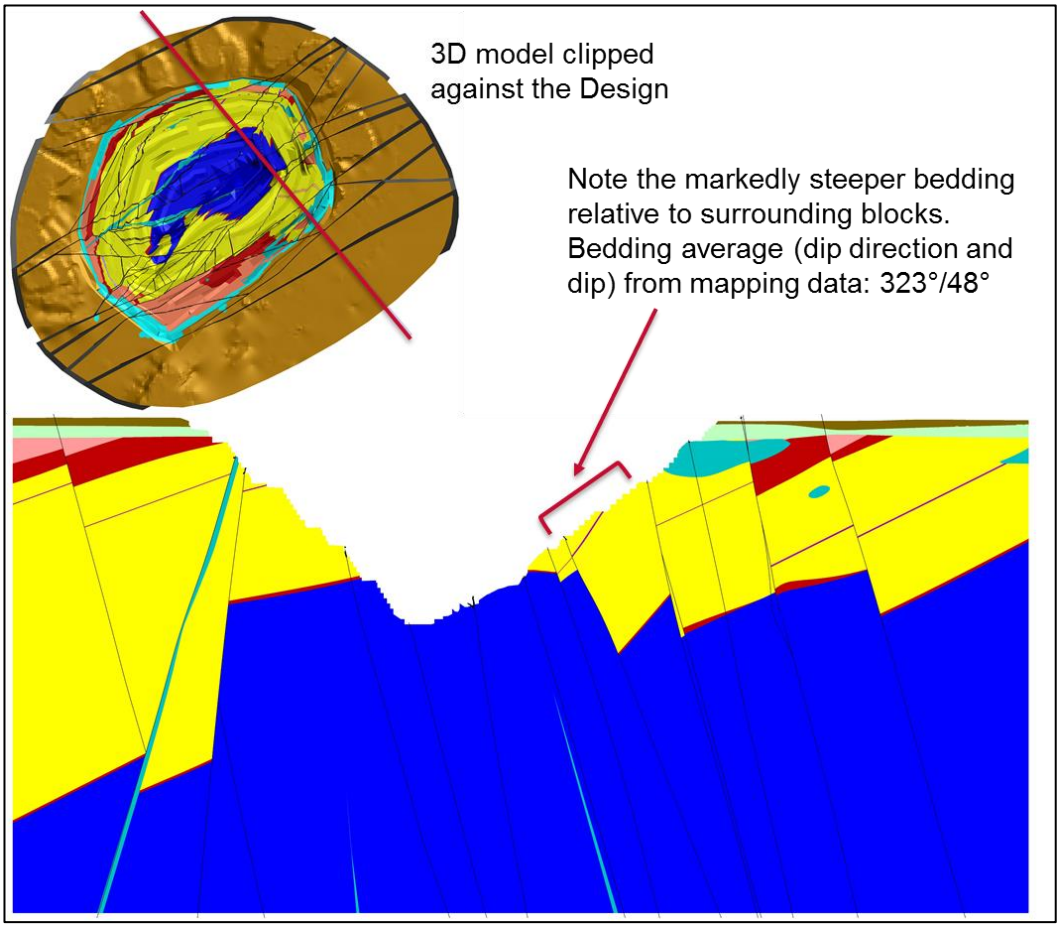


Figure 115 NW-SE trending cross-Section showing the 3D model clipped to the design surface and the relatively steeper bedding for Domain 7A (indicated) *(Basson, et al., 2016).*

The identified anomalously steep bedding, highlighted by the apparent dip analysis, has over time led to planar sliding failures affecting single to double benches. The failure of such benches in planar sliding leads to pit-ward dipping bedding surfaces that extended over 3-4 benches. Particularly to the NE part of the pit, access ramps were at risk of failure due to the locally steep bedding.

Using the methodology described herein, geotechnical risk to the future cutback was identified early and detailed stability analysis was thereafter carried out to determine the factor of safety (FS) and probability of failure for the area. The results of the stability analysis indicated lower than acceptable FS and, as mitigation, various options were considered.

Dip Slope Mining at Jwaneng to Mitigate Geotechnical Risk

Conventional mining utilises vertical bench faces and as was highlighted by the apparent dip analysis, will lead to undercutting of bedding planes in areas with unfavourable interaction between these geological features and slope orientation. This will result in single to multiple bench failures (Figure 116).



Figure 116 Planar type bench failures at Jwaneng Mine Cut 8.

In order to mitigate this risk, Jwaneng identified Dip Slope Mining as a solution ensuring safe and sustainable mining operations (Gabanakgosi, et al., 2018).

A dip slope is described as a rock slope with layered structures stretching along its inclined direction (Lee, et al., 2013) (Fisher, 2009). Dip slope mining involves excavating pit benches along a potential plane of weakness, which in the case of Jwaneng Mine Cut 8 slopes, is presented by the moderately steep dipping bedding

planes into the pit. This is done to eliminate the potential instability created by undercutting the bedding planes.

According to Gabanakgosi (2018), extensive geotechnical data collection was performed. This included geotechnical mapping utilising laser scanning, downhole tele viewer logging (OTV/ATV) as well as geological and geotechnical core logging and rock strength testing (Figure 117).

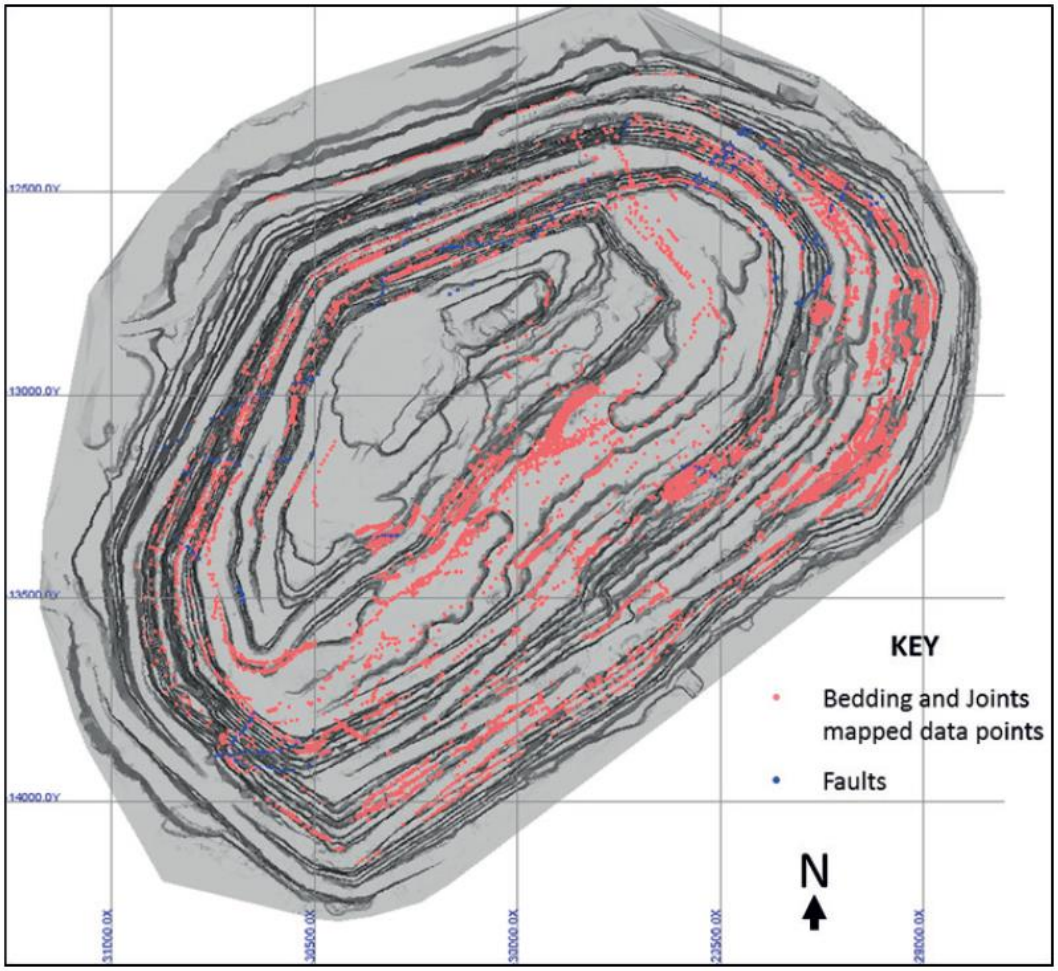


Figure 117 Geotechnical mapping coverage for Jwaneng Mine *(Gabanakgosi, et al., 2018)*

This information was critical to produce high quality geological models on which the design is based.

According to Gabanakgosi (2018), mining operations where this mining method has been implemented, include AngloGold Ashanti's Iduapriem Mine in Ghana, various Rio Tinto and BHP iron ore mines in Western Australia, several coal mines in western Canada and Newcrest's Telfer Mine in Australia. However, in contrast to these mines, fabric orientations at Jwaneng Mine show significantly more variability at a local scale due to a more complex structural evolution. This

localised variability necessitates a detailed understanding of bedding orientation for dip slope mining to be successful.

A dynamic fabric structure model was subsequently developed utilising high quality geotechnical data as input to design, i.e. detailed plans to mine to certain bedding planes.

Optimised blast designs were continuously improved to determine the most appropriate blasting parameters (hole depths, burden, spacing, blast hole layout, charge and timing) for a specific area. During drilling and charging, stringent quality checks and controls were implemented with corrective actions to address non-conformances (Figure 118) (Gabanakgosi, et al., 2018).

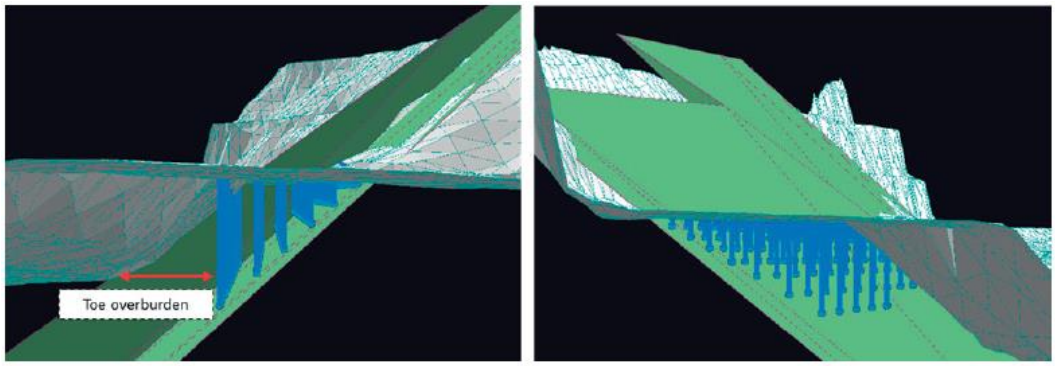


Figure 118 Blast block designs for dip slope benches. *(Gabanakgosi, et al., 2018)*

Loading of blasted material on the targeted dip slope by an excavator also had to be controlled effectively to protect the final pit boundary (Figure 119).



Figure 119 An excavator scaling and loading a final pit boundary *(Gabanakgosi, et al., 2018).*

Gabanakgosi (2018), stated that the dip slope mining had its challenges, ranging from mining space constraints and interfaces with active pushbacks, production delays associated with geotechnical data collection from exposed faces, highly variable bedding orientations as well as conversion zones from dip slope mining to conventional mining.

However, dip slope mining was implemented successfully, largely driven by high confidence in the structural geological model and accurate mining execution (Gabanakgosi, et al., 2018).

6.3.4. Summary and Conclusions

The methodology and example presented herein augments the use of 2D design sections by improving the early definition of design sectors, as inputs to the mine planning process or into focussing on geotechnical risk mitigation in specific areas. This is particularly important where the main plane(s) of anisotropy show significant changes in dip or dip direction, across various domains. This is the case at Jwaneng, where each fault-bounded block exhibits its own particular dip and dip direction due to early folding and variable rotation of fault-bounded blocks. In addition, the potentially problematic Blocks 7A and 8A occurred where there is a change in trend of pit and the future design.

The methodology has greatly assisted the early identification of the stability condition. It has allowed for forward prediction of the stability implications, based on the still-to-be-mined benches with respect to the mine design. This information

led to the accurate definition of the design (Problem statement, Requirements and constraints, Uncertainty minimisation and Concept formulation) (Stacey, 2009), and ultimately early risk mitigation through accurate and successful execution of the solution design (Dip slope mining).

Business risks associated with personnel and equipment safety as well as economic risks could have had devastating impacts on the mine's sustainability negatively affecting the economy of Botswana.

7. VALUE ADDED BY FOLLOWING THE METHODOLOGY DESCRIBED

7.1. Introduction

It is often not possible to quantify the value that results from geotechnical research and the application thereof. However, in the case of Sishen Mine, value quantification has become readily available through publication in a mining company annual report.

7.2. Value Add at Sishen Mine

Following the novel methodology described in this thesis at Sishen Mine, not only led to more effective risk mitigation, but also to the launch of a slope optimisation initiative to unlock value.

This is based on the principle that following the new methodology continuously increases confidence in the slope design by addressing geological uncertainty in potential risk areas highlighted by the 3D geometrical analysis. This was done through focussed data acquisition and more advanced stability analysis in potential risk areas.

This project also focusses on design sectors with favourable interaction of slope orientation with anisotropic units highlighted by applying the new methodology, lithologies with favourable strength characteristics where stability analysis indicates optimisation potential as well as practical layout optimisation aspects (geotechnical berms and ramps). Potential options with significant value were evaluated that determines cost saving by decreasing waste stripping for the same amount of ore as well as accessing additional deeper ore at equivalent strip ratios.

Phase 1 of the slope optimisation project was included in the Sishen 2018 Life of Mine (LOM) plan. This work unlocked significant value for Kumba Iron Ore and was the major contributor to an increase in NPV from 2017 to 2018 of approximately R10 billion (additional 50.8 million tons of ore).

Table 27 Summary of value added through process driven slope optimisation at Sishen utilising the new methodology.

Aspect	Tons	Indicative recovery (%)	Indicative iron ore price (US$ per ton)	Indicative Value (US$)
Additional ore	50.8 Mil	71	72	2.6 billion

The following are quotes from the 2018 annual reports:

- "Reserve life increased to 14 years (from 13 years in 2017), as a result of the optimised pit slope design built into the updated LoM plan life and productivity improvements."
- "Most of the annual increase can be attributed to a steepening of the pit slopes of the Sishen pit design resulting in a 50.8 Mt increase in Ore Reserves, based on advances made in the spatial geotechnical modelling field enabling a better spatial understanding of pit slope failure mechanisms, allowing for optimisation of pit slope designs." (Anglo American, 2019)
- "Sishen – in 2018 a slope optimisation project was completed which resulted in a reduction in the LoM stripping ratio from 3.89: 1 in 2017 to 3.4: 1 in 2018."

Phase 2 of the project will focus on design sectors with favourable dipping BIF slopes. The objective of this phase will be to access additional ore outside the current pit layouts without additional waste stripping. It has the potential to further extend the operating life of Sishen Mine significantly equating to significant value.

7.3. Value Add at Kolomela Mine

At Kolomela Mine to date, not only was the mine plan achieved, but increased confidence in the slope design, supported by ongoing design reconciliation described in detail earlier, led to the identification of optimisation opportunities.

The Kolomela Mine orebodies are different to that of Sishen in the sense that they are not open ended. The focus of slope optimisation at Kolomela is therefore to ensure maximum extraction of available ore while minimising waste stripping vs. adding additional ore at Sishen.

Mining of the northern part of the Leeuwfontein pit was accelerated to create a concurrent backfill opportunity. Part of this investigation included layout optimisation to mine ore that was previously outside of the pit layout (refer to Figure 120).

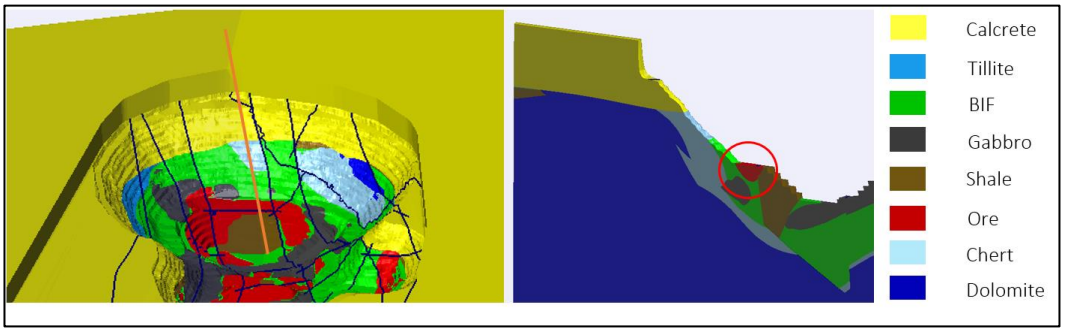


Figure 120 Section illustrating ore targeted for optimisation.

Although slope steepening was done in a small area of the pit, no slope steepening was done on the northern slopes. However, due to increased confidence resulting in lower geotechnical risk, as well as the accelerated mining of this part of the pit, the ramp system could be optimised by removing dual access and targeting ore outside of the pit layout. Table 28 summarises the total value added by accessing additional ore and decreasing waste stripping.

Table 28 Summary of value added through process driven slope optimisation at Kolomela utilising the new methodology.

Aspect	Tons	Indicative cost of waste mining (US$ per ton)	Indicative recovery (%)	Indicative iron ore price (US$ per ton)	Value (US$)
Additional ore	1 Mil	-	71	72	51 120 000
Waste saving	130000	2	-	-	260 000
				Total:	51 380 000

7.4. Conclusions

The application at operations of the research described in this thesis, unlocked significant value. Value was quantified and in the case of Sishen Mine, specifically stated in the published mining company annual report.

Although the aim of mining companies is to optimise pit slope designs to maximise returns, value protection is equally important, as was shown in the Jwaneng case study. Business risks associated with personnel and equipment safety as well as economic risks can have devastating impacts on a mine's sustainability.

8. CONCLUSIONS

The objective of the research, as was defined in the introduction, was to record the pioneering application of Discrete Fracture Networks (DFN) for anisotropic Banded Iron Formation (BIF) and Shale (SH) units, in the Northern Cape Province of South Africa, utilizing the ubiquitous joint rock mass (UJRM) modelling technique in *3DEC* to effectively account for rock mass anisotropy and scale effects.

Subsequently, the study aimed to demonstrate that the use of vertical 2D design sections in slope designs may be augmented by a new and better methodology that established the sizes and geometries of design sectors from conceptual-phase projects (exploration phase) to operational mines, based on fully-constrained, implicit 3D models and inputs from synthetic rock mass (SRM) modelling. This results in a more robust and practical suite of sector-specific design parameters, in block model format as inputs for mine design across several commodities. Application of this new methodology results in a dynamic geotechnical model that may be continuously updated and calibrated with new information (e.g. mapping from benches or mined slopes as well as downhole data for future mining areas). Such an ongoing process will lead to optimised designs and early risk mitigation, ultimately unlocking maximum value while maintaining zero harm.

The results of this methodology are dependent on the quality and quantity of input data. However, it allows one to focus ongoing and future data acquisition in areas of concern, by considering available data and, moreover, based on maps that show the continuous variation of certain parameters throughout the volume of interest. The methodology follows a risk-based approach, as the resulting focused data acquisition mitigates risk cost effectively from early project stages. It therefore addresses the fact that slope instability is one of the major sources of risk in open pit mining, largely due to data uncertainties. This was achieved as follows:

- All available data on the banded iron formation and shale units of the Northern Cape was collected and statistically analysed.
- Synthetic Rock Mass Modelling was performed by developing Discrete Fracture Networks (DFN) for the Banded Iron Formation and Shale units found in the Northern Cape utilizing the ubiquitous joint rock mass (UJRM) modelling technique in *3DEC* to account for rock mass anisotropy and scale effects.
- A new, robust methodology was developed that utilizes input from synthetic rock mass modelling, for the extraction of the spatial variation in parameters by highlighting possible areas - of any size or shape – that show unfavourable interactions with slope geometries in early stage projects, current operations and future pushbacks. Therefore, for the first time, this study describes how to fully exploit the integration of modern, smooth,

implicitly built, radial basis function derived surfaces and solids in geological/structural geological modelling as critical inputs to slope design.

- Available data was reviewed from an early stage exploration project and operational mines, namely:
    - Heuningkranz Exploration Project
    - Sishen Mine
    - Kolomela Mine
    - Jwaneng Mine
- The new methodology was applied to test its application on various geological settings and project stages.
- Results informed the design process leading to effective geotechnical risk mitigation and the unlocking of significant value.

The following Sections summarise the results and conclusions reached for each Chapter in the thesis concluding with suggestions on future research.

8.1. Synthetic Rock Mass Modelling

The most challenging aspects of slope design in moderately- to heavily-jointed rock masses relate to the impacts of in-situ joint fabric and scale effects on rock mass behaviour (Sainsbury, et al., 2008).

Chapter 2 discussed the results of the pioneering development of SRM's for BIF and shale units in the Northern Cape of South Africa, on which the economics of large iron ore mines in the Northern Cape depend heavily. It introduced the novel idea of a "concept level" SRM for early-stage exploration projects wherein certain informed assumptions may be made, based on existing knowledge and since SRM's are completely reliant on data provided by high quality, bench-scale structural mapping, which is not available on most early stage projects. Following an iterative process, these models may be tested and refined as new information becomes available.

Results indicated good agreement with explicit behaviour and consequently, implicit properties have been used in 3D geometrical analysis and mine-scale numerical models.

8.2. A New 3D Geometrical Analysis Methodology

Chapter 3 described how this novel methodology of analysing the interaction of lithological contacts, representative bedding isosurfaces and complex geological features with slope geometry, fully exploits the integration of smooth, implicitly-built radial basis function-derived surfaces and solids as critical inputs to slope design.

It augments the use of 2D design sections by providing a rational and dynamic methodology to improve the definition of design sectors, as input to the mine planning process from a very early stage. This is particularly important where the main plane(s) of anisotropy show significant changes in dip direction, which may justify domain subdivision. This technique also overcomes the situation wherein certain parts of the pit inevitably show a dramatic change in orientation with respect to strike or dip direction within a domain or sector, which have historically been addressed by more traditional means (*viz.* average or median dips).

The methodology may be utilised in early-stage projects when only modelled data, derived from radial basis function-built lithological contacts, are available. In certain instances, this may be augmented by downhole data from oriented drill core, or from dense – or closely-spaced – readings derived from optical / acoustic televiewer (OTV/ATV) analysis.

Improved and early design sector classification highlights possible areas - of any size or shape – that show unfavourable interaction with slope geometries, thereby resulting in a more robust and practical suite of sector-specific design parameters as inputs for mine design. The results also allow for more downstream, focussed data acquisition, including dedicated geotechnical drilling, to further improve dynamic geotechnical models.

In more advanced projects, a greater array of usually denser data sets is available to inform all aspects of the geotechnical model, thereby resulting in increased confidence in the results obtained from applying the methodology. During operations, instability events and slope performance reconciliation may also be plotted with respect to apparent dip or derived synthetic rock mass maps, to elucidate failures or to investigate other volumes with comparable interactions between structural features and either current pit geometries, pushbacks or final/planned slope geometries.

By applying this methodology, the slope design process can be improved significantly.

8.3. The Slope Design Process

Chapter 4 discussed the 3D geometrical analysis applied as part of an iterative process. It demonstrates how the new methodology improves the slope design process by consequently improving the understanding of mine plans and their associated implementation risks, ultimately leading to increased investor confidence, especially if applied as early as possible to facilitate optimised designs and early risk mitigation.

The methodology can be incorporated in the slope design process from early stage projects through to operational mines' planning cycles. It follows a risk-based approach as the resulting focused data acquisition, rigorous stability analysis and risk assessment in areas of concern, mitigate risk from early project stages to operational mines (future pushbacks).

It therefore addresses the fact that slope instability is one of the major sources of risk in open pit mining, largely due to data uncertainties.

8.4. Application of the Design Process, Synthetic Rock Mass Models and 3D Geometrical Analysis Methodology to Case Studies in Project Phase

Utilising the input from the SRM analysis, Chapter 5 described how the new 3D geometrical analysis methodology was successfully applied at the Heuningkranz project resulting in the definition of early stage design sectors. A geotechnical block model was developed, constrained with design sectors and populated with geotechnical design parameters as input in the mine planning process.

Early stage, focussed geotechnical data acquisition was also planned and implemented based on results obtained from the 3D geometrical analysis. New data is included in the geological and geotechnical databases to inform model updates following the suggested iterative process.

The application of the new methodology at the Heuningkranz exploration project demonstrated how early front-end loading of a project utilising the suggested iterative process, greatly improves slope design to achieve the objectives of the project stage, i.e. to look for fatal flaws and to refine the investigation with new data (Read & Stacey, 2009).

From a geotechnical engineering point of view, this was achieved as focussed data acquisition targets potential risk areas early on to allow for optimised ramp and waste dump placement leading to improved slope designs. It therefore increases confidence in one of the major drivers of this project, viz. the stripping ratio that is vital to the economic viability of the project.

8.5. Application of the Design Process, Synthetic Rock Mass Models and 3D Geometrical Analysis Methodology to Case Studies in the Operational Phase

Chapter 6 discussed Sishen Mine as a case study. Sishen Mine is a case in point that adhering to the methodology described in this thesis will consequently improve the understanding of the way mine plans interact with the underlying geology and its associated implementation risks through a dynamic geotechnical model. Ultimately it leads to increased investor confidence by unlocking maximum value without compromising the geotechnical risk profile of the mine.

The methodology was also applied at Kolomela Mine with great success. Significant value was unlocked at this mine. It was achieved without any fall of ground (FoG) related accidents due to the effective management of geotechnical risk and through effective collaboration of the Geotechnical Engineering, Mine Planning and Mining Operations Departments.

At Jwaneng Mine, the methodology has greatly assisted the early identification of the stability condition. It has allowed for forward prediction of the stability implications, based on the still-to-be-mined benches with respect to the mine design. This information led to the accurate definition of the design (Problem statement, Requirements and constraints, Uncertainty minimisation and Concept formulation) (Stacey, 2009), and ultimately early risk mitigation through accurate and successful execution of the solution design (Dip slope mining). Business risks associated with personnel and equipment safety as well as economic risks could have had devastating impacts on the mine's sustainability and consequently on the economy of Botswana.

8.6. Value added by following the methodology described

Following the methodologies and processes described in this research, as well as improving design implementation, facilitated the unlocking of value that increased Sishen Mine's Net Present Value (NPV) with approximately R10 billion from 2017 to 2018 (approx. US$ 720 000 000). A total of 50.8 million tons of additional ore was included in the 2018 Life of Mine (LOM) plan.

The Kolomela Mine case study is another case in point where this contribution facilitated the unlocking of value to a total of approximately US$ 51 million.

Although the aim of mining companies is to optimise pit slope designs to maximise returns, value protection is equally important, as was shown in the Jwaneng case study. Business risks associated with personnel and equipment safety as well as economic risks can have devastating impacts on a mine's sustainability. Also, the methodology described in this thesis has since been successfully applied at De Beers' Venetia Mine.

8.7. Suggestions for Further Research

Several authors refer to numerous case studies describing the failure or significant over-expenditure of mining projects caused by inadequate understanding of the inherent variability of the in-situ rock mass.

Hoek & Martin, (2010) noted that "the SRM approach has provided an outstanding set of tools which promise a far more realistic and reliable method of modelling rock mass behaviour than has been available in the past. At the very least this approach should enable us to calibrate traditional rock mass classification approaches used to estimate rock mass properties, but the approach also has the potential, in the long run, of replacing empirical approaches".

Therefore, research and the practical application at a variety of geological settings, of the SRM approach and contributions focusing on improving the understanding of inherent geological variability (Fillion, M.H. , 2018), should be undertaken to continuously improve and provide tools better enabling the Geotechnical Engineering fraternity to successfully deal with geological / hydrogeological uncertainty to ultimately improve investor confidence.

8.7.1. The Impact of Technology

Advancements in data acquisition techniques are never-ending, leading to the advancement of data analytics and intelligence. Future research will need to focus on enhancing Geotechnical Engineering's capability to draw value from Big Data by transforming this information to insight. Measure-while-drilling methods, capturing rock mass hardness and fracture spacing data, and producing huge data sets are an example. Although caution should be exercised with applying Geostatistical methods to geo-mechanical properties, further research will be needed to fully exploit these potential large data sets into meaningful slope design input.

Continued automation in the mining industry may result in a shift of focus for Geotechnical Engineering regarding risk assessment. Current acceptability criteria may shift towards prioritising economic risk over safety risk as personnel exposure to geotechnical hazards is reduced, i.e. mining areas having no personnel due to full automation.

REFERENCES

Admassu, Y. & Shakoor, A., 2013. DIPANALYST: A computer program for quantitative kinematic analysis of rock slope failures. *Computers & Geosciences 54*, pp. 196-202.

Altermann, W. & Hälbich, I. W., 1991. Structural history of the southwestern corner of the Kaapvaal Craton and the adjacent Namaqua realm: new observations and a reappraisal. *Precambr. Res. 52 (1)*, pp. 133-166.

Anglo American, 2019. *Anglo American Kumba Iron Ore Investors.* [Online] Available at: https://www.angloamericankumba.com/investors/annual-reporting.aspx

Anthonissen, C. & Basson, I. J., 2017. *Leeuwfontein - 2017 3D Geological Model Revision and Update,* s.l.: Report prepared for Kumba Iron Ore, Report No. TECT 011/2017R.

Anthonissen, C. J., Stoch, B., McCall, M. & Basson, I. J., 2016. *Sishen Mine: Structural Re-Interpretation and Baseline 3D Modelling in Leapfrog Geo: For Ore Resource Estimation and Geotechnical Design,* s.l.: Report No. TECT007/2016R for Kumba Iron Ore.

Barton, N. & Grimstad, E., 2014. *An illustrated guide to the Q-system following 40 years use in tunnelling.* [Online].

Barton, N. & Grimstad, E., 2014. *Forty Years with the Q-system in Norway and Abroad.* s.l., s.n.

Barton, N. R., Lien, R. & Lunde, J., 1974. Engineering classification of rock masses for the design of rock support.. *Rock Mechanics. Vol 6.,* pp. 189-236.

Basson, I. J. et al., 2017. Ore-structure relationships at Sishen Mine, Northern Cape, Republic of South Africa, based on fully-constrained implicit 3D modelling. *Ore Geology Reviews 86,* pp. 825-838.

Basson, I. J. et al., 2016. *Defining Geotechnica Design Sectors: Apparent Dip Analysis at Jwaneng Mine, Botswana.* Sun City, South Africa, SAIEG.

Basson, I. J. et al., 2018. The structural setting of mineralisation at Kolomela Mine, Northern Cape, South Africa, based on fully-constrained, implicit 3D modelling. *Ore Geology Reviews.*

Bekker, A. et al., 2004. Dating the rise of atmospheric oxygen. *Nature 427*, pp. 117-120.

Bester, M., Basson, I. & Koegelenberg, C., 2015. *A practical methodology to define geotechnical design sectors in structurally-controlled anisotropic environments.* Cape Town, The Southern African Institute of Mining and Metallurgy, Slope Stability.

Bester, M., Nel, E. & Mc Gavigan, G., 2013. *A strategic approach to the design and implementation of an effective dewatering system.* Brisbane, ACG.

Bester, M., Russell, T. & Carey, R., 2018. *Slope design reconciliation - Closing the loop.* Seville, Spain, International Symposium on Slope Stability in Open Pit Mining and Civil Engineering.

Beukes, N. J., 1983. Paleoenvironmental setting of iron-formations in the depositional basin of the Transvaal Supergroup, South Africa. *Iron-Formation: facts and problems. Developments in Precambrian Geology, 6,* pp. pp. 131-209. 558pp.

Beukes, N. J., 1986. The Transvaal sequence in Griqualand west. *Mineral Deposits of South Africa 1,* pp. 819-828.

Beukes, N. J. & Smit, C. A., 1987. New evidence for thrust faulting in Griqualand West, South Africa; implications for stratigraphy and the age of red beds. *S. Afr. J. Geol. 90 (4),* pp. 378-394.

Bidgoli, M. N. & Jing, L., 2014. Anisotropy of strength and deformability of fractured rocks. *Journal of Rock Mechanics and Geotechnical Engineering 6,* pp. 156-164.

Bieniawski, Z. T., 1988. Towards a creative design process in mining. *Mining Engineering, vol. 40,* pp. pp. 1040-1044.

Bieniawski, Z. T., 1989. Engineering rock mass classifications: a complete manual for engineers and geologists in mining, civil, and petroleum engineering. *Wiley-Interscience,* p. 272.

Bieniawski, Z. T., 1991. *In search of a design methodology for rock mechanics, Rock Mechanics as a Multidisciplinary Science.* s.l., Roegiers (ed.), Balkema, pp. pp. 1027-1036.

Bieniawski, Z. T., 1992. *Principles of engineering design for Rock Mechanics.* s.l., Tillerson and Wawersik (eds.), Balkema, pp. pp. 1031-1040.

Bieniawski, Z. T., 1993. Principles and methodology of design for excavations in geologic media. *Research in Engineering Design, vol.5,* pp. pp. 49-58.

Bye, A. R., 2003. *The development and application of a 3D geotechnical model for mining optimisation, Sandsloot open pit platinum mine, South Africa. PhD thesis,* Durban: University of Natal.

Carney, J. N., Aldiss, D. T. & Lock, N. P., 1994. *The Geology of Botswana,* s.l.: Technical Report, Geological Survey Department of Botswana.

Carney, M. & Mienie, P., 2003. Comparison of the Sishen and Sishen South (Welgevonden) iron ore deposits, N. Cape Prov., South Africa. *Appl. Earth Sci. (Trans. Inst. Min. Metall. B) 112. B5.*

Coetzee, L. L., 2001. Genetic stratigraphy of the Palaeoproterozoic Pretoria Group in the western Transvaal. *M.Sc. Thesis (unpub), Rand Afrikaans University, Johannesburg*, p. 206pp.

Cornell, D. H. & Schutte, S. S., 1996. Reply to the discussion by N.J Beukes and J Gutzmer. *Miner. Deposita 31,* pp. 246-247.

Cornell, D. H. et al., 2016. The U-Pb zircon geochronology of the Palaeoproperozoic Hartley formation porphyry by six methods with age uncertainty approaching 1 Ma.. *S. Afr. J. Geol. 119 (3),* pp. 473-494.

Creus, P. K. et al., 2019. 3D Fabric Analysis of Venetia Mine, South Africa: Using Structural Measurements and Implicitly-Modelled Surfaces for Improved Pit Slope Design and Risk Management. *Journal of African Earth Sciences 155,* pp. 137-150.

Creus, P. K. et al., 2018. Structural analysis and implicit 3D modelling of Jwaneng Mine: Insights into deformation of the Transvaal Supergroup in SE Botswana. *Journal of African Earth Sciences 137,* pp. 9-21.

Creus, P., Koegelenberg, C. & Basson, I., 2017. *Heuningkranz - Form Surface Generation, Block Modelling and Apparent Dip Analysis of Bedding Orientations,* s.l.: Tect Geological Consulting Report TECT020/2017R.

Dalstra, H. J. & Rosière, C. A., 2008. Sturctural controls on high-grade iron ores hosted by banded iron formation: a global perspective. *Rev. Econ. Geol. 15,* pp. 73-106.

Dassault Systèmes, 2019. *Dassault Systèmes.* [Online]
Available at: https://www.3ds.com/products-services/geovia/products/whittle/

De Villiers, P. R. & Visser, J. N., 1977. The glacial beds of the Griqualand West Supergroup as revealed by four deep boreholes between Postmasburg and Sishen. *Trans. Geol. Soc. South Afr. 80,* pp. 1-8.

Debswana Diamond Company (Pty) Ltd, 2015. *2015 Report to Stakeholders,* s.l.: Debswana Diamond Company (Pty) Ltd.

Deere, D. U., Hendron, A. J., Patton, F. D. & Cording, E. J., 1967. *Design of Surface and Near-Surface Construction in Rock.* New York, s.n., pp. pp. 237-302..

Dershowitz, W. S., Lee, G., Geier, J. & Lapointe, P. R., 1998. FracMan: interactive discrete feature data analysis, geometric modelling and exploration simulation. *User documentation, Seattle, WA, Golder Associates Inc.*

Dietvorst, E. J., 1988. Early Precambrian Basement uplift and block faulting along the western margin of the Bushveld Complex, Southeastern Botswana. *Journal of African Earth Sciences, 7(4),* pp. 641-651.

Dorland, H. C. et al., 2006. Precise SHRIMP U-Pb zircon age constraints on the lower Waterberg and Soutpansberg Groups, South Africa. *South African Journal of Geology, 109,* pp. 139-156.

Elmo, D., Coggan, J. S. & Pine, R. J., 2008. *Numerical analysis of pit wall deformation induced by block cave mining.* Lulea, Sweden, s.n., pp. pp. 1073-1082.

Elmo, D., Rogers, S., Stead, D. & Eberhardt, E., 2014. Discrete Fracture Network approach to characterise rock mass fragmentation and implications for geomechanical upscaling. *Mining Technology, Vol. 123, No. 3,* pp. 149-161.

Erikson, P. G., Altermann, W. & Hartzer, F. J., 2006. *The Transvaal Supergroup and its precursors.* Pretoria: The Geology of South Africa. Geological Society of South Africa.

Eriksson, P. G. et al., 1993. The Transvaal sequence: an overview. *J. Afr. Earth Sc. 16 (1-2),* pp. 25-51.

Fillion, M., 2018. *Optimizing geotechnical data collection campaigns in open pit mines, PhD thesis,* s.l.: University of Toronto, Canada.

Fillion, M. & Hadjigeorgiou, J., 2017. Quantifying the impact of additional laboratory tests on the quality of a geomechanical model. *Rock Mech Rock Eng DOI 10.1007.*

Fisher, B., 2009. Improved Characterization and Analysis of Bi-Planar Dip Slope Failures to Limit Model and Parameter Uncertainty in the Determination of Setback Distances. *PhD thesis. The Faculty of Graduate Studies (Geological Engineering), University of British Columbia.*

Friese, A. E., 2007 a. *Assessment of the tectono-structural evolution and its impact on mining in the lease area of Sishen Iron Ore Mine, Northern Cape, South Africa. Report for Kumba Iron Ore,* s.l.: Terra Explora Consulting Report, May 2007. 121pp.

Friese, A. E., 2007 b. *Assessment of tectono-structural evolution and its impact on future mining in the Sishen South project area, Northern Cape, South Africa, with implications to iron ore genesis and preservation. Report for Kumba Iron Ore,* s.l.: Terra Explora Consulting Report, June 2007, 113 pp.

Friese, A. E. & Alchin, D. J., 2007. *New insights into the formation, structural development, and preservation of iron ore deposits in the Northern Cape Province, South Africa.* s.l., The Australasian Institute of Mining and Metallurgy.

Gabanakgosi, K. et al., 2018. *A Multi-Disciplinary approach to dip slope mining in Jwaneng Mine, Botswana.* Seville, Spain, International Symposium on Slope Stability in Open Pit Mining and Civil Engineering, pp. 1408-1423.

Grenon, M. & Hadjigeorgiou, J., 2010. Integrated structural stability analysis for preliminary open pit design. *International Journal of Rock Mechanics & Mining Sciences, 47,* pp. pp.450-460.

Grenon, M. & Laflamme, A., 2011. Slope orientation assessment for open pit mines using GIS based algorithms. *Computers & Geosciences 37,* pp. pp. 1413-1424.

Hälbich, I. W. et al., 1993. The Transvaal-Griqualand West banded iron formation: geology, genesis, exploitation. *J. Afr. Earth Sc. 16 (1/2),* pp. 63-120.

Hartnady, C. H., Joubert, P. & Stowe, C. W., 1985. Proterozoic crustal evolution in southwestern Africa. *Episodes 8,* pp. 236-245.

Hilliard, P., 1999. Structural evolution and tectonostratigraphy of the Kheis Orogen and its relationship to the south western margin of the Kaapvaal Craton. *Unpub. Ph.D. Thesis. University of Durban-Westville,* p. 235pp.

Hill, P. H., 1983. *Techniques in teaching creative engineering design.* New York, s.n.

Hoek, E., Carter, T. G. & Diederichs, M. S., 2013. *Quantification of the Geological Strength Index Chart.* San Francisco, USA, 47th US Rock Mechanics / Geomechanics Symposium, p. 8.

Hoek, E., Carter, T. G. & Diederichs, M. S., 2013. *Quantification of the Geological Strength Index Chart.* San Francisco, USA, s.n.

Hoek, E. & Diederichs, M. S., 2006. Empirical estimation of rock mass modulus.. *International Journal of Rock Mechanics and Mining Sciences, 43,* pp. pp. 203-2015.

Hoek, E. & Marinos, P., 2007. A brief history of the development of the Hoek-Brown failure criterion. *Soils and Rocks,* Volume 2, p. 13.

Hoek, E. & Martin, D., 2010. *Synthetic Rock Mass Review,* Denver, March 15, 2010. Unpublished: Report prepared for Mass Mining Project.

Humphreys, H. C. & Van Bever Donker, J. M., 1987. Aspects of deformation along the Namaqua Province eastern boundary, Kenhardt District, South Africa. *Precambr. Res. 36,* pp. 39-63.

Humphreys, H. C., Van Bever Donker, J. M., Scott, W. O. & Van Schalkwyk, L., 1988. The early deformational history of the eastern Namaqua Province: new evidence from Prieska Copper Mines. *S. Afr. J. Geol. 91,* pp. 174-183.

Ilbury, C. & Sunter, C., 2005. *Games foxes play - planning for extraordinary times.* s.l.:Human & Rosseau Tafelberg.

Itasca Consulting Group, I., 2016. *3-Dimensional Distinct Element Code (3DEC), Version 5.2,* s.l.: s.n.

Kampmann, T. C., 2012. U-Pb geochronology and paleo-magnetism of the Westerberg sill, Kaapvaal Craton - support for a coherent Kaapvaal-Pilbara block (Vaalbara). *M.Sc. Thesis, Lund University, Sweden,* p. p. 36.

Koegelenberg, C. & Basson, I. J., 2018. *Heuningkranz V6 Baseline Model: Structural Re-Interpretation and 3D Modelling in LeapfrogGeo For Ore Resource Estimation and Geotechnical Design. Report prepared for Kumba Iron Ore,* s.l.: TECT014/2018R.

Kumba Iron Ore, 2019. *Kumba GIS database,* Centurion: Geosciences.

Labuz, J. F. & Zang, A., 2012. Mohr-Coulomb Failure Criterion. *Rock Mech Rock Eng,* Volume 45(Issue 6), pp. 975-979.

Laubscher, D., 1994. Cave mining - the state of the art. *Journal of the South African Institute of Mining and Metallurgy. Vol. 94(10),* pp. pp 279-293.

Lee, W. F. et al., 2013. Failure Analysis of a Highway Dip Slope Side. *Journal of Performance of Constructed Facilities, Vol. 27, Issue1.*

Lilly, P. A., 1986. *An empirical method of assessing rock mass blastibility.* s.l., Newman Combine Group, pp. 89-92.

Lilly, P. A., 1992. *The use of the Blastibility Index in the design of blasts for open pit mines.* Kalgoorlie, Western Australian School of Mines, Curtin University of Technology, pp. 421-426.

Lobatskaya, R. M. & Strelchenko, I. P., 2015. GIS based analysis of fault patterns in urban areas. A case study of Irkutsk city Russia. *Geoscience Frontiers 1-8.*

Maptek Pty Ltd, 2018. *I-Site 3D Laser Scanning Technology.* [Online] Available at: https://www.maptek.com/products/i-site/index.html

Marinos, V., Marinos, P. & Hoek, E., 2005. The Geological Strength Index: applications and limitations. *Bull. Eng. Geol. Environ. Vol. 64,* pp. pp. 55-65.

Mas Ivars, D., Deisman, N., Pierce, M. & Fairhurst, C., 2007. *The Synthetic Rock Mass Approach - A Step Forward in the Characterization of Jointed Rock Masses.* Lisbon, L. Ribeiro e Sousa, C. Olalla, and N. Grossmann (eds), The Second Half Century of Rock Mechanics, pp. 485-490.

Mas Ivars, D., Pierce, M., DeGagné, D. & Darcel, C., 2008. *Anisotropy and Scale Dependency in Jointed Rock Mass Strength - A Synthetic Rock Mass Study.* Minneapolis, s.n.

Mas Ivars, D. et al., 2011. The synthetic rock mass approach for jointed rock mass modelling. *International Journal of Rock Mechanics & Mining Sciences 48,* pp. 219-244.

Mergili, M. et al., 2014. Spatially distributed three dimensional slope stability modelling in a raster GIS. *Geomorphology 206,* pp. pp. 178-195.

Moore, J. M., Kuhn, B. K., Mark, D. F. & Tsikos, H., 2011. A sugilite-bearing assemblage from the Wolhaarkop Breccia, Bruce Fe-ore mine, South Africa: evidence for alkali metasomatism and Ar40-Ar39 dating. *Eur. J. Mineral. 23,* pp. 661-673.

Moore, M., Tsikos, H. & Polteau, S., 2000. Deconstructing the Transvaal Supergroup. *J. Afr. Earth Sc. 31 (Suppl. 1A),* pp. 52-53.

Mortimer, B., 1995. *An investigation of the geological structure at Sishen Iron Ore Mine, with special reference to slope stability,* s.l.: Kumba Internal Report.

Mortimer, B., 1995. *Report on structural geological analysis, Sishen, 1993-1995,* s.l.: Kumba Internal Report.

Park, H., Lee, J., Kim, K. & Um, J., 2016. Assessment of rock slope stability using GIS-based probabilistic kinematic analysis. *Engineering Geology 203,* pp. 56-69.

Pells, P. J., Bieniawski, Z. T., Hencher, S. R. & Pells, S. E., 2017. Rock Quality Designation (RQD): Time to Rest in Peace. *Can. Geotech. J. 54: 825-834.*

Perman, F., Sjoberg, J. & Dahnér, C., 2011. Detailed three-dimensional stress analysis of complex orebody geometry - model setup and results for the Malmberget Mine. *Continuum and Distinct Element Numerical Modelling in Geo-Engineering,* pp. Paper: 02-04.

Pierce, M., Mas Ivars, D., Cundall, P. A. & Potyondy, D. O., 2007. *A Synthetic Rock Mass Model for Jointed Rock.* Vancouver, London: Taylor & Francis Group, pp. 341-349.

Potyondy, P., 2005. *PFC Probe Logic,* s.l.: Technical Memorandum to MMT, Itasca Consulting Group, Inc.

Poulsen, B. A., Adhikary, D. P., Elmouttie, M. K. & Wilkins, A., 2015. Convergence of synthetic rock mass modelling and the Hoek-Brown strength criterion. *International Journal of Rock Mechanics & Mining Sciences 80,* pp. 171-180.

Priest, S. D., 1993. *Discontinuity Analysis for Rock Engineering.* London: Chapman & Hall.

Read, J., 2018. *Keynote address: Developments in Open Pit Slope Design since 2009.* Seville, Spain, International Symposium on Slope Stability in Open Pit Mining and Civil Engineering.

Read, J. & Stacey, P., 2009. *Guidelines for Open Pit Slope Design.* s.l.:CSIRO Publishing.

Renani, H. R., Martin, C. D., Varona, P. & Lorig, L., 2018. *Probabilistic Stability Analysis of Slopes in Highly Heterogeneous Rock Masses.* Seville, Spain,

International Symposium on Slope Stability in Open Pit Mining and Civil Engineering.

Rogers, S. F., Elmo, D., Beddoes, R. & Dershowitz, B., 2009. *Mine scale DFN modelling and rapid upscaling in geomechanical simulations of large open pits.* Santiago, Chile, International Symposium on Slope Stability in Open Pit Mining and Civil Engineering.

Ronald, E., 2017. *Mining Geology HQ.* [Online]
Available at: http://www.mininggeologyhq.com/rules-of-thumb-for-geological-modeling/

Russell, T., 2017. *Increasing Geotechnical Data Confidence through the Integration of Laser Scanner Face Mapping Data into the Sishen Iron Ore Mine Geotechnical Database, M.Sc.Eng thesis. University of the Witwatersrand,* s.l.: s.n.

Sainsbury, B., Pierce, M. E. & Mas Ivars, D., 2008. *Analysis of Caving Behaviour Using a Synthetic Rock Mass - Ubiquitous Joint Rock Mass Modelling Technique.* s.l., s.n.

Sainsbury, B., Pierce, M. & Mas Ivars, D., 2008. *Simulation of rock mass strength anisotropy and scale effects using a Ubiquitous Joint Rock Mass (UJRM) model.* s.l., s.n.

Sainsbury, D. P. & Sainsbury, B., 2013. *Three-dimensional analysis of pit slope stability in anisotropic rock masses.* Brisbane, Australian Centre for Geomechanics, pp. 683-695.

Schalkwyk, G., 2005. Genesis and Characteristics of the Wolhaarkop Chert Breccia and Associated Manganore Iron Formation. *University of Johannesburg, Johannesburg.*

Schlegel, G. C., 1988. Contribution to the metamorphic and structural evolution of the Kheis Tectonic Province, Northern Cape, South Africa. *S. Afr. J. Geol. 91 (1),* pp. 27-37.

Schütte, S. S., 1992. Ongeluk volcanism in relation to the Kalahari manganese deposits. *Unpublished Ph.D. dissertation, Durban, University of Natal, South Africa,* p. 255.

Semami, F. B. et al., 2016. New U-Pb geochronologic and palaeomagnetic constraints on the late Palaeoproterozoic Hartley magmatic event: evidence for a potential large igneous province in the Kaapvaal Craton during Kalahari assembly, South Africa. *GFF (J. Geol. Soc. Sweden) 138 (1),* pp. 164-182.

Stacey, T. R., 2009. Design - a strategic issue. *The Southern African Institute of Mining and Metallurgy,* Vol. 109(no. 3), pp. pp. 157-162.

Starfield, A. M. & Cundall, P. A., 1988. Towards a methodology for rock mechanics modelling. *International Journal of Rock Mechanics and Mining Sciences, Geomechanics Abstracts, Vol. 25, No.3,* pp. pp. 99-106.

Stead, D. & Wolter, A., 2015. A critical review of rock slope failure mechanisms. The importance of structural geology. *Journal of Structural Geology 74,* pp. pp. 1-23.

Steffen, O. K., 1997. Planning of open pit mines on risk basis. *Journal of the South African Institute of Mining and Metallurgy,* Vol. 97(No. 2), pp. pp.47-56.

Steffen, O. K., 2007. *Mine planning: its relationship to risk management.* Perth, Australian Centre for Geo-mechanics.

Stowe, C. W., 1983. The Upington Geotraverse and its Implications for Craton-Margin Tectonics. *Geological Society of South Africa. Special Publication, 10,* pp. 147-171.

Stowe, C. W., 1986. Synthesis and interpretation of structures along the north-eastern boundary of the Namaqua tectonic province, South Africa. *S. Afr. J. Geol. 89 (2),* pp. 185-198.

Sumner, D. Y. & Beukes, N. J., 2006. Sequence stratigraphic development of the Neoarchean Transvaal carbonate platform, Kaapvaal Craton, South Africa. *S. Afr. J. Geol. 109 (1-2),* pp. 11-22.

Thomas, R. J., Cornell, D. H., Moore, J. M. & Jacobs, J., 1994. Crustal evolution of the Namaqua-Natal Metamorphic Province, southern Africa. *S. Afr. J. Geol. 97,* pp. 8-14.

Tinker, J., de Wit, M. & Grotzinger, J., 2002. Seismic stratigraphic constraints on neoarchean - paleoproterozoic evolution of the Western Margin of the Kaapvaal Craton, South Africa. *S. Afr. J. Geol. 105 (2),* pp. 107-134.

Trimble Inc., 2019. *Trimble Open Pit Design.* [Online]
Available at: https://www.trimble.com/Industries/Mining/Open_Pit_Design.aspx

Van Schalkwyk, J. F. & Beukes, N. J., 1986. The Sishen iron ore deposit, Griqualand West. *Mineral Deposits of Southern Africa, Vol. I. Geol. Soc. S. Afr., Johannesburg,* pp. pp.931-956.

Van Wyk, J. P., 1980. Die geologie van die Rooinekke-Matsap-Wolhaarkop in Noord-Kaapland met spesiale verwysing na die Koegas Subgroup en die Transvaal Supergroep. *M.Sc Dissertation (unpublished) Randse Afrikaans University, Johannesburg, South Africa,* p. 159 pp.

Vatcher, J., McKinnon, S. D. & Sjöberg, J., 2016. Developing 3-D mine-scale geomechnical models in complex geological environments, as applied to the Kiirunavaara Mine. *Engineering Geology 203,* pp. 140-150.

Venter, L. J. & Deacon, J., 2017. *Sishen Detailed Stratigraphic Succession, Internal Company Presentation, Kumba Iron Ore,* s.l.: s.n.

Visser, D. J., 1944. Stratigraphic features and tectonics of portions of Bechuanaland and Griqualand West. *Trans. Geol. Soc. S. Afr. 47,* pp. 197-254.

Visser, J. N., 1969. *'n Sedimentologiese studie van die Serie Pretoria in Transvaal. PhD thesis (unpubl.),* Bloemfontein: University of the Orange Free State.

Visser, J. N., 1971. The deposition of the Griquatown Clacial Member in the Transvaal Supergroup. *Trans. Geol. Soc. S. Afr. 74,* pp. 187-199.

Vorster, A., 2001. Planning for value in the mining value chain. *The Journal of the South African Institute of Mining and Metallurgy,* pp. Sept. 2001 pp.61-65.

Xie, M., Esaki, T. & Cai, M., 2004. GIS based method for locating the critical 3D slip surface in a slope. *Computers and Geotechnics 31,* pp. 267-277.

APPENDICES

Appendix 1: Examples of a Mine Planning Cycle (annual or bi-annual) and a More Detailed Process Jointly Performed by the Mine Planning and Geotechnical Engineering Functions.

Appendix 2: Fault Confidence Rating Table.

Appendix 3: Heuningkranz Project Geological Setting.

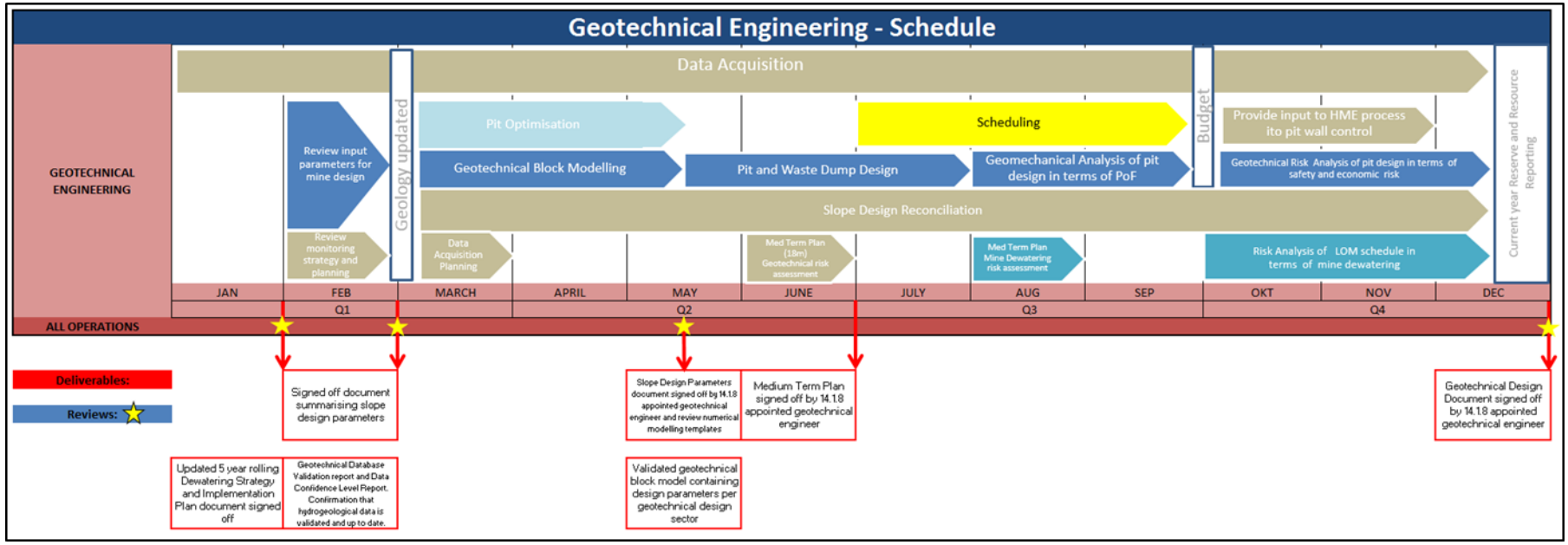
Appendix 4: Sishen Mine Geotechnical Data.

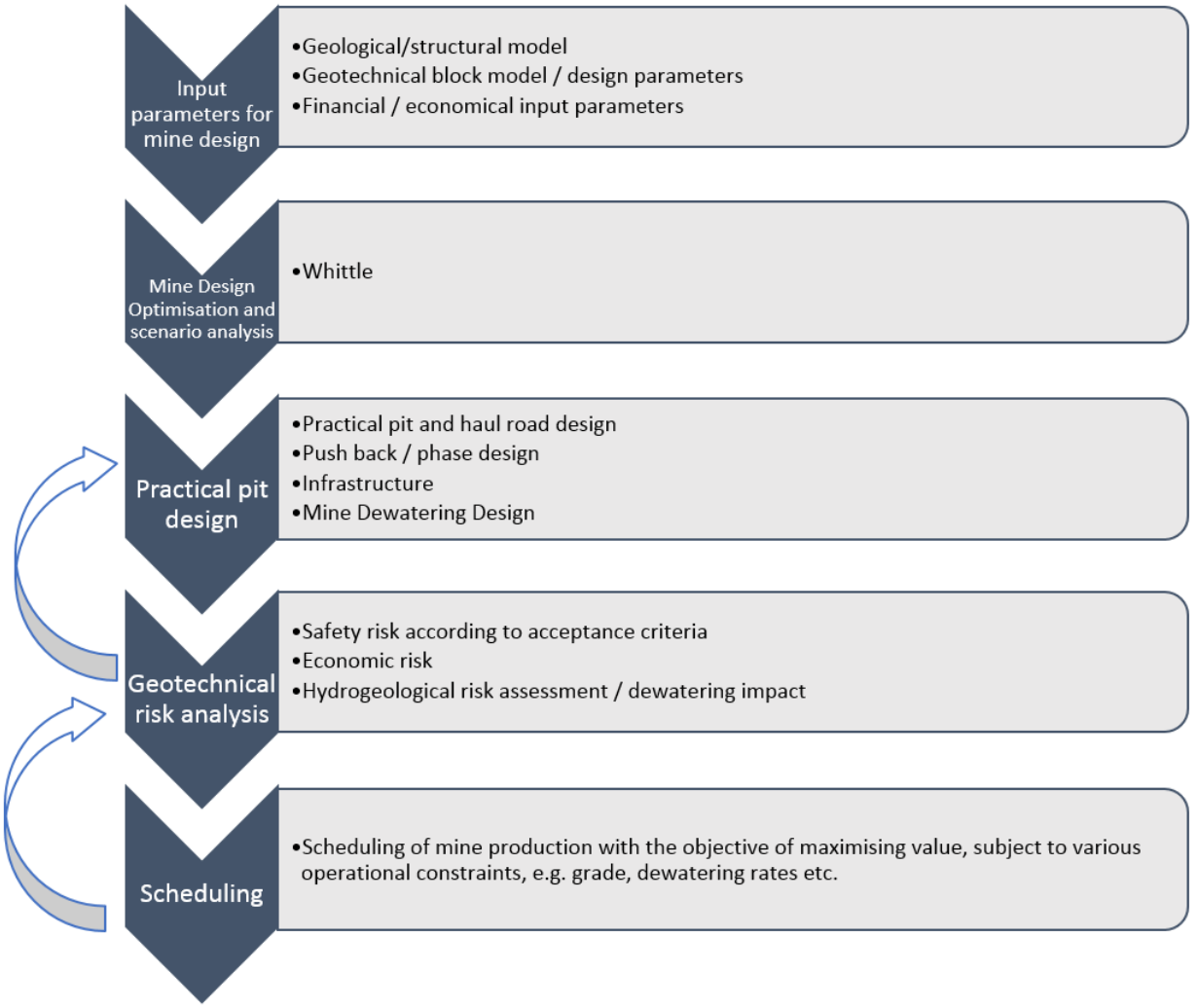
Appendix 5: Kolomela Mine Geological Setting.

Appendix 6: Kolomela Mine Geotechnical Data.

Appendix 7: Kolomela Mine Leeuwfontein Pit Stability Analysis Results.

APPENDIX 1: EXAMPLES OF A MINE PLANNING CYCLE (ANNUAL OR BI-ANNUAL) AND A MORE DETAILED PROCESS JOINTLY PERFORMED BY THE MINE PLANNING AND GEOTECHNICAL ENGINEERING FUNCTIONS.




Input parameters for mine design
•Geological/structural model
•Geotechnical block model / design parameters
•Financial / economical input parameters
Mine Design Optimisation and scenario analysis
•Whittle
Practical pit design
•Practical pit and haul road design
•Push back / phase design
•Infrastructure
•Mine Dewatering Design
Geotechnical risk analysis
•Safety risk according to acceptance criteria
•Economic risk
•Hydrogeological risk assessment / dewatering impact
Scheduling
•Scheduling of mine production with the objective of maximising value, subject to various operational constraints, e.g. grade, dewatering rates etc.

APPENDIX 2: FAULT CONFIDENCE RATING TABLE.

Supporting data	Rating
• **Geophysical data only** (e.g. magnetic, gravity or EM survey) or • **Limited data of a single type**	**1** Low 25% confidence
Minimum 2 supporting data types: • Mapping points ** (distributed along strike) • Stratigraphic evidence * ("barcoding" or significant variability of lithologies, development of conglomerate or clastic-textured units in adjacent graben or half-graben) • Significant offsets in contacts between adjacent drill holes • Geophysical evidence • Photograph • Lidar / I-sight pick or trace	**2** Moderate 60% confidence
Minimum 3 mapping data points ** and significant offsets between drillholes As well as one of the following: • Stratigraphic evidence • Geophysical data • Photographs • Lidar / I-sight picked contact or contact trace	**3** High 75% confidence
More than 3 supporting mapping data points ** **and** • Significant offsets between drill holes and • Stratigraphic evidence and • Photographs and • Geophysical evidence and • Lidar / I-sight pick or trace or • Suspected cause of instability	**1** Very high >75% confidence

Fault confidence rating table from TECT Geological Consulting for Kumba Iron Ore operations.

* Strikes of interpreted major faults must match regional trends and stereonet data. Their position, orientation and cross cutting relationships should make kinematic sense according to known deformation events in the area.

**Mapping data include scanline mapping.

APPENDIX 3: GEOLOGICAL SETTING OF THE HEUNINGKRANZ PROJECT.

Structural Setting

The Heuningkrans volume of interest is situated within the southern extent of the Maremane Dome (Figure 39), which resulted from a protracted series of tectonic events (Stowe, 1986); (Hälbich, et al., 1993); (Friese & Alchin, 2007) on the western margin of the Kaapvaal Craton. Structural studies by (Stowe, 1986), (Altermann & Hälbich, 1991) and (Hälbich, et al., 1993) concluded that the lower Transvaal Supergroup exhibits at least three major phases of compressional tectonism. The overall number of events may be significantly higher; for example, (Altermann & Hälbich, 1991) suggested that there were up to seven events. The development of this part of the Kaapvaal Craton is briefly summarised below, in chronological order and using current azimuths, from (Stowe, 1986), (Altermann & Hälbich, 1991), (Hälbich, et al., 1993), (Friese, 2007 a) (Friese, 2007 b), and (Friese & Alchin, 2007):

~2.78-2.64 Ga: Ventersdorp rift basin development. NE-SW trending faults, which formed graben boundaries, developed due to basin initiation and subsidence;

~2.64-2.6 Ga: Extrusion and deposition of the volcano sedimentary Vryburg Formation and Ventersdorp lavas;

~2.60-2.52 Ga: Development of a carbonate platform, during widespread marine transgression; consequent conformable deposition of the Schmidtsdrif and Campbell Rand Subgroup dolomites;

~2.52-2.46 Ga: Off-craton/oceanic rifting to the west, accompanied by hydrothermal deposition of manganiferous chert of the Wolhaarkop Formation. This was followed by deposition of the Asbestos Hill Subgroup (banded iron formation/Kuruman Formation);

~2.46-2.35 Ga: Incipient break-up and rifting, along a set of N-S trending, W-dipping normal faults in the Kaapvaal Craton during a "second extensional stage" (Friese & Alchin, 2007). According to (Dalstra & Rosière, 2008),

"E1" or their first extensional event occurred immediately before the "Kalahari Orogeny" (see below);

~2.35-2.25 Ga: The first phase of folding (F1) resulted from the E-verging "Kalahari Orogeny". (Altermann & Hälbich, 1991) cite the >2.24 Ga or pre-Makganyene development of the Uitkomst cataclasite as part of this event, which they attribute to a bedding-parallel thrust. F1 folds were predominantly N-S trending; therefore, the main axis of the Maremane Dome is effectively a 2.35-2.25 Ga F1 anticline or an F2-tightened F1 anticline. Pre-existing, predominantly rift-related normal faults were inverted and underwent a component of strike-slip reactivation, associated with this eastward tectonic vergence; their adjacent, uplifted blocks were eroded. An additional feature of this event appears to be the formation of conjugate NE- and SE-trending strike-slip faults which are radially

distributed around the eastern curve of the Maremane Dome. This orogeny also caused uplift and erosion of underlying units, including the Ghaap Group, to form the Postmasburg Unconformity, which is pivotal in regional ore development and/or preservation. The deposition of the Makganyene Formation of the Lower Postmasburg Group, which has a minimum age of 2.22 Ga, probably resulted from this event;

~2.24-1.83 Ga: Reactivation of faults related to both the N-S trending passive margin rift and the Ventersdorp Rift, causing deposition of the fault-controlled or fault-bounded, volcano sedimentary/volcaniclastic Upper Postmasburg Group. Ongeluk lavas signify the peak of mafic lava extrusion at c. ~2.22 Ga, via feeder dykes that exploited reactivated NNE- to NE-trending faults (Friese & Alchin, 2007). (Dalstra & Rosière, 2008) correctly inferred that dykes locally recrystallized ores within the Manganore Iron Formation at Sishen. Within this interval, deposition of clastic sediments in the form of conglomerate, "grit", quartzite and shale of the lower Olifantshoek Supergroup took place at ~2.05-1.93 Ga, thereby forming and terminating the deposition of the Gamagara/Mapedi Formation, which formed within a shallow-water rift environment (Beukes, 1983). The second extensional event or "E2" of (Dalstra & Rosière, 2008) occurred during or shortly after this period, as reactivated normal faults displaced or offset the lower Olifantshoek Group, although such structures tend to predate the Kheis Orogeny (see below). Apparently overlapping in age with this extensional event is the formation of south-verging folds and thrusts, which, according to (Altermann & Hälbich, 1991), are the oldest post-Matsap event at 2.07-1.88 Ga;

~1.83-1.73 Ga: The Kheis Orogeny or tectono-metamorphic event, like the Kalahari Orogeny, showed eastward tectonic vergence that was accompanied by thrusting and folding (Stowe, 1986); (Beukes & Smit, 1987); (Altermann & Hälbich, 1991); (Hälbich, et al., 1993). The Kheis Orogeny is more precisely dated at ~1780 Ma, using a 39Ar-40Ar metamorphic age derived from the Groblershoek Schist Formation of the Olifantshoek Supergroup (Schlegel, 1988). Rift structures of the Postmasburg Group and Olifantshoek Supergroup depositional settings were reactivated while F2 folding and thin-skinned thrusting occurred along major unconformities and lithological contacts. In some areas, F1 folds were tightened co-axially during F2 folding. In the Sishen area, thrusting was concentrated at the shale-dominated, tectonised margins of a quartzite member within the upper Olifantshoek Group; these horizons are termed "tectonised shale" in drill core, although this sequence appears to be very poorly developed at the Heuningkranz prospect. (Friese, 2007 b) and (Friese & Alchin, 2007) have termed these and other low-angle thrusts "principal décollements";

~1.15-1.0 Ga: The NNW-directed Lomanian (Namaqua-Natal) Orogeny caused deformation along the southern margin of the Kaapvaal Craton. The effects of this were manifold: reactivation and buckling of N-S trending normal and inverted normal faults, reactivation of the 2.35-2.24 Ga NE- and SE-trending conjugate strike-slip faults, usually with upthrow to the SE and SW, respectively, the

development of ENE-trending F3 folds, which may have contributed to broad F2/F3 fold interference patterns (Mortimer, 1995). This may also have contributed to the geometry of the Maremane Dome, which is effectively a large-scale "Ramsay style" interference fold with a radial set of fractures/faults, in which conjugate relationships may still be observed. The Dimoten and Ongeluk-Witwater Synclines, wherein the Postmasburg Group is preserved, are situated towards the eastern foreland of the Maremane Dome.

It has been suggested that the interference or interSection of F2 synclines and F3 synclines has resulted in deep, steep-sided, circular or ovoid depressions in which ore (and banded iron formation) is notably thicker (Mortimer, 1995). This must be weighed against other models which suggest that areas of very thick, deep ore occupy palaeosinkholes, i.e. occur within palaeokarst topography within the Campbell Rand Subgroup. A third model is that of (Dalstra & Rosière, 2008), which advocates a close association between structures and mineralisation and/or between structures and the preservation of mineralisation. Due to the complex structural and stratigraphic evolution of the area, it is entirely possible that there is a component of all three mechanisms present in and around a given deposit, albeit substantially complicated by variable preservation. However, at Heuningkranz, there is the possibility that there has been a hydrothermal overprint of a pre-existing, partially mineralized sequence, thereby affecting shale, quartzite and possibly other lithologies.

Subsequent tectonism, including the breakup of Gondwana and Pan-African reworking, had only a minor effect on the modelled volume. Regionally, Bushveld-age gabbroic rocks intruded into the Ghaap and Postmasburg Groups within a clearly-defined NE-trending graben, essentially accommodated by the reactivation of Ventersdorp faults (Friese & Alchin, 2007). These gabbroic units appear to be more evident in the Kolomela area, approximately 17km from Heuningkranz. Figure 39 shows the Heuningkranz and Langverwacht model limits, within the regional setting of the Maremane Dome. The Heuningkrans prospect occurs to the west of the broad, doubly-plunging Maremane Dome and to the north/northwest of a series of small domes – including the Wolhaarkop Dome – which have anticlinal long axes that parallel the F1 fold axis of the Maremane Dome. These domes are doubly-plunging, such that Heuningkranz occurs to the NW of the northernmost smaller dome, essentially adjacent to a broad anticline. A series of N-S to NNE-trending anastomosing faults, which are essentially parallel to the curve of the western margin of the Maremane Dome, occur throughout the area. Due to the regional "Pre-Kheis"/Kalahari and/or Kheis deformation events, which involved the inversion of older normal faults and predominantly eastwards tectonic vergence and transport, these structures may comprise inverted or partially inverted normal faults, reverse faults, and/or breached fold hinge zones. Cross-cutting these structures and thereby cross-cutting the general strike of lithologies, are predominantly NW-SE-trending structures. These are one component of a regional conjugate joint/fault set/couple (i.e. NW-SE and NE-SW) that formed due to eastwards tectonic vergence. Due to refolding of the Maremane Dome (F2?), and

the influence of the ca. 1 Ga Namaqua-Natal event, these structures were reactivated, thereby offsetting – occasionally in a vertical sense - N-S trending structures and units. Such faults may have a quantifiable effect on pit shells or mine design, for example in the Leeuwfontein Pit at Kolomela. Based on the regional geology and Heuningkranz' structural position on the frontal toe of the Kheis orogeny in the west, the main features or geometries expected are:

1) Relict, primary sub-basin/graben/half-graben NNW-SSE to N-S geometries or structures with preserved, partially inverted normal faults with their adjacent high-energy sediments, including conglomerate, hematite rich conglomerate, gritstone and intercalated shale;

2) Low-angle, thin-skinned thrusting, with accompanying mesoscale to microscale features with kinematic indicators, also evident at Kolomela and Heuningkranz core and in thrusts within banded iron formation at Kolomela's Leeuwfontein pit;

3) A predominantly SSE to SE-directed tectonic vergence and transport direction, exhibited by the asymmetry of meso-scale and small-scale folds (evident at Kolomela), and the overall east-convex shape of the Maremane Dome;

4) Blind thrusts ranging from parallel to bedding to moderately transgressive and top-to-the-SSE, typically characterized by breached folds (the former evident at Kolomela);

5) Local back-thrusting may occur, particularly on the eastern margins of the Maremane Dome and smaller secondary domes, i.e. Wolhaarkop Dome. Examples of these include NW-verging thrusts at Kolomela;

6) Broad imbrication of lithological units indicated by duplication/stacking, inversion and/or lensing of units along thrusts;

7) Tectonic "removal" or displacement of ore and other horizons along thrusts, evident at Heuningkranz;

8) NNE-SSW trending folds, with varying amplitudes;

9) Folding of bedding above and sub-parallel to thrust planes, resulting in locally very steep dips of bedding and laminations, expressed as very low Alpha-angles in drill core;

10) NW-SE or NE-SW trending, sub-vertical strike-slip faults that transect the entire pit and which may offset or displace the relict or primary sub-basin/half-graben geometry.

Tectonostratigraphy

The Transvaal Supergroup occurs in two main basins: the Griqualand West Basin and the Transvaal Basin. In turn, the former has been subdivided into two sub-basins (Prieska and Ghaap Plateau). Heuningkranz is situated within the Ghaap

Plateau sub-basin and a distinct tectonic unconformity subdivides modelled lithologies into two packages. Above the unconformity, andesitic lavas of the Ongeluk Formation and various clays, diamictite, sands and calcrete dominate. Below, lithologies consist predominantly of dolomite, chert breccia, shale and quartzite. The modelled sequence is assigned to the following, from the base upwards (refer to Figure 68):

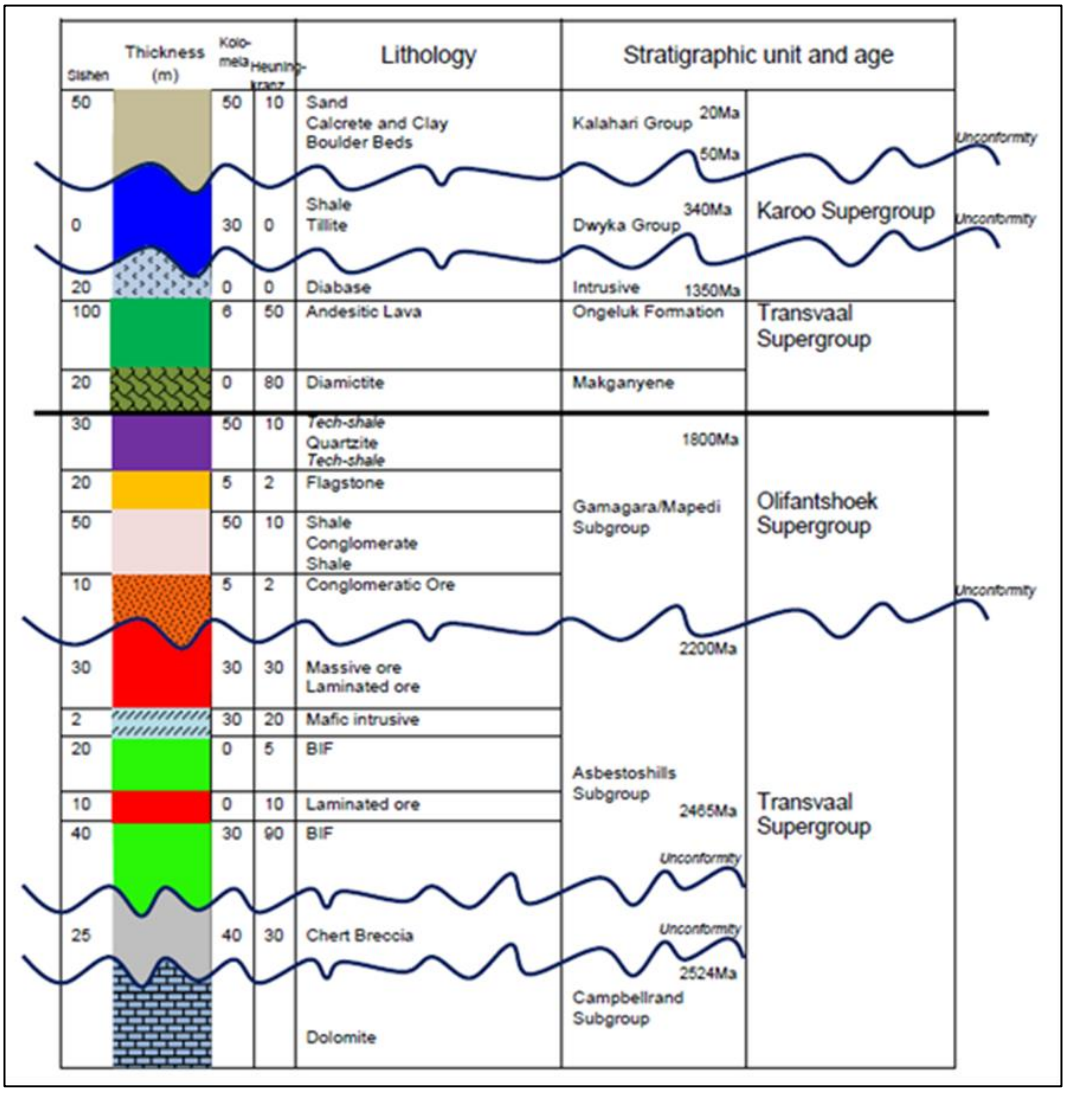


Figure 3-1: Stratigraphic succession in the Heuningkranz area

Ghaap Group

The base of the Ghaap Group is constituted by the Campbell Rand Subgroup that has a lower age of 2.555Ga ±19 Ma. Modelled lithologies of this group should predominantly comprise the Kogelbeen Formation, which consists of dolomite (DOL), limestone and chert. Carbonate units in the vicinity of the modelled volume have been described by (Beukes, 1983) as being predominantly clastic and ferruginous with localized ankerite-rich chert beds. Dolomite of the Kogelbeen Formation is unconformably overlain by chert breccia (CH) of the Wolhaarkop

Formation. The ferruginous Wolhaarkop Formation was deposited - or preserved - in local depressions, probably on a relict karstic topography or surface. Chert and chert breccia are believed to have formed in a shallow-water setting, which was periodically exposed to the atmosphere (Van Wyk, 1980) (Van Schalkwyk & Beukes, 1986). Their exposure over Heuningkranz is limited to several very deep drill holes that usually intersect the uppermost few meters of dolomite. Stratigraphically upwards chert, chert breccia(s) and "wad", comprising the Wolhaarkop Formation or the Wolhaarkop Breccia, grade upwards into banded iron formation (BIF) of the ~2.52-2.43 Ga Asbestos Hills Subgroup, occasionally interlayered with Penge shale (see below) (Beukes, 1983) (Van Schalkwyk & Beukes, 1986). This breccia is siliceous and locally Mn-, Fe- (or haematite)-rich. Its composition and texture suggest an exposed, relict, karstic topography or surface, or a solution-collapse breccia that formed in a shallow-water setting that was periodically exposed to the atmosphere. The Penge Formation, located in the Transvaal Basin, correlates with the Asbestos Hill Subgroup of the Griqualand West and Prieska Sub-basins. Banded iron formation (BIF) forms the base of what is locally known as the Kuruman Formation of the Asbestos Hills Subgroup.

The Asbestos Hill Subgroup is divided into three formations, namely the Kliphuis, Kuruman and Daniëlskuil Formations. The Kliphuis Formation is transitional between the underlying carbonates of the Campbell Rand Subgroup and BIF of the Kuruman Formation. Overlying this is BIF of the Daniëlskuil Formation, which is believed to be reworked Kuruman-type BI. BIF of this formation is typically regarded as both granular and less finely-laminated than that of the Kuruman Formation. However, BIF of both the Kuruman and Daniëlskuil Formations are regarded as being chemically similar. Lastly, sediments of the Asbestos Hill Subgroup are, in parts, para-conformably and unconformably overlain by the Koegas Subgroup that defines a depositional hiatus prior to the onset of upwards-shallowing conditions of the Griqualand West basin (Beukes, 1983). Five formations are distinguished, namely the Pannetjie Formation, Doradale Formation, Kameelfontein and Naragas Formations, and Heynskop Formation. These formations are characterized by upwards-coarsening sequences of shale, siltstone and quartzite, while individual cycles are identified by (stromatolitic) carbonate and jasperoidal iron-formation at the base. In the Heuningkranz/Langverwacht area, Koegas units have been tectonically juxtaposed or thrusted over younger units of the Gamagara Subgroup (see below) and Postmasburg Group (see below) along, eastwards/foreland directed thrusts (i.e. Black Ridge Thrust) activated during the ca. 1.83 Ga Kheiss Orogeny.

Gamagara Subgroup

The Sishen Formation of the Gamagara Subgroup (SHG) disconformably overlies the Daniëlskuil Formation of the Asbestos Hill Subgroup. This disconformity is a c. 380 Ma period of erosion and probable uplift, between 2.43 Ga and 2.05 Ga. "Gritty" or conglomeratic ore may directly overly this unconformity. Across the broader Kolomela exploration area, this is termed "conglomeratic iron ore"

(HEMCGT). It is generally accepted that this formed by reworking of underlying laminated or clastic-textured ore, particularly in areas that have experienced significant downthrow adjacent to faults and/or possibly in palaeo channels. These units appear to be very thin and sparsely distributed.

The Sishen Formation forms the bulk of the Palaeoproterozoic Transvaal/Olifantshoek Supergroup. It overlies banded iron formation along an unconformable contact (Friese, 2007 a) (Friese, 2007 b). The package overlying HEMCGT consists of conglomerate (CGT) and shale (SH/SHG/SHT) of the remainder of the Sishen Formation, which apparently culminates in a quartzite unit. However; thin, patchy quartzites are also evident throughout shale. It may also be completely absent in places, particularly where units have been upthrown and/or eroded at anticlinal crests, above regional domes or on broad anticlines.

Postmasburg Group

Basal diamictites (DMT) of the Postmasburg Group unconformably overlie the Asbestos Hills and Gamagara Subgroups. DMT's are sporadically developed in palaeo channels and as such are not continuous over the entire area. Basal diamictites are believed to be of glacial origin (Visser, 1969) and occur high in the stratigraphic sequence, although still below the andesitic lavas of the Ongeluk Formation. Notwithstanding low-angle thrusting and low-angle tectonic inversion, basaltic-andesitic lavas (LAV) of the Ongeluk Formation extruded disconformably over the basal diamictites of the Postmasburg Group. The age of this LAV unit is constrained to 2.222 Ga ±13 Ma (Cornell & Schutte, 1996). It should be noted that the extent of low angle or sub-horizontal offset is currently unknown, although this should intuitively be greater near the orogenic front to the west of the Heuningkranz area.

Kalahari Group

Sediments of the Kalahari Group overlie the basaltic-andesitic lavas overlying the Gamagara Group. This group comprises sand, pebble, clay and calcrete.

Intrusive bodies

Drill holes intersect several significant and densely-spaced intervals of diabase and gabbro. The collective spatial distribution indicates an inter-connected system of intrusions consisting of a major sub-vertical and SSW-NNE trending dyke, offset in a sinistral sense in the central part and relatively thin, sub-horizontal sills that are parallel to bedding and/or low-angle thrusts. Ongoing modelling at Kolomela Mine reveals that the effects of gabbro intrusions, particularly gabbro sills, has had a profound effect on the position and geometry of orebodies and, consequently, on the designs of pits.

Major Structural Trends

In absence of high confidence mapping or the explicit identification of major faults or thrusts, major structures are necessarily interpreted and derived from mostly

geophysical data (airborne gravity and magnetic surveys) and lithological logs. These structures are used to subdivide the area into smaller fault bounded blocks.

Geophysical data outlines significant ore mineralization (dense gravity anomalies) below the proposed tectonic unconformity, but importantly also indicates prominent NNE-NE to SSW-SW-trending, high-angle normal faults.

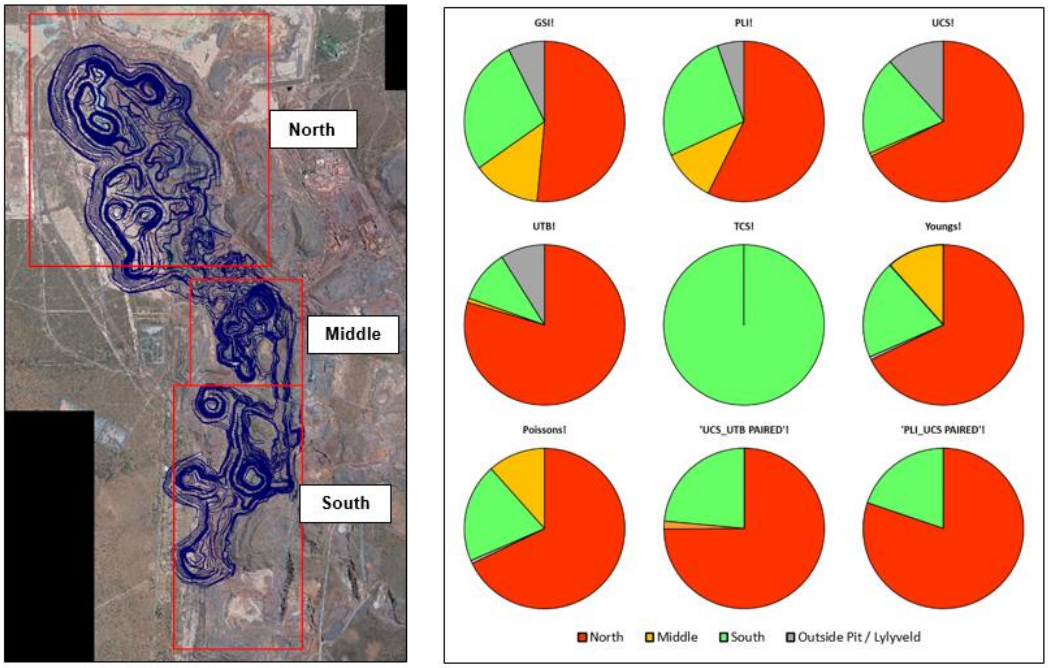
The geometry and full kinematic characteristics of these normal faults are not clear; however regional trends on the western margin of the Maremane Dome and marginal effects of the frontal propagation of the Kheis fold-and thrust belt suggests gentle SE to ESE vergence of normal faults, possible subsequent inversion and with a small component of dextral strike-slip. Such lateral (oblique slip) displacement along normal faults have been documented, but is less significant. Typical high-angle structures, i.e. inverted normal faults, are interpreted as likely listric graben-type faults initiated during the 2.64 Ga Ventersdorp rift basin formation that was later reactivated/inverted during the 1.83 Ga Kheis Orogeny. Geophysical data and cross-cutting structural relationships also indicate a set of sub-vertical, conjugate, SE-NW and SW-NE trending faults along which the southern blocks appear marginally upthrown. The origin of these faults are unclear, but late kinematic and differential strike-slip (dextral?) movement during eastwards propagation of the Kheis Orogeny, and subsequent north to north-westwards directed Namaqua orogeny could have contributed to movement along these faults. The latter event, causing southern blocks to be upthrown, is suggested to have caused erosion, affecting preservation of high grade hematite ore. Heuningkranz straddles the eastern frontal margin of the Kheis Belt and is characterized by a distinct tectonic unconformity at the base of the Postmasburg Group, which overrides shale and sandstone of the Gamagara Subgroup. Regionally, this tectonic unconformity represents a continuity of the Blackridge Thrust, which largely follows the frontal margin of the Kheis Belt. The thrust plane is identified by the base of the Postmasburg Group and, as such, is marked by the lowermost interval of either (Ongeluk Formation) lava or diamictite. Previous Heuningkranz models have shown the thrust plane to be remarkably laterally continuous with a consistent top-to-the-SE verging geometry and with no clear offset by other structures. This indicates that earlier faults, i.e. faults that predate the Kheis Orogeny, are largely constrained below the Blackridge Thrust, a scenario comparable to the geology of Sishen Mine. The effects of broadly eastwards directed stress of the Kheis Orogeny is transgressive throughout the Heuningkranz sequence, even below the Blackridge Thrust, as low angle thrusts imbricate, stack and, in parts, invert the stratigraphy.

APPENDIX 4: SISHEN MINE GEOTECHNICAL DATA.

Summary of sample numbers for all test data at Sishen Mine.

	Rockmass		Lab Tests			Elastic Properties		Paired Sampled	
	GSI	PLI	UCS	UTB	TCS	Young's	Poisson's	Mi Calculation (UCS / UTB Paired Samples)	Point Load UCS Factor (UCS / PLI Paired Samples)
BIF (BIF, LY, LYT)	600	3143	82	63	41	33	33	21	50
Calcrete (CC, KK)	174	314	74	103	0	54	54	46	94
Conglomerate (CGT, KGT)	135	571	1	1	0	1	1	1	2
Diabase (DI)	31	239	6	9	0	3	3	6	12
Dolomite (DOL)	80	299	9	2	0	1	1	0	0
Hematite (HEM, EKG, EL)	369	1577	9	0	0	1	1	0	0
Lava (LAV, LAW)	135	1575	86	152	0	63	63	25	128
Manganese Marker (MN, MM, MNE, CH, CHM)	407	1781	36	33	0	25	25	33	61
Quartzite (QTZ, FLS)	255	1049	21	22	0	20	20	16	49
Shale (SH, SHM, SHT, SKT)	777	1921	66	35	0	29	29	23	41
Total (Including Misc. lithology)	3194	12826	444	457	41	250	250	187	480

Test samples per mining area.



Results of small sample theory assessment of Sishen's Geotechnical Data.

	Rockmass	Lab Tests				Elastic Properties		Paired Sampled		
	GSI	PLI	UCS	UTB	TCS	Youngs	Poissons	Mi Calculation (UCS / UTB Paired Samples)	Point Load UCS Factor (UCS / PLI Paired Samples)	
Notes	>100 = Green, >50 = Yellow, <50 = Red (No targeted sampling program - general borehole logging)	>200 = Green, >100 = Yellow, <50 = Red (No targeted sampling program - general borehole logging)	Small Sample Theory: >80% Confidence = Green, > 5 Samples = Yellow, < 5 Samples = Red	Small Sample Theory: >80% Confidence = Green, > 5 Samples = Yellow, < 5 Samples = Red	>15 Samples = Green, 5 to 15 Samples = Yellow <5 Samples = Red (Low Priority Sampling)	Small Sample Theory: >80% Confidence = Green, > 5 Samples = Yellow, < 5 Samples = Red	Small Sample Theory: >80% Confidence = Green, > 5 Samples = Yellow, < 5 Samples = Red	>10 Samples = Green, 5 to 10 Samples = Yellow <5 Samples = Red Cannot apply Small Sample Theory)	>10 Samples = Green, 5 to 10 Samples = Yellow <5 Samples = Red Cannot apply Small Sample Theory)	**Sampling Notes**
BIF (BIF, LY, LYT)										
Actual Sample Count	600	3143	82	63	41	33	33	21	50	
Distribution	Normal	Lognormal	Lognormal	Lognormal	-	Normal	Lognormal	-	-	Sufficient Samples
Confidence Interval (%)	-	-	90	88	-	99	98	-	-	
Samples Required	-	-	29	25	-	6	8	-	-	
Calcrete (CC, KK)										
Actual Sample Count	174	308	80	109	0	54	54	46	94	
Distribution	Normal	Lognormal	Lognormal	Lognormal	-	Normal	Normal	-	-	Sufficient Samples
Confidence Interval (%)	-	-	92	98	-	88	100	-	-	
Samples Required	-	-	24	20	-	22	6	-	-	
Conglomerate (CGT, KGT)										
Actual Sample Count	135	571	1	1	0	1	1	1	2	
Distribution	Normal	Lognormal	Lognormal	Lognormal	-	Normal*	Normal*	-	-	Min 5 UCM / UTB / Point load paired samples to be collected (Low sampling priority)
Confidence Interval (%)	-	-	0	0	-	0	0	-	-	
Samples Required	-	-	5	5	-	5	5	-	-	
Diabase (DI)										
Actual Sample Count	31	238	7	10	0	3	3	10	12	
Distribution	Normal	Lognormal	Lognormal*	Lognormal*	-	Normal*	Normal*	Lognormal*	-	Min 5 UCM / UTB paired samples to be collected for Youngs / Poissons/UTB (Low sampling priority)
Confidence Interval (%)	-	-	47	65	-	0	0	65	-	
Samples Required	-	-	14	11	-	5	5	11	-	
Dolomite (DOL)										
Actual Sample Count	80	299	9	2	0	1	1	0	0	
Distribution	Normal	Lognormal	Lognormal*	Lognormal*	-	Normal*	Normal*	-	-	Min 5 UCM / UTB paired samples to be collected for Youngs / Poissons/UTB (Low sampling priority)
Confidence Interval (%)	-	-	59	0	-	0	0	-	-	
Samples Required	-	-	13	5	-	5	5	-	-	
Hematite (HEM, EKG, EL)										
Actual Sample Count	369	1577	9	0	0	1	1	0	0	
Distribution	Normal	Lognormal	Lognormal*	Lognormal*	-	Normal*	Normal*	-	-	Min 5 UCM / UTB paired samples to be collected for Youngs / Poissons/UTB
Confidence Interval (%)	-	-	71	0	-	0	0	-	-	
Samples Required	-	-	8	5	-	5	5	-	-	
Lava (LAV, LAW)										
Actual Sample Count	135	1572	89	155	0	63	63	25	128	
Distribution	Normal	Lognormal	Normal	Normal	-	Normal*	Normal*	-	-	Sufficient Samples
Confidence Interval (%)	-	-	99	100	-	100	100	-	-	
Samples Required	-	-	14	8	-	5	5	-	-	
Manganese Marker (MN, MM, MNE, CH, CHM)										
Actual Sample Count	407	1779	38	33	0	25	25	33	61	
Distribution	Normal	Lognormal	Normal	Lognormal	-	Normal*	Normal*	-		Sufficient samples according to Small Sample Theory - Area specific analysis required.
Confidence Interval (%)	-		82	79	-	92	96	-		
Samples Required	-		19	21	-	8	6	-		
Quartzite (QTZ, FLS)										
Actual Sample Count	255	1049	21	22	0	20	20	16	49	
Distribution	Normal	Lognormal	Lognormal*	Lognormal*	-	Normal*	Normal*	-	-	5 UCS samples (down from 14) required according to small sample theory.
Confidence Interval (%)	-	-	62	76	-	97	93	-	-	
Samples Required	-	-	26	16	-	6	7	-	-	
Shale (SH, SHM, SHT, SKT)										
Actual Sample Count	777	1921	66	35	0	29	29	23	41	
Distribution	Normal	Lognormal	Lognormal	Lognormal	-	Normal*	Normal*	-	-	12 UCM/UTB Paired sampled required. Further UTB Small Sample iterations to be done.
Confidence Interval (%)	-	-	77	27	-	50	82	-	-	
Samples Required	-	-	42	188	-	24	13	-	-	

*Distribution Assumed, not enough data to calculate.

Key	
High Confidence - Sufficient Samples	
Medium Confidence - Some Samples Required	
Low Confidence - Insufficient / No samples	
Low Priority - Test type / Material properties currently not required	

Note: All material types that currently have low confidence or low priority are not present on final pit boundaries or stability analyses results are not sensitive to these parameters.

APPENDIX 5: GEOLOGICAL SETTING OF KOLOMELA MINE.

Stratigraphy

"The Griqualand West Basin of the Transvaal Supergroup is well-preserved in the Northern Cape of South Africa. The base of the Ghaap Group (Transvaal Supergroup) comprises the ca. 2.6–2.43 Ga Campbellrand Subgroup (Eriksson, et al., 1993) (Moore, et al., 2000), conformably overlying the Schmidtsdrif Subgroup. The Wolhaarkop Breccia or Wolhaarkop Formation, which unconformably overlies dolomite, is a siliceous chert breccia, locally enriched in manganese and/or hematite and comprising angular to subrounded chert fragments in a grey-brown chert matrix. (Van Wyk, 1980) and and (Van Schalkwyk & Beukes, 1986) suggest an exposed, relict, karstic topography accompanied by solution-collapse in a periodically-exposed shallow-water setting (Moore, et al., 2011). The Wolhaarkop Formation grades upwards into undisturbed or partly brecciated and folded ironstones of the Manganore Formation (Van Schalkwyk & Beukes, 1986), which is the local term for the Kuruman Iron Formation, occasionally interlayered with shale of the ca. 2.52–2.43 Ga Asbestos Hills Subgroup (Beukes, 1983) (Van Schalkwyk & Beukes, 1986). The upper portion of the Manganore/Kuruman Iron Formation shows Fe enrichment to ore grade. The Gamagara/Mapedi Formation (Beukes & Smit, 1987) has an age of ca. 2.05–1.83 Ga and overlies banded iron formation at an un conformable contact. It consists of a thick sequence of younger clastic sediments, including shale, quartzite and conglomerate. Hematitic conglomerate, which marks the base of the Olifantshoek Supergroup, typically constitutes lower-grade ore at the eroded upper contact of the Manganore/Kuruman Iron Formation. The unconformity represents approximately 380 myr of erosion and uplift, between 2.43 Ga and 2.05 Ga, at the Manganore Iron Formation-Gamagara/Mapedi Formation contact. Due to its deposition on a densely-faulted footwall, the Gamagara/Mapedi Formation varies greatly in thickness or is completely absent. West of the Maremane Dome, diamictite of the Makganyene Formation (De Villiers & Visser, 1977) and basaltic andesite/andesite of the Ongeluk Formation (both part of the Postmasburg Group) were thrust eastwards over Gamagara Formation sediments, along what has been interpreted as a thrusted unconformity or tectonic unconformity, termed the Blackridge Thrust (Beukes & Smit, 1987) or Makganyene Unconformity. This feature is one of several forward-propagating splays that have created thin klippe or outliers within the foreland of the thrust front. These units are primarily preserved in synclines flanking the Wolhaarkop Dome (Schütte, 1992), but have been removed by erosion over up-faulted, anticlinal or domal areas, thereby exposing dolomite. Tholeiitic basaltic andesite of the Ongeluk Formation, extruded underwater in a marginal basin of the Kaapvaal Craton (Schütte, 1992). The age of the Ongeluk lavas effectively assigns a maximum age to the Mapedi Formation, which postdates the Great Oxidation event (GOE) (Bekker, et al., 2004) by a minimum of 100 myr. Shale, of the Sishen Member in the Gamagara Formation, is generally overlain by purplish-white Marthaspoort quartzite followed by further green to red shales of the uppermost Paling Member. The region hosting the Mapedi Formation has experienced only low-grade metamorphism, with maximum temperatures of 110–170°C and pressures less than 2 kbar. Makganyene diamictite is massive to poorly-bedded and contains lenses of pebbly sandstone, siltstone, shale and mudstone, interpreted as piedmont glacial and glaciofluvial assemblages by (Beukes, 1983) and (Visser, 1971). Dwyka glaciation removed a significant

interval of the stratigraphy and redeposited this as tillite (Visser, 1971), notably preserved in the Kapstevel North/South and Leeuwfontein model volumes, during the Cretaceous. Tertiary regional erosion produced calcrete, dolocrete, clay and pebble layers of the Kalahari Group, deposited unconformably over older lithologies; however, this cover is extremely thin to completely absent in the Kolomela area. Several diabase dykes and sills occur in the region. (Carney & Mienie, 2003) noted significant gabbroic sills that separate iron ore from the banded iron formation. Kapstevel South shows at least two gabbroic sills that transgress the orebody, while Leeuwfontein contains an extensive and laterally-persistent sill that consistently underlies the main orebody across its full extent. (Friese & Alchin, 2007) suggested that gabbro intruded into the Griqualand West Supergroup during the late Proterozoic. The stratigraphic succession for the Kolomela area is illustrated in Figure 102.

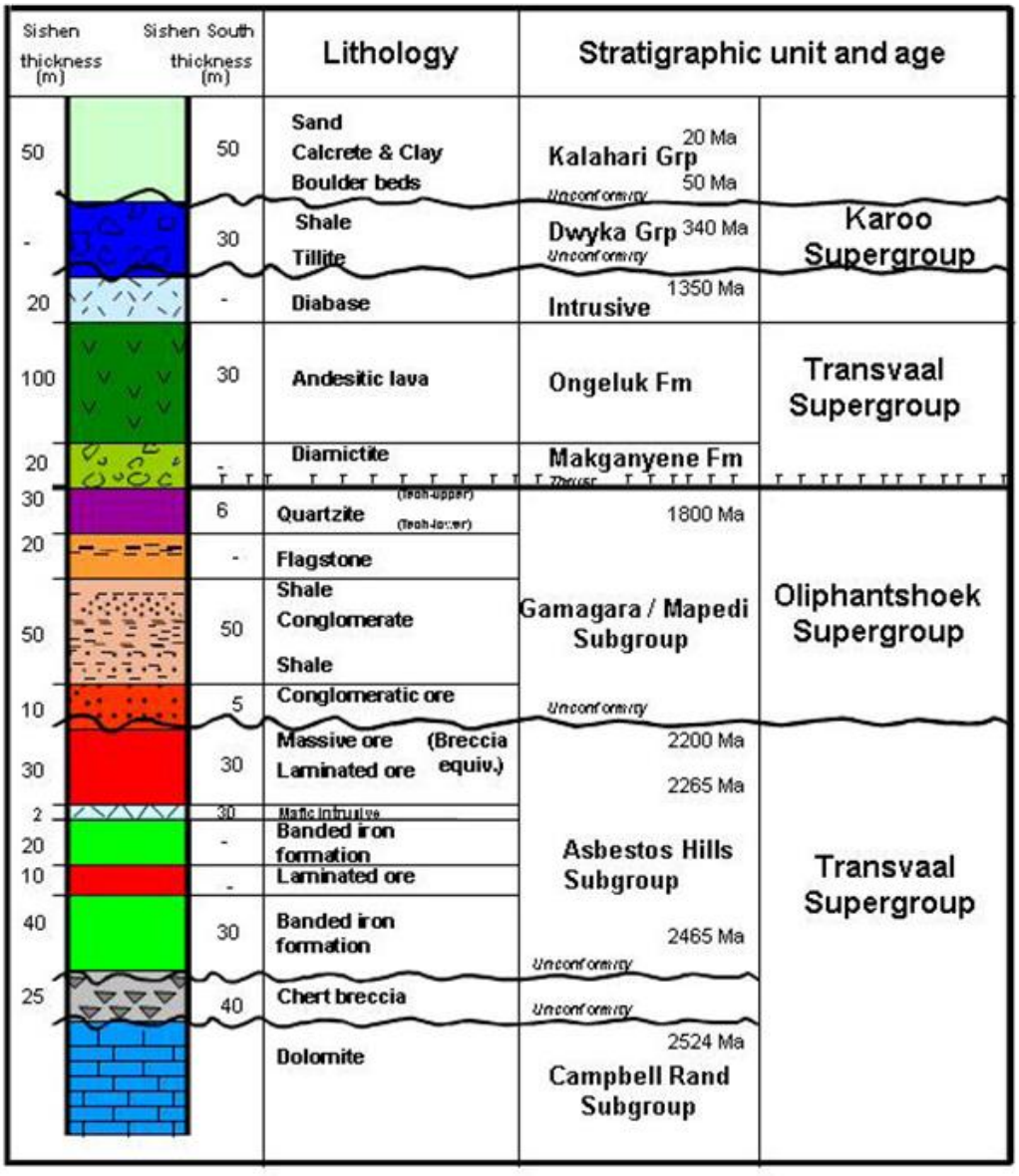


Figure 5-1: Kolomela stratigraphic succession

Structural Evolution

This portion of the southwestern to western Kaapvaal Craton and its overlying sequences have undergone polyphase deformation, according to van (Van Schalkwyk & Beukes, 1986), (Stowe, 1986), (Hilliard, 1999), (Carney & Mienie, 2003), (Friese & Alchin, 2007), (Altermann & Hälbich, 1991) and (Beukes & Smit, 1987). (Hälbich, et al., 1993) and (Hilliard, 1999) refer to extensive deformation in the lower portions of the Transvaal Supergroup and its ore-bearing zones. The formation of the Ventersdorp Rift Basin around 2.78–2.64 Ga initiated with the deposition of the Campbellrand dolomite, Wolhaarkop chert and BIF of the Ghaap Group, followed by a series of orogenic events, separated by hiatuses or extensional events. A new baddeleyite U-Pb age of 2442 ± 5Ma was obtained for the intracratonic Westerbergsill, which intruded banded iron formation of the Kuruman Formation of the Transvaal Supergroup to the south of Kolomela, displaying folding that trends tangentially to the Maremane Dome (Kampmann, 2012). The ~2.35–2.25 Ga east-verging Kalahari Orogeny formed NS trending F_1 folds, generated the Uitkomst cataclasite (Altermann & Hälbich, 1991) and inverted rift-related faults. Uplift and erosion of lithologies at this time, including those of the Ghaap Group, led to the formation of the Postmasburg Unconformity, commonly cited as being instrumental in supergene Fe-enrichment models. Between ~2.24 and1.83Ga, reactivation of rift-related faults caused deposition of the volcano sedimentary to volcaniclastic Upper Postmasburg Group. Ongeluk lavas mark the peak of mafic lava extrusion at c.~2.22 Ga. Deposition of clastic sediments in the form of conglomerate, "grit", quartzite and shale of the lower Olifantshoek Supergroup took place at ~2.05–1.93 Ga, thereby forming the Gamagara/Mapedi Formation within shallow-water rifts (Beukes, 1983). The emplacement of the Hartley Large Igneous Province, to form the Hartley Formation, took place at 1923 ±6 Ma to 1915.2 ±1.1 Ma (Semami, et al., 2016); (Cornell, et al., 2016). The Eburnean or E_2 extensional event (Dalstra & Rosière, 2008) resulted in reactivated normal faults displacing or offsetting the lower Olifantshoek Supergroup. South-verging folds and thrusts, according to (Altermann & Hälbich, 1991), occurred between 2.07 and 1.88 Ga. From 1.83 to 1.73 Ga, the Kheis or Kheis-Koranna Orogeny or tectonometamorphic event, like the Kalahari Orogeny, showed eastward tectonic vergence, thrusting, folding (Stowe, 1986); (Beukes & Smit, 1987); (Altermann & Hälbich, 1991); (Hälbich, et al., 1993); (Hilliard, 1999) and inversion or further inversion of older, long-lived normal faults. Rift structures of the Postmasburg Group and Olifantshoek Supergroup depositional settings were reactivated and inverted, while F_2 folding and thin-skinned thrusting occurred along major unconformities, lithological contacts and the BlackridgeThrust at the base of the lower Ongeluk lavas and Makganyene diamictite. The Groblershoek Schist Formation of the Olifantshoek Supergroup yields an 39Ar-40Ar metamorphic age of ~1780 Ma (Schlegel, 1988) and constrains the age of the Kheis Orogeny, which resulted in numerous deformational features within the Griqualaland West Supergroup (Hilliard, 1999). Possibly Bushveld-age gabbroic rocks intruded the Ghaap and Postmasburg Groups, a process partly accommodated by the reactivation of Ventersdorp faults (Friese & Alchin, 2007). The third orogenic event, to the south of the Kolomela area, comprises the ~1.35–1.0 Ga NNW-directed Lomanian (Namaqua-Natal) Orogeny, which caused deformation along the southern margin of the Kaapvaal Craton. This formed a large-scale, dextral shear system, which shows numerous,

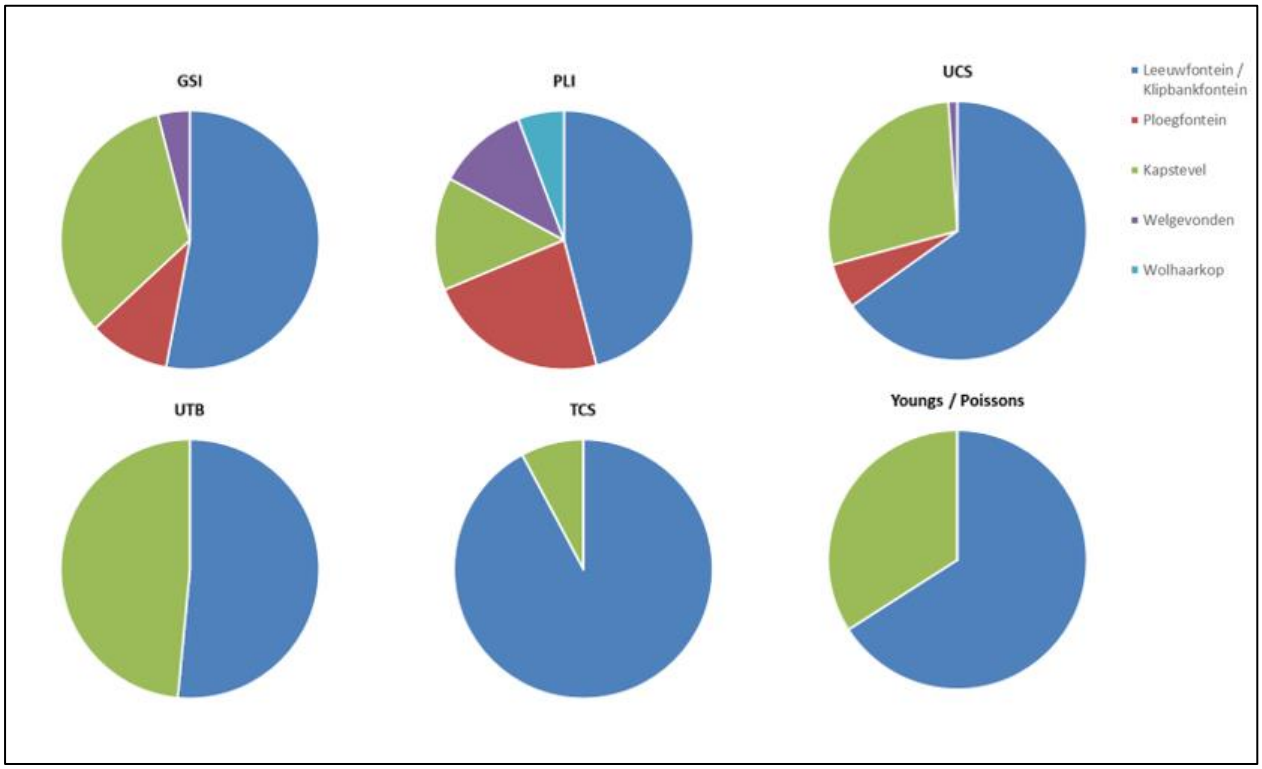
parallel, smaller-scale, right-lateral shears to the north of it. The effects of this event are manifold: reactivation, segmentation and buckling of N-S trending normal and inverted normal faults; reactivation of the 2.35–2.24 Ga NE- and SE-trending, conjugate, strike-slip faults, usually with uplift to the SE and SW, respectively, and the development of ENE-trending F_3 folds. This event was probably responsible for an overall northward dip of approximately 3° across the Maremane Dome and the emplacement of magnetite along major NW-SE trending faults (e.g. the Griquatown Fault Zone; (Erikson, et al., 2006). The Lomanian Orogeny also caused broad F_2/F_3 fold interference patterns (Hilliard, 1999) (Mortimer, 1995), particularly in units above the Blackridge Thrust, best observed at Sishen Mine (Basson, et al., 2017), as well as refolding, segmentation and buckling of thrusts, normal faults and inverted normal faults. The "asymmetry" of the Maremane Dome, mimicked on a smaller scale by the Wolhaarkop Dome to the west of its southern termination, may have partly resulted from dextral shearing in the Namaquan part of the Namaqua-Natal Orogeny. Subsequent tectonism, including the breakup of Gondwana and Pan-African reworking, appear to have had only a minor effect on the region".

APPENDIX 6: KOLOMELA MINE GEOTECHNICAL DATA.

Summary of all test data at Kolomela Mine.

	Rock mass	Lab Tests				Elastic Properties	
	GSI	PLI	UCS	UTB	TCS	Youngs	Poissons
Calcrete (CC, KK)	90	515	42	20	26	18	18
Tillite (TIL, DMT)	47	494	23	20	6	18	18
Clay (CL, KL, PEB)	8	10	8	0	11	8	8
Gabbro (GAB)	124	480	33	14	2	22	22
Quartzite (QTZ, KWT)	28	308	5	3	0	5	5
Shale LF, KF and PF (SH, SK, SKC, SKT, SKB, SHG, SHT)	72	163	43	30	18	39	39
Shale KS (SH, SK, SKC, SKT, SKB, SHG, SHT)	164	111	46	32	9	46	46
Congolmerate (CGT, KGX)	3	94	0	0	0	0	0
Conglomerate Ore (HCGT, KGT, KGE, KGC, KTE)	41	214	1	0	0	0	0
Laminated Ore (LE, KTE, HEM)	118	419	9	17	0	7	7
BIF (BIF, LY, LYX, LYK, LYA, LYB)	185	613	29	15	38	23	23
Chert (CH, CBR)	66	203	13	10	5	13	13
Dolomite (DOL)	44	242	7	8	0	7	7
Lava (LAV, LAW)	33	504	3	0	0	0	0
Total (Including Misc lithology)	1023	4370	237	150	113	182	182

Test samples per pit.



Results of small sample theory assessment of Kolomela's Geotechnical Data.

KOLOMELA GEOTECHNICAL DATA SAMPLE COUNT SUMMARY

	Rockmass	Lab Tests						Elastic Properties			
	GSI	PLI	UCS	CL%	UTB	CL%	TCS	Youngs	CL%	Poissons	CL%
Calcrete (CC, KK)	97	515	42	69	20	82	26	18	58	18	80
Tillite (TIL, DMT)	54	494	23	49	20	50	6	18	33	18	83
Clay (CL, KL, PEB)	9	10	8	35	0	0	11	8	34	8	81
Gabbro (GAB)	126	480	33	70	14	64	2	22	60	22	96
Quartzite (QTZ, KWT)	30	308	5	69	3	54	0	5	100	5	98
Shale (KF,LF, PF)	72	163	43	86	30	65	18	39	70	39	98
Shale (KS)	164	111	46	80	32	72	9	46	72	46	96
Congolmerate (CGT, KGX)	4	94	0	0	0	0	0	0	0	0	0
Conglomerate Ore (HCGT, KGT, KGE, KGC, KTE)	41	214	1	0	0	0	0	0	0	0	0
Laminated Ore (LE, KTE, HEM)	119	419	9	54	17	98	0	7	99	7	62
BIF (BIF, LY, LYX, LYK, LYA, LYB)	188	613	29	89	15	59	38	23	96	23	93
Chert (CH, CBR)	66	203	13	59	10	76	5	13	79	13	79
Dolomite (DOL)	44	242	7	82	8	72	0	7	77	7	80
Lava (LAV, LAW) Welgevonden	33	504	3	53	0	0	0	0	0	0	0
Total (Averages*)	1047	4370	262	61.2%	169	53.2%	115	206	59.8%	206	72.8%

From	To
0	59
60	79
80	100
Engineering Justification	

Note: Conglomerate (coloured blue, engineering justification) is not present on final pit boundaries and therefore stability analyses are not sensitive to its parameters. An ongoing, focussed data acquisition plan is in place to address uncertainty for all other material types prioritising BIF, gabbro and shale (taking into account the conceptual failure model at Kolomela Mine).

APPENDIX 7: KOLOMELA MINE LEEUWFONTEIN PIT STABILITY ANALYSIS RESULTS.

